Development of a Spheroid Model to Investigate Drug-Induced Liver Injury

Thesis submitted in accordance with the requirements of the University of Liverpool for the degree of Doctor of Philosophy

By

Harriet Josephine Gaskell

August 2016

Declaration

This thesis is the result of my own work. The material contained within this thesis has not been presented, nor is currently being presented, either wholly or in part for any other degree or qualification.

Harriet Josephine Gaskell

This research was carried out in the Department of Pharmacology and Therapeutics, The University of Liverpool, UK, in collaboration with AstraZeneca.

Contents

Abstract

Drug induced liver injury is a major problem for the pharmaceutical industry and health services. Yet 30-40 % of human hepatotoxins go undetected during *in vitro* studies. Hence, more predictive *in vitro* liver models are a critical requirement for preclinical screening of compounds demonstrating hepatotoxic liability. 3D liver spheroids show promise as a novel model to investigate drug-induced liver injury with preliminary studies indicating the ability of spheroids to detect hepatotoxins as well as displaying an enhanced functional lifespan compared to 2D monocultures.

The aim of this thesis was to develop an improved *in vitro* model to investigate drug-induced liver injury. A viable C3A spheroid model with a lifespan of 32 days was successfully optimised. A characterisation of the spheroid model was performed, revealing direct cell-cell contacts, 3D morphology and cellular polarisation, hence recapitulating corresponding features of human liver tissue. Subsequently, liver-specific functions were investigated in the C3A spheroids and were found to display zonation, functional transporters, CYP enzyme activity, albumin production, urea synthesis and functional mitochondria. After validating the biology of the model, the ability of the spheroids to detect hepatotoxins was examined. The C3A spheroid model correctly identified 66.6 % of hepatotoxins to have a risk of liver injury, a higher predictive value than a 2D model.

As hepatocytes only represent 60 % of the cells in the liver it was predicted that including non-parenchymal cells in the C3A spheroid model would cause increased sensitivity to hepatotoxins. Indeed when C3A spheroids were co-cultured with endothelial cells or immune cells they correctly predicted more compounds to have a risk of human hepatotoxicity, improving their predictivity to 91.6 % and 83.3 % respectively.

It has been established that novel biomarkers of liver injury HMGB1, keratin 18 and miR-122 have enhanced sensitivity when compared to current clinical diagnostic markers, however they have not been extensively analysed *in vitro*. It was determined that keratin 18 could be quantified from the C3A spheroid model and provides important mechanistic insight into the mechanism of cell injury occurring.

Mitochondrial damage is implicated in up to 50 % of human hepatotoxins. It was hypothesised that by analysing mitochondrial function in more detail one could reveal the mechanism of action by which a compound might be causing toxicity. Mitochondrial dysfunction could be successfully analysed in the C3A spheroids, which were found to be more sensitive to mitochondrial toxins than 2D cells.

To conclude; C3A spheroids act as a human-relevant *in vitro* model with the potential to be incorporated into an initial drug safety screen, replacing 2D models with poor sensitivity and specificity. Results suggest that the inclusion of non-parenchymal cells may be advantageous to liver models. Furthermore the analysis of endpoints including clinical biomarkers and mitochondrial function may improve the sensitivity of the drug screen.

Acknowledgments

I would firstly like to thank Dominic Williams, the MRC and AstraZeneca for giving me the opportunity to carry out this PhD. I am honoured to have spent the last 4 years dedicated to this project, I have thoroughly enjoyed planning and executing this research and writing this thesis was extremely rewarding. Next I would like to acknowledge all of my supervisors; Dan, Dom, Jean, Parveen, Ruth and Steve. thank you for your contribution to this project, your guidance and support.

I believe a special thanks has to go to Jon. Without your continuous patience, extensive knowledge and thorough lab wisdom I don't know where I would be. Your help has been immeasurable, thank you.

There is an extensive list of people in Liverpool that I need to thank over the last 4 years. To everybody that I have had the delight of sharing an office with, thank you for consoling me when I needed it most and for the endless delightful discussions. G27a, I'll miss you. To all who contributed to an inappropriate conversation with me over lunch, thank you for keeping me entertained and enlightening me on a diverse range of subjects, we have all learnt a lot. I can't forget anyone who has helped me to eat an entire bag of cheesy poofs, everyone who has listened to me rant about spheroids and everyone whom I have had the pleasure of sharing a night in Brooklyn Mixer with. Your friendship has been priceless to me. You have made this PhD more enjoyable than I ever could have imagined.

Finally, I would like to mention my family. Codford, thank you for always taking an interest in my PhD, I appreciate that you have always taken the time to ask me what I'm doing in the lab and support me throughout, despite it probably sounding extremely complicated and boring. Thank you to Dad and Jos for being there when I needed a break, for feeding me tonnes of food and for the millions of cups of tea; and to Dot and Nancy for helping me to put things into perspective. To me bezzie Ally Fazakerley, you have been by my side throughout this journey. Thank you for helping me to make the most of my experience in Liverpool, it would not have been the same without you there, luvyababez xoxo. And finally to Sidney, thank you for just being Sidney.

Publications

H. Gaskell, D. P. Williams, S. D. Webb, P. Sharma. The role of non-parenchymal cells in a 3D liver spheroid model. *Manuscript in prep* (2016)

H. Gaskell, P. Sharma, H. Colley, C. Murdoch, D. P. Williams, S. D. Webb. Characterisation of a functional 3D C3A liver spheroid model, Toxicology Research, DOI: 10.1039/C6TX00101G, (2016)

H. Gaskell, P. Sharma, H. Colley, C. Murdoch, D. Antoine, J. G. Sathish, D. P. Williams, S. D. Webb. Development and Characterisation of a functional 3D liver spheroid model, Toxicology Letters, 238 (2) p 176, (2015).

H. Gaskell, L. Walker, F. Miyajima, D. Antoine, M. Pirmohamed. Development of a Meso-Scale Discovery® Multi-Array® Assay to Quantify High Mobility Group Box-1. Manuscript in preparation (2014).

Abbreviations

ADME	Adsorption, Distribution, Metabolism, Excretion
ADR	Adverse drug reactions
ALT	Alanine transaminase
AP	Alkaline phosphates
AST	Aspartate aminotransferase
ATP	Adenosine triphosphate
BSA	Bovine serum albumin
CD	Cluster of differentiation
ck18	caspase-cleaved keratin 18
C_{max}	Maximum serum concentration of a drug after dosing
CMFDA	5-chloromethylfluorescein diacetate
CO_2	Carbon dioxide
CPS1	Carbamoyl phosphate synthetase 1
CYP	Cytochrome P450
DAMPs	Damage-associated molecular pattern molecules
DILI	Drug-Induced Liver Injury
DMSO	Dimethyl sulfoxide
DNA	Deoxyribonucleic acid
ECAR	Extracellular acidification rate
ECM	Extracellular matrix
ELISA	Enzyme-linked immunosorbent assay
EM	Electron Microscopy
EMEM	Eagle's minimal essential medium
ETC	Electron transport chain
FBS	Fetal bovine serum
fk18	Full length keratin 18
g	Grams
GGT	Glutamate dehydrogenases
GS	Glutamine synthetase
GSMF	Glutathione-methylfluorescein
H&E	Haematoxylin and eosin
HMGB1	High mobility group box-1
IC_{10}	Concentration of a drug to cause 10 % reduction in cell viability (highest non cytotoxic concentration)
IC_{50}	Concentration of a drug to cause 50 % reduction in cell viability
IL	Interleukin
JC-1	Tetraethylbenzimidazolylcarbocyanine iodide
kD	kilo Daltons
L	Litre
LOT	Liquid-overlay technique

LSEC	Liver sinusoidal endothelial cells
miR	microRNAs
µ-	Micro-
m-	Milli-
m	Meter
M	Molar
min	Minute
mol	Moles
MRI	Magnetic resonance imaging
MRP	Multidrug resistance protein
MSOT	Multispectral Optoacoustic Tomography
n-	Nano-
NAPQI	N-acetyl-p-benzoquinone imine
NMR	Non-mitochondrial respiration
NPC	Non-parenchymal cells
O_2	Oxygen
OCR	Oxygen consumption rate
OXPHOS	Oxidative phosphorylation
PBS	Phosphate buffered saline
PFA	Paraformaldehyde
Pgp	P-glycoprotein
p-	Pico-
RNA	Ribonucleic acid
ROS	Reactive oxygen species
RT	Room temperature
SEM	Standard error of the mean
SRC	Spare respiratory capacity
TBST	Tris-Buffered Saline with 0.05 % Tween20
TNF	Tumour necrosis factor
U	Units
ULA	Ultra-low adherence
2D	Two dimensional
3D	Three dimensional

Chapter 1

General Introduction

Contents

1.1 Introduction

Adverse drug reactions (ADR) are a constant major concern for pharmaceutical industries, regulatory authorities, as well as the patients themselves. Type A, dose-related ADR are common, predictable and caused by the primary pharmacology of the drug. Type B-F reactions are rarer but much more complicated. Type B ADR are less common and unrelated to the therapeutic drug action, making them harder to predict and treat. Chronic ADR, type C, are both time and dose-related, whereas type D ADR are mainly time-related with a delayed onset. Drug reactions can also occur after withdrawal of a compound, known as type E reactions. The final type of ADR is type F, where an unexpected failure of therapy is observed, most frequently due to interactions with other drugs (Edwards and Aronson 2000). Drug-induced liver injury (DILI) remains a prominent cause of ADR (Olsen and Whalen 2009; Russo et al. 2004; Sgro et al. 2002). Lack of understanding of the mechanisms of human DILI could be a reason for this. Predictive and relevant *in vitro* models of human DILI may help researchers identify the key events and mechanisms initiating DILI, along with aiding drug screening.

This thesis describes the development and analysis of a novel *in vitro* liver model through the use of 3D cell culture techniques as well as investigating the toxicological predictivity of the model.

1.2 Drug-induced liver injury

Drug side-effects are a major cause of liver damage, with 52 % of acute liver failure cases attributed to DILI (Norris et al. 2008; Ostapowicz et al. 2002). Exposure to hepatotoxic compounds have varying severities, including mild asymptomatic changes, symptoms similar to acute or chronic liver diseases, or can result in liver failure, usually requiring a liver transplant (Navarro and Senior 2006). However, liver transplants are not a sustainable treatment for liver injury as not only is it a complicated procedure but donor tissue is limited. In addition 20-25 % of patients die before a liver becomes available for transplantation (Liou and Larson 2008; Norris et al. 2008; Reuben et al. 2010).

Many therapeutic compounds can cause DILI. This is often unrelated to the therapeutic mechanism of action, hence more complicated to diagnose and treat. The mechanism of toxicity of hepatotoxic drugs varies from compound to compound and the exact mechanism by which a drug causes injury being often disputed or unconfirmed. Some drugs have been shown to cause toxicity by the formation of a reactive metabolite, such as paracetamol (acetaminophen) (James et al. 2003; Srivastava et al. 2010). Cytochrome P450 (CYP) enzymes convert acetaminophen to the toxic metabolite, NAPQI (N-acetyl-p-benzoquinone imine), once other metabolic pathways are saturated. NAPQI further depletes the antioxidant glutathione in hepatocytes leading to the formation of reactive oxygen species (ROS), mitochondrial damage, covalent binding and cytokine release (James et al. 2003). All of these mechanisms contribute to hepatocyte injury and liver damage; however the complete mechanism is still debated. Other compounds have been suggested to cause DILI by primarily immune mediated mechanisms. Diclofenac has been shown to cause immuno-allergic reactions, including clinical observations of hypersensitivity, production of antibodies and liver failure upon re-challenge (Boelsterli 2003). Reactive metabolites, 5-OHdic and N,5-dihydroxydiclofenac, are

also produced with this compound, resulting in mitochondrial dysfunction, NADPH consumption and oxidative stress (Boelsterli 2003; Bort et al. 1999). Fialuridine is another compound with as yet unconfirmed toxicological mechanisms. The majority of evidence suggests that the damage caused by fialuridine is due to mitochondrial toxicity, with substantial research pursuing this investigation into mitochondrial damage (Honkoop et al. 1997; McKenzie et al. 1995). Trovafloxacin is another compound which causes idiosyncratic DILI, potentially through immune mediated inflammatory stress mechanisms (Beggs et al. 2014; Shaw et al. 2010). More research into elucidating the mechanism by which compounds cause DILI could help pharmaceutical companies to design out these liabilities in the future and consequently creating safer compounds.

After initiation of liver injury, the liver attempts to repair damaged tissue. The liver has a high regenerative capacity in comparison to other human organs (Michalopoulos 2007). After DILI, an inflammatory response occurs, as immune cells infiltrate to remove debris, followed by the regenerative response where the hepatocytes proliferate until the original number of cells are present, often within 1-2 days, with full re-establishment of liver mass within 8- 15 days (Michalopoulos 2007). During this period, communication between multiple liver cell types is crucial for efficient regeneration.

DILI is the leading cause for drug attrition during pre-clinical evaluation and the main reason for drug withdrawal from the market, which is extremely costly for pharmaceutical companies (Bell and Chalasani 2009; Lasser et al. 2002; Watkins 2005). Predictive *in vitro* and *in vivo* liver models are essential during initial drug screening in order to detect ADR early in the drug discovery process. Nonetheless, current models have poor sensitivity to human hepatotoxins, with only 60-70 % of hepatotoxins detected in gold standard *in vitro* models (Gomez-Lechon et al. 2004; Xu et al. 2008) and approximately 50 % detected in animal models (Olsen and

Whalen 2009). Hence more predictive liver models are required in order to reduce the number of toxic compounds making it into humans.

1.4 Human liver physiology and function

The liver is a vital organ, situated below the diaphragm in the abdominal-pelvis region and in humans consists of four lobules, weighing approximately 1.5 kg in total (Bacon. B. R. et al. 2006; Cotran 2005). The liver is connected to the hepatic artery carrying blood from the aorta, and the portal vein carrying blood from the gastrointestinal tract, spleen and pancreas. Bile canaliculi collect bile produced from the liver which drains via the bile ducts into either the duodenum or the gall bladder (Bacon. B. R. et al. 2006). The portal triad is a group of structures, including the hepatic artery, portal vein, bile duct, lymphatic vessels and vagus nerve which sits at the edge of the liver lobule. Each liver lobe is made up of around one million lobules, around 1 mm by 2 mm, which are hexagonal in shape with the central vein at the core (Figure 1.1). This arrangement leads to zonation of each lobule; the periportal region (zone 1) closest to the vasculature and therefore supplied with highly oxygenated blood and nutrients, perivenous region (zone 3) nearest to the central vein, with lower oxygen and nutrient supply, and the transitional region (zone 2) in between the two (Bacon. B. R. et al. 2006; Godoy et al. 2013). The consequence of this is functional zonation, whereby hepatocytes in different zones of the lobule express different liver functions.

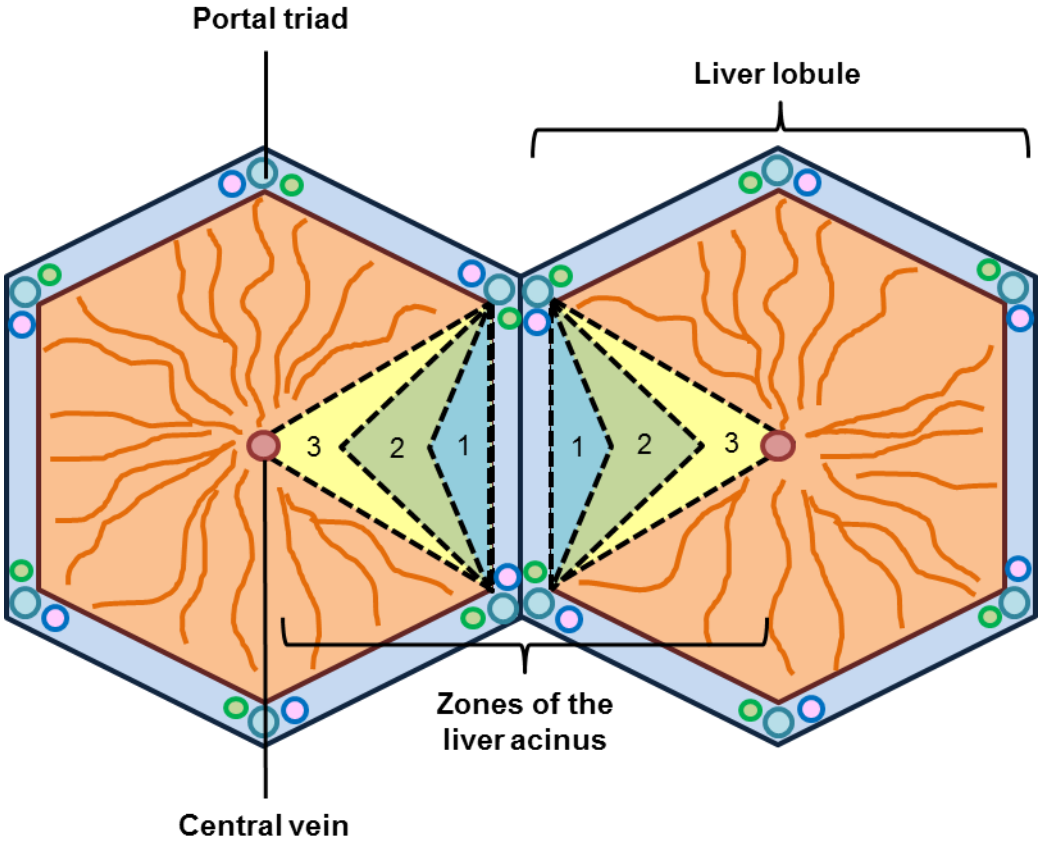

Figure 1.1. Illustration of the liver lobule. The liver lobule is arranged with the central vein in the middle and the portal triad (hepatic artery, portal vein, bile duct, lymphatic vessels and vagus nerve) on the periphery. This leads to zonation of the liver acinus (zone 1 closest to the oxygenated blood supply, zone 2 intermediately and zone 3 nearest to the central vein).

The liver has a multitude of important functions. Firstly, bile formation is a key function of the liver involving the hepatocytes excreting electrolytes and solutes from the plasma, then transporting them into the bile canaliculi (Bacon. B. R. et al. 2006). Metabolism of compounds is another key liver function. This includes the metabolism of xenobiotics, bilirubin, cholesterol, lipoproteins, ammonia, carbohydrate and fatty acids (Bacon. B. R. et al. 2006). In addition, the liver functions to store glycogen and vitamins, produces various hormones and urea and albumin synthesis (Bacon. B. R. et al. 2006; Cotran 2005).

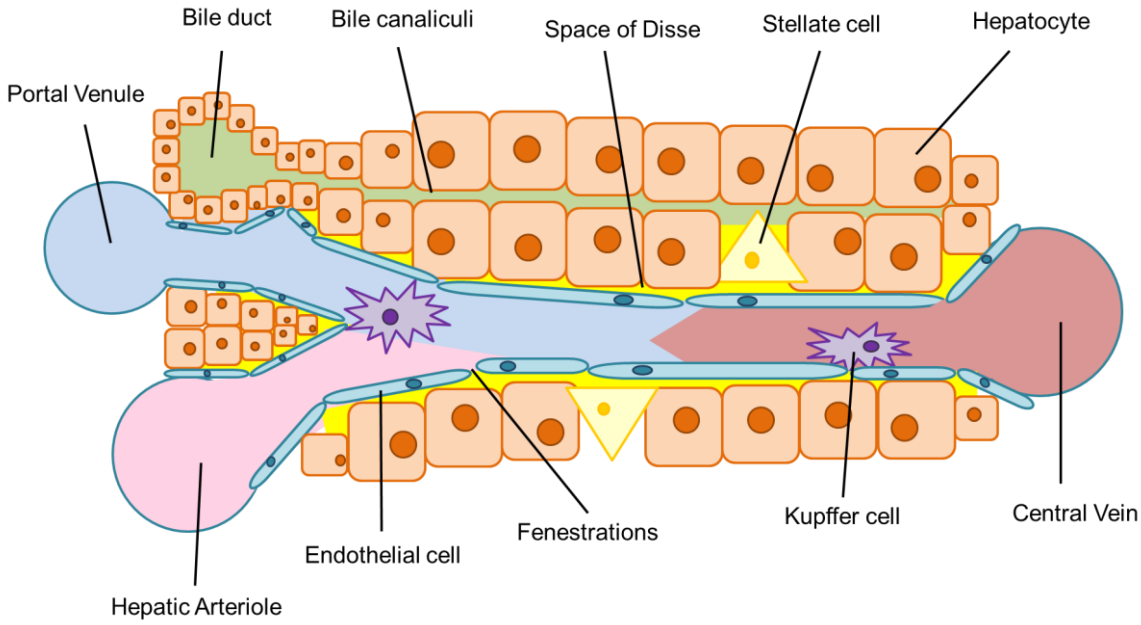

Figure 1.2. Illustration of the liver sinusoid. The liver sinusoid is composed of multiple cell types and structures. Hepatocytes make up the majority of cells in the sinusoid and produce bile. Bile canaliculi form between adjacent hepatocytes and take waste products into the bile ducts. Endothelial cells line the blood vessels and possess fenestrations to monitor the passage of molecules and cells. Kupffer cells and infiltrating macrophages circulate in the blood stream with the ability to migrate throughout the sinusoid. Stellate cells inhabit the space of Disse between the sinusoid and the hepatocytes.

1.4.1 Role of hepatocytes in the liver

The main functioning cell type in the liver is the hepatocyte, occupying 80 % of the liver volume and 60 % of the total cell number (Bacon. B. R. et al. 2006). The hepatocytes sit in a plate along the lobule and are exposed to capillaries on either side, also known as the liver sinusoids, allowing a consistent supply of blood (Figure 1.2) (Bacon. B. R. et al. 2006). Adjacent hepatocytes are connected with tight-junctions and form bile canalicular structures which run perpendicular to the capillaries (Gissen and Arias 2015). Hepatocytes are functionally polarised cells, with specific transporters localised to the basolateral (sinusoidal) membrane or the apical (canalicular) membrane, allowing specific molecules to be taken up or secreted from the cells. The structural and functional polarity of hepatocytes go hand-in-hand for efficient liver function; for example some substances may be taken up by hepatocyte transporters from the capillaries and must be secreted by a different transporter into the bile, or metabolised and transported back into the blood stream (Bacon. B. R. et al. 2006; Gissen and Arias 2015; Godoy et al. 2013). As the homeostasis of many molecules are controlled by hepatocytes, multiple enzymes, such as those involved phase I and II metabolism, must be expressed in order to perform these important physiological functions. Hepatocytes also express many plasma proteins, including albumin, protease inhibitors, transporters and inflammatory modulators (Bacon. B. R. et al. 2006; Lippincott. J. B 1993).

1.4.2 Role of non-parenchymal cells in the liver

Non-parenchymal cells (NPC) reside alongside hepatocytes in the liver and contribute 40 % of the total cell number (Bacon. B. R. et al. 2006). These cell types play an important part in maintaining liver structure and correct functionality.

Furthermore, the phenotype and function of NPC dramatically changes once the liver is damaged, contributing significantly to the liver's recovery process as well as potentially furthering insult to the tissue (Godoy et al., 2013). The second largest cell population in the liver, comprising 19 % of the cells, are the sinusoidal endothelial cells (LSEC) which function to line the capillaries in the liver. This allows the regulation of substances between the circulation and the liver (Kmiec 2001). These cells have large fenestrations to allow molecules such as hormones, toxins, nutrients and plasma proteins to flow freely between the plasma and the liver, with the ability to prevent larger molecules entering. LSEC have additional roles within the liver including scavenger functions and clearance of endotoxins and bacteria by receptor mediated mechanisms, playing a role in both immunological tolerance and liver regeneration (Anderson 2015; Ding et al. 2010; Limmer and Knolle 2001). During liver injury LSEC alter their function and morphology, enlarging their fenestrae, secreting IL-1, detecting DAMPs (damage-associated molecular pattern molecules) and enhanced tethering to leukocytes in order to allow for liver repair and regeneration (Godoy et al. 2013; Michalopoulos 2007).

Kupffer cells make up 15 % of the cells in the liver and are the resident macrophage in this organ, residing within the capillaries (Bouwens et al. 1986; Kmiec 2001). Like all macrophages, the Kupffer cells migrate around the liver and function to engulf infiltrating bacteria and cell debris, recruit neutrophils and encourage liver repair. In addition to this, during liver injury Kupffer cells release pro-inflammatory cytokines such as IL-1β, TNFα and IL-6 (Wheeler 2003). Kupffer cells additionally have an important role in regulating liver regeneration (Michalopoulos 2007). This is accomplished by releasing anti-inflammatory cytokines alongside the ability to recruit other cells to the liver, including neutrophils, natural killer cells and monocytes (Godoy et al. 2013; Kolios et al. 2006).

Stellate cells (also known as perisinusoidal cells or Ito cells) are pericytes located between the sinusoid and hepatocytes in the perisinusoidal space of Disse and comprise of 6 % of the population of cells in the liver (Bacon. B. R. et al. 2006). Once activated, the main function of the stellate cell is the formation of scar tissue during liver fibrosis. This involves chemotaxis, chemokine secretion, contractility and proliferation of stellate cells. This cell type can also detect DAMPs and can be activated by the release of cytokines from Kupffer cells, aiding liver regeneration (Godoy et al. 2013; Michalopoulos 2007). However, in a healthy liver, stellate cells are inactivated and in a quiescent state. At this point their main function is storing vitamin A and displaying neuronal and neuroendocrine markers (Kordes et al. 2008; Kordes et al. 2009; Kordes et al. 2007).

Other cell types in the liver include fibroblasts, which function to maintain the structural integrity of connective tissue when in their inactive state, producing collagen, fibres and other substances found in the extracellular matrix (ECM). Fibroblasts are activated in response to tissue damage, leading to excessive production of ECM components, which can lead to liver fibrosis and eventually cirrhosis (Guyot et al. 2006). Neutrophils and macrophages can also both migrate into the liver during injury (Mantovani et al. 2011). Neutrophils have increased tethering to LSEC and produce ROS during liver damage and infiltrating macrophages are alternately activated and produce TNFα, IL-1, IL1RA, TGFβ and IL-10 and act pro-apoptotic towards neutrophils (Godoy et al. 2013).

1.5 Current liver models used to investigate DILI

There are numerous models in which one can investigate human DILI. The most relevant option is to study the *in vivo* situation, for example through conducting clinical trials. This would give the most accurate and relevant representation of human DILI. However, this is not always possible, has broad ethical implications, and many rare toxicities are still undetected in clinical trials. Therefore researchers must find different 'models' in which to investigate DILI. Figure 1.3 lists some of the most common systems used to recapitulate a human liver, highlighting the main drawbacks of each technique.

Animal models are legally required for safety and efficacy testing of all new pharmaceuticals. In general, *in vivo* studies are highly predictive of organ toxicity and essential in order to ascertain a full organism response to a chemical (Research. 2004). However, species, environmental and genetic differences between animals and humans can result in dangerous chemicals going undetected *in vivo*. Liver injury is particularly hard to predict, with only 50 % of human hepatotoxins detected in animal models and poor concordance between animal and human toxicity data (Olsen and Whalen 2009; Olson et al. 2000a). Many compounds cause rare idiosyncratic reactions and these often can't be detected in the small number of genetically similar animals used to test for toxicity (Lee 2003), as well as many compounds going undetected in clinical trials due to the rarity of the toxicity (Stricker 1992). Furthermore, there are ethical restrictions to the use of animals, as well as rules against certain experiments or procedures being performed *in vivo* (Krewski et al. 2010).

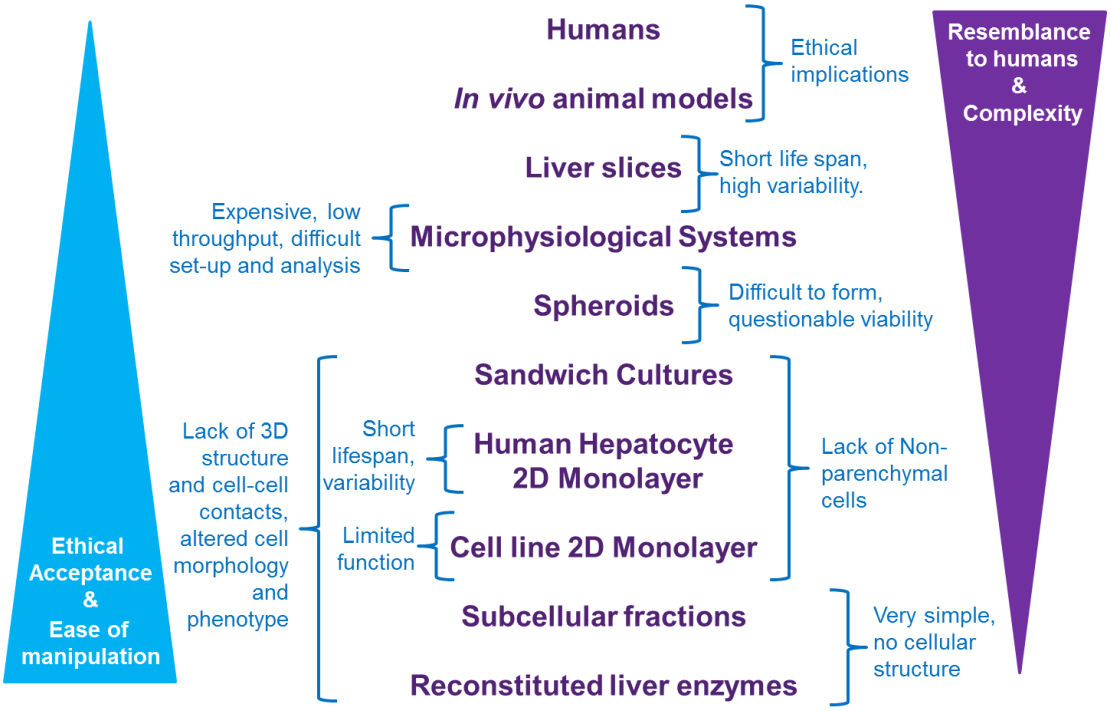

Figure 1.3. The increasing complexity of liver models. Numerous liver models are available for the investigation of DILI. These models range from the closest resemblance to humans with highest complexity to the most ethically accepted and easy to manipulate systems. Clinical trials and animal' studies are legally required and provide whole organisms responses to drug compounds, however they bare ethical restrictions as to what and how many experiments can be performed. Liver slices can be studied in more detail *ex vivo*, however they can't be sustained for prolonged periods. Complex 3D models, also known as microphysiological systems, recapitulate the liver microenvironment with the ability to include multiple cell types and microfluidics, however this comes at the cost of high expense and difficult set-up and analysis. Spheroids display 3D cell structures and can include multiple cell types but have yet to be validated for key parameters and biological characteristics. Varies cell types can be cultured in a simple 2D model, including human hepatocytes or immortalised cell lines, which are easy to manipulate and analyse, yet this leads to lower functionality and altered morphology. The most simplistic *in vitro* models include subcellular fractions or liver enzymes, which although useful, provide limited information on the whole cell response.

For this reason, human-relevant *in vitro* liver models are essential during initial drug screening in order to detect ADR early in the drug discovery process. *In vitro* liver models range from liver slices taken from an animal or human, to reconstituted liver enzymes. These models differ in their likeness to human liver, complexity and ethical acceptance. For instance, liver slices contain all of the primary cells and structures of an *in vivo* animal liver and can be analysed in detail with little restrictions. Conversely, they have a short lifespan and can be complicated to manipulate and analyse. Reconstituted liver enzymes might reflect the metabolic functions of a human liver but are simple, giving little insight into other important liver parameters (such as cellular dysfunction or drug transporter effects). The majority of *in vitro* liver models focus on hepatocytes or their immortalised alternatives, as not only are they the most common cell type in the liver but are also responsible for the majority of the liver-specific functions, such as the endogenous and xenobiotic metabolism, synthesis and secretion of substances and bile production (Godoy et al. 2013; Lippincott. J. B 1993). However, the liver is a complicated tissue with a diverse structure and multiple cell types. NPC constitute up to 40 % of the total cell number in the liver, contributing significantly to the intricate liver structure as well as having an important role in correct liver function (Bacon. B. R. et al. 2006). Hence a co-culture liver model may better represent the human liver. Increasingly complex cell culture techniques are becoming available and are beginning to be incorporated into drug screens.

Currently 30-40 % of hepatotoxic drugs still remain undetected during *in vitro* drug screening, despite efforts to increase the sensitivity of these models, leading to potentially dangerous compounds being continued throughout development (Garside et al. 2014; O'Brien et al. 2006; Xu et al. 2008). Hence novel, appropriate, human-relevant, *in vitro* liver models are a necessity in order to identify human

toxins before they reach animal or clinical trials. Commonly used *in vitro* models, their limitations and potential improvements are discussed in detail below.

1.5.1 *In vitro* liver models used to investigate DILI: Primary human hepatocytes

Hepatocytes can be isolated from human liver biopsies and cultured as a 2D monolayer *in vitro*; they are still considered by many to be the gold standard *in vitro* model for assessing DILI (Gomez-Lechon et al. 2004). Animal hepatocytes are more freely available and less costly, resulting in an array of research using rodent, canine or even porcine hepatocytes. However, species differences, such as variations in metabolism and pharmacokinetics of compounds, impact the predictivity of the model potentially rendering animal hepatocytes inappropriate for detecting human hepatotoxins (Olson et al. 2000b). Primary human hepatocytes when isolated and cultured correctly, show phase I and II metabolic enzyme activity, glucose metabolism, ammonia detoxification, albumin secretion and other functional markers for up to 72 hours in culture (Knobeloch et al. 2012). Cultured human hepatocytes thus act as a valuable model for drug metabolism and acute toxicity studies (Donato et al. 2008).

Nonetheless, there are disadvantages of using this cell type as a liver model. Firstly, not only is the availability of human liver tissue sometimes limited, especially for the amounts required for pharmaceutical drug testing, but often that which is available is from a damaged liver which has been removed because of a cancer and may have other existing pathologies or previous damage (Godoy et al. 2013). Consequently, the quality of the hepatocytes isolated is dependent on the quality of the donor tissue. Additionally, there is a large variation between donors when using

human liver tissue, as some hepatocytes are more susceptible to toxicity or more metabolically competent than others, thus the variation in responses of the cells can be large and unpredictable (Donato et al. 2008; LeCluyse et al. 2005). Pooling hepatocytes from multiple donors may help to overcome this issue, however this is not always an option. Another complication is the isolation procedure itself, with the technique of isolating hepatocytes from both human and animal liver being fairly complex and requiring advanced skills and techniques, where multiple problems and limitations can arise (Godoy et al. 2013; LeCluyse et al. 2005). Once isolated, hepatocytes rapidly lose their phenotype and function in 2D cultures *in vitro*, typified by a decrease in phase I and II enzyme activity, decreased glucose metabolism and ammonia detoxification and lower albumin secretion, as well as morphological and structural changes (Godoy et al. 2013; Gomez-Lechon et al. 2004; Khetani et al. 2015b). This reduction in liver-specific function and phenotype limits the use of primary hepatocytes to no more than 72 hours in 2D culture, meaning that only acute testing can be performed (Godoy et al. 2013).

1.5.2 *In vitro* liver models used to investigate DILI: Immortalised human liver cell lines

An alternative to using primary hepatocytes are immortalised cell lines, mainly derived from human hepatocellular carcinomas which overcomes any species differences associated with using animal derived cells. The main advantages of using liver cell lines over primary human hepatocytes are the higher proliferative capability and therefore long lifespan, ease of availability, stable phenotype, easy handling and the absence of any donor variations (Donato et al. 2008; Gerets et al. 2012; LeCluyse et al. 2012; O'Brien et al. 2006). In spite of this, the lower liver-specific functions displayed by these cell types are their main downfall, as many

human hepatocarcinoma cell lines do not express all of the metabolizing enzymes seen *in vivo*, or have levels of enzymes which are not physiologically relevant (Guo et al. 2011; Khetani et al. 2015b; LeCluyse et al. 2012).

HepG2 cells are the most commonly used human liver cell line and therefore the best characterised. These cells are derived from a hepatocellular carcinoma and are epithelial-like and non-tumorigenic (LeCluyse et al. 2012). This cell line can biotransform numerous xenobiotic compounds and is able to secrete typical liver plasma proteins including albumin, fibrinogen and transferrin. However, gene expression levels of phase I and II biotransformation enzymes of these cells cultured in 2D are substantially lower than those found in primary human hepatocytes (LeCluyse et al. 2012). This lack of enzyme function indicates that the HepG2 model is not fully representative of the phenotype of a human hepatocyte and is therefore unlikely to accurately detect human hepatotoxins that require metabolic activation. Further research has revealed that HepG2 cells have a sensitivity of 80 % to hepatotoxins, yet a specificity of 40 % when using non-liver toxins (Atienzar et al. 2014). This may be an improvement on other screening techniques; however, one cannot be confident in this model due to the lower functional profile of these cells. HepG2 cells have been studied in detail as an attempt to improve their toxicological predictivity and function. In order to express increased levels of specific enzymes, HepG2 cells have been transfected with different CYPs and used for specific drug metabolism studies (Vermeir et al. 2005).

C3A cells were selected as a clonal derivative of HepG2 cells with some advantages, chosen for their strong contact-inhibited growth characteristics, as well as high-albumin production, alpha fetoprotein and transferrin synthesis and are able to grow in glucose deficient media (LeCluyse et al. 2012; Nibourg et al. 2012). This derivative of HepG2 cells appears to better represent a primary hepatocyte,

however, more research is required on these C3A cells in order to elucidate their potential as a liver model.

Another liver cell line under investigation is HepaRG, a terminally differentiated human hepatocellular carcinoma cell. These cells produce both hepatocyte-like or cholangiocyte-like cells and can then be differentiated into mature hepatocyte-like or biliary-like cells using dimethyl sulfoxide (DMSO) (LeCluyse et al. 2012; Nibourg et al. 2012). HepaRG cells have been shown to express phase I and II enzymes, including specific CYPs, with high drug metabolising potential (Guillouzo et al. 2007). The cells additionally produce albumin, urea and lactate and have been shown to have functional transporters (Guillouzo et al. 2007; Nibourg et al. 2012). Nevertheless, these increases in enzyme expression are artificial in that they are strongly dependant on the high concentrations of DMSO in the cell culture media (LeCluyse et al. 2012).

More recently stem cell research has shown potential for *in vitro* liver modelling, including mesenchymal, fibroblast, embryonic and induced pluripotent stem cells, which can be differentiated into human hepatocytes. These cells show many morphological and functional features of hepatocytes, including drug metabolising activity, albumin secretion, drug transportation, glycogen storage (Godoy et al. 2013). However some functions are still suboptimal and there is question over whether these cells are truly differentiated into mature hepatocyte-like cells (Guguen-Guillouzo et al. 2010); nonetheless research is ongoing (Nibourg et al. 2012). Other immortalised cells, including Huh7, FLC-4/5/7, FA2N-4, have similar advantages and disadvantages which have been reviewed (Godoy et al. 2013; Nibourg et al. 2012).

1.5.3 *In vitro* liver models used to investigate DILI: NPC co-culture models

It may be essential to include all relevant cell types for complete recapitulation of the liver *in vitro* and in order to improve the predictive value of these models. There is evidence to suggest that including NPC in *in vitro* liver models can produce a more *in vivo*-like microenvironment, with enhanced liver functions. It has been found that including LSEC in primary rat hepatocyte culture models resulted in CYP function being maintained for up to 48 days, with hepatocyte differentiation markers, such as albumin, transferrin and hepatocyte nuclear factor-4, present up to day 37 and consistent urea synthesis for 28 days (Kang et al. 2013). Similar results have been observed with HepG2 cell culture, where the addition of endothelial cells caused CYP enzymes to be induced to a higher degree than in a monoculture (Ohno et al. 2009). This indicates that endothelial cells help to regulate CYP enzymes and transporter gene pathways. This research provides evidence that the presence of endothelial cells increases and maintains hepatocyte function *in vitro*. Interestingly, the reverse is also seen, as hepatocytes improve and regulate endothelial cell function. Hepatocytes are able to signal to LSEC to regulate the expression of adhesion receptors, allowing the increase or decrease of lymphocyte adhesion, hence aiding the repair of the liver after injury (Adams et al. 2010). Few studies have investigated the effects of endothelial cell co-culture on sensitivity of a model to hepatotoxins and further research is essential to elucidate the role of these cells in DILI.

Kupffer cells have been found to influence hepatocyte function, for example when included in a hepatocyte culture system metabolic functions were increased (Yagi et al. 1998). Additionally, it has been revealed that co-culturing Kupffer cells with hepatocytes alters the hepatocyte function in response to an inflammatory stimulus that would otherwise have no effect on the hepatocytes alone (West et al. 1986). Kupffer cells can also detect and respond to hepatocyte stress and damage from

hepatotoxins *in vitro*, with increased activity of Kupffer cells and release of cytokines (Kegel et al. 2015). The production of these inflammatory factors would not occur in a monoculture liver model, therefore the inclusion of Kupffer cells may increase the ability of the model to detect certain hepatotoxins. Other immune cells have been investigated in liver models, for example monocytic cell line THP-1 cells. Huh-7 liver cells were co-cultured with THP-1 cells and produced an increase in pro-inflammatory and stress-related gene expression after treatment with the hepatotoxin troglitazone, as well as increased drug metabolism and sensitivity when compared to a Huh-7 monoculture (Edling et al. 2009).

Additionally, stellate cells have an important role in liver homeostasis. One study by Kasuya *et al.* describes the essential role of stellate cells in the communication between hepatocytes and endothelial cells (Kasuya et al. 2011). Kostadinova *et al.* 2013 studied a co-culture model including hepatocytes, Kupffer cells, endothelial cells and stellate cells which revealed that liver function can be maintained for up to 3 months (Kostadinova et al. 2013). This included increased albumin, transferrin and fibrinogen production, increased urea synthesis and increased CYP inducibility when compared to a monolayer culture of hepatocytes alone. The co-culture model also responded to inflammatory stimuli, likely due to the inclusion of Kupffer cells in the model. Moreover, the co-cultured cells displayed a toxic response to hepatotoxins, whereas monolayer cultures of hepatocytes did not (Kostadinova et al. 2013) indicating that the inclusion of NPC is necessary to improve the predictive value of the model. Hence, there is building evidence that the inclusion of NPC in an *in vitro* liver model may more realistically recapitulate liver structure, function and response to toxins.

1.5.4 *In vitro* liver models used to investigate DILI: 3D liver models

There remains a need for more sophisticated *in vitro* liver models to better recapitulate liver physiology. One suggestion for how to achieve this is by enhancing the cells microenvironment to be more *in vivo*-like. The main disadvantage of standard *in vitro* liver models is that cells have a completely different morphology and structural arrangement than *in vivo*. In the human liver, cells have a 3D morphology and structural organisation, with direct cell-cell contacts to neighbouring cells which is important for cell signalling. Hepatocytes have both structural and functional polarity, with a polygonal 3D morphology, specific orientation and localised transporter functions (Gissen and Arias 2015). When cultured in 2D, hepatocytes flatten and spread out, losing their 3D cell-cell contacts and limiting signalling pathways. Additionally 2D hepatocytes have an altered phenotype as the cells dedifferentiate and lack polarisation, resulting in cellular proliferation and a loss of many crucial functions (Gomez-Lechon et al. 1998; Semler et al. 2000; Wells 2008).

The ECM is an important factor to consider when culturing cells, as this acts as a scaffold for the adhesion of cells, as well as a signalling platform (Gissen and Arias 2015). The stiffness of the ECM in the liver alters the function of multiple cell types and can result in changes to albumin production, migration and flattening of cells (Semler et al. 2000; Wells 2008). Consequently many research groups have investigated the effects of culturing cells in a 3D environment free of artificial ECM in order to more accurately model the liver microenvironment.

There are multiple ways in which cells can be cultured in 3D. A frequently used culture technique is sandwich culture, where hepatocytes are placed between layers of ECM components such as collagen or Matrigel. This technique is not a complete 3D organization of cells but has been shown to promote a more *in vivo*-like

hepatocyte morphology with less flattening, cell-cell contacts, increased polarisation, prolonged viability and functionality (Dunn et al. 1991). Multiple cell types can be applied to the sandwich culture technique to allow diffusion of cellular signals between cell types but with no direct cell-cell contact. However, a key disadvantage of this model is the variation in ECM components such as Matrigel and the effects these products have on cell phenotype.

One of the most common ways for cells to be cultured in full 3D orientation is by using scaffolds. Various types of scaffolds exist, one of which are hydrogel scaffolds which hepatocytes can be embedded within. These hydrogels have been shown to improve function further than sandwich culture (Moghe et al. 1997). Cells can also be seeded into 3D scaffolds made of natural or artificial ECM, allowing cells to migrate into these structures and form 3D tissues. For example, scaffolds in the form of 'sponges' can be used; cells can be seeded into the sponge matrix, forming small 3D aggregates within the pores of the scaffold (Godoy et al. 2013). Micropatterning has emerged as a technique allowing modification of cell and ECM interactions and accurate placement of cells, thereby controlling their microenvironment. This technique has shown potential at improving and prolonging hepatocyte function (Gerlach et al. 2003; Zinchenko et al. 2006). A very novel culture technique involves the use of 3D printing, where cells and biological materials can be automatically printed into a certain design in order to create tissues, accurately controlling the placement of multiple cell types and structures (Murphy and Atala 2014). The difficulty with all of these scaffold-based techniques are as follows: (1) developing the correct material for cells to adhere to and (2) ensuring that the size and shape of the structures are appropriate for optimal cell function, the diffusion of signalling molecules, waste products, nutrients and oxygen. Moreover these techniques are often practically difficult to set up, with a complicated harvesting and analysis of cells not to mention costly and variable in their output. A

more high-throughput and readily available 3D culture technique would be desired from a drug screening perspective.

1.5.5 *In vitro* liver models used to investigate DILI: Liver spheroids

Spheroids, also known as microtissues or organoids, are small, round 3D clusters of cells. Molds or scaffolds can be used to facilitate the formation of spheroids (Wong et al. 2011), or they can form naturally as the cells self-assemble to form a 3D spherical structure. Figure 1.4 illustrates some of the different techniques commonly used to create spheroids (Lee et al. 2013; Materne et al. 2015; Ramachandran et al. 2015; van Zijl and Mikulits 2010). All of these methods have been used to create spheroids, however as with most 3D culture techniques, reproducibility is a problem, with variation in spheroid size, shape, viability, proliferation and functionality (Friedrich et al. 2009; van Zijl and Mikulits 2010). In addition some of these techniques are more complex than others, requiring specialist equipment and often spheroids must be harvested before performing any analyses. Scaffold-free methods for creating spheroids include the hanging-droplet technique, low adherent round-bottomed cell culture plates and rocked or stirred cultures which allow cells to self-assemble and form tissue aggregates. Spheroids produced by these methods form extensive direct cell-cell contacts and produce their own ECM, which may overcome the negative effects seen with other 2D and 3D liver models. Moreover, these spheroids display an *in vivo*-like liver structure, including cuboidal cell morphology, polarised hepatocytes and structural similarities such as bile canaliculi formation (Peshwa et al. 1996). Evidence clearly suggests that spheroids cultured using a scaffold-free method better represent human liver morphology and function compared to a 2D monolayer culture (Peshwa et al. 1996; Wong et al. 2011). Plate-based methods, such as the hanging-drop technique and low adherent round bottom plates offer the advantage of producing one aggregate per well, removing

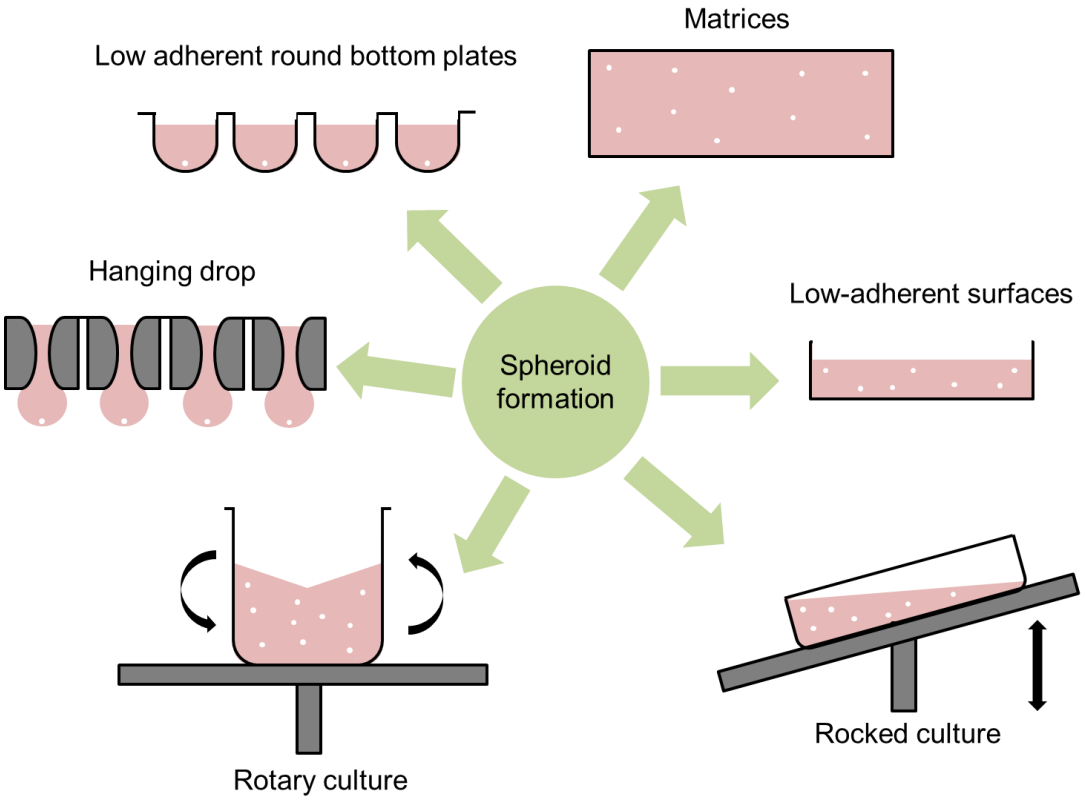

Figure 1.4. An illustration of the different approaches used to create 3D spheroids. The techniques used to create spheroids vary in complexity and include the use of rotatory or rocked culture, as well as low adherent surfaces, matrices and hanging-drop techniques in order to stimulate cells to aggregate in clusters.

the need to harvest spheroids after formation, as well as making drug treatment much easier.

Spheroids can be formed from primary hepatocytes or liver cell-lines and research shows that both have been shown to display enhanced, more *in vivo*-like functionality and a longer lifespan compared to 2D monolayer cultures. Primary human hepatocytes survive and are functional in spheroids for up to 4 weeks, sustaining phase I and II enzyme expression, albumin and urea synthesis alongside expression of liver-specific markers. Additionally bile canaliculi structures can be visualised in the spheroids, indicating polarisation of hepatocytes and the expression of hepatic transporters (Messner et al. 2013; Tostoes et al. 2012).

Furthermore, spheroids produced from numerous different liver cell lines have shown enhanced function when cultured in 3D, overcoming the main inadequacies of using immortalised hepatocarcinoma cell lines in 2D. For example Huh7 cells can be cultured in spheroids and show expression of phase I and II enzymes as well as polarisation of various receptors (Sainz et al. 2009). Investigations into HepG2 cell spheroids revealed that they have higher albumin production and metabolic activity as well as over-expression of genes involved in xenobiotic and lipid metabolism and more liver-like structures when compared to 2D cultures (Chang and Hughes-Fulford 2009; Mueller et al. 2011). Additionally, studies have been performed on C3A spheroids showing increases in liver-specific functions and potential enhanced sensitivity to hepatotoxins than 2D cultures (Fey and Wrzesinski 2012; Wrzesinski and Fey 2013; Wrzesinski et al. 2013), however multiple parameters still need to be elucidated. HepaRG cells have been cultured as spheroids and show a significant improvement in albumin and AboB production, increases in liver specific gene expression and activity, and induction of CYP enzymes when compared to 2D cultured cells (Takahashi et al. 2015; Wang et al. 2015). Hence the spheroid model overcomes many limitations of 2D cell culture, is extremely adaptable and can be used with a wide variety of different cell types.

Spheroids can be created with multiple cell types, often referred to as organoids as they better recapitulate an *in vivo* organ. Hepatocytes have been co-cultured with hepatic stellate cells, showing the same morphological and structural changes as with monoculture spheroids but superior CYP function and expression, up to 30 % increases in albumin production sustained for 2 months (Riccalton-Banks et al. 2003; Thomas et al. 2005; Wong et al. 2011). Hepatocytes have also been co-cultured with Kupffer cells and endothelial cells in spheroids, showing viability for 35 days, expression of transporters and sensitivity to some hepatotoxins (Messner et al. 2013). The location of different cell types can be studied in spheroids in order to

establish the reorganisation of multiple cell types over time (Dorst et al. 2014; Godoy et al. 2013). Despite the fact NPC have been included in many liver spheroid models, little research has gone into investigating the specific effects or roles of the NPC in the system compared to monocultures.

Cells cultured in spheroids are viable for a longer period than in 2D cultures, allowing for long-term cultures with the possibility of repeated-dose toxicity studies (Godoy et al. 2013). In addition, the quick and simple culture technique requires limited expertise and allows for high-throughput analysis, all of which are major advantages for a pharmaceutical drug screen. Furthermore, the *in vivo*-like phenotype, structure and functionality could result in spheroids being more predictive of human hepatotoxins and result in a useful model for the investigation of liver injury (Fey and Wrzesinski 2012; Godoy et al. 2013; Tostoes et al. 2012).

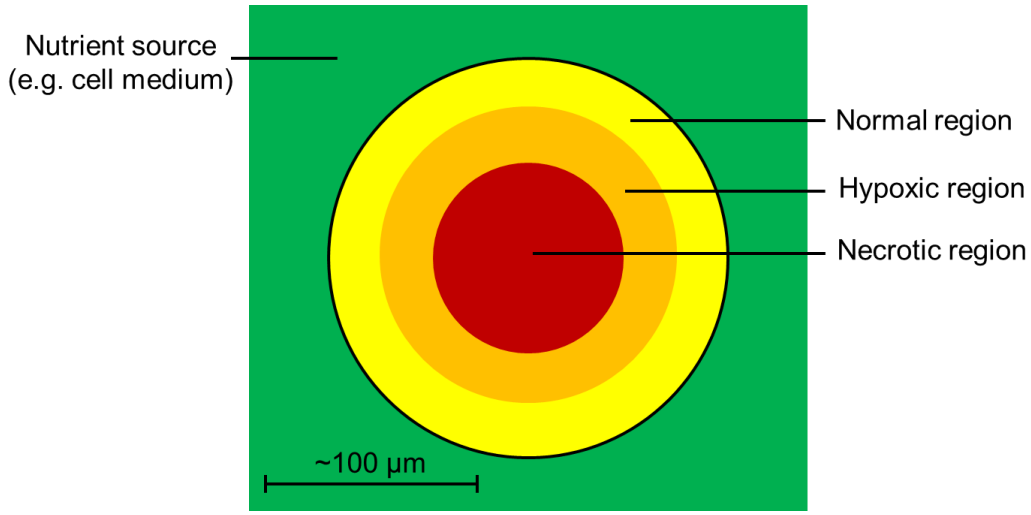

Figure 1.5. A diagram illustrating oxygen and nutrient gradients throughout a spheroid. The outer layer of the spheroid has normal oxygen and nutrient concentrations. Further into the spheroid, oxygen and nutrient concentrations decrease, with necrosis occurring in the spheroid core.

Nonetheless, like most *in vitro* models there are some disadvantages and unresolved issues when it comes to culturing spheroids. Spheroids can develop hypoxic cores, where the central cells undergo necrosis (Figure 1.5). This is due to the lack of diffusion of oxygen and nutrients into the spheroid core and build-up of cell debris and waste products in the centre. It has been reported that oxygen can diffuse 100 - 150 µm through tissue, suggesting that spheroids under 200 - 300 µm radius would have a healthy core (Asthana and Kisaalita 2012; Curcio et al. 2007; Olive et al. 1992). In addition to this, oxygen concentrations effect hepatocyte functionality as the demand for oxygen in these cells is 10 times higher than other cell types, and studies have shown that increased oxygen uptake rates can lead to increased liver-specific functions (Cho et al. 2007).

A different theory states that a lack of nutrients to cells is the cause of apoptotic cell death and that this occurs whilst oxygen is present (Funatsu et al. 2001; Grimes et al. 2014; Kasinskas et al. 2014). However, little research has thoroughly investigated the essential parameters required in order to avoid necrotic core formation, which could be influenced by culture technique, cell type, cell number and culture duration. Furthermore, few studies on liver spheroids have confirmed cell viability or oxygen concentrations over a prolonged period and throughout the spheroid core. It is essential to avoid a necrotic core in a liver model as this would distort any toxicity data collected from the spheroid model if pre-existing cell damage was present. Conversely, this gradient may be advantageous, as oxygen and nutrient gradients exist throughout the liver sinusoid, leading to zonation of the lobule. Hence it is important that these factors are investigated thoroughly during validation of a spheroid culture system.

1.5.6 *In vitro* liver models used to investigate DILI: Microfluidic liver systems

One of the disadvantages of *in vitro* models is the artificial way in which medium is sequentially renewed and drug treatment acutely added. This results in non-steady state conditions, depletion of substrate and accumulation of product (Gebhardt et al. 2003). Microfluidics systems are a way to overcome some of these issues, with continuous perfusion of medium through the cell culture (Bhatia and Ingber 2014). There is also suggestion that the shear stress created by the flow of medium is complimentary to the cells and their phenotype (Lee et al. 2013). Moreover, evidence has revealed that microfluidics causes maintenance of more *in vivo*-like system as the consistent low concentrations of nutrients, oxygen and metabolites has been shown to improve liver-specific functions in hepatocytes as well as improve cell viability in these systems (Esch et al. 2015; Gebhardt et al. 2003; Lee et al. 2013; Tostoes et al. 2012).

Research on C3A hepatoma cells cultured in a microfluidic device showed liver-specific functions, including gluconeogenesis, ureagenesis and albumin synthesis, with almost comparable levels to primary hepatocytes (Filippi et al. 2004). These systems can now be created in microchip size, resulting in a more practical sized device. The HepaTox Chip is a microfluidic device with multiple channels representing the microvessels and allowing the maintenance of hepatocyte functions and more realistic dosing strategies (Toh et al. 2009). Some research groups have combined 3D culture with microfluidics and show promising results with maintenance of a liver-specific phenotype for weeks (Domansky et al. 2010; Esch et al. 2015; Lee et al. 2013; Tostoes et al. 2012). More sophisticated culture systems such as complex hollow-fibre bioreactors are being developed, consisting of a complex scaffold onto which cells are seeded, with a flow of media through the system (Gerlach et al. 2003; Williams D et al. 2012).

Some limitations to these complex models are also apparent. The perfusion of media can result in the loss or disaggregation of cells from the system, especially as the cells proliferate and can become over confluent. Therefore, the use of microfluidics devices for long-term culture may not be appropriate. Moreover the effect of shear stress on the cells has yet to be fully elucidated and could be potentially damaging to the system (Lee et al. 2013). Little investigation has gone into confirming the sensitivity of microphysiological systems such as liver-on-a-chip devices, with some evidence suggesting poor detection of human hepatotoxins (Toh et al. 2009). Major drawbacks of all perfusion models are the complicated and costly set-up and maintenance of the system, difficult analysis and extraction of data, large number of cells required and low throughput nature. This means that the model is often not amenable to high-throughput or long-term drug screening. Despite potential for these complex 3D liver models to more accurately recapitulate *in vivo* liver tissue, this kind of system may not be appropriate as an *in vitro* liver model for drug screening.

In conclusion, numerous *in vitro* liver models are available, ranging in complexity and each of which has promises and drawbacks to their use for investigating DILI. A summary of the advantages and disadvantages of some of the currently available *in vitro* liver models are shown in in Table 1.1.

In vitro model	Advantages	Disadvantages
Primary human hepatocytes	• Most liver-like cell • Liver-specific functions • Enzyme activity • Well established	• Limited availability • Large variability • Short lifespan
Immortalised human liver cell lines	• Unlimited lifespan • Inexpensive • Little variability • Easy to culture • Well established	• Limited enzyme activity • Poor liver-specific function • Low specificity
NPC co-cultures	• Includes more relevant cell types • Increased liver-specific functions • Increase CYP enzyme activity	• Limited availability of primary cells • Limited lifespan • More complex to create
Spheroids	• *In vivo*-like cell morphology • Liver-specific functions • Prolonged lifespan • High-throughput • Multiple cell types available	• Necrotic core formation • Variability in spheroid size and formation • Difficult analysis
Complex 3D models	• *In vivo*-like cell morphology • Multiple cell types available	• Low-throughput • Expensive • High variability • Difficult analysis • Complex to set up • Large number of cells required
Microfluidics devices	• *In vivo*-like microenvironment • Liver-specific functions	• Low-throughput • Expensive • Difficult analysis • Need further investigation • Complex to set up

Table 1.1 Advantages and disadvantages of commonly used *in vitro* liver models.

1.3 Biomarkers of DILI

Clinical trials are legally required in order to determine the safety and efficacy of a compound in human subjects. Early diagnosis of DILI can be troublesome and often requires an invasive liver biopsy. Serum biomarkers are often utilised for a simpler, non-invasive diagnosis of liver injury. Appropriate, sensitive biomarkers of DILI are needed not only to monitor liver function and potential injury during clinical trials but also in order to aid patient diagnosis and treatment of DILI. A biomarker is a characteristic objectively measured as an indicator of a normal biological, pathological or pharmacological process. To screen for liver injury, blood or serum can be analysed for biomarkers, as any biomolecules released by the liver will enter the circulation. Biomarkers of liver injury can include metabolites, proteins or RNAs. Protein biomarkers released from the liver during injury include aminotransferases, such as alanine transaminase (ALT), aspartate aminotransferase (AST), glutamate dehydrogenases (GGT) and alkaline phosphates (AP), with the first two proteins indicating hepatocellular injury and the latter indicating cholestatic injury (Laverty et al. 2010). The degree of liver injury occurring can be estimated from the degree of activity or concentration of these enzymes in the blood stream.

1.3.1 Current clinical biomarkers of DILI

ALT is the most commonly utilised biomarker analysed by pharmaceutical companies and regulatory agencies for the detection of DILI (Dufour et al. 2000), with an elevation over twice the upper limit of normal (40 IU/L) indicating liver damage (Antoine et al. 2009a; Benichou 1990). Additionally, total bilirubin levels (TBL) can be analysed as a measure of liver function with elevations indicating a decline in liver function. ALT elevations are often seen before changes in TBL, however even ALT cannot predict liver injury at an early time point, as once these

biomarkers are significantly raised in the serum severe liver damage may have already ensued.

Other problems exist with the currently used clinical biomarkers. First, elevations of these molecules in serum could often indicate conditions other than DILI, as these markers are not organ specific. An example of this would be that ALT and AST could be raised due to damage to another organ system such as the heart, as well as indicating non-related liver diseases including fatty liver disease or viral hepatitis (Antoine et al. 2013; Antoine et al. 2012; Antoine et al. 2009a; Ozer et al. 2008; Zhou et al. 2013). In addition, even if the biomarkers do reveal DILI in a patient, the elevation of ALT doesn't always correlate with the extent of injury and levels can vary between patients (Ozer et al. 2008). The currently used biomarkers are also relatively insensitive, being unable to detect mild or early liver injury. The lack of translatable biomarkers may be the cause of the poor concordance between animal and human toxicity data, leading to only 50 % of hepatotoxins being detected *in vivo* (Olson et al. 2000b). It is clear that the criteria for diagnosing DILI must be improved and novel methods of detecting liver injury investigated. Research into finding novel biomarkers of DILI is underway in order to potentially overcome the problems with current clinical biomarkers of DILI. A perfect biomarker would be organ specific, have a higher sensitivity and earlier serum detection, as well as giving insight into the mechanism or cause of injury and the severity of the condition. Figure 1.6 shows a selection of clinical and novel biomarkers, their mechanistic insight and the time at which they are released after onset of DILI. Some of these novel biomarkers are discussed below.

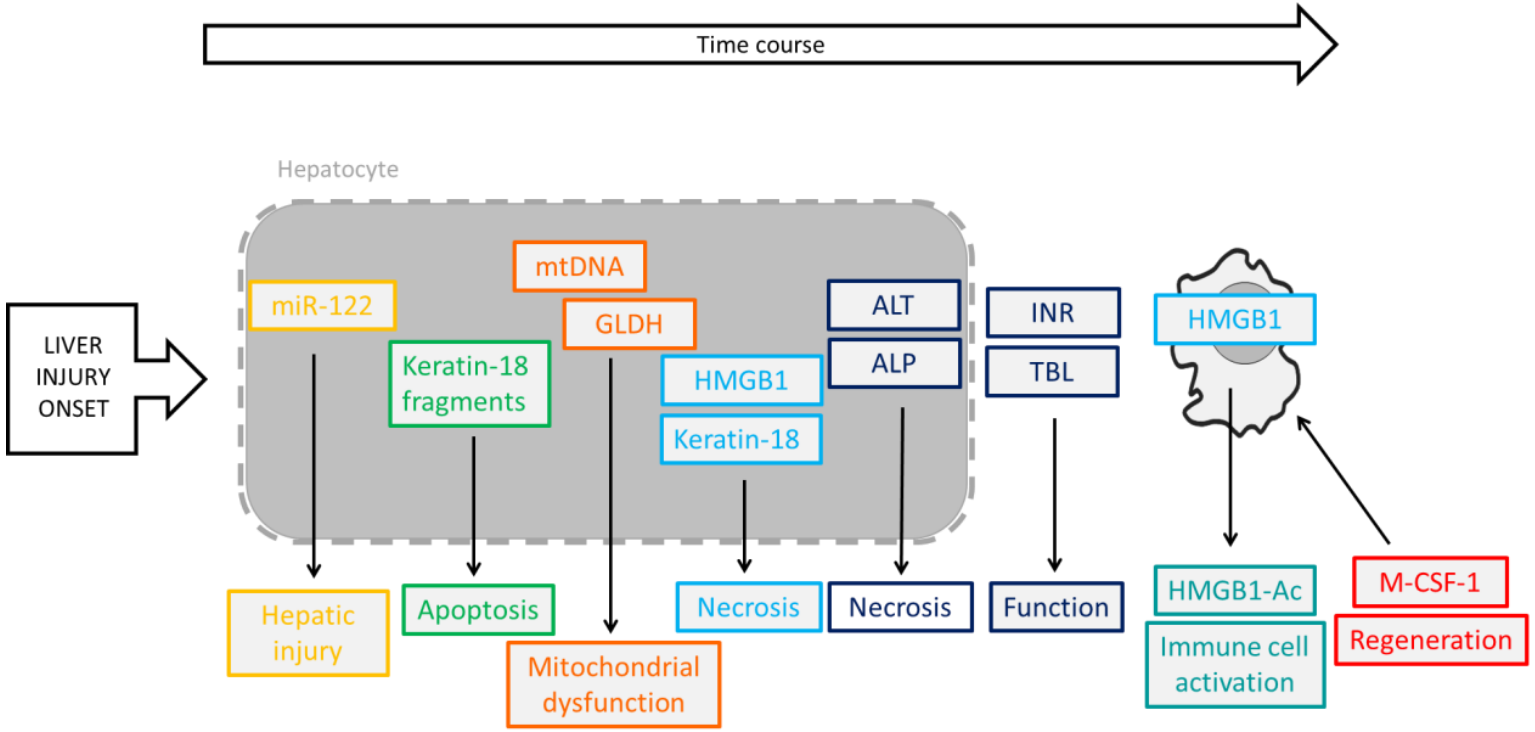

Figure 1.6. Current and novel biomarkers of DILI. Schematic represents the time course and location of release of each biomarker from the onset of liver injury. Current clinical biomarkers ALT, ALP, INR and TBL (dark blue) are released late after the onset of injury. ALT and ALP are released from hepatocytes once they necrose, and along with INR and TBL which are detected in serum once a significant reduction in liver function has occurred. Novel biomarker miR122 (yellow) is released from hepatocytes early after the onset of injury, along with keratin 18 which reflects the levels of apoptotic (green) and necrotic (blue) hepatocytes. Damage to hepatocyte mitochondria can be detected through the measurement of mtDNA and GLDH (orange). HMGB1 is initially released from hepatocytes once they necrose (blue) and later released from immune cells (cyan), along with M-CSF-1 as a marker of liver regeneration. Courtesy of Joanna Clarke, University of Liverpool.

1.3.2 Novel biomarkers of DILI: HMGB1

One novel biomarker that has been identified as a possible indicator of liver injury is high mobility group box-1 (HMGB1). HMGB1 is a component of all nucleated cells; it is essential for life and is usually found in the nucleus where it binds to DNA and regulates transcription (Bianchi and Beltrame 1998; Calogero et al. 1999). This protein also has additional functions which are thought to be stimulated by modification of its structure. Once reduced HMGB1 acts as a chemoattractant; partially oxidised HMGB1 has pro-inflammatory cytokine activity whereas terminal oxidation of the protein abrogates these functions (Janko et al. 2013; Kazama et al. 2008; Venereau et al. 2012; Yang et al. 2012). Extracellularly, HMGB1 can modulate the immune response as it aids the regeneration of damaged tissue, secretes cytokines, recruits neutrophils as well as controlling inflammation of the surrounding area (Scaffidi et al. 2002; Wang et al. 1999; Yamada and Maruyama 2007).

This extracellular release of HMGB1 occurs in two phases. Firstly, hypoacetylated-HMGB1 is passively released from both apoptotic and necrotic cells, which occurs early on during liver injury (Antoine et al. 2009b; Bell et al. 2006; Evankovich et al. 2010; Nystrom et al. 2012). A delayed release of oxidised HMGB1 occurs via release from activated immune cells such as macrophages, which triggers the release of hyperacetylated HMGB1 as an immune response to the injury. Consequently HMGB1 has been investigated as a mechanistic biomarker of liver injury, as it is released into serum post liver injury and the different isoforms distinguish between early and late liver injury and liver regeneration. Research has revealed that levels of HMGB1 are increased in the serum of patients following acetaminophen overdose and concentrations correlate with the extent of necrosis occurring in the liver (Antoine et al. 2012; Antoine et al. 2009b). When compared to ALT analysis, HMGB1 was able to predict the extent of liver injury and likelihood of

survival more accurately and at an earlier time point (Antoine et al. 2013; Antoine et al. 2012; Antoine et al. 2009b). Thus, there is potential for HMGB1 to be used as a clinical serum biomarker to predict the extent of liver injury (Andersson and Rauvala 2011; Yamada and Maruyama 2007).

1.3.3 Novel biomarkers of DILI: Keratin-18

Another protein that has been investigated as a potential biomarker of DILI is keratin 18. Keratins are highly expressed by epithelial cells such as hepatocytes, and are responsible for cell structure and integrity (Ku et al. 2007; Omary et al. 2002). Keratin 18 is specifically expressed by hepatocytes and research has found that the full length protein (fk18) is passively released by necrotic cells, whereas caspase-cleaved keratin 18 (ck18) is released as a result of apoptotic cell death (Biven et al. 2003; Cummings et al. 2006). These proteins have been found to be released into the serum early on during DILI and their levels correlate well with histological data on the extent of injury (Antoine et al. 2009b). Keratin 18 was found to be a more sensitive biomarker of liver injury than ALT (Antoine et al. 2013) and was more accurate at predicting the severity and outcome of DILI, as well as being specifically released from the liver (Antoine et al. 2012). An additional advantage of this protein is the ability to distinguish between different modes of cell death, thus giving mechanistic insight to the type of liver damage occurring, as well as being hepatocyte-specific (Antoine et al. 2009b).

1.3.4 Novel biomarkers of DILI: miR-122

Specific microRNAs (miR) also have potential to act as biomarkers of DILI. miR consist of single stranded non-coding regulatory RNA, which are typically very small

at approximately 20 nucleotides. Some miR have been shown to be stable extracellularly in body fluids such as blood and urine (Szabo and Bala 2013; Zhou et al. 2013). Hence these molecules have the potential to be used as biomarkers of various conditions as their levels correlate with injury occurring from specific origins. miR-122 functions to maintain homeostasis of hepatic cholesterol and lipid metabolism (Castoldi et al. 2011; Krutzfeldt and Stoffel 2006). There is also evidence that miR-122 acts as a tumour suppressor gene (Bai et al. 2009; Kutay et al. 2006). miR-122 was found to be elevated in the serum of patients with various different liver diseases (Cermelli et al. 2011; Xu et al. 2011) and further research revealed miR-122 as a hepatocyte-specific marker of DILI, with levels in plasma correlating well with the extent of liver injury after treatment with various hepatotoxins (Antoine et al. 2013; Harrill et al. 2012; Starkey Lewis et al. 2011; Zhang et al. 2010). miR-122 is released into the bloodstream very early on after initiation of liver injury. When compared to using ALT levels to predict DILI, miR-122 had a higher sensitivity and specificity (Starkey Lewis et al. 2011; Zhang et al. 2010) and moreover was found to be highly enriched in the human liver, therefore acting as a tissue-specific biomarker (Liu et al. 2009; Sempere et al. 2004). As an additional advantage miR-122 is conserved across multiple species, meaning that it could be measured in preclinical *in vivo* models and extrapolated to clinical studies (Chang et al. 2004).

A major caveat with all clinical biomarkers of DILI is that these molecules tend not to be, or have difficulty being, assessed *in vitro*. Only few biomarkers, such as ALT, are analysed in animal studies and show correlations with clinical data (Lea et al. 2016), however the current lack of translatable biomarkers is a problem which needs addressing in order to fully understand the causes and mechanisms of DILI. If clinical DILI biomarkers could be assessed more easily *in vitro*, this may aid the drug screening process and prevent ADR further along in the drug development process.

1.6 Aims and Objectives

The overall aim of this thesis was to create a more representative *in vitro* liver model in order to investigate DILI. In order to achieve this, six objectives were created.

Aim 1: To develop a novel *in vitro* liver spheroid model, optimising key parameters and characterising essential liver-specific structural and morphological components.

In order to investigate DILI an appropriate *in vitro* model, representative of a human liver, is essential. The aim was to overcome some of the numerous disadvantages of current liver models and in turn create a more realistic, human-relevant *in vitro* model. Lack of liver-like structures was identified to be a key downfall of current liver models, alongside the short lifespan, unavailability and large variation of primary liver cells. The plan was to use a 3D cell culture technique with an immortalised liver cell line to create a liver model. Key parameters investigated included viability and lifespan, cellular morphology, 3D structure and proliferation.

Aim 2: To confirm liver-specific functionality in the liver spheroid model and compare this to other liver models.

The second aim was to overcome another major caveat of current *in vitro* liver models: functionality. Liver cell lines are known for their poor representation of human liver function, yet evidence suggests that 3D cell culture could improve upon this. By investigating key liver-specific functions, such as zonation, metabolic activity, synthesis of compounds and bile transport, the project intended to confirm liver-like functioning of the liver spheroid model and compare this to 2D cell cultures.

Aim 3: To investigate the ability of the liver spheroid model to detect human hepatotoxins and compare this to other liver models.

The ability of a liver model to detect hepatotoxicity is the most important determinant of whether the model is appropriate to investigate DILI. Current *in vitro* liver models have poor sensitivity and many hepatotoxic compounds go undetected. Therefore the third aim was to reveal the ability of the liver spheroid model to detect a range of compounds with a risk of DILI. The sensitivity of this spheroid model could then be compared with other 2D and 3D *in vitro* liver models.

Aim 4: To determine whether the inclusion of NPC alters the sensitivity or specificity of the liver spheroid model to hepatotoxins.

The majority of *in vitro* models used to investigate DILI rely solely on hepatocytes or their immortalised alternatives, yet 40 % of the liver is populated by NPC. Previous research indicates that co-culturing hepatocytes with NPC can create a model with more liver-like functionality. How these cells affect sensitivity of a liver model to hepatotoxins, however, has not been elucidated. The fourth aim of this thesis was to create a co-culture spheroid model and investigate how the addition of NPC alters the ability of the liver model to detect hepatotoxicity.

Aim 5: To elucidate whether the measurement of novel biomarkers is possible from the *in vitro* liver spheroid model and if this can provide additional information about the mechanism of hepatotoxicity.

Current clinical diagnostic biomarkers of DILI have weaknesses and research indicates that novel alternatives provide organ-specific and mechanistic information about the injury occurring. Despite this, biomarkers of liver injury are not commonly quantified from *in vitro* liver models. It was investigated whether novel biomarkers of DILI could be quantified from cell-based liver models and whether this could provide additional mechanistic information into the type of cell damage occurring and potentially increase the sensitivity of the liver spheroid model to hepatotoxins.

Aim 6: To confirm whether mitochondrial dysfunction caused by hepatotoxins can be detected in the liver spheroid model.

DILI is thought to occur by an array of different mechanisms and 50 % of hepatotoxins cause injury through mitochondrial dysfunction (Begriche et al. 2011; Boelsterli and Lim 2007). Mitochondria are integral to cell survival, hence the ability to detect mitochondrial liabilities in an *in vitro* model could greatly reduce the number of toxic compounds making it to clinic. The final aim was to determine whether mitochondrial liabilities could be correctly identified in the liver spheroids and whether this may give mechanistic insight into how some common hepatotoxins are causing liver injury.

Chapter 2

Development of a C3A Liver Spheroid Model

Contents

2.1 Introduction

Predictive *in vitro* liver models are essential during initial drug screening in order to conduct an accurate risk assessment leading to better candidate selection early in the drug discovery and development process. Current drug safety screens only detect 60-70 % of hepatotoxins (Xu et al. 2008). The rapid decline in function and viability of human hepatocytes *ex vivo* and inter-donor variability is a major limitation of their use (Donato et al. 2008; Gomez-Lechon et al. 2004; Khetani et al. 2015b; LeCluyse et al. 2005). Furthermore immortalised hepatocarcinoma cell lines, such as HepG2, C3A, Huh7 and HepaRG, demonstrate low functionality and an altered phenotype compared to human hepatocytes *in vivo* (Godoy et al. 2013; Guo et al. 2011; LeCluyse et al. 2012). Hence investigations into developing novel *in vitro* liver models are underway.

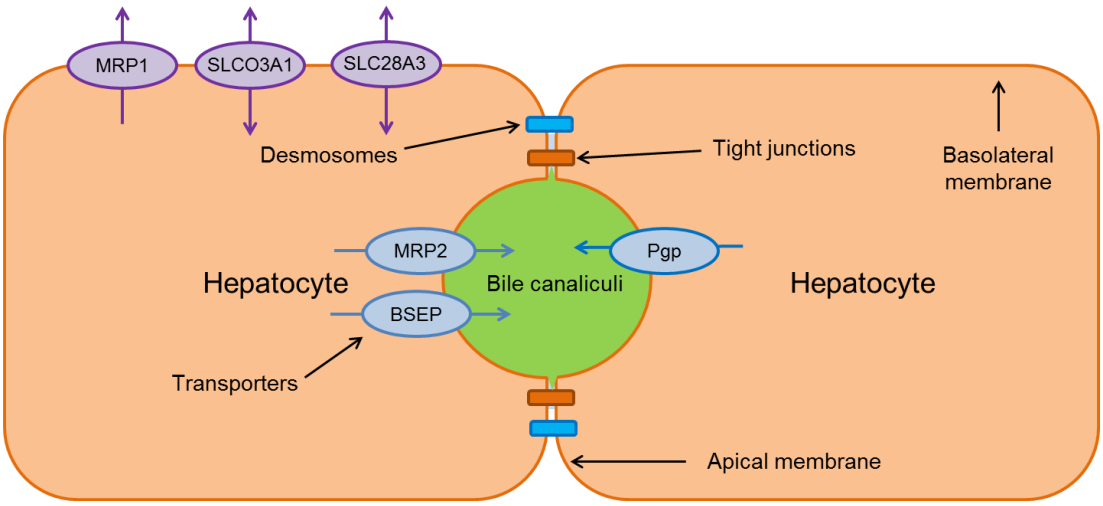

Figure 2.1. Illustration of the polarisation of hepatocytes. Tight junctions and desmosomes form on the apical membrane between adjacent hepatocytes and the membrane of each hepatocyte distorts to form a bile canaliculi structure. Transporters are localised to specific membranes in order for efficient transport. For example MRP1, SLCO3A1 and SLC28A3 are localised to the basolateral membrane whereas MRP2, Pgp and BSEP are expressed on the canalicular membrane and export compounds into the bile.

A key disadvantage of commonly used *in vitro* models is a lack of 3D structure, which has a significant effect on the hepatocyte morphology, function, phenotype, signalling and toxicological response (Gomez-Lechon et al. 1998; Semler et al. 2000; Wells 2008). Figure 2.1 illustrates the polarisation of hepatocytes *in vivo* along with the formation of desmosomes and tight junctions, creating bile canaliculi between the apical membranes and localised expression of hepatic transporters. For example MRP2 and Pgp are transporters localised to the canalicular membrane of hepatocytes and transport organic anions and efflux lipophilic cations from the cell respectively (Esteller 2008). The microenvironment, secondary structures and specific polarisation of hepatocytes is vitally important to their function (Godoy et al. 2013). It is possible that in order to create a more relevant liver model, one must recapitulate these 3D structural characteristics.

A simple, inexpensive and high-throughput method of culturing cells in 3D is by creating spheroids (Friedrich et al. 2009; Godoy et al. 2013; van Zijl and Mikulits 2010; Wong et al. 2011). The use of spheroids as a model for screening of hepatotoxins is fairly novel, in contrast to other areas of research where spheroids are a well-established 3D cell culture technique (van Zijl and Mikulits 2010). Preliminary research into liver spheroids has shown promising results. For instance, hepatocarcinoma cell lines when cultured in 3D spheroids display more liver-like structures and functions than monolayer cultures (Chang and Hughes-Fulford 2009; Fey and Wrzesinski 2012; Mueller et al. 2011; Sainz et al. 2009; Takahashi et al. 2015). C3A cells are a subclone of HepG2 cells selected for their strong contact-inhibited growth characteristics, as well as high-albumin production and transferrin synthesis and are able to grow in glucose deficient media (Nibourg et al. 2012). This cell line may therefore have advantages over other hepatocarcinoma cells when cultured in spheroids, with their reduced proliferation rate which is more representative of the *in vivo* situation and potentially allowing the cells to be cultured

for longer periods (Wrzesinski et al. 2013). Previous studies of C3A spheroids have revealed superior function over 2D cultures, including increased cholesterol and urea release, as well as glycogen synthesis (Fey and Wrzesinski 2012; Wrzesinski and Fey 2013; Wrzesinski et al. 2013). Despite the increasing interest and use of 3D liver models, little research has gone into determining the most reliable method of spheroid formation and culture, as well as optimisation of key parameters such as spheroid size, proliferation, viability, cellular morphology and internal structure (Asthana and Kisaalita 2012; Curcio et al. 2007; Olive et al. 1992). Additionally, further investigation into the liver-specific functionality and sensitivity of this model is necessary before it can be considered for drug screening purposes.

The aim of this work was to develop and optimise a liver spheroid model and perform an initial characterisation. C3A cells were chosen in order to create spheroids with the advantages of being human derived, easy to obtain and culture, little variability and reduced proliferation rate once in 3D. Scaffold-free techniques were adopted to create spheroids for their ease, reproducibility, high-throughput nature and to avoid the detrimental effects of scaffolds or ECM.

Hypothesis 1: C3A cells cultured in 3D spheroids would be viable for a prolonged period of time, with a reduced proliferation rate.

Hypothesis 2: C3A spheroids will display a more *in vivo*-like internal structure including 3D morphology, direct cell-cell contacts and polarisation characteristics leading to an overall increased likeness to human liver tissue.

2.2 Materials and Methods

Agarose type V high gelling temperature (A3768), agarose low electroendosmosis (EEO) (A9539), fetal bovine serum (FBS), penicillin-streptomycin, 1 x phosphate buffered saline (PBS), paraformaldehyde (PFA), Triton X-100, Tween20, Tris, bovine serum albumin (BSA), DMSO, doxorubicin were purchased from Sigma Aldrich, Missouri, USA. C3A cells and Eagle's minimal essential medium (EMEM) were purchased from LGC standards, Middlesex, UK. Ultra-Low Adherence (ULA) plates were purchased from Corning, NY, USA. Cell Titer-Glo assay was purchased from Promega, Madison, USA. MRP2 (ab3373), MRP1 (ab24102), SLC22A3, SLC03A1 and Pgp (ab8189) antibodies were purchased from Abcam, Cambridge, UK. Prolong Gold (P36930), Hoechst (H3570) and Alexa Fluor 568 phalloidin (A12380) were purchased from Life Technologies, Carlsbad, CA, USA. Alexa Fluor 488 Donkey Anti-Mouse (R37114) was purchased from Invitrogen, Carlsbad, CA, USA. M65 and M30 ELISA kits were purchased from Peviva, Stockholm, Sweden. BSEP antibody was purchased from ThermoFisher Scientific, MA, USA.

2.2.1 Spheroid formation and cell culture

C3A cells were maintained in EMEM supplemented with 10 % FBS and 1 % penicillin-streptomycin under standard cell culture conditions. C3A cells were used between passage 5 and 15 for all experiments. C3A cells were not mycoplasma tested or characterised before use. For 2D monolayer experiments 40,000 C3A cells/well were seeded, left to adhere for 24 hours and confirmed to be 100 % confluent before analysis.

Spheroids were created using two techniques, the liquid-overlay technique (LOT) and ULA plates. The LOT was performed as previously described (Yuhas et al., 1977). 100 µL of molten sterile 1.5 % Agarose (high gelling temperature) dissolved in EMEM was added per well to flat-bottomed 96-well cell culture plates and left to

set to form a low-adherence surface (Figure 2.2). C3A cells were seeded onto either LOT or ULA plates at different cell densities (500 - 2500 cells/well) in 100 µL media, centrifuged for 5 min at 1000 rpm and left for 72 hours to form spheroids. The outer 36 wells of the plate were not used due to inconsistencies occurring from differences in oxygen and humidity (Figure 2.3). 50 % of the media was renewed twice weekly and spheroids were cultured for up to 32 days. Cell numbers were counted by trypsining cells in spheroids (pool of 3 spheroids) and counting cell

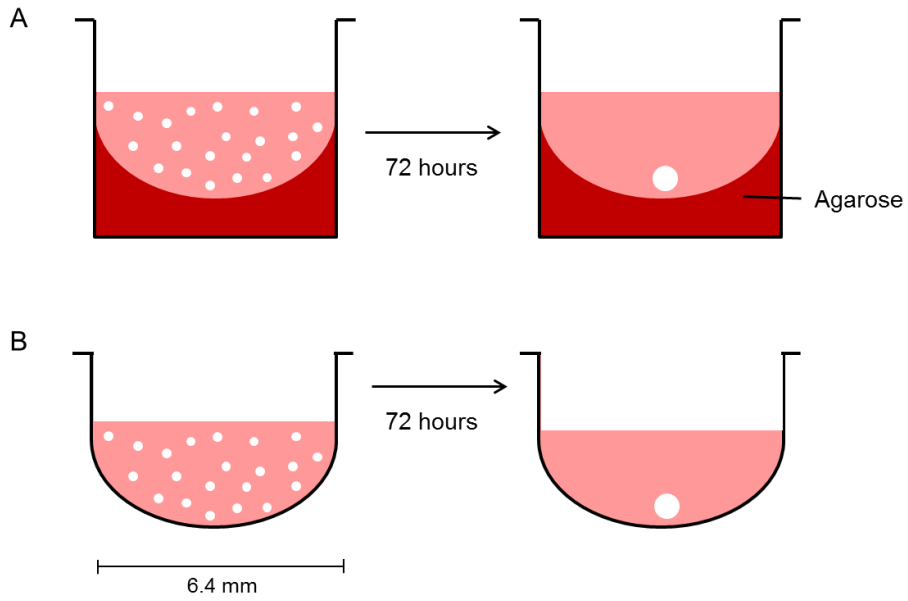

number using a haemocytometer.

Figure 2.2. Illustration of spheroid formation using the LOT and ULA plates. Both (**A**) the LOT and (**B**) ULA plates were investigated. For the LOT agarose was added to each well of a flat-bottom 96-well plate and left to set.

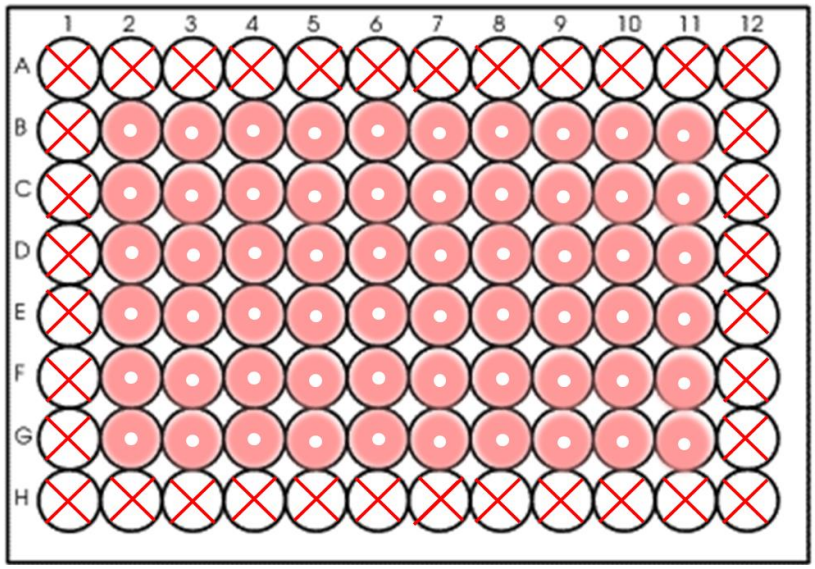

Figure 2.3. Spheroid and cell culture plate layout. When culturing spheroids or cells in monolayer on 96-well plates, only the inner 60 wells were used, as the outer 36 wells has inconsistencies in spheroid formation and cell density.

2.2.2 Phase contrast microscopy to measure spheroid morphology and diameter

Spheroid diameter and morphology was analysed by light microscopy using a phase-contrast microscope (ECLIPSE TS100/100-F, Nikon). Photographs were captured using a digital camera head (DS-Vi1, Nikon) and a stand-alone controller and display unit (DS-L3, Nikon). Spheroid diameter was measured from these images (n=9) (where not symmetrical the maximum diameter was measured).

2.2.3 Histological analysis for the analysis of cell morphology and proliferation.

Spheroids were washed in PBS, fixed for 1 hour in 4 % PFA and embedded in 2 % Agarose (low EEO) in 4 % PFA then paraffin embedded. Tissue sections were cut and stained with haematoxylin and eosin (H&E) or immunostained for Ki-67 as previously described (Colley et al., 2011). Briefly tissue sections had wax removed

with Histoclear, were hydrated in decreasing concentrations of ethanol, stained with haematoxylin, then eosin and next dehydrated in increasing concentrations of ethanol and cleared using Histoclear. Immunostaining for Ki-67 was carried out by Julie Haigh at the Department of Veterinary Pathology, Leahurst Campus, University of Liverpool, UK.

2.2.5 Keratin 18 cell death quantification by ELISA

Total keratin 18 and ck18 in pooled spheroid supernatant (10 wells) were quantified using M65 and M30 ELISA kits respectively, according to the manufacturer's protocol. All incubations were performed at room temperature (RT). Samples were diluted as appropriate and 25 µL of standard and sample added to the pre-coated ELISA plate, followed by 75 µL M65 or M30 conjugate and incubated on a plate shaker at 60 rpm for 2 or 4 hours respectively. The wells were washed 5 times with 250 µL Wash Buffer and incubated for 20 min with 200 µL TMB substrate in the dark. 50 µL stop solution was added, the plate shaken for 10 seconds, then after 5 min the absorbance read at 450 nm using a microplate reader (Thermo Scientific Varioskan Flash). Apoptotic cell death was represented by the ck18 concentration, total cell death represented by total keratin 18, and necrotic cell death calculated from the total cell death minus apoptotic cell death.

2.2.6 Transmission electron microscopy

Spheroids were pooled (10 wells) and fixed at day 10 of culture and processed for electron microscopy (EM). Transmission EM was performed by Alison J Beckett, Biomedical EM Unit, School of Biomedical Sciences, University of Liverpool and images taken using FEI Tecnai G2 Spirit 120KV bioTWIN.

2.2.7 Immunofluorescent analysis of spheroids

Spheroids were transferred to ULA plates, washed three times in PBS and fixed with 4 % PFA for 1 hour at 4 °C. Spheroids were washed again then permeabilized with 0.5 % Triton X-100 in Tris-Buffered Saline with 0.05 % Tween20 (TBST) overnight at 4 °C and next blocked with 0.1 % Triton X-100/3% BSA in TBST for 2 hours at RT. Primary antibody diluted in 0.1 % Triton X-100 /1 % BSA in TBST were then incubated with the spheroids overnight at 4 °C. Multidrug resistance protein-2 (MRP2) and P-glycoprotein (Pgp) antibodies were used at a 1:20 dilution. Other transporters MRP1, BSEP, SLCO3A1 and SLC28A3 were analysed, but could not be optimised for use with spheroids. Spheroids underwent three 1 hour washes with 1 % Triton X-100 in TBST then incubated with secondary Alexa Fluor 488 Donkey Anti-Mouse antibody diluted at 1:1000, Hoechst diluted at 1:5000 and phalloidin diluted at 1:250 in 0.1 % Triton X-100 /1 % BSA in TBST overnight at 4 °C. Spheroids were washed for 1 hour and finally mounted with Prolong Gold onto a glass microscope slide. Maximum intensity projection images of spheroids were taken on Zeiss microscope using 40 × oil objective.

2.2.8 Immunofluorescent analysis of 2D monolayers

Cells were washed in PBS for 30 min at 4 °C then fixed with 2 % PFA for 30 min at 4 °C. Cells were permeabilized with two 15 min washes in 0.2 % Tween-20/ 0.5 % Triton X-100 in PBS at 4 °C and blocked for 30 min in 5 % BSA/ 0.2 % Tween-20/ 0.5 % Triton X-100 in PBS at RT. The primary antibody was diluted in 5 % BSA/ 0.2 % Tween-20/ 0.5 % Triton X-100 in PBS and incubated with cells overnight at 4 °C. Cells underwent three 15 min washes in 0.2 % Tween-20/ 0.5 % Triton X-100 in PBS then incubated with secondary Alexa Fluor 488 Donkey Anti-Mouse antibody diluted at 1:1000, Hoechst diluted at 1:5000 and phalloidin at diluted 1:250 in 5 % BSA/ 0.2 % Tween-20/ 0.5 % Triton X-100 in PBS for 1 hour at RT. Cells underwent

three 15 min washes in PBS and finally were mounted with Prolong gold onto a glass microscope slide. Images were taken on Zeiss microscope using 40 × magnification with oil objective.

2.2.9 Statistical analysis

Data are representative of at least three independent experiments (n=3) and expressed as mean ± SEM. Graphs and statistical analyses were performed using GraphPad Prism 5. A Shapiro-Wilk normality test was performed on all data sets. Data which passed normality tests underwent analysis by a two-way ANOVA, those which did not underwent a non-parametric Kruskal-Wallis test. Significance was determined from a p value < 0.05. **** p<0.0001, *** p< 0.001 ** p<0.01, * p< 0.05.

2.3 Results

2.3.1 Comparison of spheroid formation techniques

C3A cells with a seeding density of 2500 cells/well successfully created spheroids using both the LOT and ULA plates, with the cells in each well aggregating to form a single spheroid (see Figure 2.2).

Spheroids created by LOT were generally more spherical and uniform in shape compared to those created on ULA plates which had a more irregular structure with a less defined outer perimeter throughout the culture period (Figure 2.4A). The diameter of the spheroids gradually increased over the culture period of 25 days, with very similar growth curves from both techniques (Figure 2.4B). Due to a more consistent, spherical morphology all further spheroids were generated using the LOT.

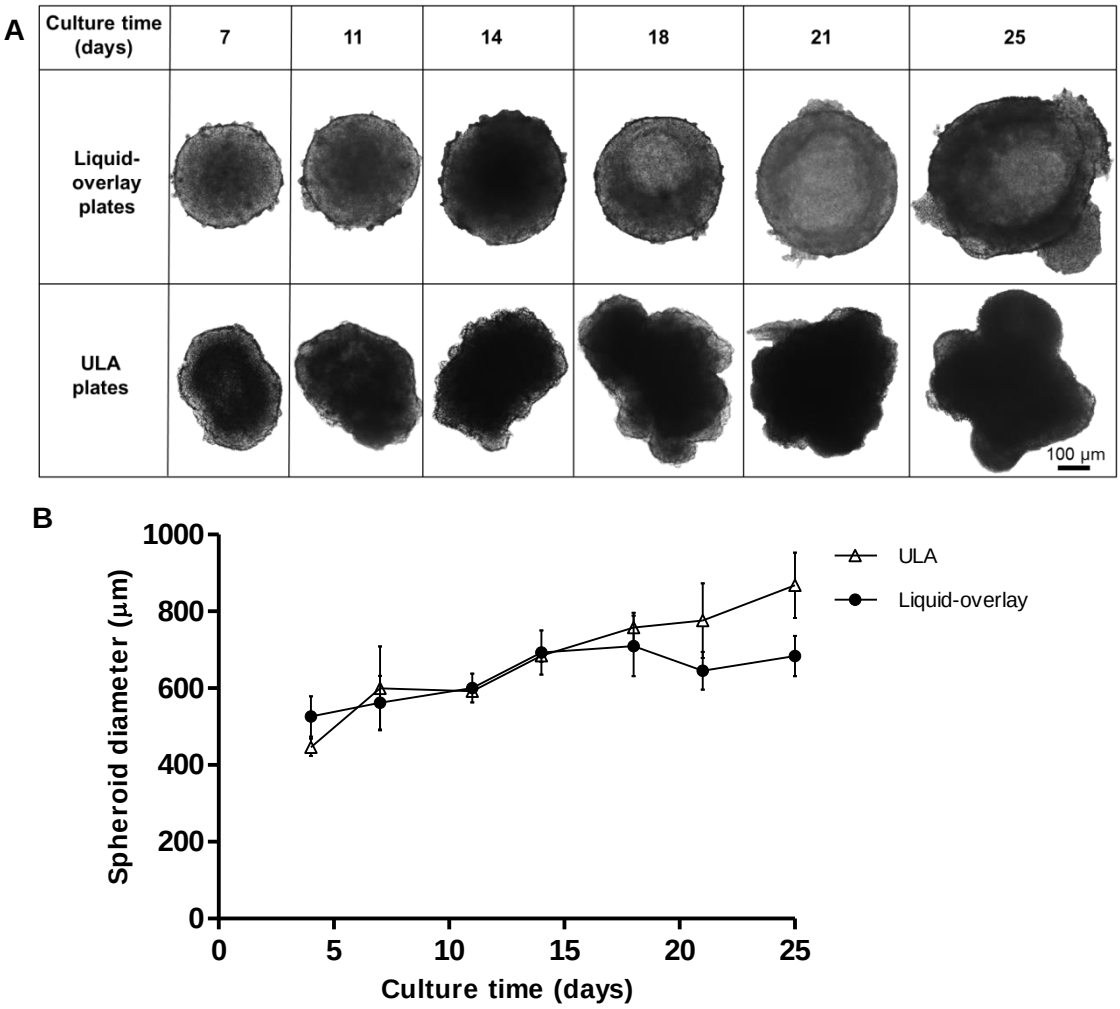

Figure 2.4. Comparison of spheroid formation techniques. (**A**) Phase-contrast images of representative spheroids cultured from 2500 cells on LOT or ULA plates over 25 days. Scale bar = 100 µm. (**B**) Growth curve of spheroids cultured by liquid-overlay technique (black circle) or ULA plates (clear triangle). Spheroid diameter (µm) was plotted against culture time (days). Data are represented as mean ± SEM (n=3 in triplicate).

2.3.2 Optimisation of spheroid starting cell number

Next, the effect of different starting cell numbers on spheroid formation, size and shape over time was investigated. Spheroids were formed by LOT from 500, 750, 1000, 1500, 2000 or 2500 C3A cells and cultured for 32 days. Brightfield microscopy was used to measure spheroid diameter and morphology every 2-3 days (Figure 2.5A). Spheroid size versus time for each cell number is plotted in Figure 2.5B.

All starting cell numbers resulted in the formation of spheroids with varying sizes and morphology. Spheroids created from 500 cells gradually increased in diameter over 32 days from 237.0 ± 14.3 µm to 432.9 ± 111.4 µm in diameter, however these spheroids were less uniform and less stable in shape, resulting in disaggregation of some cells (Figure 2.5A and 2.5B). Spheroids with a starting cell number of 750 or 1000 cells steadily grew over 32 days, starting with a diameter of 289.4 ± 26.5 µm and 343.2 ± 73.3 µm at day 4 and increasing to 407.7 ± 92.3 µm and 539.5 ± 39.5 µm at day 32 respectively, and maintained a uniform spherical shape over the course of the culture. Spheroids created from higher starting cell numbers, 1500, 2000 or 2500 cells, increased in size more rapidly, reaching much larger diameters of 624.5 ± 59.5 µm, 730.0 ± 112.0 µm and 759.1 ± 83.5 µm, as well as becoming irregular in shape (Figure 2.5A and 2.5B). From this data, 750 to 1000 cells was determined to be an optimal range of cell number, as these spheroids remained uniform in shape over the 32 days, with little variation in post establishment size and the smallest diameter. However 2500 cell spheroids have also been subsequently used in the analysis as a comparison.

Next, cell numbers were counted in the optimised 1000 cell spheroids over 32 days (Figure 2.6). Cell number can be seen to increase over time, with a typical sigmoidal pattern, reaching a plateau around day 21 of culture, indicating reduced

proliferation and senescence. The 1000 cell spheroids reached a maximum of just over 60,000 cells at the end of the culture period.

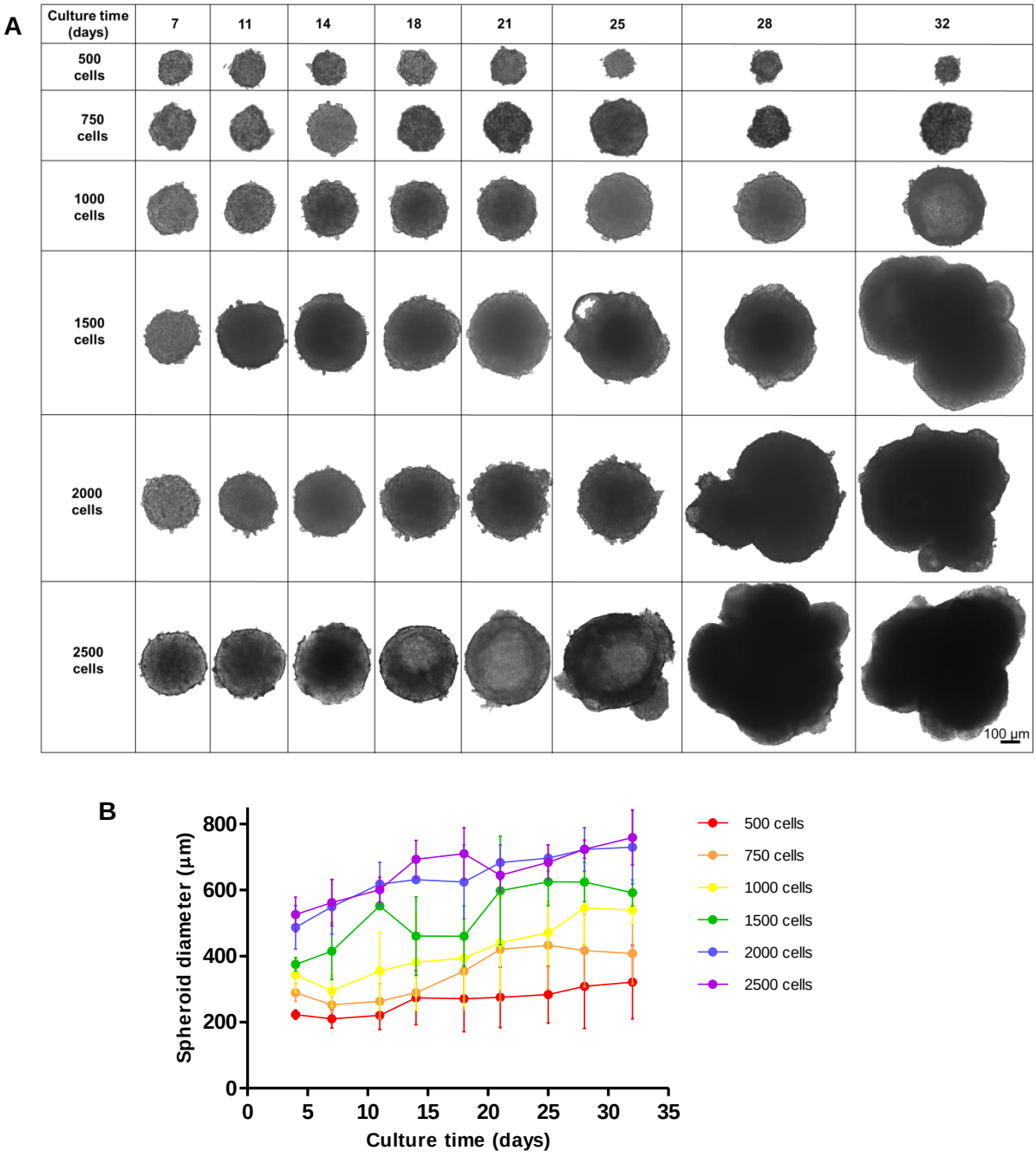

Figure 2.5. Effect of starting cell number on spheroid size and morphology. Spheroids were created from 500, 750, 1000, 1500, 2000 and 2500 C3A cells and cultured for 32 days. (**A**) Phase-contrast images of representative spheroids, images taken at day 7, 11, 14, 18, 21, 25, 28, 32. Scale bar = 100 µm. (**B**) Growth curve of spheroids over 32 days. Spheroid diameter (µm) was plotted against culture time (days). Data are represented as mean ± SEM (n=3 from 5 repeats).

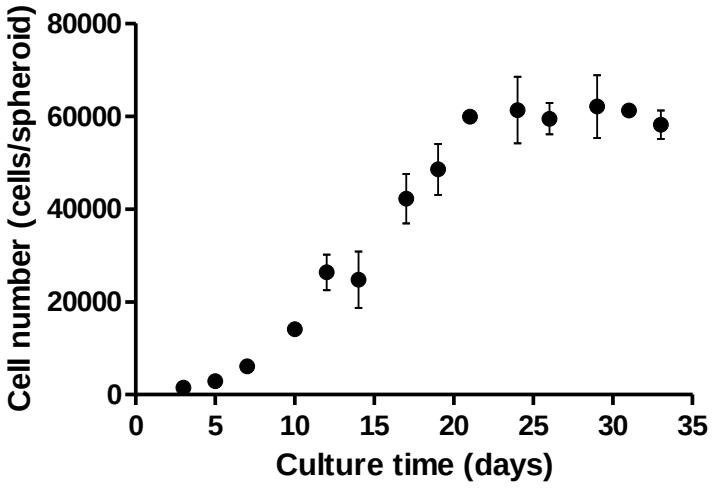

Figure 2.6. Spheroid cell count. Spheroids were created from 1000 C3A cells and cultured for 32 days and cell number counted per spheroid. Spheroid cell number is plotted against culture time (days). Data are represented as mean ± SEM (n=3 in triplicate).

2.3.3 Internal spheroid structure

In order to analyse the internal structure of the C3A spheroids and to visualise cell morphology and arrangement over 32 days, H&E staining was performed (Figure 2.7). Staining of spheroids with a starting cell number 750 cells revealed a compact, uniform structure, with a defined outer perimeter (Figure 2.7). Cells within these spheroids had a cuboidal 3D morphology with direct cell-cell contacts, as seen in the liver *in vivo* (Krishna 2013). Correlating with cell growth data (Figure 2.5), the 750 cell spheroids are seen to increase in size and stay uniformly spherical throughout the culture period with only very small amounts of apoptosis visible on the H&E staining at later stages of culture past day 18. On the other hand in the larger 2500 cell spheroids small patches of cell death started to occur around day 14 and, by day 18, a necrotic core had formed. Additionally, by day 25 the 2500 cell spheroids became misshapen and their growth started to rapidly increase, resulting in the spheroids disaggregating and losing structural integrity (Figure 2.7).

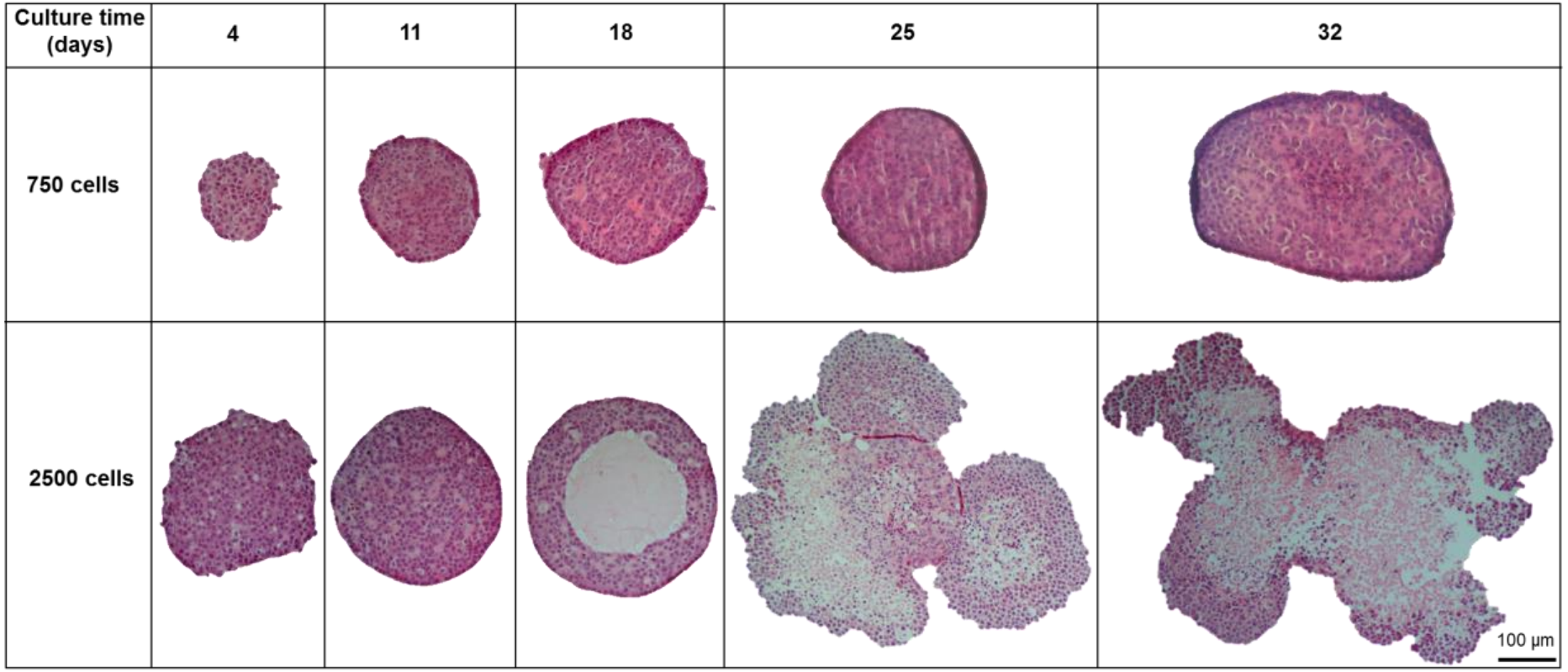

Figure 2.7. Spheroid internal structure and morphology. Spheroids were created by LOT from 750 or 2500 C3A cells and fixed at day 4, 11, 18, 25 and 32 of culture, paraffin embedded, sectioned and stained with H&E. Images represent mid-sections through the spheroids. Scale bar = 100 µm.

EM was performed and cell microstructures analysed. Figure 2.8 A-C shows images taken throughout the spheroids. Spheroids were observed to be viable, with a defined cell membrane and numerous mitochondria, an intact nuclear membrane and Golgi. It is clear that the cells are in a 3D morphology and numerous direct cell-cell contacts were visible. Overall the cell morphology was comparable to that of liver tissue (Figure 2.8 D and E). It was also possible to identify multiple bile canalicular structures throughout the spheroids (Figure 2.8 C), which can be confirmed by the formation of tight junctions and desmosomes at either end of a deformation in the cell membrane between adjacent cells (Farquhar and Palade 1963), as schematically illustrated in Figure 2.1.

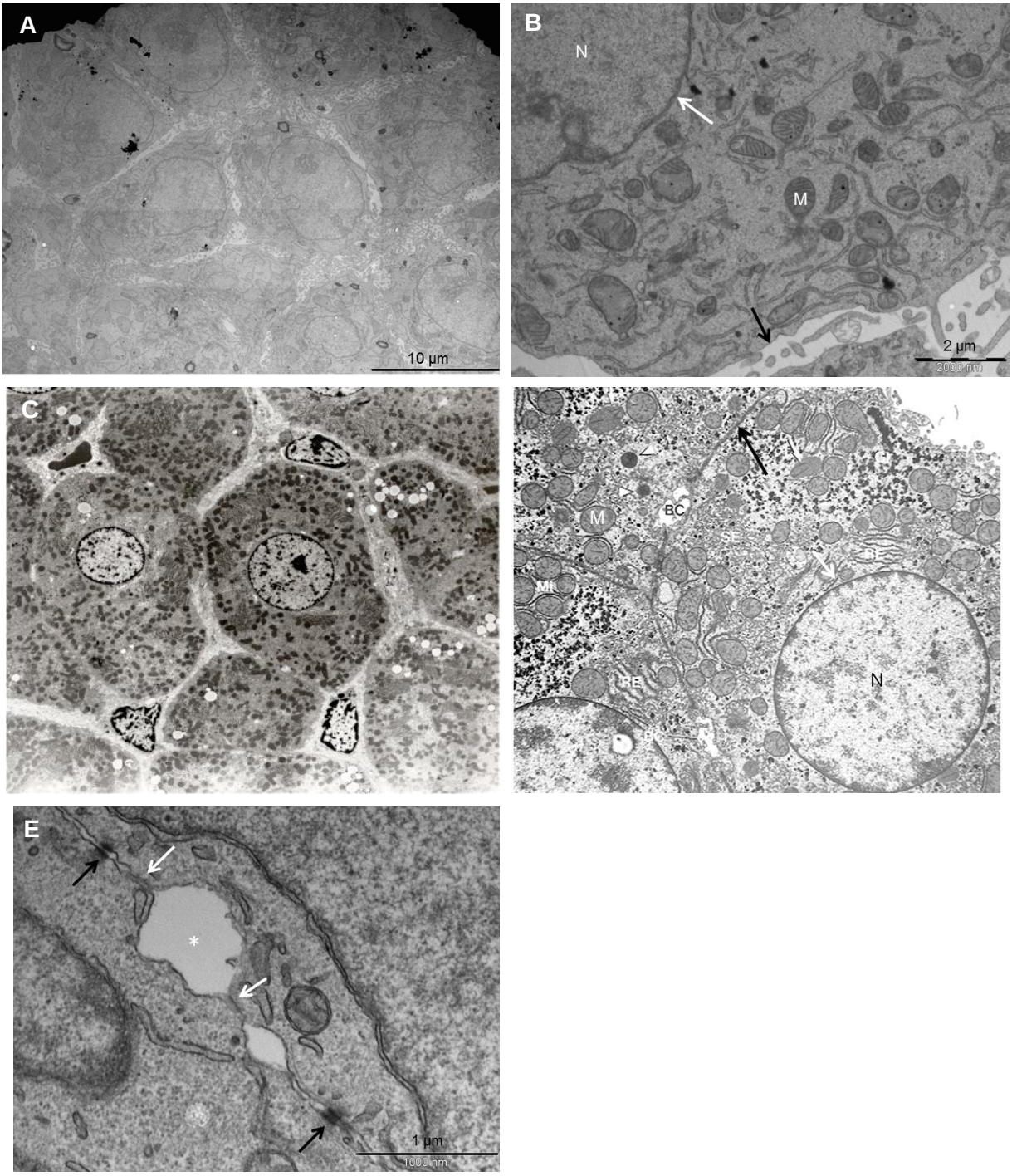

Figure 2.8. Electron microscopy of C3A spheroids. Spheroids were created by LOT and for transmission electron microscopy. (**A**) shows a section of a typical C3A spheroid and (**B**) at a higher magnification, indicating the nucleus (N), mitochondria (M), nuclear membrane (white arrow) and plasma membrane (black arrow). (**C**) and (**D**) are images of human liver tissue for comparison taken from (Dutkowski et al. 2006) and Dr R C Wagner, University of Delaware. (**E**) shows an example of the formation of bile canalicular structures (star) indicated by a space between adjacent cells connected by desmosomes (black arrow) and tight junctions (white arrow) at either end. Images of spheroid were taken using an electron microscope. Scale bars = 10 µm, 2 µm and 1 µm respectively.

2.3.4 Cell death analysis in spheroids

The release of cell death biomarkers was quantified from spheroids of different sizes (Figure 2.9). Keratin 18 was analysed to distinguish between apoptotic and necrotic cell death in the spheroids. It was revealed that significantly higher levels of necrosis in the larger 2500 cell spheroids compared to the 1000 cell controls. 3485.5 ± 133.1 U/L of necrotic keratin 18 was detected in spheroids created from 2500 cells and cultured for 24 days, whereas over 10 times less, 243.7 ± 80.9 U/L, was detected in 1000 cell spheroids cultured for 10 days. There was however no significant difference in the levels of apoptosis in the different culture conditions, staying in the range 241.3 to 945.8 U/L (Figure 2.9A). In addition to this, necrosis appears to be the leading mechanism of cell death in the larger and older spheroids, supporting the histology data which appears to show a necrotic core only in the larger 2500 cell spheroids (Figure 2.7, bottom row). The amount of cell death was also compared against the corresponding spheroid diameter for each culture condition (Figure 2.9B). Necrosis was observed to significantly increase once spheroids reach a critical diameter of around 700 µm, correlating with histology which shows necrotic core formation once spheroids reach 700 µm. Extending the culture time to 24 days increased necrosis further in the larger spheroids (Figure 2.9B).

Next the cumulative basal levels of cell death in 1000 cell spheroids were determined over a culture period of 33 days (Figure 2.10). The levels of apoptotic and necrotic biomarker release did not change significantly over a 32 day period. Slightly higher levels of necrosis were detected at day 3 of culture 0.27 ± 0.19 U/L/cell, with apoptosis at 0.063 ± 0.007 U/L/cell. For the remainder of the culture period the levels of necrosis decreased and apoptosis increased until day 33 at 0.21 ± 0.05 U/L/cell and 0.06 ± 0.05 U/L/cell respectively.

A

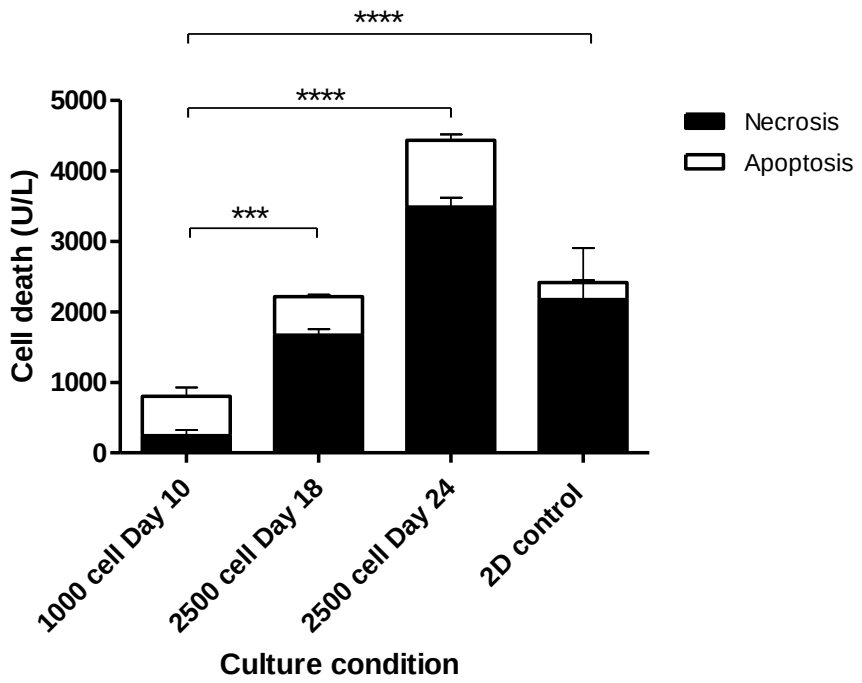

B

Culture condition	Spheroid diameter (µm)	Apoptosis (U/L)	Necrosis (U/L)	Total cell death (U/L)
1000 cell Day 10	354.9	557.3	243.7	801.0
2500 cell Day 18	709.89	545.6	1667.7 ***	2213.3
2500 cell Day 24	683.86	945.8	3485.5 ****	4431.3
2D control 24 hr	-	241.3	2174.4 ****	2415.7

Figure 2.9. Comparison of basal cell death in spheroids of different sizes. Biomarkers of apoptosis (ck18) and total cell death (total keratin 18) were analysed by ELISA in supernatants of spheroids of different sizes and culture times, and compared to a 2D monolayer control. (A) Total cell death (U/L), split into apoptotic (white) and necrotic (black) are plotted against culture condition; (B) Table showing cell death values obtained compared to culture condition and corresponding spheroid diameter (µm) Data are represented as mean ± SEM (n=3 using 20 replicates). **** $p<0.0001$, *** $p< 0.001$ for necrotic keratin 18 compared to 1000 cell day 10.

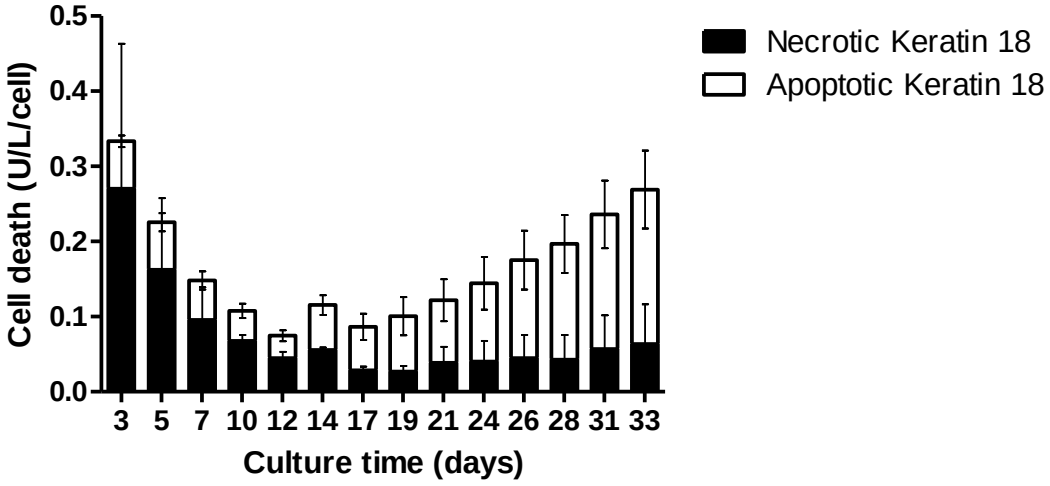

Figure 2.10. Keratin 18 release from spheroids over time. Biomarkers of apoptosis (cleaved keratin 18) and total cell death (full-length keratin 18) were analysed in supernatants of spheroids over a 33 day culture period. Total cell death, split into apoptotic (white) and necrotic (black) are plotted against culture condition. Data are represented as mean ± SEM (n=3 using 20 replicates).

2.3.5 Spheroid proliferation rate

Proliferation of the cells in the spheroids was analysed over the first 18 days of culture using Ki-67 staining in spheroids created from 750 or 2500 cells. Nuclei stain blue with haematoxylin and proliferating cells appear brown, stained with Ki-67. A reduction in the amount of proliferating cells can be seen in Figure 2.11A, with those that are proliferating mainly located to the periphery of the spheroids. At day 4, 59.50 ± 3.5 % and 50.60 ± 2.3 % of the cells in the spheroids were proliferating for spheroids created from 750 and 2500 cells respectively (Figure 2.11B). At day 11 significantly less proliferation was occurring and after 18 days in culture only 32.43 ± 6.1 % and 7.40 ± 1.3 % of cells were proliferating in 750 and 2500 cell spheroids respectively (Figure 2.11B). This correlates with the cell number data in Figure 2.6, as cells initially have a higher proliferation rate as cell number rapidly increases, this then decreases by around day 18 as the cell number levels off and proliferation rate decreases.

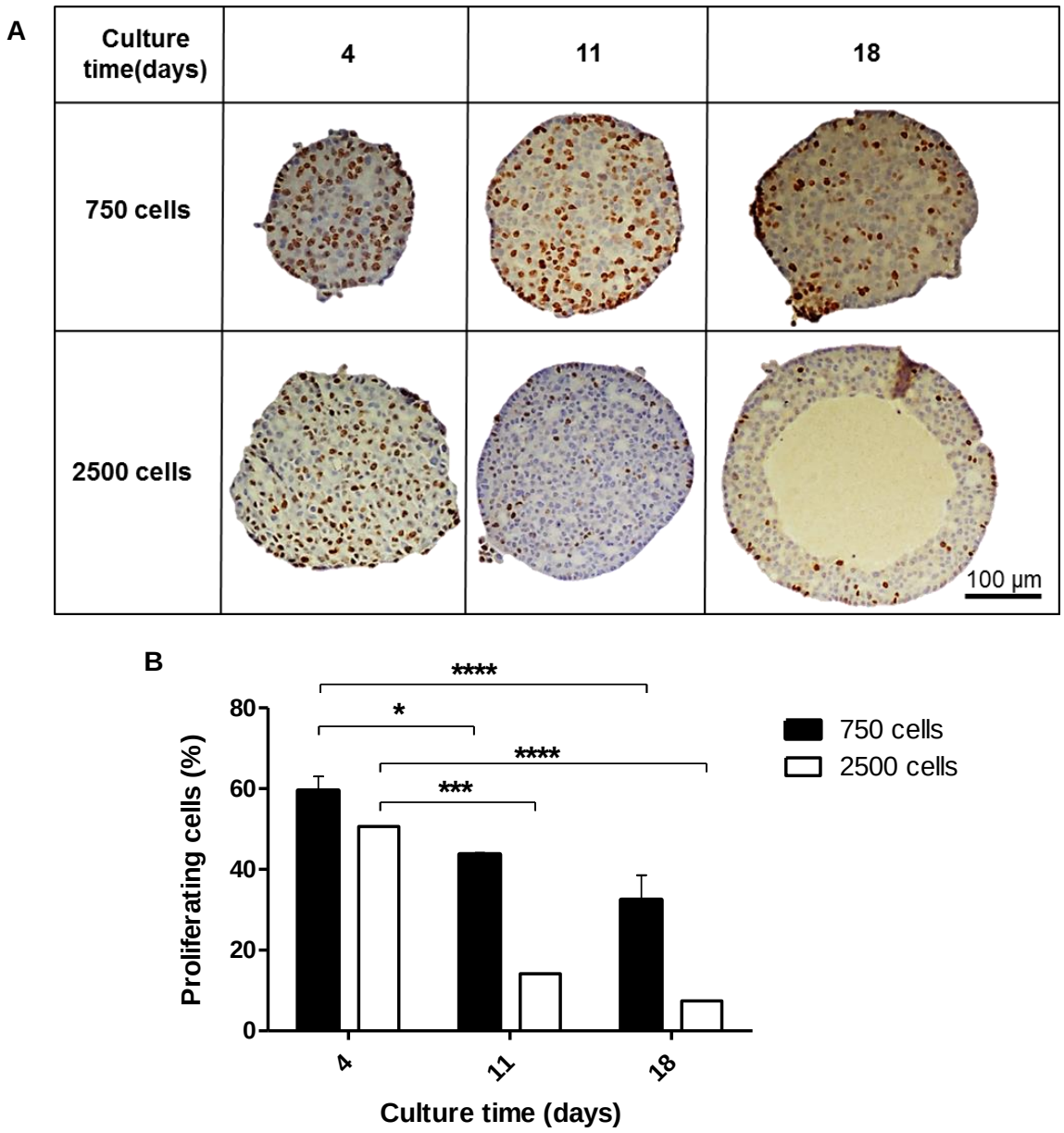

Figure 2.11. Proliferation of cells within the spheroids. Spheroids were created by LOT from 750 or 2500 C3A cells and fixed at day 4, 11 and 18 of culture, paraffin embedded, sectioned and stained with ki67 (brown) to stain proliferating cells, and haematoxylin (blue) to stain the nuclei. (A) Images of spheroid mid-sections. Scale bar =100 µm; (B) Graph showing proliferating cells (%) plotted against culture time (days). Data are represented as mean ± SEM (n=3), **** p<0.0001, *** p< 0.001, * p<0.05 compared to day 4.

2.3.6 Polarisation of C3A cells in spheroids

One of the key features of hepatocytes is their ability to polarise. This involves the formation of bile canaliculi between adjacent cells, as well as the polarisation of key transporters to either the apical or basolateral membranes (see Figure 2.1 for schematic) (Gissen and Arias 2015; Godoy et al. 2013). Immunofluorescence was used to analyse the internal structure of the spheroids over time. Spheroids were fixed and stained with Hoechst (blue) to stain the nuclei and phalloidin (red) to visualise F-actin structures, then imaged by confocal microscopy (Figure 2.12). After 4 days in culture, actin filaments were observed forming between cells within the spheroid (Figure 2.12A). After 11 days in culture, these actin structures could be seen joining together to create an interconnected network of secondary structures throughout the spheroid (Figure 2.12B).

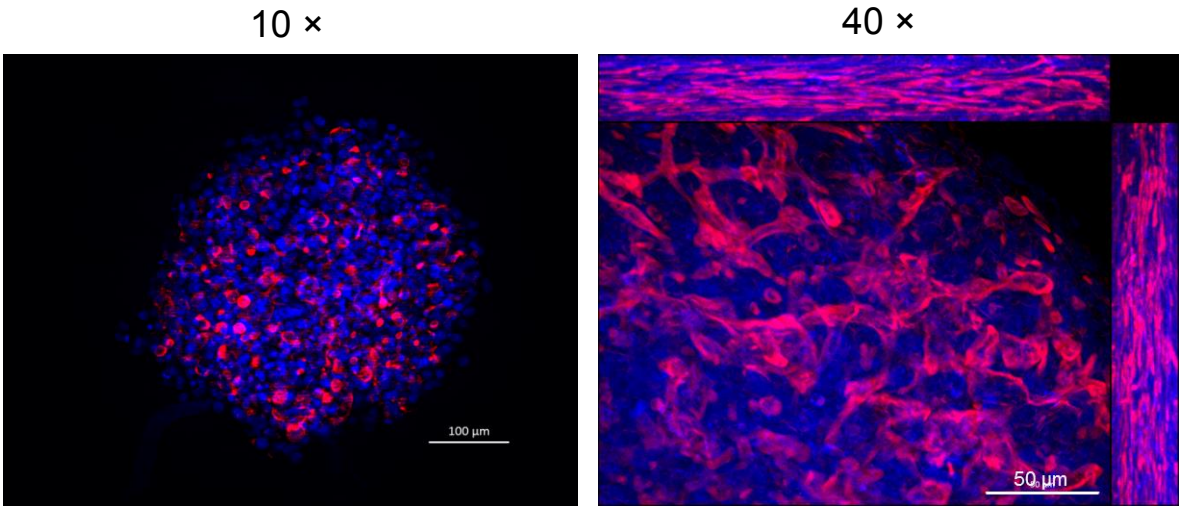

Figure 2.12. Secondary structure formation in spheroids. Spheroids were cultured by LOT, fixed and stained with Hoechst (blue) to stain the nuclei and phalloidin (red) to stain F-actin. Maximum intensity projection images were taken using a Zeiss Axio Observer microscope at 10 × (4 day old spheroids) and 40 × (11 day old spheroids) magnification respectively. Scale bars = 100 µm and 50 µm respectively.

The expression of MRP2 and Pgp transporters was used to confirm whether the actin structures observed were the result of cellular polarisation and the formation of bile canaliculi, and whether or not culture time or spheroid size affected this process. Spheroids of different starting cell numbers were analysed over 18 days for MRP2 and Pgp expression. Figure 2.13 shows the expression of MRP2 and Figure 2.14 the expression of Pgp in spheroids created from 750, 1500 or 2000 cells. The staining pattern of these transporters emulated the F-actin structures seen previously (Figure 2.12). The secondary structures could be seen forming after 4 days of culture regardless of the starting cell number, and appeared to elongate and join together over time, forming an interconnected network of canalicular-like structures (Figure 2.13 and 2.14). The same staining pattern for MRP2 and Pgp were not observed in the corresponding 2D monolayer culture (Figure 2.13 and 2.14, bottom row).

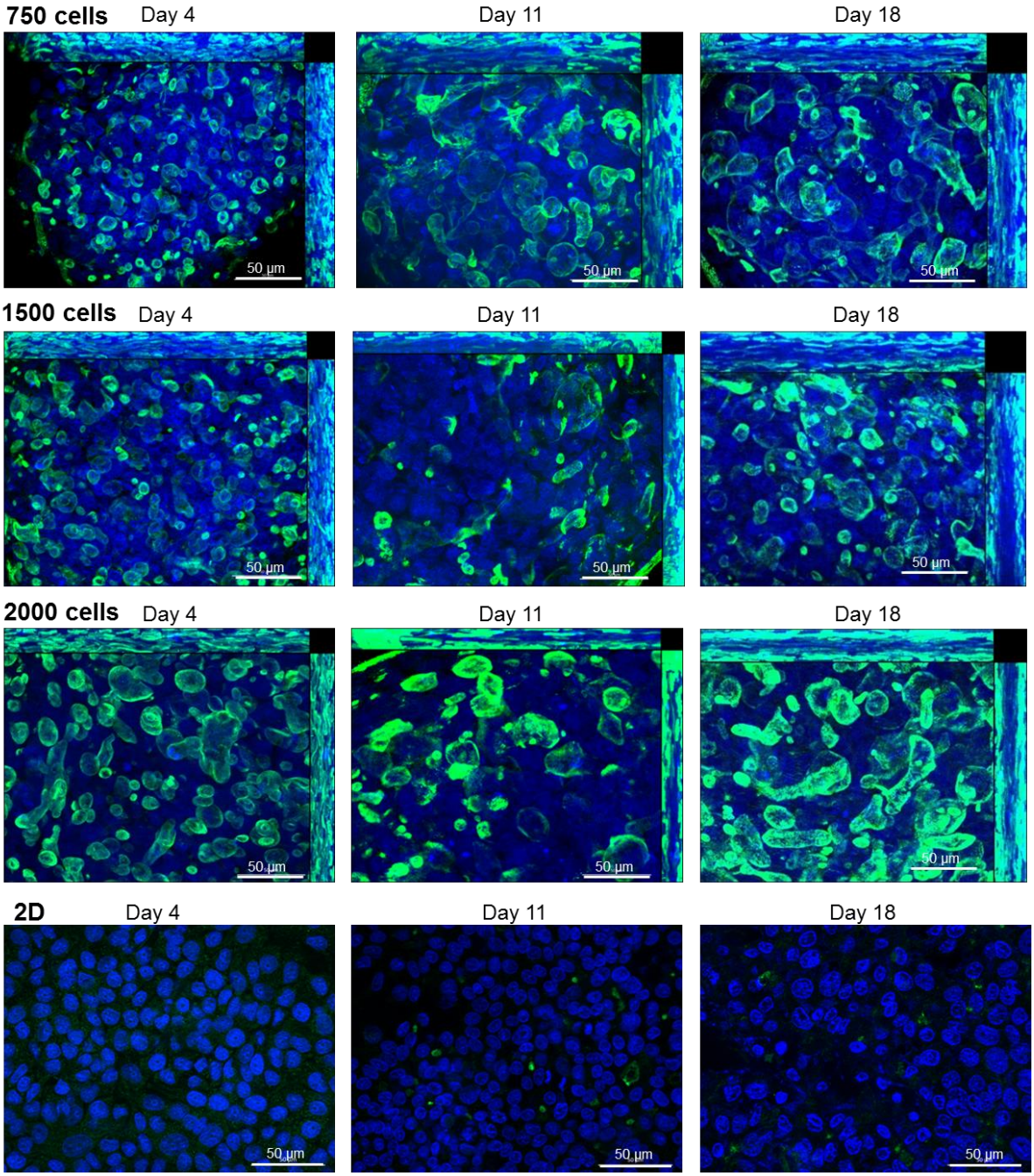

Figure 2.13. MRP2 transporter location in spheroids. Spheroids were created from 750, 1500, 2000 C3A cells by LOT or C3A cells were cultured in a 2D monolayer and fixed at day 4, 11 and 18 of culture. Immunofluorescent staining was performed for the canalicular transporter MRP2 (green) and Hoechst (blue) to stain the nuclei. Maximum intensity projection images were taken using a Zeiss Axio Observer microscope at 40 × magnification. Scale bars = 50 µm.

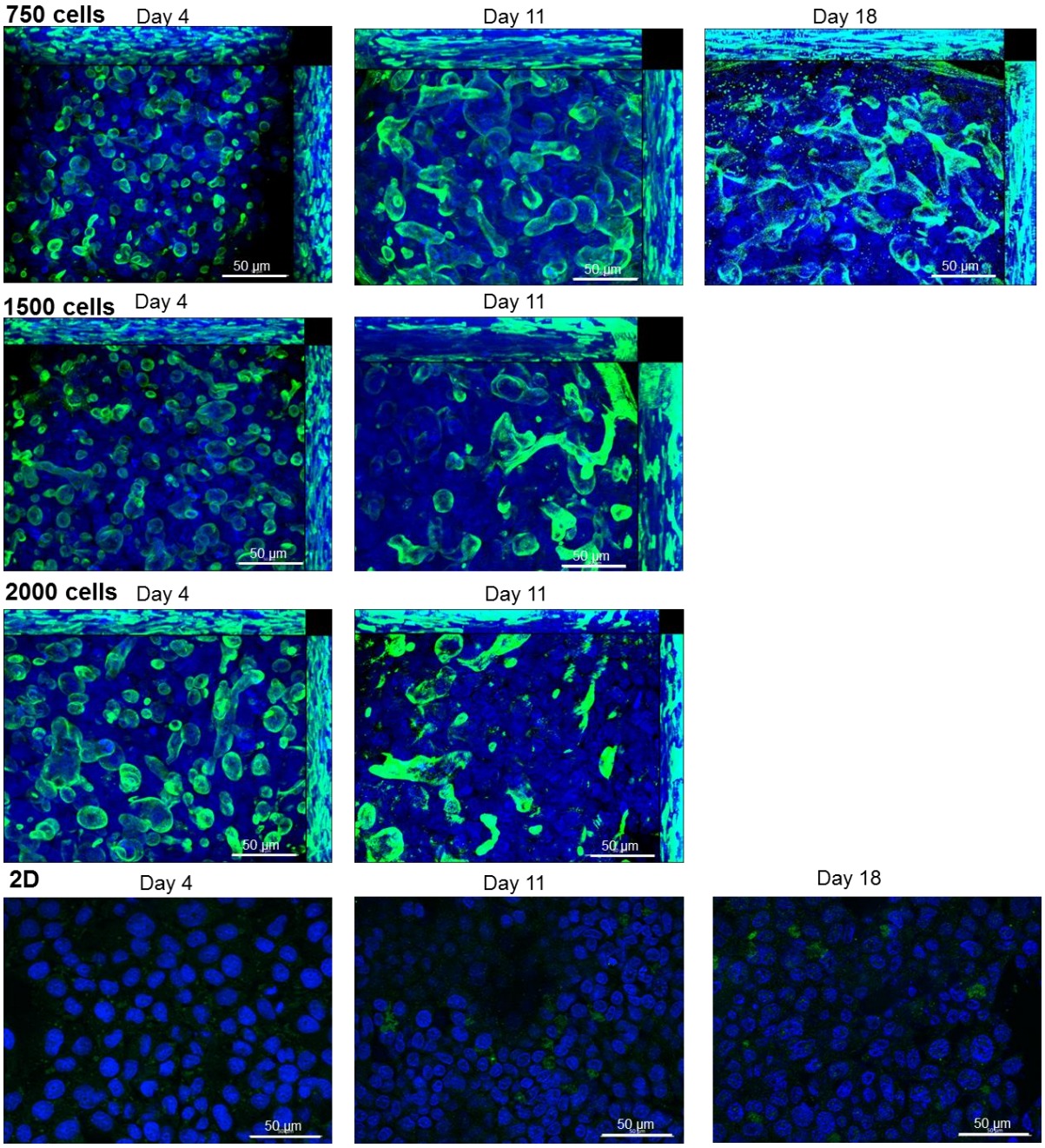

Figure 2.14. Pgp transporter localisation in spheroids. Spheroids were created from 750, 1500, 2000 C3A cells by LOT or C3A cells were cultured in a 2D monolayer and fixed at day 4, 11 and 18 of culture. Immunofluorescent staining was performed for the canalicular transporter Pgp (green) and Hoechst (blue) to stain the nuclei. Maximum intensity projection images were taken using a Zeiss Axio Observer microscope at 40 × magnification. Scale bars = 50 µm. Some of the day 18 spheroids were unable to be mounted onto a microscope slide due to increased size.

2.4 Discussion

3D *in vitro* models are becoming more widely used when investigating drug toxicity. Multiple companies now offer spheroids to be shipped ready for use in drug toxicity testing, such as InSphero (InSphero 2016). Research has shown the potential for liver spheroid models to be more predictive for hepatotoxicity than commonly used 2D liver models, as well as being more amenable to high-throughput screening and long-term repeat dose studies (Fey and Wrzesinski 2013; Godoy et al. 2013; Mueller et al. 2011; Tostoes et al. 2012). However many parameters had not been thoroughly investigated in spheroid models and there were relatively few direct comparisons between liver spheroids and other 2D models.

In this chapter a technique for creating liver spheroids from the C3A cell line was developed and optimised. C3A cells, a derivative of HepG2 cells, were chosen for this model as they exhibit strong contact-inhibited growth characteristics, consequently when cultured in a spheroid these cells do not proliferate to the same extent as other hepatocarcinoma cell lines (Wrzesinski and Fey 2013). This also better emulates primary cells which bear limited proliferation capacity. As with other liver cell lines cultured in 2D, C3A cells have disadvantages including limited expression of metabolizing enzymes and lack of liver-specific functions (Guo et al. 2011; LeCluyse et al. 2012), however the advantages over primary cells include unlimited replication potential, stable phenotype, absence of donor variation as well as ease of availability (Donato et al. 2008; LeCluyse et al. 2012).

In this study, C3A spheroids were created and characterised and found to be uniform and reproducible using the LOT, which has not been previously reported to have been used with this cell type. The LOT is a well-established technique and has been used to create spheroids from numerous different cell types in the past (Dorst et al. 2014; Herzog et al. 2015). Creating spheroids by this method was rapid

and demonstrated a high degree of reproducibility (coefficient of variation 0.53 or less for spheroid diameter); also it does not require an extensive tissue engineering background, making this model far more user-friendly. The cost-effectiveness of the model and amenability to both high-throughput and repeat-dose studies makes it a promising model for toxicological studies (Godoy et al. 2013). The optimised spheroids remained viable for 32 days of culture with a maximum diameter of 407.8 ± 92.3 µm, and uniform in shape and size. Histological and EM analysis revealed cuboidal cell morphology within the spheroids, with direct cell-cell contacts similar to the *in vivo* liver structure, hence overcoming the multitude of structural and phenotypic problems with culturing cells in 2D (Gomez-Lechon et al. 1998; Semler et al. 2000; Wells 2008). The C3A spheroid model therefore recapitulates the human liver more so than the corresponding 2D cell models.

One disadvantage of using spheroids for drug testing is that necrosis can occur within the spheroid core, distorting toxicity data. Despite this problem, few researchers have analysed the extent of necrosis when using liver spheroids. It has been estimated that oxygen and nutrients can diffuse through approximately 100 - 150 µm of tissue (Asthana and Kisaalita 2012; Curcio et al. 2007; Olive et al. 1992), however the size or time at which liver spheroids develop necrosis at the core has not been specifically determined. To complicate things further, factors such as cell type, cell number, culture time, culture technique and scaffold interactions may all have an impact on the development of necrosis in a spheroid model. The data generated in this chapter optimised starting cell number to create uniform reproducible spheroids, and after culture for 32 days the optimised spheroids do not possess a necrotic core, with only very low degree of apoptosis and necrosis detected over a 32 day culture period. It was determined that once the C3A spheroids exceed approximately 700 µm in diameter a necrotic core can be seen to have developed and there were significantly increased detectable levels of necrotic

biomarker. Therefore, C3A spheroids exceeding this critical size were deemed unusable to accurately determine the toxicological effect of a compound since they are likely to be structurally unstable, with pre-existing necrosis at the core.

In vivo, hepatocytes are structurally and functionally polarised (Gissen and Arias 2015; Godoy et al. 2013). The formation of bile canaliculi structures between cells in the C3A spheroids confirms the structural polarity of the spheroids, and was confirmed using EM and immunofluorescence. It was also identified that the spheroids displayed functional polarity, as MRP2 and Pgp - transporters known to be localised to the canalicular membrane of hepatocytes *in vivo* – were found to be expressed on the canalicular membrane (Esteller 2008; Wrzesinski et al. 2014). These polarisation features were not reproduced in 2D monolayers. The expression of these transporters is important, as not only do they have vital roles in liver homeostasis, but are also involved in the transport of drugs into, and export from, hepatocytes (Jedlitschky et al. 2006; Sharom 2011). Dysfunction of these transports can lead liver damage and cholestasis. Other basolateral and canalicular transporters were analysed, however the method used could not be optimised. Analysis of other hepatic uptake and export transporters would be valuable to this research.

Other studies have used C3A cells to create spheroids, such as Wrzesinski's group, who created C3A spheroids on AggreWell plates and transferred them into a microgravity bioreactor for culture (Fey and Wrzesinski 2012; Wrzesinski and Fey 2013; Wrzesinski et al. 2013). Characterisation was performed on their spheroids, such as analysis of spheroid size and viability (Wrzesinski and Fey 2013; Wrzesinski et al. 2013). More recently the same group have investigated the changes which occur once cells are cultured in 3D, finding key differences in cell architecture, metabolism and compound synthesis, growth and genetics (Wrzesinski et al. 2014). The C3A spheroids created in this chapter displayed similar overall characteristics to

those created by Wrzesinski's group, including similar growth curves and comparative structural similarities. A scaffold free approach for creating spheroids was also adopted in this thesis in order create direct cell-cell contacts and to reduce any ECM effects (Gomez-Lechon et al., 1998; Semler et al., 2000; Wells, 2008), however the LOT was much simpler than that used by Wrzesinski's group.

2.4.1 Conclusion

Spheroids show promise as a novel *in vitro* liver model, including a prolonged lifespan, structural similarities with the liver *in vivo*, good reproducibility and amenability to high-throughput screening. A reproducible technique for creating uniform C3A spheroids was developed. The optimised spheroids were created from 750-1000 C3A cells and were viable for 32 days, displaying a reduced proliferation rate, an *in vivo*-like cell morphology as well as 3D direct cell-cell contacts, polarised cells, bile canaliculi formation and localised hepatic transporters.

Chapter 3

Functional Characterisation of a C3A Liver Spheroid Model

Contents

3.1 Introduction

The liver is a vitally important organ, with multiple functions essential for human survival. The main function of the liver is the metabolism of compounds, including hormones, xenobiotics, carbohydrates, lipids as well as the production of albumin, urea, amino acids, lipoprotein and cholesterol (Cotran 2005; Lippincott. J. B 1993). The expression and function of key metabolic enzymes is essential in order for hepatocytes to metabolise and synthesise compounds. Additionally, functional transporters are needed for the liver to exocytose and endocytose important molecules (Cotran 2005; Godoy et al. 2013). Many of these metabolites or by-products need excreting hence hepatocytes have transporters to secrete bile into the canaliculi and bile ducts in order to remove these substances from the liver (Gissen and Arias 2015). Mitochondrial integrity is crucial to ensure correct functioning of hepatocytes, as these organelles are responsible for respiration and producing energy through metabolism (Cooper 2000). Some of these functions occur in specific zones of the liver, as the liver displays functional heterogeneity due to zonation of the liver lobule. Some of these key functions of the liver are summarised in Figure 3.1.

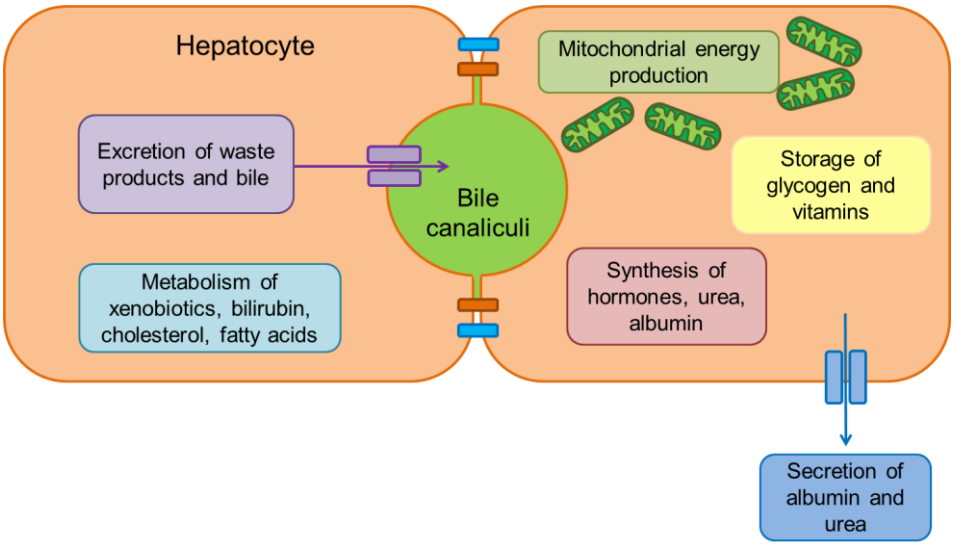

Figure 3.1. The functional roles of hepatocytes. An illustration of the key functions of hepatocytes including the synthesis of substrates and compounds, enzymatic metabolism, secretion of important molecules, excretion of substances into bile canaliculi and efficient energy production through mitochondrial respiration.

Expression of liver-specific markers, albumin and urea synthesis, metabolic enzyme expression, increased enzyme function and transporter function, have been determined to be increased in 3D liver models (Chang and Hughes-Fulford 2009; Sainz et al. 2009; Tostoes et al. 2012). This may overcome one of the key disadvantages of liver cell lines in that they display reduced liver function in 2D culture (Guo et al. 2011; LeCluyse et al. 2012). A more accurate liver model displaying increased liver-specific functions may help to broaden one's understanding of the mechanisms of liver injury and potential toxic drug targets, allowing researchers to create more efficacious drugs whilst designing-out toxicities. Hence, determining the functionality of *in vitro* liver models has become a priority in the aim to create more human-relevant drug screening systems. Despite the increased research into this area there is still much more to investigate in 3D liver models, and the functionality of C3A spheroids has yet to be fully determined or compared to current 2D liver models.

In the previous chapter a technique for creating spheroids using C3A hepatoma cells was developed and optimised. This work next planned to elucidate the liver-specific functionality and phenotype of the C3A spheroids and compare this with a corresponding 2D culture model.

Hypothesis: C3A spheroids will display liver-like functions which will be an improvement upon corresponding 2D culture model.

3.2 Materials and Methods

L-glutamine, sodium pyruvate, 1 x PBS, PFA, Triton X-100, Tween20, Tris, BSA, DMSO and glucose were purchased from Sigma Aldrich, Missouri, USA. C3A cells and EMEM were purchased from LGC standards, Middlesex, UK. Cell-Tak was purchased from Corning, NY, USA. GS, CPS1, CYP2E1, CYP3A4 and GAPDH antibodies, Albumin Human ELISA Kit (ab108788) and Urea Assay Kit (ab83362) were purchased from Abcam, Cambridge, UK. Prolong Gold (P36930), Hoechst (H3570), Alexa Fluor 568 phalloidin (A12380) and Cell Tracker 5-chloromethylfluorescein diacetate (CMFDA) (C7025) were purchased from Life Technologies, Carlsbad, CA, USA. M65 and M30 ELISA kits were purchased from Peviva, Stockholm, Sweden. XF^{e}96 cell culture microplates, spheroid microplates, extracellular flux assay kits, calibrant and base medium minimal DMEM were all purchased from Seahorse Bioscience, Massachusetts USA. Bradford reagent was purchased from Bio-Rad, Hertfordshire, UK.

3.2.1 Spheroid formation and cell culture

C3A cells were maintained and cultured in monolayers as previously described (Section 2.2.1). Spheroids were created using the LOT from 1000 C3A cells as described previously (Section 2.2.1).

3.2.2 Analysis of MRP2 and Pgp transporter function

Spheroids and monolayers were incubated with 5 µM CMFDA with or without 25 µM MK571 (MRP inhibitor) and 12.5 µM PSC833 (Pgp inhibitor) in EMEM for 30 min at 37 °C. CMFDA is membrane permeable until it enters the cells and is converted to glutathione-methylfluorescein (GSMF), a cell impermeable substrate for MRP2 and Pgp. Cells and spheroids were washed in PBS and prepared for immunofluorescence analysis as previously described (Section 2.2.7).

3.2.3 Preparation of cell lysates

Supernatant samples were stored at -80 °C. Monolayer cells were lysed using 100 µL lysis buffer made up of 250 mM sucrose, 50 mM Tris-HCl pH 7.4, 5 mM $MgCl_2$, 1 mM β-mercaptoethanol, 1 % Triton X-100. Spheroids were pooled (20 wells), washed in PBS, and lysed using 100 µL lysis buffer with 1 % Triton X-100, and stored at -80 °C. Samples were sonicated before analysis to ensure thorough lysis of spheroids.

3.2.4 Bradford assay for quantification of protein content

Standards in the range 0 - 0.5 mg/mL BSA were added to a 96-well plate. Samples were diluted as appropriate in dH_20. 200 µL Bradford Reagent was added per well and the absorbance measured at 570 nm. Protein concentrations were calculated using values obtained from the standard curve.

3.2.5 Western blot analysis for the expression of zonation and hepatocyte markers

50 µg of each sample was denatured at 80 °C before being analysed by SDS-PAGE on a 10 % acrylamide gel. The proteins were then transferred to a nitrocellulose blotting membrane then blocked using 10 % non-fat milk in Tween-Tris Buffered Saline (TBST). Membranes were probed with primary antibodies carbamoylphosphate synthetase I (CPS1), glutamine synthetase (GS), CYP3A4 and GAPDH at 1:1000 dilutions overnight in 10 % non-fat milk in TBST. Membranes were washed in TBST and bound antibody detected using secondary antibodies anti-rabbit IgG-peroxidase (1:10000), anti-mouse IgG-peroxidase (1:10000) incubated for 2 hours. Protein bands were visualised by enhanced chemiluminescence on X-ray developer film. GAPDH was analysed to ensure even loading of samples.

3.2.6 Histological analysis of functional zonation and hepatocyte markers

Spheroids were fixed, sectioned and stained with haematoxylin and CYP2E1 or CPS1 as previously described (Section 2.2.3). Immunohistochemistry was carried out by Julie Haigh at the Department of Veterinary Pathology, Leahurst Campus, University of Liverpool, UK.

3.2.7 Measurement of CYP activity by quantification of metabolites using Mass Spectrometry

Spheroids and 2D monolayer cells were washed twice in Williams E phenol-red free medium. Cells were treated with 1 mM testosterone and 0.25 mM dextromethorphan in Williams E medium for 24 hours. Spheroids or cells were pooled (from 12 wells), cells were washed in Williams E medium then stored at – 80 °C until analysis. Quantification of metabolites 6β-OH-testosterone and Dextrorphan by Mass Spectrometry was performed by Rowena Sison-Young at the University of Liverpool, UK.

3.2.8 Quantification of albumin release by ELISA

Albumin release from spheroids and monolayers into supernatant was quantified using Albumin Human ELISA Kit (Abcam), according to the manufacturer's protocol. Supernatant was pooled (4 wells) and collected 4 days after media change, twice weekly over 32 days and stored at -80 °C until analysis. All incubations were performed at RT. Albumin standards were prepared and 50 µL added to the wells of a pre-coated 96-well plate, along with samples for analysis, and incubated for 1 hour. The plate was washed 5 times with 200 µL wash buffer and incubated with 50 µL biotinylated albumin antibody for 30 min. The plate was washed as previously described and incubated with 50 µL SP conjugate for a further 30 min. Again the

plate was washed and incubated with 50 µL Chromagen solution for 20 min then 50 µL stop solution added. The absorbance was read at 450 nm using a microplate reader (Thermo Scientific Varioskan Flash). The albumin concentration in the samples was calculated using values obtained from the standard curve and normalised to average cell number.

3.2.9 Quantification of urea release

Urea release from spheroids and monolayers into supernatant was quantified using a Urea Assay Kit (Abcam), according to the manufacturer's protocol. Supernatant was pooled (4 wells) and collected 4 days after media change, twice weekly over 32 days and stored at -80 °C until analysis. Urea standards were prepared and 50 µL added to the wells of a 96-well plate, along with samples for analysis, and incubated with 50 µL urea reaction mix for 1 hour at 37 °C, protected from light. The absorbance was read at 570 nm using a microplate reader (Thermo Scientific Varioskan Flash). Urea concentration in the samples was calculated using values obtained from the standard curve and normalised to average cell number.

3.2.10 Visualisation of mitochondrial location

Mitochondria were visualised by incubating spheroids with 1 µM JC-1 (tetraethylbenzimidazolylcarbocyanine iodide) for 1 hour, then washed in PBS, incubated with Hoechst for 10 min, then washed once again and mounted onto a microscope slide as previously described (Section 2.2.7)

3.2.11 Analysis of mitochondrial function by oxygen consumption analysis

Mitochondrial function was analysed using Seahorse XF technology. For 2D monolayer experiments C3A cells were seeded onto Seahorse cell culture microplates at 40,000 cells/well 24 hours before experimentation. The sensor cartridge from the extracellular flux assay kit was hydrated in XF calibrant at 37 °C in

a non-CO_2 incubator overnight. For experiments on spheroids, the Seahorse spheroid microplate was coated with Cell-Tak (200 µL in 2.8 mL 0.1 M sodium bicarbonate), incubated for 1 hour at 37 °C, washed twice with 200 µL sterile H_2O and left to air-dry. Seahorse medium was prepared using 25 mM glucose, 2 mM L-glutamine and 1 mM in base medium minimal DMEM (Seahorse), pH adjusted to 7.4 and heated to 37 °C. The spheroid microplate was then filled with 175 µL Seahorse medium and one spheroid carefully transferred into the centre of each well. The outer wells of the Seahorse culture plates were filled with 175 µL media only and used to calculate background values (see Figure 3.2). 2D monolayer cells were washed in Seahorse medium then 175 µL medium added to each well. For 2D experiments final compound concentrations had been previously optimised as 1 µM oligomycin, 0.25 µM FCCP, 1 µM antimycin-A and 1 µM rotenone (data not shown). For spheroid experiments twelve different conditions were used (A-L) in order to optimise drug concentrations (Table 3.1). Appropriate concentrations of each compound were made up in Seahorse medium. 25 µL each compound was added to the corresponding port on the sensor cartridge, A-D in the order of injection (Figure 3.2). Cells and spheroids were incubated for 1 hour in a non-CO_2 incubator before the experiment. A Cell Mito Stress Test was then performed using Seahorse XF^e96 Extracellular Flux Analyser and Wave software which analyses oxygen consumption rate (OCR) and extracellular acidification rate (ECAR). Cells and spheroids were finally washed in PBS and lysed before performing a Bradford assay for protein quantification. Data was analysed using Seahorse XF Mito Stress Test Report Generator and data normalised to protein content. 6 wells of spheroids or 2D monolayer wells were used for each experiment.

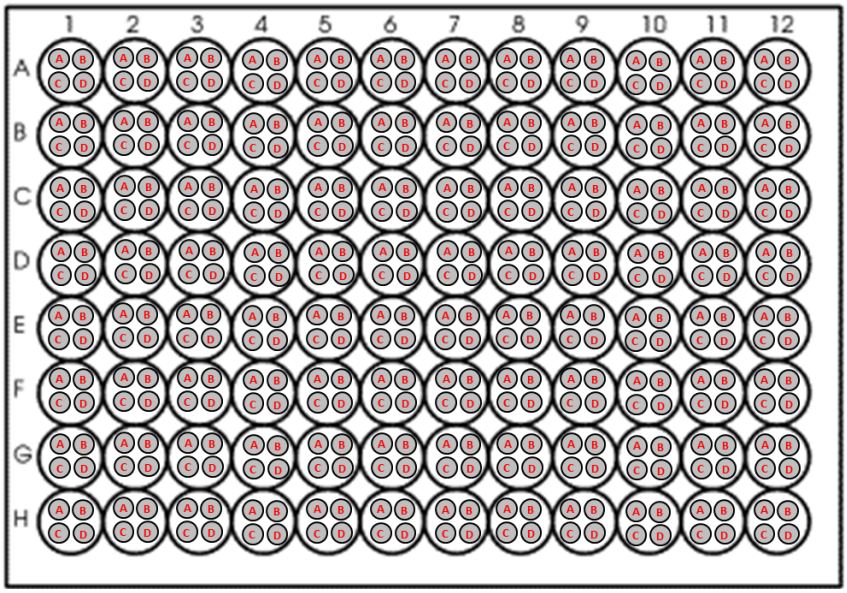

Figure 3.1. Seahorse sensor cartridge layout. Each well contains 4 ports, A, B, C and D. Compounds are added to the following ports in order of injection; (A) oligomycin, (B) FCCP, (C) antimycin-A and rotenone.

Condition	Oligomycin concentration μM)	FCCP concentration (μM)
A	1	1.5
B	1	2
C	1	3
D	1	3.5
E	3	1.5
F	3	2
G	3	3
H	3	3.5
I	5	1.5
J	5	2
K	5	3
L	5	3.5

Table 3.1. Optimisation of Cell Mito Stress Test for spheroids. Varying concentrations of oligomycin and FCCP were analysed using twelve conditions (A-L) in order to optimise the Mito Stress Test for use with C3A spheroids.

Compound	Port	Injection volume (µL)	Final volume in well (µL)	Injection concentration
Oligomycin	A	25	200	8 ×
FCCP	B	25	225	9 ×
Antimycin- A	C	25	250	10 ×
Rotenone	C	25	250	10 ×

Table 3.2. Calculation of compound dilutions for Seahorse experiments.

3.2.12 Statistical analysis

Data are representative of at least three independent experiments (n=3) and expressed as mean ± SEM. Graphs and statistical analyses were performed using GraphPad Prism 5. A Shapiro-Wilk normality test was performed on all data sets. Data which passed normality tests underwent analysis by a two-way ANOVA, those which did not underwent a non-parametric Kruskal-Wallis test. Significance was determined from a p value < 0.05. **** p<0.0001, *** p< 0.001 ** p<0.01, * p< 0.05.

3.3 Results

3.3.1 Confirmation of transporter function in spheroids

Previously it was determined that key canalicular transporters were expressed in the spheroid model (Section 2.3.4), as MRP2 and Pgp polarise to the canalicular membrane in C3A spheroids, forming a bile canalicular network. In this chapter it was investigated whether or not these transporters were functionally active. MRP2 and Pgp functionality was determined using fluorescently labelled CMFDA by immunofluorescence. This compound is membrane permeable and can passively enter cells, however once inside cells it is converted to glutathione-methylfluorescein (GSMF), a membrane impermeable compound which can only be excreted from cells via transport through function MRP and Pgp transporters. In the spheroids there was limited retention of CMFDA (green) within cell cytoplasm and an accumulation and co-localisation of the compound within secondary canalicular-like structures (red) (Figure 3.3A). Blocking MRP and Pgp transporters resulted in CMFDA being retained in the cell cytoplasm (Figure 3.4). This suggests that CMFDA was actively transported out of the cells by MRP2 and Pgp into the canalicular structures. 2D monolayer C3A cells retained CMFDA within the cell cytoplasm (Figure 3.3B) and no transport out of the cells was observed.

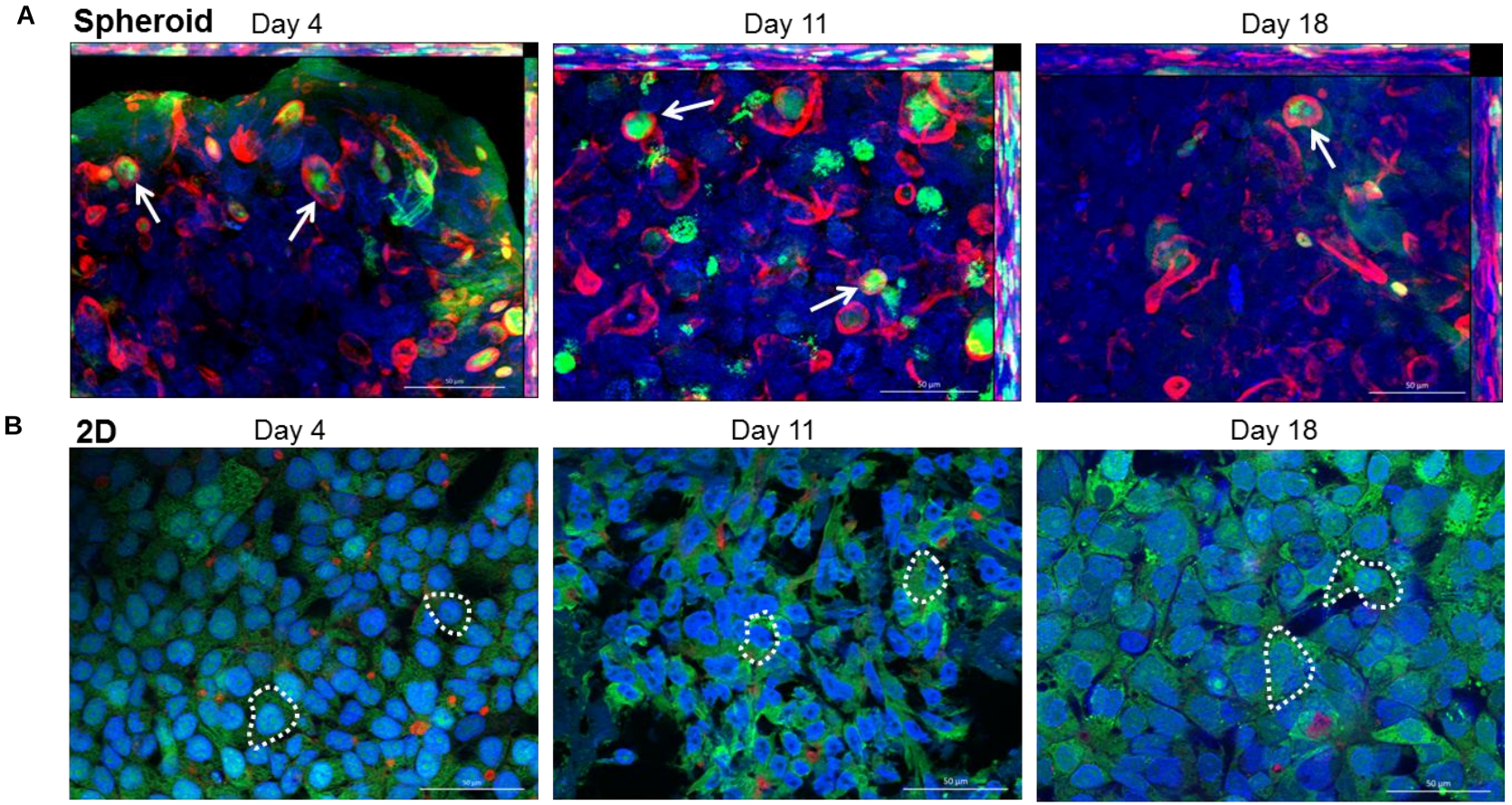

Figure 3.2. Transporter function in spheroids. (**A**) Spheroids or (**B**) 2D C3A cells were cultured for 4, 11 or 18 days and then incubated with CMFDA (green) an MRP and Pgp transporter substrate for 30 min, washed, fixed and stained with Hoechst (blue) to stain the nuclei and phalloidin (red) to stain F-actin. Snap images were taken using a Zeiss Axio Observer microscope at 40 × magnification. Dotted line indicates an example of a cell where CMDFA is retained within the cell cytoplasm. Arrow indicates the canalicular-like structures containing CMFDA. Scale bars = 50 µm.

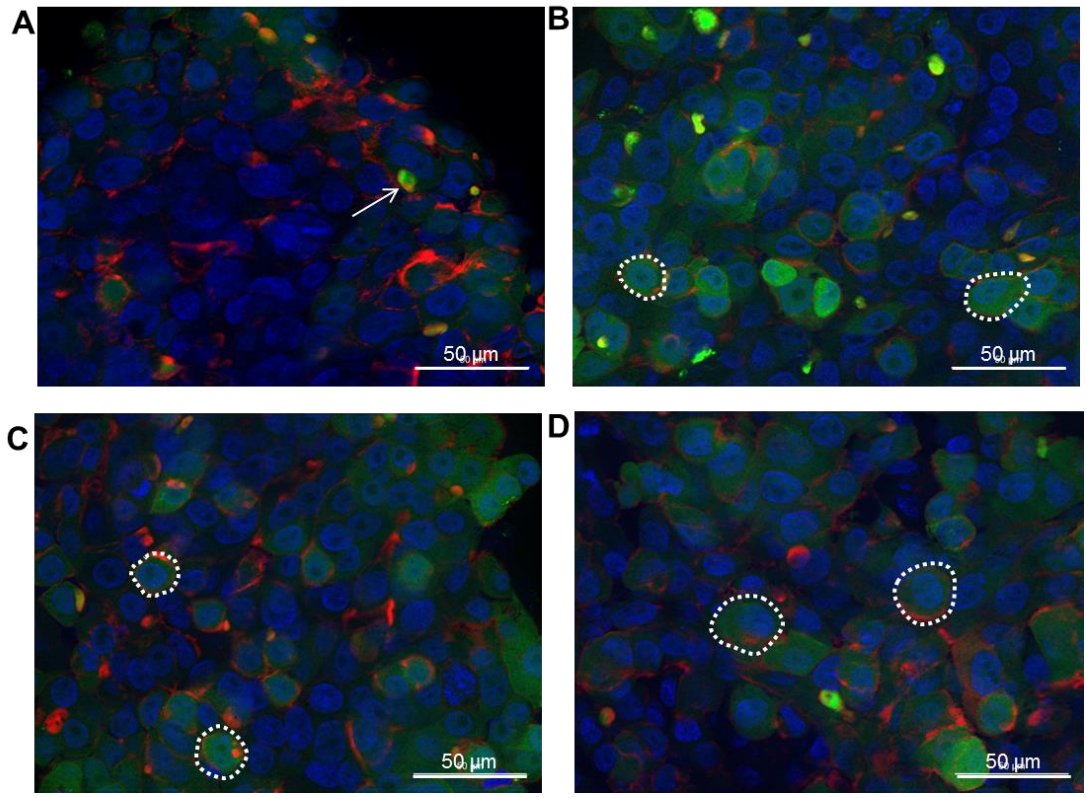

Figure 3.3. Transporter inhibition in spheroids. Spheroids were incubated with (**A**) CMFDA (green) only; (**B**) CMFDA and MK571 (MRP inhibitor); (**C**) CMFDA and PSC833 (Pgp inhibitor); (**D**) CMFDA, MK571 and PSC833 for 30 min. Spheroids were washed, fixed and stained with Hoechst (blue) to view the nuclei and phalloidin (red) to view F-actin. Snap images were taken using a Zeiss Axio Observer microscope at 40 × magnification. Dotted line indicates an example of a cell where CMDFA is retained within the cell cytoplasm. Arrow indicates the canalicular-like structures containing CMFDA. Scale bars = 50 µm.

3.3.2 Functional zonation in spheroids

Specific functional markers were probed for in order to assess liver zonation and functional heterogeneity. Figure 3.5 indicates some of the zonated functions of the human liver which can be used as zonation markers. CPS1 is an enzyme of the urea cycle which catalyses the metabolism of ammonia and bicarbonate to carbamoylphosphate and can be utilised as a marker for periportal and intermediate areas of the liver (Gebhardt 1992; Koenig et al. 2007; Poyck et al. 2008). GS is involved in the conversion of ammonia and glutamate to glutamine and can be used as a marker of perivenous regions (Gebhardt 1992; Winkler et al. 2015). Western blot was used to analyse the expression of these two zonation markers and it was found that they were both expressed in the C3A spheroids (Figure 3.6A). Next the spheroids were stained for CPS1 and it was found to be expressed near the periphery of the spheroid, an area with the highest oxygen concentrations, similar to the periportal area of the liver lobule (Figure 3.6B).

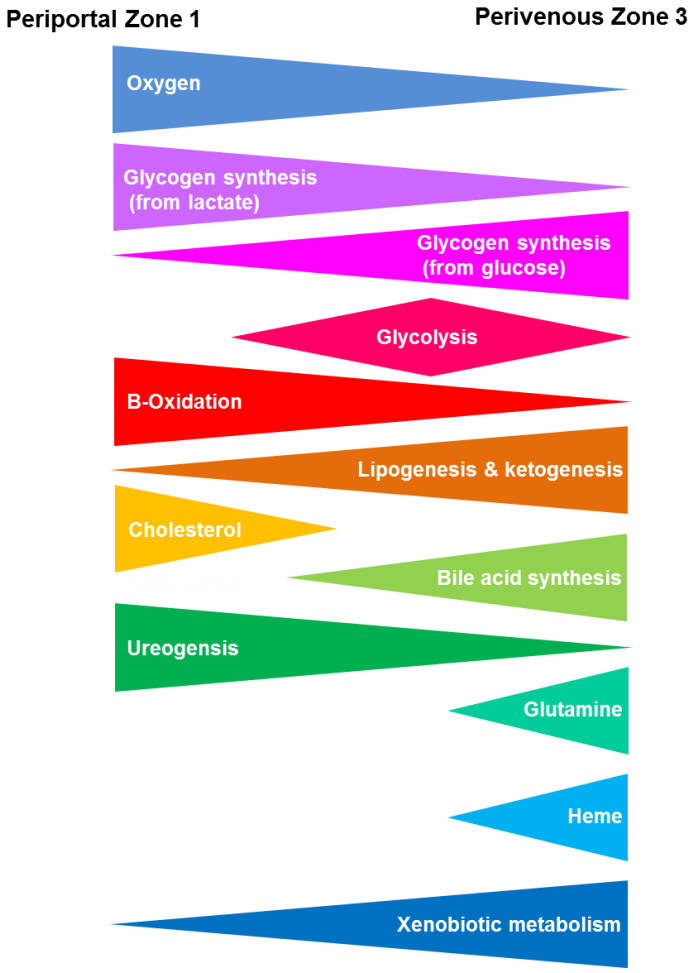

Figure 3.5. Markers of liver zonation. Due to the zonation of the liver, specific liver functions are carried out in particular zones, as illustrated in the above diagram. The zonated functional activity can be used to probe for markers of specific liver zones.

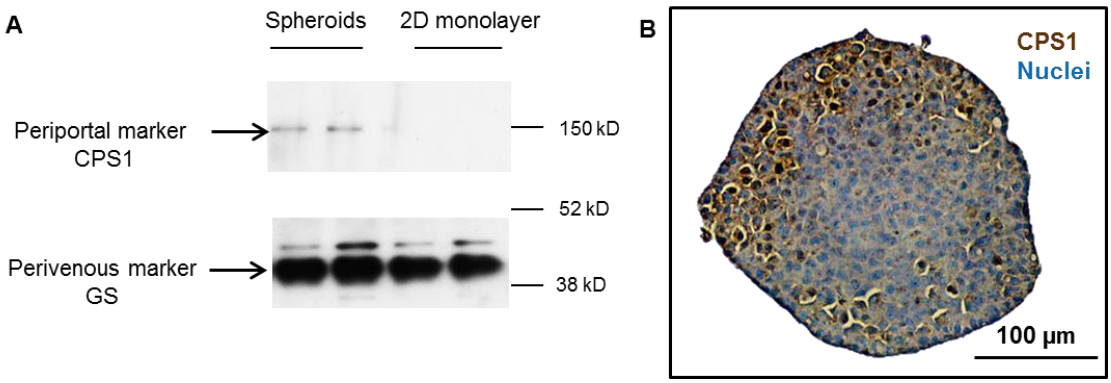

Figure 3.4. Functional heterogeneity in spheroids. (**A**) Spheroids and 2D monolayer C3A cells were analysed in duplicate by western blot for zonation markers CPS1 and GS. (**B**) Spheroids were fixed at day 18 of culture, paraffin embedded, sectioned and stained with CPS1, a periportal marker (brown) and haematoxylin (blue) to stain the nuclei. Scale bar = 100 µm.

3.3.3 Expression of hepatocyte specific markers

In order to determine the presence of key liver-specific enzymes involved in drug metabolism, expression of CYP3A4 and CYP2E1 was analysed. A western blot was performed for CYP3A4 and Figure 3.7A shows clear expression of this enzyme in the spheroid cultures and 2D. Subsequently the spheroids were stained for CYP2E1 using immunohistochemistry. CYP2E1 was observed to be expressed in the spheroid, indicating that the spheroids express this liver-specific functional marker (Figure 3.7B).

Keratin 18 is a hepatocyte-specific protein responsible for cell structure and integrity and is only expressed in liver cells (Ku et al. 2007; Omary et al. 2002) The expression of keratin 18 was also analysed in C3A spheroids, which can be seen to be expressed in cells within the spheroid to a higher degree than 2D cultures (Figure 3.7A).

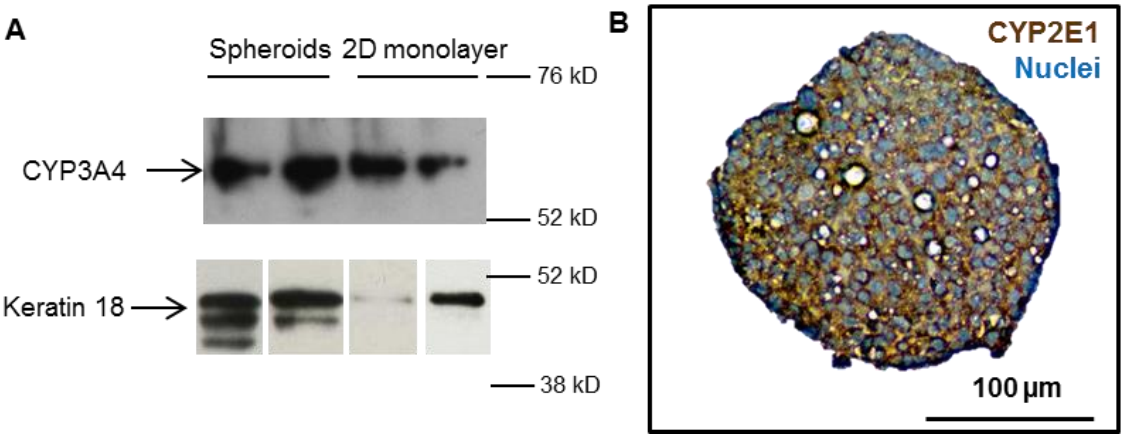

Figure 3.7. Expression of hepatocyte-specific markers in spheroids. (**A**) western blot for CYP3A4 and keratin 18 expression in spheroids and 2D monolayer cells in duplicate. (**B**) Spheroids were fixed at day 11 of culture, paraffin embedded, sectioned and stained with CYP2E1 antibody (brown) and haematoxylin (blue) to stain the nuclei. Scale bar = 100 µm.

3.3.4 CYP enzyme activity

The metabolic capacity of the C3A spheroids was next analysed. Spheroids were treated with two compounds, testosterone and dextromethorphan, which are metabolised by CYP3A4 and 2D6 respectively. The metabolites of these two compounds were quantified as an indication of the activity of these two CYP enzymes in spheroids and compared to 2D cultures (Figure 3.8). The highest production of the CYP3A4 testosterone metabolite, 6β-OH-testosterone, was in C3A spheroids at day 3 of culture at 8.01 ± 2.1 nM/spheroid. Likewise, day 3 spheroids also produced the highest quantities of Dextrorphan, the CYP2D6 dextromethorphan metabolite, also, at 0.062 ± 0.01 nM/spheroid. When normalised to cell number, the CYP activity in 2D monolayer C3A cells could be compared to spheroids (Figure 3.9). 2D monolayer cells had a lower CYP3A4 and 2D6 activity than day 3 spheroids. Reported Dextrorphan values in human hepatocyte spheroids are around 11.6 nM, higher than the values observed in C3A spheroids (Bell et al. 2016). Reported CYP3A4 activity values from 2D primary hepatocytes range from around 5 – 350 pmol/mg, and CYP2D6 from 1- 60 pmol/mg, with equivalent values in C3A spheroids being 14,907 pmol/mg and 115 pmol/mg respectively (Hewitt et al. 2007).

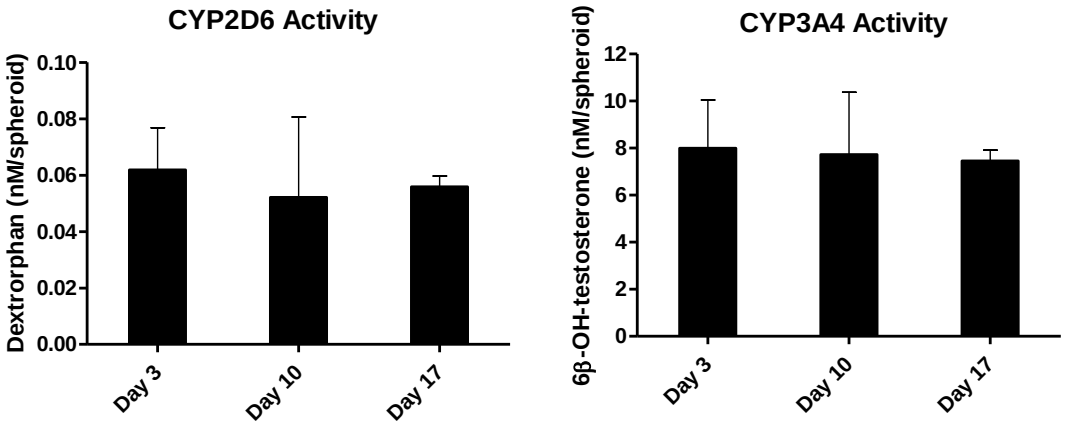

Figure 3. 8. CYP enzyme activity in spheroids. Spheroids were incubated with 1 mM testosterone and 0.25 mM dextromethorphan hydrobromide for 24 hours. Supernatant and cell samples were collected and analysed by mass spectrometry for metabolite formation. CYP2D6 and CYP3A4 enzyme activity were represented by the quantification of metabolites 6ß-OH-testosterone and Dextrorphan (nM/spheroid) respectively. Data are represented as mean ± SEM (n=3 from 12 replicates).

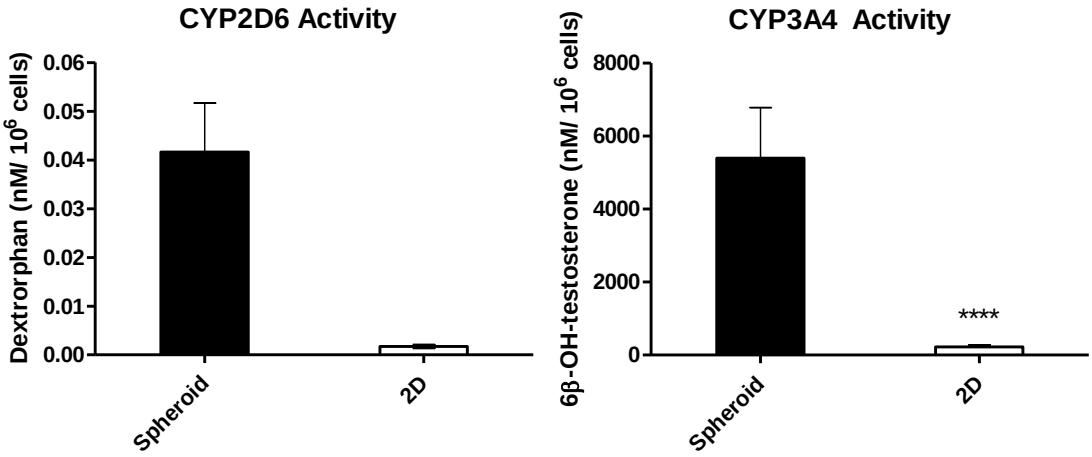

Figure 3.9. CYP enzyme activity is higher is spheroids than 2D cells. Spheroids and C3A cells cultured as a monolayer were incubated with 1 mM testosterone and 0.25 mM dextromethorphan hydrobromide for 24 hours. Supernatant and cell samples were collected and analysed by mass spectrometry for metabolite formation. CYP2D6 and CYP3A4 enzyme activity were represented by the quantification of metabolites 6ß-OH-testosterone and Dextrorphan (μM/10^6 cells) respectively. Data are represented as mean ± SEM, **** p<0.0001 (n=3 from

3.3.5 Production of albumin and urea

A major function of the liver is the metabolism and synthesis of vital substances, two of which are albumin and urea, commonly utilised to asses liver-specific function (Bacon. B. R. et al. 2006; Cotran 2005). Albumin and urea production from spheroids was quantified over 32 days. Albumin production increased over the 32 day culture period to a maximum cumulative release of 9.14 ± 3.5 pg/cell (Figure 3.10A). This was compared to 2D monolayer cultured C3A cells which were seen to produce a maximum of 1.91 ± 0.42 pg/cell albumin after 8 days of culture, significantly less than in 3D culture. Urea production from C3A spheroids peaked early on at day 4 with 0.46 ± 0.06 pmol/cell of urea released, with the production residing at around 0.2 pmol/cell for the remainder of the culture period (Figure 3.10B). Less urea was produced from monolayer cultured C3A cells, with a maximum of 0.016 ± 0.001 pmol/cell urea produced on day 4.

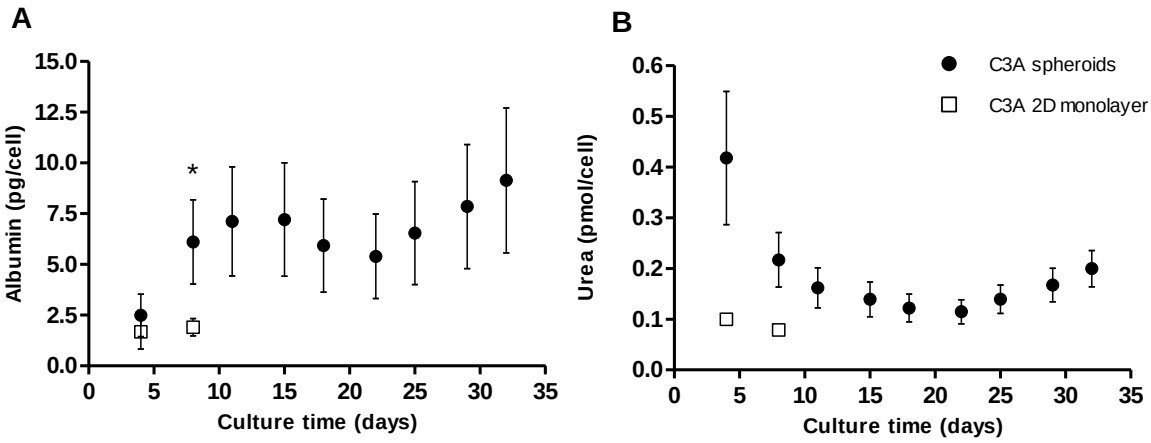

Figure 3.10. Albumin and urea production in spheroids. Supernatant samples from spheroids were analysed over 32 days, with 2D C3A cells used as a comparison. (**A**) Albumin and (**B**) urea release were quantified in spheroid (black circle) and monolayer (black square) supernatant and plotted against culture time (days) . Data are represented as mean ± SEM, * $p<0.05$ (n=3 in triplicate).

3.3.6 Mitochondrial function in spheroids

Firstly mitochondrial expression and location were analysed in C3A spheroids using immunofluorescence. Figure 3.11 shows mitochondria (red) in relation to nuclei (blue) in the spheroids. Mitochondria were observed to be distributed throughout the C3A cell cytoplasm and appeared to be in abundance. Due to the 3D nature of the spheroids the staining could not be seen in all of the cells in the image due to limitation of cell penetration of the microscope which has a maximum depth of 20 nm.

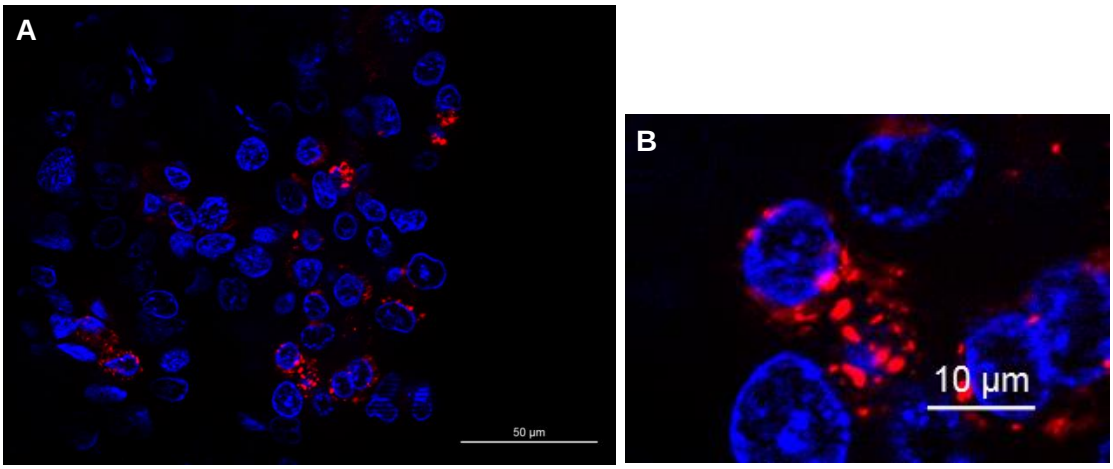

Figure 3.11. Mitochondrial location in spheroids. Spheroids were incubated with 1 µM JC-1 mitochondrial stain (red) then nuclei stained (blue) and imaged by confocal microscopy at 40 × magnification and represented as snap images. (**A**) shows a section throughout the spheroid; (**B**) shows a close-up of one cell. Scale bars = 50 µm.

In order to analyse the function of mitochondria in the spheroids mitochondrial respiration was measured using Seahorse technology and a Mito Stress Test. This analysis works by calculating OCR and ECAR through measurement of oxygen and free proton concentrations present in the culture (Hill et al. 2012; SeahorseBioscience 2016). Figure 3.12 represents a typical OCR curve produced from a Mito Stress Test with the sequential addition of oligomycin, FCCP and antimycin A and rotenone. These drugs each challenge the mitochondria

complexes within the Electron Transport Chain (ETC) in order to calculate specific respiratory parameters and elucidate how the mitochondria are functioning. Oligomycin inhibits ATP synthase (mitochondrial complex V), therefore any decrease in OCR after its addition is estimated to be the amount of respiration linked to ATP production (Hill et al. 2012). FCCP was added next, acting as a proton uncoupler as the mitochondrial membrane becomes permeable to protons, this OCR value allows one to calculate the maximal potential respiration of the system being tested (Hill et al. 2012). Finally non-mitochondrial oxygen consumption can be analysed by adding rotenone and antimycin-A, mitochondrial complex I and III inhibitors respectively, to inhibit the respiratory chain (Hill et al. 2012). Firstly concentrations of oligomycin and FCCP were optimised to ensure that the assay was appropriate for use with spheroids. Table 3.1 shows the concentrations of each compound used in the optimising conditions. Ideally, during the Mito Stress Test basal OCR would be clearly above 0, with a significant decrease after the addition of oligomycin and an increase back above the basal level after addition of FCCP, finally with antimycin-A and rotenone brining the OCR down below the previous values seen, resulting in a curve comparable to Figure 3.12. Figure 3.13 shows the OCR curves produced in the Mito Stress Test in C3A spheroids under each condition tested. From this data it seemed clear condition H produced the most informative OCR curve, thus these concentrations were used in future experiments on spheroids. 2D monolayer experiments had been previously optimised for the concentrations 1 µM oligomycin, 0.25 µM FCCP, 1 µM antimycin-A and 1 µM rotenone (Kamalian et al. 2015).

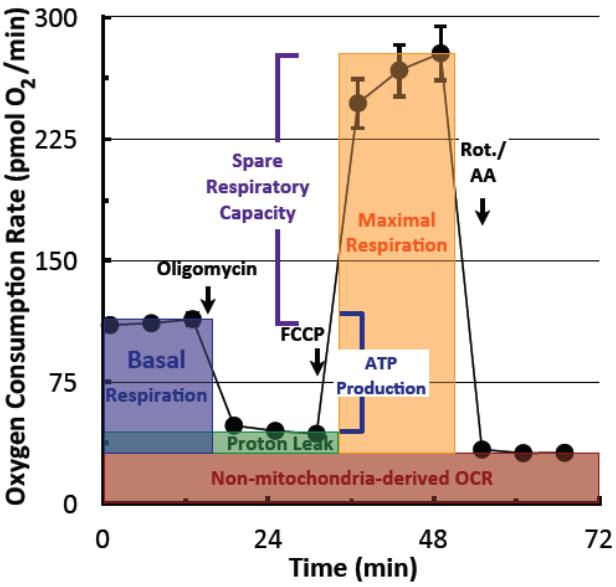

Figure 3.12. Representative OCR curve from a Mito Stress Test. A typical graph plotting OCR (pmol O_2/min) against time (min) during a Mito Stress Test with the sequential addition of oligomycin, FCCP, antimycin-A and rotenone. The calculation of basal respiration, proton leak, ATP-linked respiration, spare respiratory capacity and non-mitochondrial respiration are depicted. Image taken from Seahorse Bioscience.

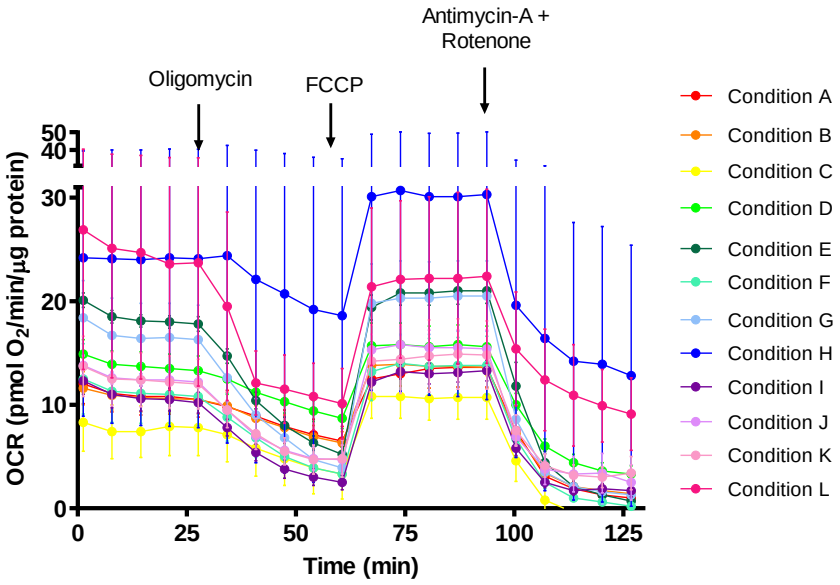

Figure 3.13. Optimisation of spheroid Mito Stress test. A Mito Stress test was performed on 10 day cultured spheroids using Seahorse technology using a range of conditions (A-L). Raw OCR values (pmol O_2/min/µg protein) were plotted against time (min). Data represent mean ± SEM (n=1, 6 replicates).

The experiment on spheroids was first carried out to establish a baseline of normal mitochondrial function. The spheroids responded to the Mito Stress Test as expected, similar to the typical OCR curve in Figure 3.12. OCR values for C3A spheroids and 2D monolayers are plotted in Figure 3.14. Spheroids had slightly lower overall OCR than 2D monolayer cells, and spheroids had higher variation in OCR, however there was no significant difference between the two culture conditions. Extracellular acidification rate (ECAR) was also analysed. Acidification of culture medium is primarily a result of glycolytic turnover and concomitant lactate production, an alternative non-mitochondrial method of ATP production in cells (Dranka et al. 2011). ECAR was found to be significantly higher in spheroids than 2D cultures, at 7.6 ± 3.8 compared to 3.26 ± 1.63 mpH/min/µg protein (Figure 3.15).

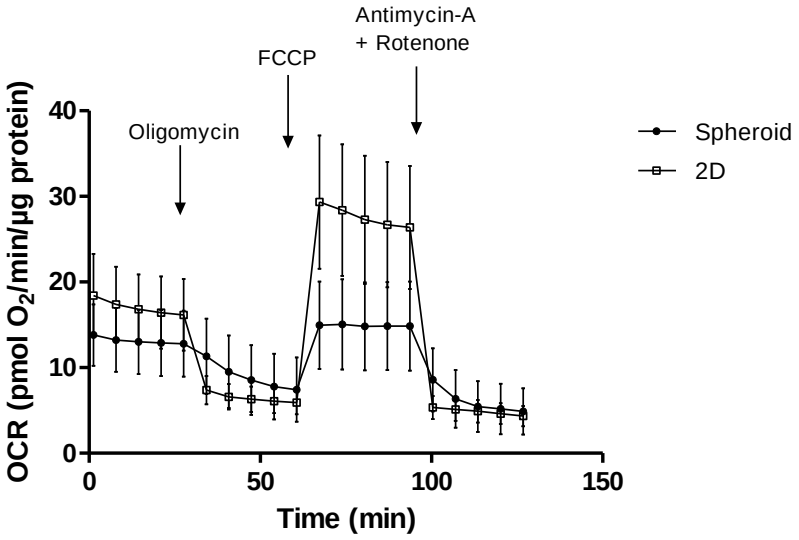

Figure 3.14. OCR in C3A spheroids and 2D. A Mito Stress test was performed on 10 day cultured spheroids and 2D C3A cells using Seahorse technology. Raw OCR values (pmol O_2/min/10^3 cells) were plotted against time (min). Data represent mean ± SEM (n=3, 6 replicates).

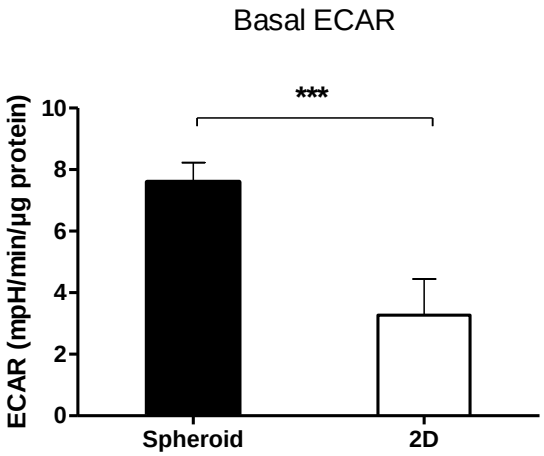

Figure 3.15. ECAR in C3A spheroids and 2D. ECAR was measured in 10 day cultured spheroids and 2D C3A cells using Seahorse technology. Basal ECAR values (mpH/min/10^3 cells) were plotted against culture condition. Data represent mean ± SEM, *** p<0.001 (n=6, 6 replicates).

Further respiratory parameters were calculated from the Mito Stress Test (Figure 3.16). Basal respiration in spheroids was found to be 7.9 ± 1.2 pmol O_2/min/µg protein, compared to 11.8 ± 3.0 pmol O_2/min/µg protein in 2D monolayer cultures. ATP production was 5.35 ± 0.5 O_2/min/µg protein in spheroids and 10.2 ± 2.8 O_2/min/µg protein in 2D. Proton leak was higher than 2D monolayer cultured cells at 2.57 ± 1.1 O_2/min/µg protein. Non-mitochondrial respiration (NMR) was similar in both culture conditions. The only significant difference in mitochondrial function observed between spheroids and monolayer cultures C3A cells was the maximal respiratory capacity and corresponding spare respiratory capacity (SRC), with spheroids having significantly lower values, for example SRC in spheroids was 2.35 ± 1.5 O_2/min/µg protein compared to 13.2 ± 3.8 O_2/min/µg protein in 2D.

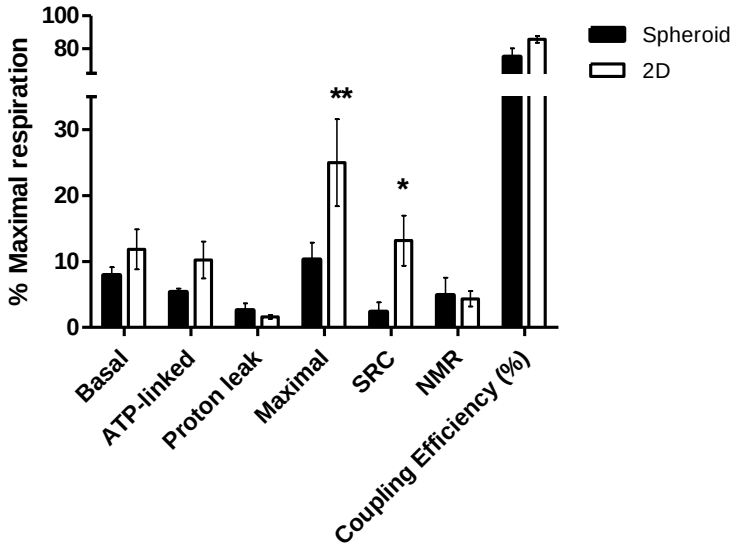

Figure 3.16. Spheroid mitochondrial function. A Mito Stress Test was performed on 10 day cultured spheroids and 2D C3A cells using Seahorse technology and mitochondrial respiratory parameters calculated and plotted as a percentage of maximal respiration. Basal respiration, ATP-linked respiration, proton leak, maximal respiration, spare capacity, non-mitochondrial respiration and coupling efficiency are plotted for each culture condition. Data represent mean ± SEM, ** $p<0.01$, * $p<0.05$ (n=3, 6 replicates).

3.4 Discussion

After discovering that it was possible to recapitulate certain aspects of the liver microstructures in a 3D *in vitro* model it was then decided to investigate the liver-specific functionality of C3A spheroids and compare this with a corresponding 2D model.

The ability of hepatocytes to produce bile, excrete waste products and transport compounds is essential for their proper functioning. Accumulation of a florescent bile substrate in bile canalicular structures in spheroids was confirmed, with little remaining within the cell, indicating that canalicular transporters in the spheroid were functional. It was further confirmed that MRP2 and Pgp were indeed responsible for this transport by blocking these transporters. CMFDA was not transported in monolayer cultured C3A cells, likely due to lack of expression of MRP2 and Pgp, improper polarisation of cells (shown in Section 2.3.4), or inactive transporters when cultured in 2D. Since this work was carried out MRP2 function in HepG2 spheroids has been confirmed (Mueller et al. 2011; Ramaiahgari et al. 2014) indicating that this happens in multiple cell lines once cultured in 3D.

The liver is well known to have functional zonation, as periportal and perivenous hepatocytes have different functions and therefore different expression markers (Bacon. B. R. et al. 2006). This zonation is perhaps partially due to the oxygen and nutrient gradients throughout the liver sinusoid produced by relative distances to the vascularisation. It was revealed that C3A spheroids recapitulate some of the functional heterogeneity of the liver that occurs *in vivo* by confirming that both these periportal and perivenous markers were expressed in the spheroids. CPS1 was expected to be expressed in areas of the liver lobule nearest to the oxygenated blood supply. CPS1 was stained for and was clearly expressed in the peripheral regions on the spheroid, with a similar expression pattern to *in vivo*, indicating

spatiotemporal similarity of C3A spheroids with a human liver lobule (Koenig et al. 2007). To the knowledge of the author this functional heterogeneity has not been proven previously in an *in vitro* liver model. The results suggest that C3A spheroids recapitulate functions from each zone in one spheroid, giving spheroids the potential to perform the zonated functions of the liver lobule.

One of the main functions of the human liver is the homeostasis of numerous molecules and substances, including the metabolism and breakdown of compounds, detoxification of xenobiotics as well as the synthesis of substances (Bacon. B. R. et al. 2006; Lippincott. J. B 1993). Many of the metabolic processes in the liver are performed by various phase I CYP enzymes, which are vital for efficient liver function (Koenig et al. 2007). Hence, as an indicator of liver-specific functionality the CYP enzyme expression and activity were analysed in the spheroids. CYP2E1 and CYP3A4 were both found to be expressed in the C3A spheroids. These two enzymes are responsible for the metabolism of numerous xenobiotics, including acetaminophen and diclofenac (James et al. 2003). CYP expression had previously been confirmed in liver spheroids created from other cell types (Chang and Hughes-Fulford 2009; Sainz et al. 2009; Tostoes et al. 2012) and this is now confirmed to be true for C3A spheroids. The activity of CYP3A4 and CYP2D6 were further quantified. Both enzymes were found to be functional in C3A spheroids over 17 days in culture, with significantly higher metabolism than 2D cultured C3A cells. Interestingly, the levels of CYP activity appeared to be higher in C3A spheroids than that reported for 2D human hepatocytes, yet lower than hepatocyte spheroids (Bell et al. 2016; Hewitt et al. 2007). In order to fully determine the metabolic capability of the model, phase II enzymes, such as UGT, could be analysed.

It was additionally confirmed that the spheroids were able to synthesise and secrete albumin and urea, with higher values of albumin and urea produced in spheroids than the corresponding 2D model. This indicates synthetic and metabolic function in

C3A liver spheroids as albumin and urea production are important physiological functions of hepatocytes *in vivo* (Bacon. B. R. et al. 2006; Cotran 2005; Khetani et al. 2015a), and builds on the evidence that cells cultured in spheroids have superior functionality to those cultured in 2D. However, it has been suggested that 2D C3A cells produce urea without a completely functional urea-cycle through arginase II (Mavri-Damelin et al. 2008). The expression of CPS1 in the spheroids indicates that parts of the urea cycle are present, however from the results presented in this chapter it cannot be confirmed that the other enzymes involved in the urea cycle are functional or that the synthesis of urea is through an active detoxification of ammonia through the urea cycle. One possibility is that C3A cells cultured in 2D do not display zonated functions, and therefore might lack expression of periportal functions such as the urea cycle, whereas spheroid culture may overcome this limitation by expressing the enzymes necessary for the detoxification of ammonia through the urea cycle. It was also found that the spheroids expressed the hepatocyte-specific marker keratin 18, this protein is only expressed in liver cells, with vital roles in maintaining cell integrity and structure. This indicates that C3A spheroids are able to express proteins exclusively localised to hepatocytes, hence recapitulating the cells in a human liver. Other groups have additionally analysed liver-specific functions in their C3A spheroids, revealing cholesterol and urea secretion (Fey and Wrzesinski 2012; Wrzesinski and Fey 2013). The pattern of urea release from 'Wrzesinski's' spheroids did not correlate with the results presented in this chapter, as they saw an increase over 45 days in culture unlike the rise and fall observed in the C3A cells presented here (Wrzesinski et al. 2013).

Mitochondria are vitally important to the cell, producing energy through metabolism. ATP is produced by mitochondria via oxidative phosphorylation (OXPHOS) of nutrients, creating a proton gradient across the inner mitochondrial membrane as part of the ETC (Cooper 2000). Toxic by-products of OXPHOS are oxygen free

radicals and ROS, which have the capability of damaging DNA, proteins, lipids and other molecules, potentially leading to oxidative stress and cellular dysfunction. Correct mitochondrial function is therefore essential to a cell's phenotype and for efficient cell function and homeostasis.

Mitochondria were present in abundance throughout the spheroid cytoplasm and looked viable in the electron microscopy images presented previously (see Section 2.3.3). Mitochondrial function was analysed in the spheroids under normal culture conditions and compared to 2D cultured C3A cells. The basal respiration reflects the sum of all cellular processes consuming oxygen. In C3A spheroids the basal respiration was comparable to that seen in 2D. Respiration linked to ATP production from C3A spheroids had a similar value to 2D cultures, suggesting that the ATP demand of the cell is similar regardless of culture condition. A decrease in the amount of ATP-linked respiration could mean a damaged electron transport chain. Proton leak occurs when OXPHOS is incompletely coupled, with high values potentially indicating mitochondrial injury, however spheroids showed similar values for proton leak as monolayer cultures. C3A spheroids had low levels of NMR which occurs from any other oxygen consuming process occurring within the cell, high levels could be due to increased ROS production (Divakaruni et al. 2014; Hill et al. 2012). Another important parameter is the coupling efficiency, the amount of ATP turnover compared to baseline levels, which was again comparable in C3A cells cultured in 2D or 3D. The small differences in how C3A cells respired in 2D and 3D spheroids were generally not significant and overall the cells responded similarly regardless of culture condition. An interesting observation was a significantly lower maximal respiration and SRC in spheroids compared to 2D monolayers. Maximal respiration tells one the peak respiration that can occur within the cell, with the SRC being the difference between the basal and maximal respiration. The SRC gives information about the ability of the cell to respond to increased energy demand, and

the C3A spheroids had fairly low reserve capacity. This may indicate that the spheroids may be less able to cope with increased energy demand or stress than 2D cultured cells. Higher ECAR values were also observed in spheroids, potentially indicating a higher glycolytic capacity when C3A cells are cultured in 3D. Overall, the analysis of mitochondrial function indicates that the spheroids were viable and functional with efficient energy production through OXPHOS as well as glycolysis and functional mitochondria, with minor differences between C3A cells cultured in 2D or spheroid culture.

The multiple functional differences observed between C3A cells cultured in 2D and 3D could be due to a number of factors. Wrzesinski *et al.* have shown metabolic changes induced by 3D cell culture. Increased glucose metabolism, hence glycolysis, was observed in their spheroids, as well as reduced complex VI oxidative phosphorylation and reduced ATP synthase (Wrzesinski et al. 2014). More recently significant proteome alterations in mitochondrial function, oxidative phosphorylation and the TCA cycle occur once hepatocytes were cultured in 2D, whereas spheroid cultures had a similar prolife as liver tissues (Bell et al. 2016). This suggests that the bioenergetic profile of cells in 2D is unlike that of the *in vivo* liver, whereas spheroid culture behaves more alike liver tissue, and supports the data presented here. Other cell types when cultured in 3D have shown a metabolic shift to increase glycolysis (Longati et al. 2013), similar to the results in C3A spheroids. It has been suggested that an increase in metabolism acts as a way of intracellular and extracellular signalling (Jones and Bianchi 2015), which could be the cause of the differences in metabolism observed in 3D culture. Without comparing the values obtained from C3A spheroids to those obtained in *in vivo* tissue it is hard to speculate as to whether or not these metabolic changes are advantageous or deleterious to the culture model. Regardless, the results presented show improvements in many liver-specific functions in C3A spheroids when compared to

these cells under standard monolayer culture, suggesting that the cells in spheroids are becoming more like primary liver cells, hence it is possible that the changes in mitochondrial respiration and energy metabolism observed are an adaptation, or cause, of this differentiation of cells into a more liver-like phenotype.

Since this work began, other research groups have looked at the effect of 3D cell culture on the phenotype of *in vitro* liver models and support the building evidence that liver functions are increased once cells are cultured in spheroids. Multiple studies have now shown increases in albumin and urea synthesis, CYP expression and transporter function in liver spheroids when compared to 2D or sandwich culture using multiple different liver cell types (Chan et al. 2016; Ramaiahgari et al. 2014; Takahashi et al. 2015; Wang et al. 2015; Xia et al. 2016).

Interestingly, C3A cells have been tested in microfluidics devices, and although some liver-specific functions have been elucidated, mainly albumin and urea production, there has been minimal direct comparisons with 2D cultures (Baudoin et al. 2011; Filippi et al. 2004), Hence, there is insufficient evidence to show that microfluidics devices are in any way superior to 2D or spheroid cultures. Additionally these systems are practically difficult to maintain and low-throughput as well as being more costly that spheroid culture. Therefore, C3A spheroids show promise as a simple 3D cell culture system with the added benefit of superior liver-specific function compared to corresponding 2D cell models.

3.5 Conclusion

The disadvantages of liver cell lines, primarily the reduction of liver functionality, are often a justification to avoid the use of these cells during *in vitro* drug screening. Nonetheless there is growing evidence that improved cell culture condition can reverse the limitations of some liver cell lines, resulting in a functional, reproducible,

more cost-effective and high-throughput liver model. C3A spheroids show enhanced liver-specific functions compared to the same cell type cultured in 2D, including active transporters, expression of hepatocyte-specific markers, CYP enzyme activity and albumin and urea synthesis. Furthermore mitochondrial functionality and functional heterogeneity were revealed in the spheroid model. The results presented in this chapter support the conclusion that when cultured in spheroids, cells display increased liver-like phenotype and function.

Chapter 4

Toxicological Predictivity of a C3A Liver Spheroid Model

Contents

4.1 Introduction

More predictive *in vitro* liver models are essential in order to decrease the number of toxic compounds being progressed into *in vivo* studies and clinical trials. It is possible that the C3A spheroid model, with its numerous advantages over 2D cell culture, may be more predictive of compounds which cause DILI in humans. This hypothesis was tested by performing a screen of hepatotoxins in C3A spheroids in order to determine the sensitivity of the model to compounds with a risk of DILI in humans.

The majority of *in vitro* liver models concentrate on hepatocytes, or their immortalised alternatives (Godoy et al. 2013; Lippincott. J. B 1993), however NPC, such as LSEC, Kupffer cells and stellate cells, also have vital physiological roles in the liver and importantly, during liver injury and regeneration (Godoy et al. 2013; Kmiec 2001; Michalopoulos 2007). There is some evidence to suggest that the inclusion of NPC in *in vitro* models has a role not only in maintaining the phenotype and function of hepatocytes, but the response of the liver to hepatotoxins (Edling et al. 2009; Kang et al. 2013; Ohno et al. 2009; West et al. 1986; Yagi et al. 1998). Therefore, it may be essential to include NPC for complete recapitulation of the liver *in vitro* and in order to improve the sensitivity of liver models to human hepatotoxins. Nonetheless, no study prior to the start of this work had elucidated the specific effects of different NPC on the ability of an *in vitro* liver model to detect DILI.

As well as preclinical screening being extremely important, clinical tests are legally required before a compound can be marketed for use. Current clinical DILI biomarkers however have multiple disadvantages including poor sensitivity, a delay in elevations in the serum and lack of organ specificity, to name a few (Antoine et al. 2013; Antoine et al. 2012; Antoine et al. 2009a; Ozer et al. 2008; Zhou et al. 2013). Understandably, research is now focusing on novel biomarkers of DILI, such as

HMGB1, keratin 18 and miR-122, which have each been found to be more accurate at predicting the likelihood of survival and extent of injury than ALT (Antoine et al. 2013; Antoine et al. 2012; Antoine et al. 2009b; Starkey Lewis et al. 2011; Zhang et al. 2010). Surprisingly, circulating biomarkers are not routinely analysed during initial *in vitro* drug screening, with different criteria used *in vitro* to determine the likelihood of a compound being hepatotoxic. This could be an inadequacy of the biomarkers, the *in vitro* models, or both. Furthermore, despite building evidence in support of these novel biomarkers of DILI, there is still more research needed into their use *in vitro.* Research into HMGB1, keratin 18 and miR-122 in preclinical liver models could further scientists' understanding of their mechanisms of release and role during liver injury, as well as potentially aiding the sensitivity of *in vitro* models used for safety testing.

In this chapter, the first aim was to determine the sensitivity of C3A spheroids to a panel of human hepatotoxins and compare this to corresponding 2D and 3D liver models. Secondly, it was investigated whether including NPC in C3A spheroids would further improve the ability of the model to detect hepatotoxins. Finally, there was an investigation into whether novel DILI biomarkers could be quantified from spheroid cultures and whether or not this analysis could enhance the predictive value of the model as well as giving additional insight into the type of cellular injury occurring after treatment with hepatotoxins.

Hypothesis 1: Spheroids will be sensitive to a range of hepatotoxic compounds and will show increased susceptibility to this toxicity compared to 2D monolayer cells.

Hypothesis 2: Spheroids co-cultured with NPC will have an enhanced susceptibility to hepatotoxins, detecting a higher number of DILI compounds than monoculture spheroids.

Hypothesis 3: The quantification of novel biomarkers *in vitro* will increase the sensitivity of the model and provide additional information as to the mechanism of cell death caused by hepatotoxins.

4.2 Materials and Methods

L-glutamine, RPMI-1640, PBS and all drug compounds were purchased from Sigma Aldrich, Missouri, USA. LSEC were purchased cryopreserved from ScienCell, Carlsbad, CA, USA. THP-1 cells were purchased cryopreserved from The European Collection of Authenticated Cell Cultures, Salisbury, UK. Cell Titer-Glo assay was purchased from Promega, Madison, USA. M6 keratin 18 antibody was purchased from Peviva, Stockholm, Sweden. Endothelial cell medium and bovine plasma fibronectin was purchased from Caltag Medsystems, Buckingham, UK. White 96-well flat-bottomed plates were purchased from Greiner Bio-One, Stonehouse, UK. HMGB1 rabbit polyclonal antibody and CD31 antibody were purchased from Abcam, Cambridge, UK.

4.2.1 Cell culture

C3A cells were maintained and cultured in monolayers as previously described (Section 2.2.1). LSEC were maintained in endothelial cell medium on fibronectin coated cell culture flasks. THP1 cells were cultured in RPMI-1640 supplemented with 1 % L-glutamine and 1 % penicillin-streptomycin and all cells were cultured in standard conditions. For 2D monolayer experiments cells were used at 100 % confluence.

4.2.2 Spheroid formation and culture

Spheroids were created using the LOT from 1000 C3A cells as described previously (Section 2.2.1). LSEC co-culture spheroids were formed by seeding 850 C3A cells and 150 LSEC/well in 50 % supplemented EMEM/ 50 % endothelial cell medium (media optimised for maximal cell viability, data not shown), centrifuged at 1000 rpm and incubated for 72 hours to form spheroids. THP1 co-culture spheroids were created by seeding 1000 THP1 cells/well onto 830 C3A cell spheroids in 50 %

supplemented EMEM/ 50 % supplemented RPMI-1640 (media optimised for maximal cell viability, data not shown) and allowing the cells to infiltrate throughout the spheroid for at least 24 hours (24 hours gave maximum cell infiltration, data not shown). Tri-culture spheroids were created by infiltrating THP1 cells into LSEC co-culture spheroids as above.

4.2.3 Visualisation of compound penetration throughout spheroids

Spheroids were treated with 3 µg/mL doxorubicin for 24 hours. Spheroids were washed in PBS, fixed in 4 % PFA for 1 hour then incubated with Hoechst diluted 1:5000 in 0.1 % Triton X-100 /1 % BSA in TBST for 1 hour. Spheroids were imaged in 3D by LightSheet fluorescence microscopy (Zeiss LightSheet Z.1).

4.2.4 Hepatotoxin treatment of spheroids

Spheroids were treated at day 3 or day 10 of culture with hepatotoxic compounds diluted in 0.5 % DMSO in medium for 4 days with repeat dosing after 2 days. 2D monolayer C3A cells were treated with compounds for 24 hours.

4.2.5 Cell viability analysis

Cell viability was analysed using the Cell Titer-Glo assay (Promega) according to the manufacturer's instructions. 100 µL of Cell Titer-Glo reagent was added to spheroids or monolayers in 100 µL media. For spheroids the plates were then agitated using an orbital shaker at 55 rpm for 15 min to induce cell lysis. 100 µL lysate was transferred to a white 96-well flat-bottomed plate and the luminescence measured by a microplate reader (Thermo Scientific Varioskan Flash). Media alone with Cell Titre-Glo reagent was used as a blank control and subtracted from sample values. Cell viability was calculated as a percentage of untreated vehicle control samples. Three replicates were used for each experiment (n=3). A dose-response curve was plotted and IC_{50} and IC_{10} values determined from the curve or

extrapolated. The likelihood of the compound causing DILI was predicted by calculating Cytotoxicity-based Safety Margin (SM) = IC_{10} / C_{max} in order to account for compound exposure and compounds with a SM value below 20 were determined hepatotoxic (Bell et al. 2016; Richert et al. 2016; Sison-Young et al. 2016). C_{max} values and IC_{10} values from InSphero human hepatocyte spheroid data were obtained from the collaboration with AstraZeneca.

4.2.6 Visualisation of NPC in spheroids

Immunofluorescent analysis of spheroids was performed as previously described (Section 2.2.7) in order to visualise NPC. CD31 primary antibody was used at 1:50 dilution to detect LSEC. THP1 cells were pre-incubated with 5 µM CMFDA (cell tracker) for 30 min, then washed once in RPMI-1640 before seeding onto C3A spheroids.

4.2.7 Preparation of cell lysates

Cell lysates were prepared as previously described (Section 3.2.3).

4.2.8 Bradford assay for quantification of protein content

Bradford assays were performed as previously described (Section 3.2.4).

4.2.9 Biomarker quantification from cell lysates by western blot

Western blots were performed as previously described (3.2.5). Antibody concentrations were as follows: HMGB1 (1:1000), GAPDH (1:10000), M6 for ck18 (1:500). Membranes were stripped using 2 % SDS 0.7 % β-mercaptoethanol, 12.5 % 0.5 M Tris and re-probed using M6 for fk18 (1:5000) for 1 hour. GAPDH was analysed to ensure even loading of samples.

4.2.10 Keratin 18 cell death quantification from spheroid supernatant by ELISA

Spheroids were pooled (20 replicates) and supernatant separated from cell mass. Keratin 18 was quantified in supernatant using M65 and M30 ELISA kits as previously described (Section 2.2.5).

4.2.11 miR-122 quantification from spheroid supernatant by PCR

Spheroids were pooled (20 replicates) and supernatant separated from cell mass. miR-122 quantification was performed by Joanna Clarke, Department of Molecular and Clinical Pharmacology, University of Liverpool, as previously described (Starkey Lewis et al. 2011). Briefly miR was firstly extracted and purified using a miRNeasy kit followed by RNeasy MinElute Cleanup Kit (Qiagen). Reverse transcription and real-time quantitative PCR were then performed using Taqman.

4.2.12 Statistical analysis

Data are representative of at least three independent experiments (n=3) and expressed as mean ± SEM. Graphs and statistical analyses were performed using GraphPad Prism 5. A Shapiro-Wilk normality test was performed on all data sets. Data which passed normality tests underwent analysis by a two-way ANOVA, those which did not underwent a non-parametric Kruskal-Wallis test. Significance was determined from a p value < 0.05. **** p<0.0001, *** p< 0.001 ** p<0.01, * p< 0.05. Sensitivity was calculated as the number of true positives ÷ (number of true positives + number of false negatives). Specificity was calculated as the number of true negatives ÷ (number of true negatives + number of false positives).

4.3 Results

4.3.1 Drug penetration throughout the spheroids

The first investigation was to confirm compound penetration and ascertain whether or not all the cells within the spheroids are being exposed to compounds added exogenously. A C3A spheroid, with a diameter of approximately 200 µm, was treated with doxorubicin and imaged using LightSheet microscopy in order to analyse compound penetration. Doxorubicin was chosen as this is an autofluorescent chemotherapeutic compound and therefore its penetration throughout the spheroid could be easily visualised. Separate images were taken throughout the z-plane of the spheroid to visualise throughout the entire spheroid core. Figure 4.1 shows the spheroid after treatment with doxorubicin (green) for 24 hours, with nuclei shown in blue. Doxorubicin can be seen fluorescing throughout the spheroid core in the median section through the spheroid (Figure 4.1A), as well as throughout the periphery (Figure 4.1B), thus confirming that this compound is likely in contact with every cell in the spheroid and that the drug response observed is present within all cells.

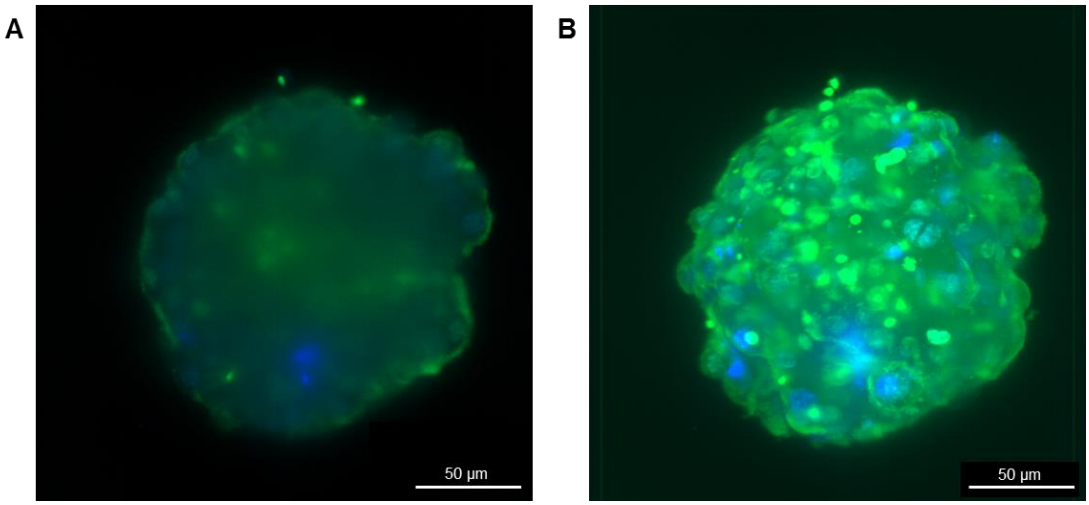

Figure 4.1. Drug penetration throughout the spheroid. Spheroids were cultured by LOT, treated with 3 µg/ml doxorubicin (green) for 24 hours, fixed, stained with Hoechst (blue) to stain the nuclei and imaged by Zeiss LightSheet Z.1 microscope at 40 × magnification. (**A**) Represents a mid-section through the spheroid and; (**B**) a maximum projection image. Scale bars = 50 µm.

4.3.2 Sensitivity of C3A spheroids to human hepatotoxins compared to 2D C3A cells

Cell viability was analysed after drug treatment in order to determine the toxicological effect of the drug on C3A spheroids. Spheroids and C3A cells cultured in a 2D monolayer were first treated with varying concentrations of four hepatotoxic compounds, acetaminophen, diclofenac, fialuridine and trovafloxacin. A 4 day repeat-dosing regimen could be used for spheroids, as their viability over this period was previously confirmed, however 2D cultures were given acute doses as these cells become over-confluent and lose viability once cultured for over 48 hours. A dose-dependent reduction in cell viability, determined by measuring ATP levels, was observed in the spheroids in response to all four hepatotoxins (Figure 4.2, black circle). Acetaminophen, diclofenac, trovafloxacin and fialuridine were all significantly more toxic to C3A spheroids than C3A monolayers, indicated by significantly lower cell viability (Figure 4.2). IC_{50} values, the concentration at which a 50 % reduction in cell viability is observed, were calculated from this data and listed in Table 4.1. Acetaminophen had an IC_{50} value of 7212 µM in spheroids and 33,826 µM in monolayers. Spheroids were also significantly more sensitive to trovafloxacin, with an IC_{50} value of 65 µM in spheroids compared to 440 µM in 2D cultures, as well as fialuridine, which had an IC_{50} value of 251 µM in 3D culture and 380 µM in 2D (Table 4.1). In the monolayer cultures diclofenac did not have a toxic response at the concentrations used, although the IC_{50} value is reported to be around 763 µM in HepG2 monolayer cultures (Bort et al. 1999) and was found to be 295 µM in the C3A spheroids (Table 4.1).

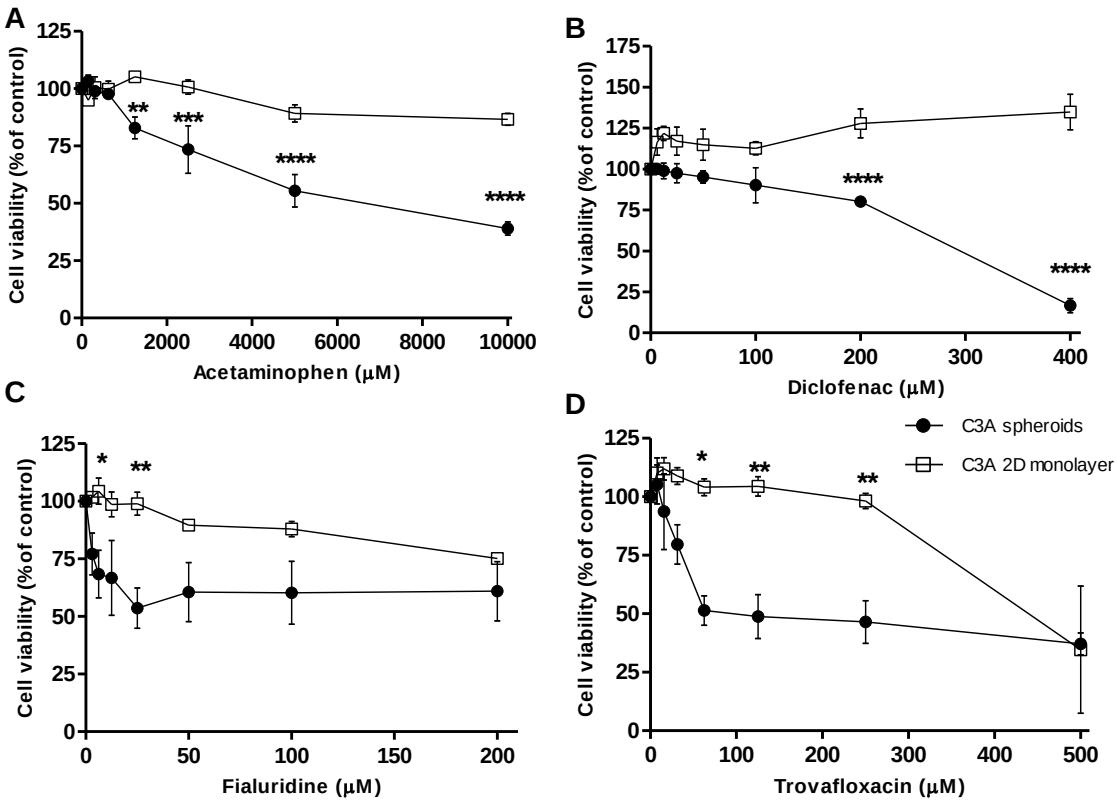

Figure 4.2. Spheroids show a toxic response to hepatotoxins. Spheroids and 2D C3A cells were treated with (**A**) acetaminophen; (**B**) diclofenac; (**C**) fialuridine and (**D**) trovafloxacin. Cell viability was analysed and plotted as a percentage of vehicle control. Data are represented as mean ± SEM, **** p<0.0001, *** p<0.001, ** p<0.01, * p<0.05 (n=3 in triplicate).

Compound	IC_{50} value in C3A spheroids (µM) 4 day repeat dosing	IC_{50} value in C3A 2D monolayer (µM) 24 hr acute dosing
Acetaminophen	7212 **	33,826
Diclofenac	295 ***	> 400
Fialuridine	251	380
Trovafloxacin	65	440

Table 4.1. The sensitivity of spheroids and 2D C3A cells to hepatotoxins. Spheroids and 2D C3A cells were treated with four hepatotoxins. Cell viability was analysed and IC_{50} values calculated. Data are represented as mean values, **** p<0.0001, *** p<0.001, ** p<0.01, (n=3 in triplicate).

In order to determine whether culture time or spheroid size affected the response of the spheroids to hepatotoxins, this toxicological analysis was repeated on 10 day old spheroids. Figure 4.3 shows that there was no significant difference between the toxicological response of the spheroids to acetaminophen, diclofenac, fialuridine or trovafloxacin at day 3 or day 10 of culture.

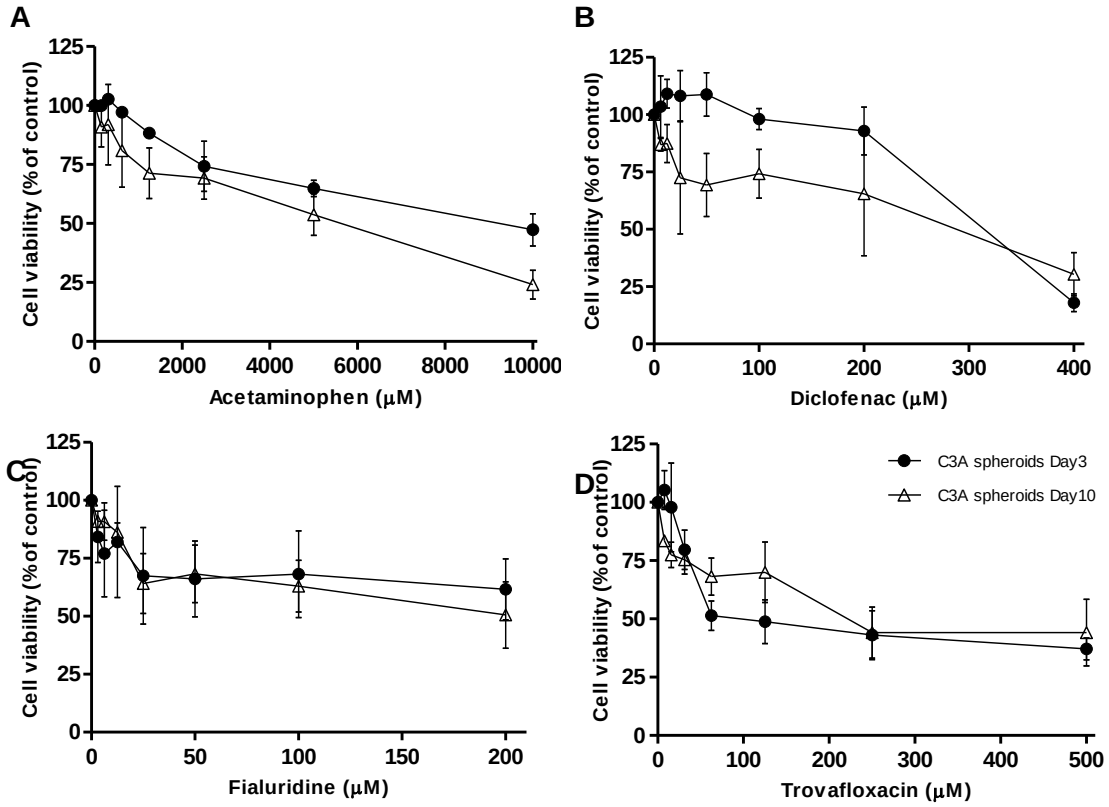

Figure 4.3. Culture time does not affect spheroids response to hepatotoxins. Spheroids were cultured for 3 days or 10 days, and treated with (**A**) acetaminophen; (**B**) diclofenac; (**C**) fialuridine and (**D**) trovafloxacin. Cell viability was analysed and plotted as a percentage of untreated control. Data are represented as mean ± SEM (n=3 in triplicate).

Subsequently, a further eleven compounds were analysed in the C3A spheroids, eight of which are known to cause clinical liver injury and three which acted as DILI negative compounds. These compounds were chosen due to their broad mechanisms of action, range of DILI symptoms and inability to be detected preclinically. Table 4.2 provides information of each of the hepatotoxic compounds tested. All DILI compounds caused a toxic response in C3A spheroids to some degree, confirmed by a dose-dependent decrease in cell viability (Figure 4.4 A-H). IC_{50} values were calculated for each compound and compared to values obtained from literature for a 2D C3A or HepG2 model, as well as 2D and sandwich cultured human hepatocyte models (Table 4.3). Every compound other than amiodarone and pioglitazone had a lower IC_{50} value in spheroids than that reported for a 2D C3A or HepG2 cell model (Bort et al. 1999; Donato et al. 2008; Ju et al. 2015; Lin and Will 2012). Interestingly, IC_{50} values for 9 out of 12 compounds were lower in spheroids than those reported in human hepatocyte cultures, with fialuridine, nefazodone, tolcapone, entacapone and perhexiline even lower than in sandwich cultured hepatocytes. One of the negative DILI compounds was non-toxic to the spheroids at the concentrations tested, the other two had a similar effect in spheroids as reported for 2D cultures.

Compound	DILI undetected in:	Clinical DILI	Proposed mechanism of action	References
Acetaminophen	Clinical trials	Fatal liver failure	Reactive metabolite	(Ju et al. 2015; Tujios and Fontana 2011)
Diclofenac	Clinical trials	High concern DILI, acute or chronic liver disease	Immunoallergic, mitochondrial dysfunction, reactive metabolite, transporter inhibition	(Boelsterli 2003; Bort et al. 1999; Kia et al. 2015; Tujios and Fontana 2011)
Fialuridine	Preclinical screening	Fatal liver injury	Mitochondrial dysfunction	(Honkoop et al. 1997; McKenzie et al. 1995)
Trovafloxacin	Clinical trials	Hepatotoxicity and liver failure	Inflammatory stress	(Beggs et al. 2014; Shaw et al. 2010)
Ximelagatran	Clinical trials	Elevated DILI biomarkers and hepatotoxicity	Unknown	(Keisu and Andersson 2010; Schutzer et al. 2004)
Nefazodone	Clinical trials	Severe DILI, black box warning, fatal liver injury	Toxic metabolites, transporter inhibition	(Choi 2003; Kalgutkar et al. 2005; Kostrubsky et al. 2006; O'Brien et al. 2006)
Bosentan	Clinical trials	Severe DILI, black box warning, rare	Transporter inhibition	(Eriksson et al. 2011; Fattinger et al. 2001; Lea et al. 2016)
Amiodarone	Clinical trials	Severe DILI, black box warning, fatty liver disease, phospholipidosis	Mitochondrial dysfunction, lysosomal dysfunction, toxic metabolite	(Bandyopadhyay et al. 1990; Begriche et al. 2011; Dake et al. 1985; Kia et al. 2015; Zahno et al. 2011)
Troglitazone	Clinical trials	Severe DILI, acute liver failure, withdrawn	Toxic metabolite, mitochondrial injury, lysosomal dysfunction, transporter inhibition	(Kaplowitz 2005; Loi et al. 1999; Loi et al. 1997; Smith 2003)
Tolcapone	Clinical trials	Severe DILI, withdrawn, fatal acute liver injury	Toxic metabolite, transporter inhibition	(Borges 2003; Gebhardt 1992; Jorga et al. 1999; Olanow 2000)
Entacapone	Clinical trials	Elevated DILI biomarkers, hepatotoxicity	Unknown	(Fisher et al. 2002)
Perhexiline	Clinical trials	Severe DILI, withdrawn	Improper metabolism and excretion, transporter inhibition, lysosomal dysfunction	(Amoah et al. 1986; Ashrafian et al. 2007; Fromenty and Pessayre 1997)

Table 4.2. DILI compounds. A range of hepatotoxins, their clinical manifestations and suggested mechanisms of action.

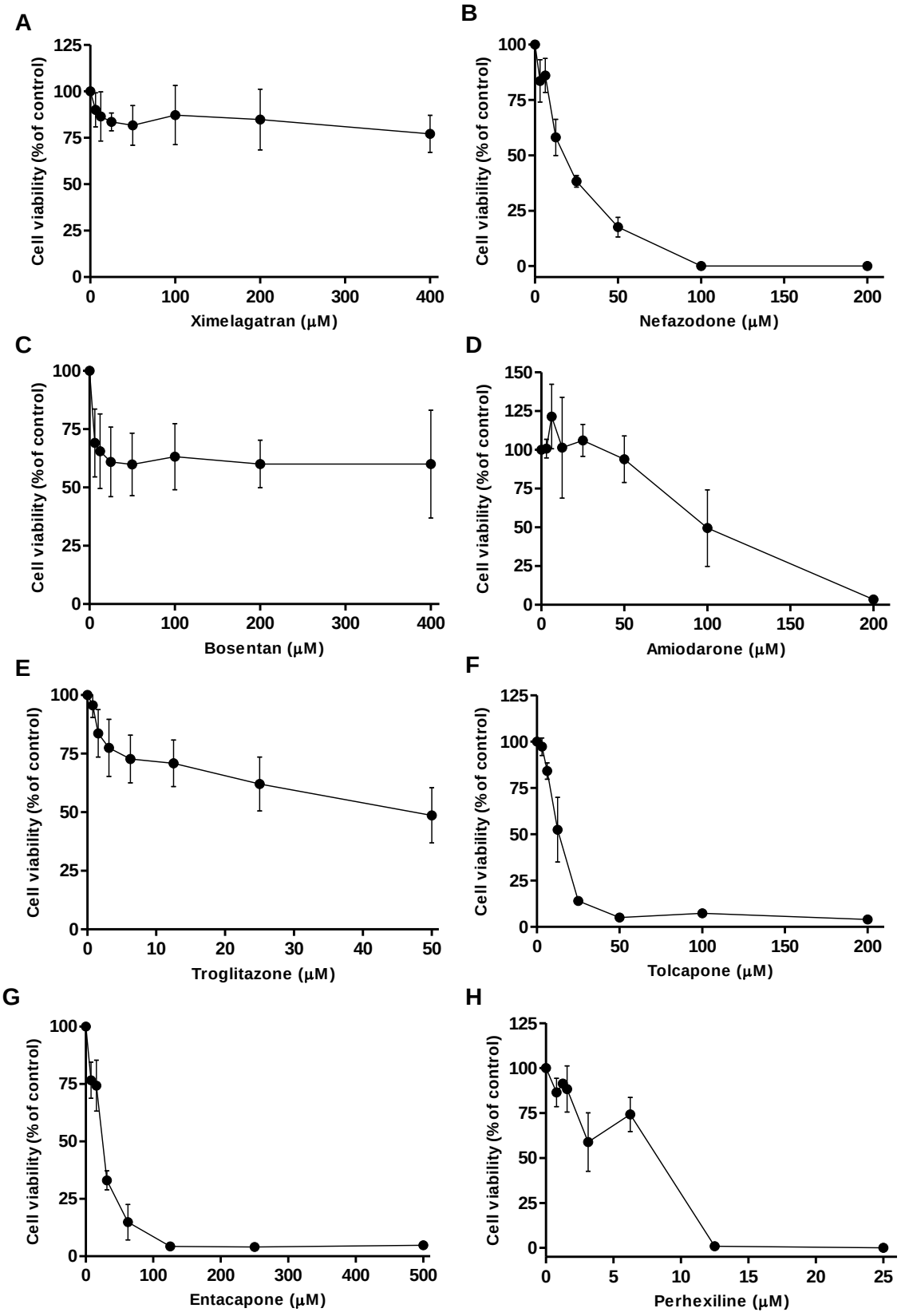
A
Cell viability (% of control)
Ximelagatran (μM)
B
Cell viability (% of control)
Nefazodone (μM)
C
Cell viability (% of control)
Bosentan (μM)
D
Cell viability (% of control)
Amiodarone (μM)
E
Cell viability (% of control)
Troglitazone (μM)
F
Cell viability (% of control)
Tolcapone (μM)
G
Cell viability (% of control)
Entacapone (μM)
H
Cell viability (% of control)
Perhexiline (μM)

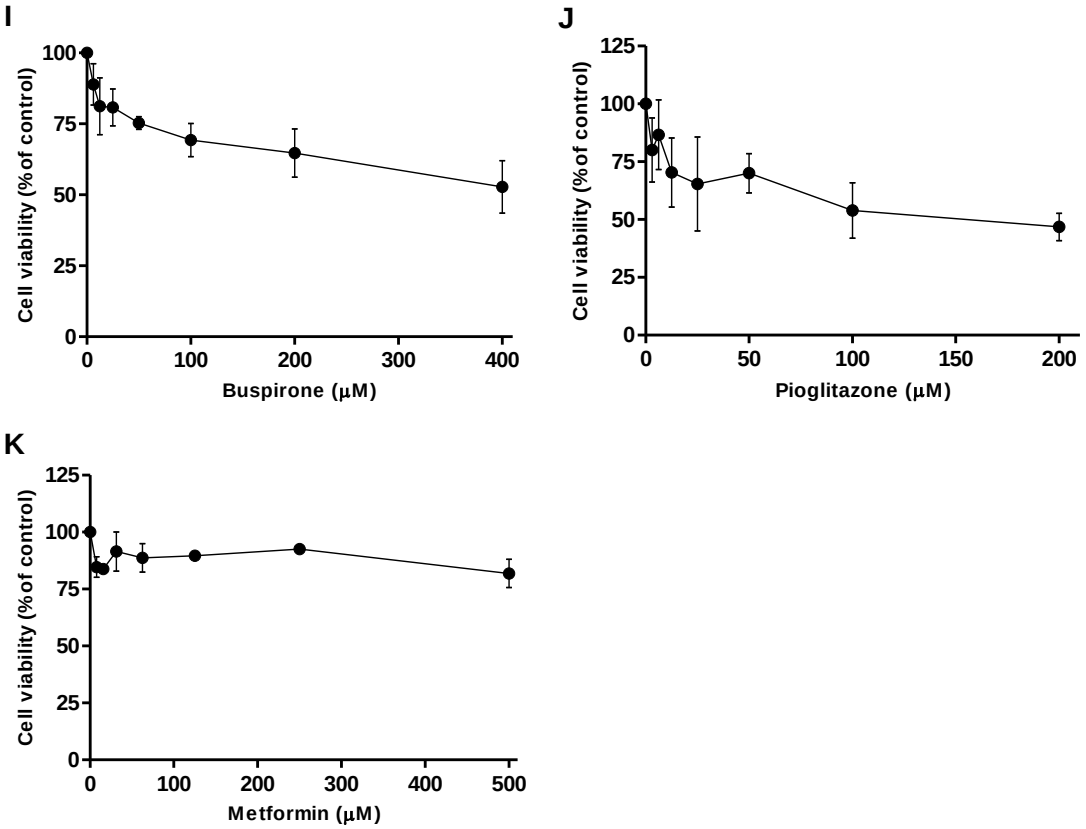

Figure 4.4. Spheroids show a toxic response to a range of hepatotoxins. Spheroids were treated with (**A-H**) eight additional hepatotoxins and (**I-K**) three negative DILI controls. Cell viability was analysed and plotted as a percentage of vehicle control. Data are represented as mean ± SEM (n=3 in triplicate).

Compound	IC_{50} value in C3A spheroids (μM) 4 day repeat dosing	Published IC_{50} value for C3A/HepG2 2D monolayer (μM)	Published IC_{50} value in human hepatocyte 2D/ sandwich (μM)	Reference
Acetaminophen	7212	22,800	20,000 / 3000	(Ju et al. 2015; Richert et al. 2016)
Diclofenac	295	763	400 / 200	(Bort et al. 1999; Richert et al. 2016)
Fialuridine	206	> 400	> 1000	(Richert et al. 2016)
Trovafloxacin	65	> 1000	> 200 / 200	(Ramaiahgari et al. 2014; Richert et al. 2016)
Ximelagatran	> 400	> 500	> 200 / 150	(Kamalian et al. 2015; Richert et al. 2016)
Nefazodone	15	20	20	(Lin and Will 2012; Richert et al. 2016)
Bosentan	> 400	> 3000	> 200	(Ramaiahgari et al. 2014)
Amiodarone	98	>500	> 200 / 20	(Donato et al. 2008; Lin and Will 2012)
Troglitazone	43	121	15	(Lin and Will 2012; Richert et al. 2016)
Tolcapone	11	> 500	20 / 17	(Kamalian et al. 2015; Richert et al. 2016)
Entacapone	22	> 500	200 / 22	(Kamalian et al. 2015)
Perhexiline	8	10	12	(Kamalian et al. 2015; Richert et al. 2016)
Buspirone	386	> 500	> 200	(Donato et al. 2008)
Pioglitazone	145	> 100	> 200	(Lin and Will 2012; Richert et al. 2016)
Metformin	> 500	> 500	> 1000	(Kamalian et al. 2015; Richert et al. 2016)

Table 4.3. The sensitivity of spheroids to hepatotoxins. Spheroids were treated with twelve known hepatotoxins and three negative DILI controls (red). Cell viability was analysed IC_{50} values calculated. 2D monolayer IC_{50} values for C3A/ HepG2 or human hepatocytes were obtained from literature. Data are represented as mean values.

4.3.3 Toxicological predictivity of C3A spheroids compared to human hepatocyte spheroids

Human hepatocyte spheroid data was obtained from AstraZeneca. The same 15 compounds were tested using the same repeat-dosing protocol on InSphero primary human hepatocyte spheroids. When comparing IC_{10} values C3A spheroids were more sensitive than InSphero spheroids to all but three hepatotoxins, acetaminophen, diclofenac and amiodarone (Table 4.4). For example trovafloxacin had an IC_{10} values of 22 µM in C3A spheroids compared to 100 µM in InSphero spheroids, and fialuridine caused no toxicity whatsoever in the InSphero spheroids, whereas a decline in cell viability was detected in the C3A model. The cytotoxicity safety margin (SM) was calculated from the highest non-toxic concentrations (IC_{10}) and known exposure values (C_{max}) as published previously (Mueller et al. 2015; Richert et al. 2016; Sison-Young et al. 2016) and an SM value lower than 20 indicated a risk of DILI. Table 4.4 lists the SM values for C3A or InSphero spheroids, with DILI risk indicated in green. Using data from InSphero human hepatocyte spheroids, 8 out of 12 compounds were correctly detected as hepatotoxic. C3A spheroids successfully detected 10 out of 12 compounds to have a risk of DILI, leaving only ximelegatran and amiodarone going undetected. However one of the non- DILI compounds were falsely detected as having a risk of DILI in C3A spheroids. This corresponded to a sensitivity of 90.9 % and specificity of 66 % for C3A spheroids, and sensitivity of 88 % and specificity of 66 % for the InSphero spheroids.

Compound	C_{max} (µM)	IC_{10} value (µM)		SM (DILI risk detected when SM<20)	
		InSphero spheroids	C3A spheroids	InSphero spheroids	C3A spheroids
Acetaminophen	139	300	1463	2.15	10.5
Diclofenac	7.99	50	110	6.25	13.7
Fialuridine	0.64	-	2	-	3.13
Trovafloxacin	19.7	100	22	5	1.12
Ximelagatran	0.30	30	7	100	23.3
Nefazodone	4.26	30	2	7	0.47
Bosentan	7.39	100	2	14	0.27
Amiodarone	0.81	20	42	25	51.8
Troglitazone	6.39	5	1	1	0.16
Tolcapone	47.6	20	5	0.4	0.11
Entacapone	4.34	100	5	23	1.15
Perhexiline	2.16	2	0.5	1	0.23
Buspirone	0.01	-	7	-	70
Pioglitazone	2.95	30	2	10	0.67
Metformin	7.75	-	-	-	-

Table 4.4. The ability of C3A spheroids and human hepatocyte spheroids to predict DILI risk. Spheroids were treated with twelve known hepatotoxins and three negative controls (red). Cell viability was analysed and IC_{10} values calculated. DILI risk was predicted by calculating the Cytotoxicity-based Safety Margin (SM) = IC_{10} / C_{max} and compounds with a SM value below 20 were determined hepatotoxic (indicated as green). C_{max} values were obtained from literature and InSphero human hepatocyte spheroid data obtained from AstraZeneca. Data are represented as mean values.

4.3.4 The location of NPC in co-culture spheroids

The next aim was to create a NPC co-culture spheroid model. LSEC were incorporated into the C3A spheroids at a ratio which most closely represented that seen *in vivo*, optimised to be 15 % LSEC, 85 % C3A cells. Immunofluorescence confirmed the survival and location of endothelial cells in the co-cultured spheroids for 18 days (Figure 4.5) using an endothelial-specific marker CD31. THP1 cells were infiltrated into the pre-formed C3A spheroids and were visualised to have migrated into the spheroid core and distributed throughout after a 24 hour incubation with C3A spheroids (Figure 4.6).

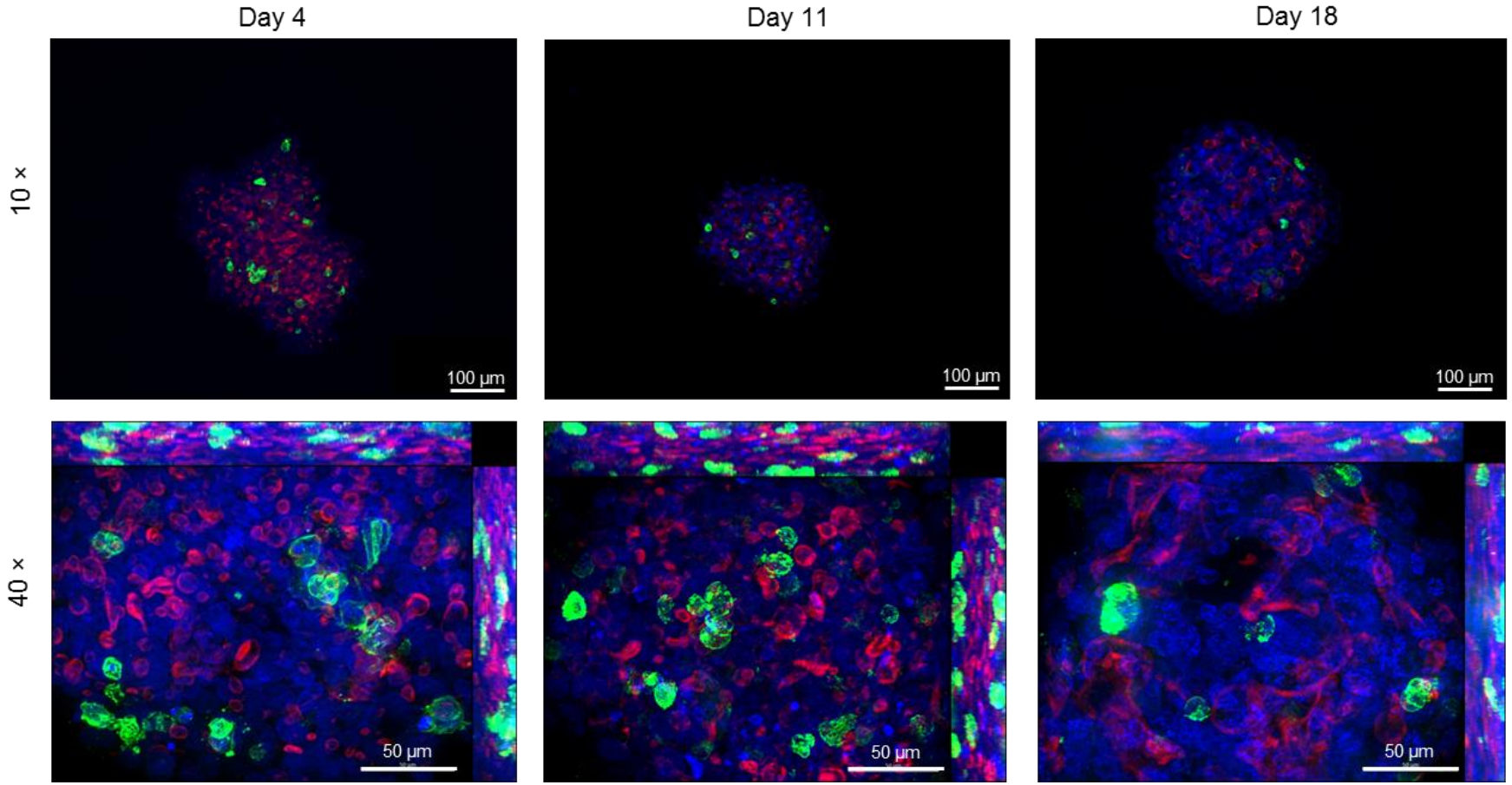

Figure 4 5. LSEC location in spheroids. LSEC co-culture spheroids were created on liquid-overlay plates and fixed at day 4, 11 and 18 of culture. Immunofluorescent staining was performed for the endothelial cell marker CD31 (green), nuclei (blue) and F-actin (red) and imaged by confocal microscopy at 10 × and 40 × and represented as maximum intensity projection images. Scale bars = 50 µm.

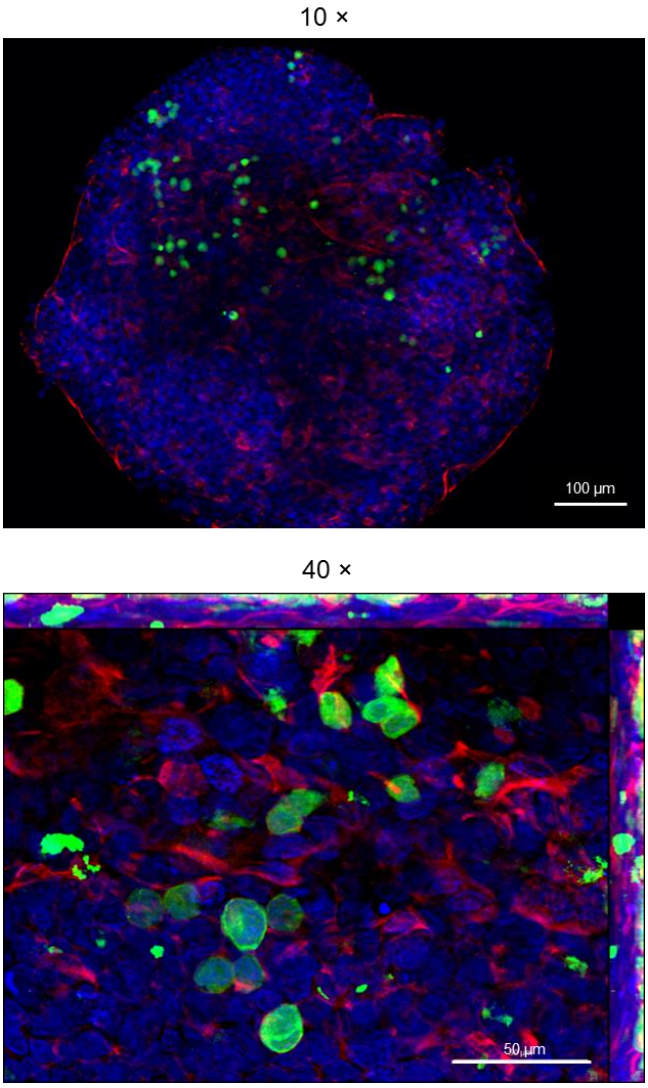

Figure 4.6. THP-1 cell infiltration into spheroids. Spheroids were created from 850 C3A cells on liquid-overlay plates and cultured for 10 days. THP-1 cells (green) were added to the spheroids and left to infiltrate for 24 hours. Spheroids were stained for nuclei (blue) and F-actin (red) and imaged by confocal microscopy at 10 × and 40 × and represented as maximum intensity projection images. Scale bars = 100 µm, 50 µm.

4.3.5 Sensitivity of NPC co-culture spheroids to human hepatotoxins

Toxicological analysis was performed using the same panel of 15 compounds as previously on both co-culture and tri-culture spheroids (Table 4.2). Both co-cultures responded in a similar manner to the hepatotoxic insult, and dose dependent toxicity was observed in all models (Figure 4.7A-L). LSEC co-culture spheroids (red) were observed to be slightly more sensitive to the majority of hepatotoxins, 9 out of 12, compared to monoculture spheroids, however not significantly. THP1 co-cultures (blue) and tri-cultures (green) also appeared to be more sensitive than both C3A and LSEC co-culture spheroids to the majority of hepatotoxins. For example, acetaminophen, diclofenac, trovafloxacin and ximelegatran caused significantly more toxicity to tri-culture spheroids than C3A monoculture spheroids at one or more concentrations. IC_{50} values for each compound were calculated as an indication of the sensitivities of each co-culture model (Table 4.5). Acetaminophen, diclofenac, fialuridine, ximelegatran, bosentan and perhexiline had lower IC_{50} values in both all NPC co-culture models compared to C3A spheroids. Troglitazone and tolcapone also had lower values in spheroids containing LSEC, and trovafloxacin had lower IC_{50} values in those incorporating THP1 cells. For example, acetaminophen had an IC_{50} value of 7212 µM in monoculture spheroids, 4400 µM in LSEC co-culture spheroids, 3200 µM in THP1 co-culture spheroids and 1700 in tri-culture spheroids (Table 4.5). When analysing the non-DILI compounds, LSEC co-culture spheroids were less sensitive to buspirone and pioglitazone than C3A spheroids, although THP1 co-culture spheroids appeared to be more sensitive to pioglitazone at high concentrations (Figure 4.7M-O and Table 4.5).

The SM for each compound was then calculated in order to determine whether DILI would be detected in each co-culture model, and compared to previous values obtained from C3A spheroids and InSphero spheroids (Table 4.6). All NPC co-culture models correctly identified amiodarone to be hepatotoxic, however

ximelagatran was still determined to be safe in all spheroid models, despite the significantly increased sensitivity (Table 4.6). Using this criteria these results determined a sensitivity of 91.6 % and a specificity of 66 % for LSEC and THP-1 co-culture spheroids, and 90.9 % sensitvity for tri-culture spheroids.

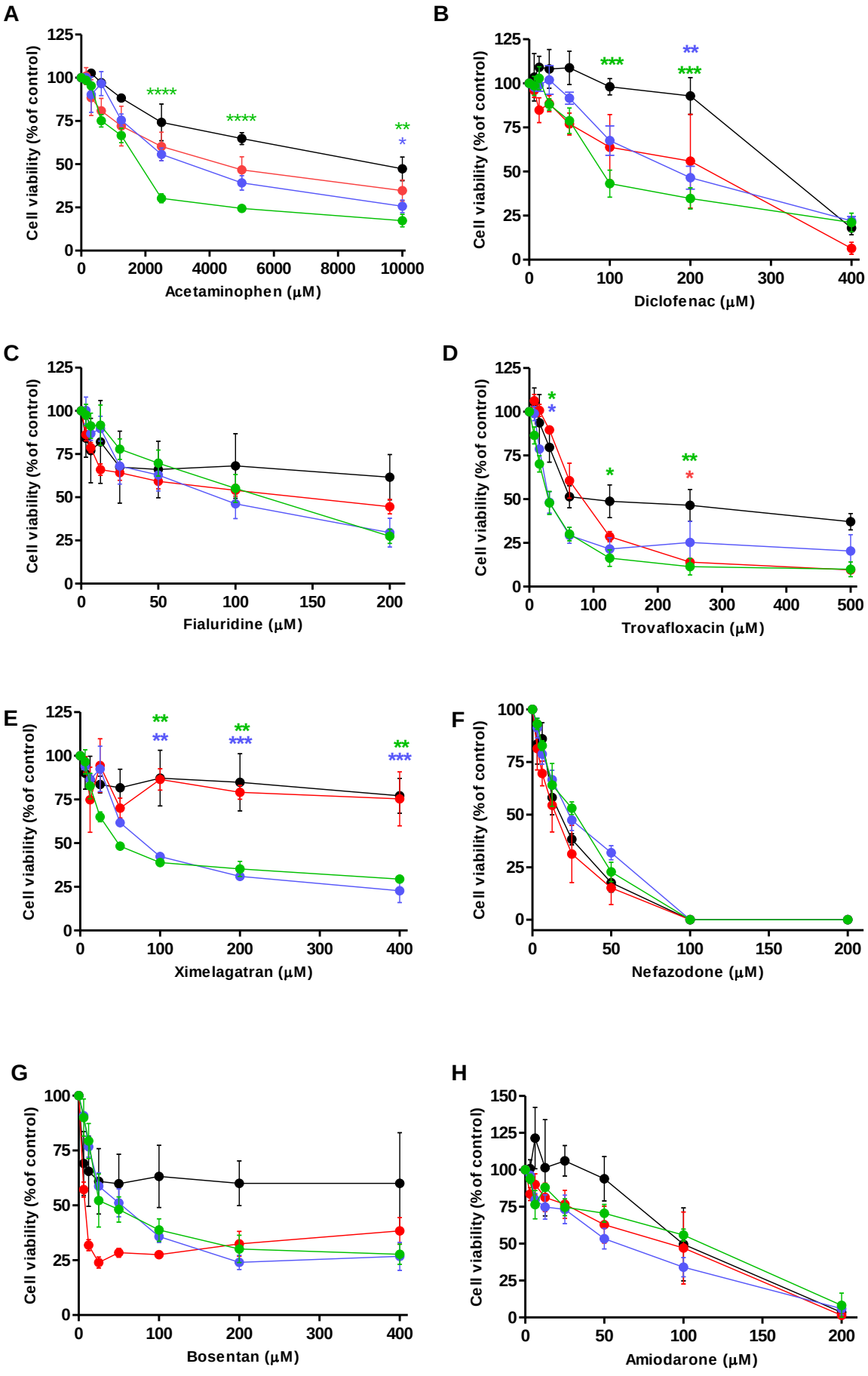
A
Cell viability (%of control)
Acetaminophen (µM)
B
Diclofenac (µM)
C
Fialuridine (µM)
D
Trovafloxacin (µM)
E
Ximelagatran (µM)
F
Nefazodone (µM)
G
Bosentan (µM)
H
Amiodarone (µM)

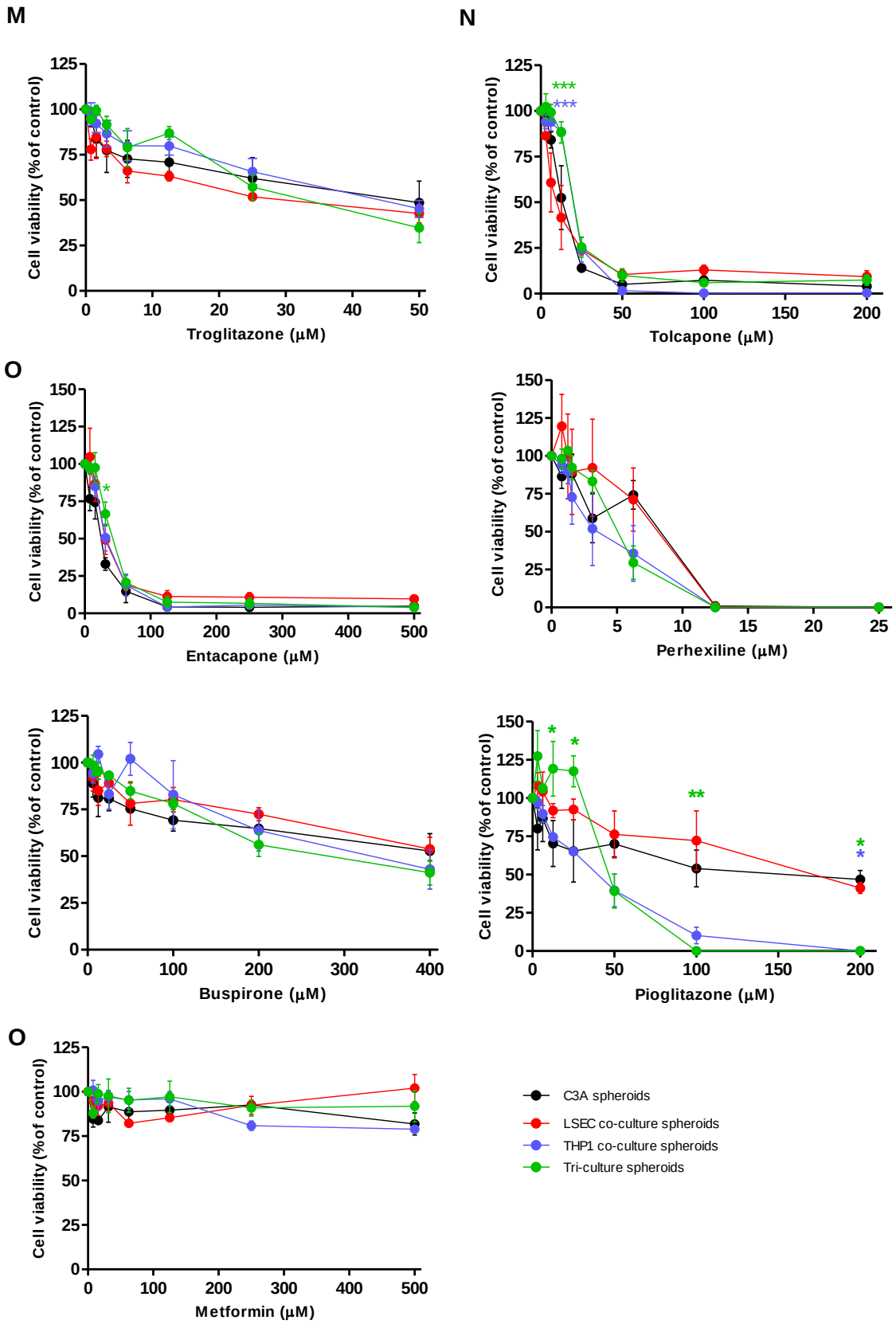

Figure 4.5. The addition of NPC leads to increased sensitivity to hepatotoxins. Co-culture and tri-culture spheroids were treated with; (**A-L**) twelve hepatotoxins; and (**M-O**) three negative DILI controls. Cell viability was analysed and plotted as a percentage of vehicle control. Data are represented as mean ± SEM, **** p<0.0001, *** p<0.001, ** p<0.01, * p<0.05 compared to C3A monoculture spheroids (n=3 in triplicate).

Compound	IC_{50} value (μM)			
	C3A spheroids	LSEC co-culture spheroids	THP1 co-culture spheroids	Tri-culture spheroids
Acetaminophen	7212	4400	3200	1700
Diclofenac	295	199	180	85
Fialuridine	219	140	85	117
Trovafloxacin	65	78	28	30
Ximelagatran	1427	581	75	45
Nefazodone	15	18	23	28
Bosentan	373	7	52	30
Amiodarone	98	89	55	113
Troglitazone	43	28	44	32
Tolcapone	11	9	18	19
Entacapone	22	25	32	40
Perhexiline	8	7.8	3.4	4.3
Buspirone	386	430	330	270
Pioglitazone	145	166	38	44
Metformin	> 500	> 500	> 500	> 500

Table 4.5. The sensitivity of NPC co-culture spheroids to hepatotoxins. Co-culture and tri-culture spheroids were treated with twelve hepatotoxins and three negative DILI controls (red). Cell viability was analysed and IC_{50} values calculated. Data are compared against IC_{50} values obtained for C3A monoculture spheroids, green indicates a lower value than C3A spheroid control, pink indicates higher value. Data are represented as mean values.

Compound	C_{max} (μM)	IC_{10} value (μM) for spheroids					SM (DILI risk detected when SM<20) for spheroids				
		InSphero	C3A	LSEC co-culture	THP1 co-culture	Tri-culture	InSphero	C3A	LSEC co-culture	THP1 co-culture	Tri-culture
Acetaminophen	139	300	1463	234	287	400	2.15	10.5	1.68	2.06	2.8
Diclofenac	7.99	50	110	13.4	52	22	6.25	13.7	1.68	6.51	2.7
Fialuridine	.64	-	2	2	7	15	-	3.13	3.13	10.9	23.4
Trovafloxacin	19.7	100	22	31	12	7	5	1.12	1.57	0.61	0.35
Ximelagatran	.30	30	7	7	15	9	100	23.3	23.3	50	30
Nefazodone	4.26	30	2	2.5	4	4	7	0.47	0.59	0.94	0.94
Bosentan	7.39	100	2	4	7	7	14	0.27	0.54	0.95	0.95
Amiodarone	.81	20	42	2	4	9	25	51.8	6.71	4.94	11.1
Troglitazone	6.39	5	1	0.5	2	3.5	1	0.16	0.08	0.31	0.55
Tolcapone	47.6	20	5	3	10	12	0.4	0.11	0.06	0.21	0.25
Entacapone	4.34	100	5	15	13	20	23	1.15	3.5	2.9	4.6
Perhexiline	2.16	2	0.5	1.5	1.1	1.3	1	0.23	0.69	0.51	0.60
Buspirone	.01	-	7	10	59	32	-	70	100	590	3200
Pioglitazone	2.95	30	2	29	6	32	10	0.67	9.8	2.0	10.8
Metformin	7.75	-	-	-	-	-	-	-	-	-	-

Table 4.6. Ability of co-culture spheroids to predict DILI risk. Co-culture and tri-culture spheroids were treated with twelve hepatotoxins and three negative DILI controls (red). Cell viability was analysed and IC_{10} values calculated. DILI was predicted by calculating the Cytotoxicity-based Safety Margin (SM) = IC_{10} / C_{max} and compounds with a SM value below 20 were determined hepatotoxic (indicated as green). C_{max} values were obtained from literature and InSphero human hepatocyte spheroid data obtained from the collaboration with AstraZeneca. Data are represented as mean values.

4.3.6 Analysis of DILI biomarkers in spheroid lysates

The next question asked was whether novel serum biomarkers could be analysed in the C3A spheroid *in vitro* model. Spheroids were treated with acetaminophen, diclofenac and fialuridine, previously shown to cause toxicity in the C3A spheroids (see Figure 4.2). HMGB1 was analysed by western blot in the spheroid and monolayer cell lysates after drug treatment. The expression of HMGB1 in the cells didn't appear to change regardless of drug type or dose (Figure 4.8). Culture condition also had no effect on HMGB1 expression.

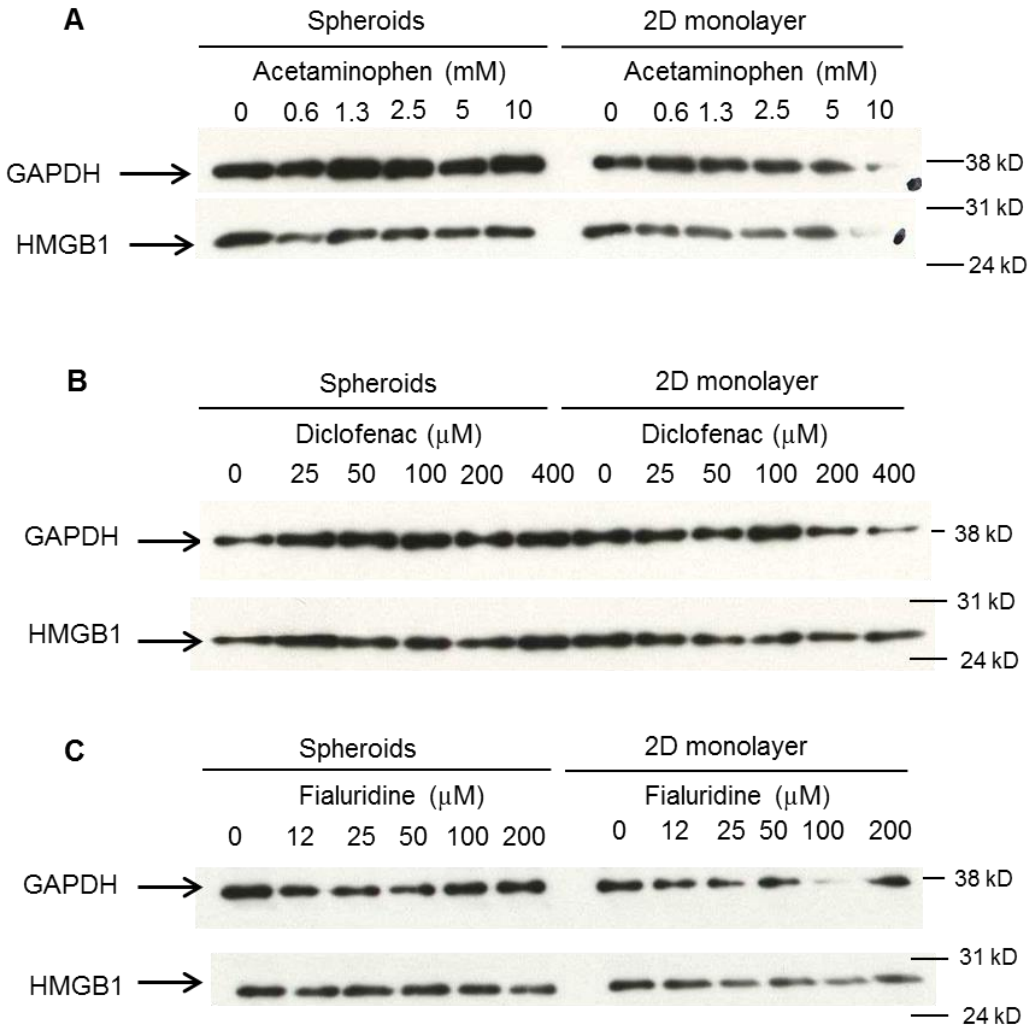

Figure 4.8. HMGB1 biomarker analysis in spheroid lysates. Spheroids and 2D C3A cells were treated with hepatotoxins (**A**) acetaminophen, (**B**) diclofenac and (**C**) fialuridine, 20 spheroids pooled, lysed and HMGB1 analysed by western blot. Data represents one experiment of three repeats.

4.3.7 Analysis of keratin 18 in spheroid supernatant

The release of apoptotic and necrotic forms of keratin 18 were then analysed from spheroid supernatant after treatment with four hepatotoxins previously shown to cause cell death in C3A spheroids (see Figure 4.2). Apoptosis was determined using ck18 concentrations and necrosis determined by subtracting ck18 values from total keratin 18. A dose dependent increase in apoptosis was observed after spheroids were treated with all four compounds (Figure 4.9A and B). This correlated well with previous cell viability data (Figure 4.2). Necrosis did not show the same correlation, as levels fluctuated from dose to dose for every compound. For fialuridine, although overall cell death was unchanged the levels of necrosis appeared to decrease as fialuridine concentration increased. This was repeated on C3A cells cultured in 2D, giving slightly different results to spheroids. Much smaller changes in apoptosis were observed after acetaminophen and diclofenac concentrations increased, and concentrations of necrosis followed no clear trend for any of the compounds (Figure 4.9A and B). Overall, the levels of apoptosis and necrosis were similar whether cells were cultured in 2D or 3D, despite the previous observation of difference in sensitivity of the two models (Figure 4.2).

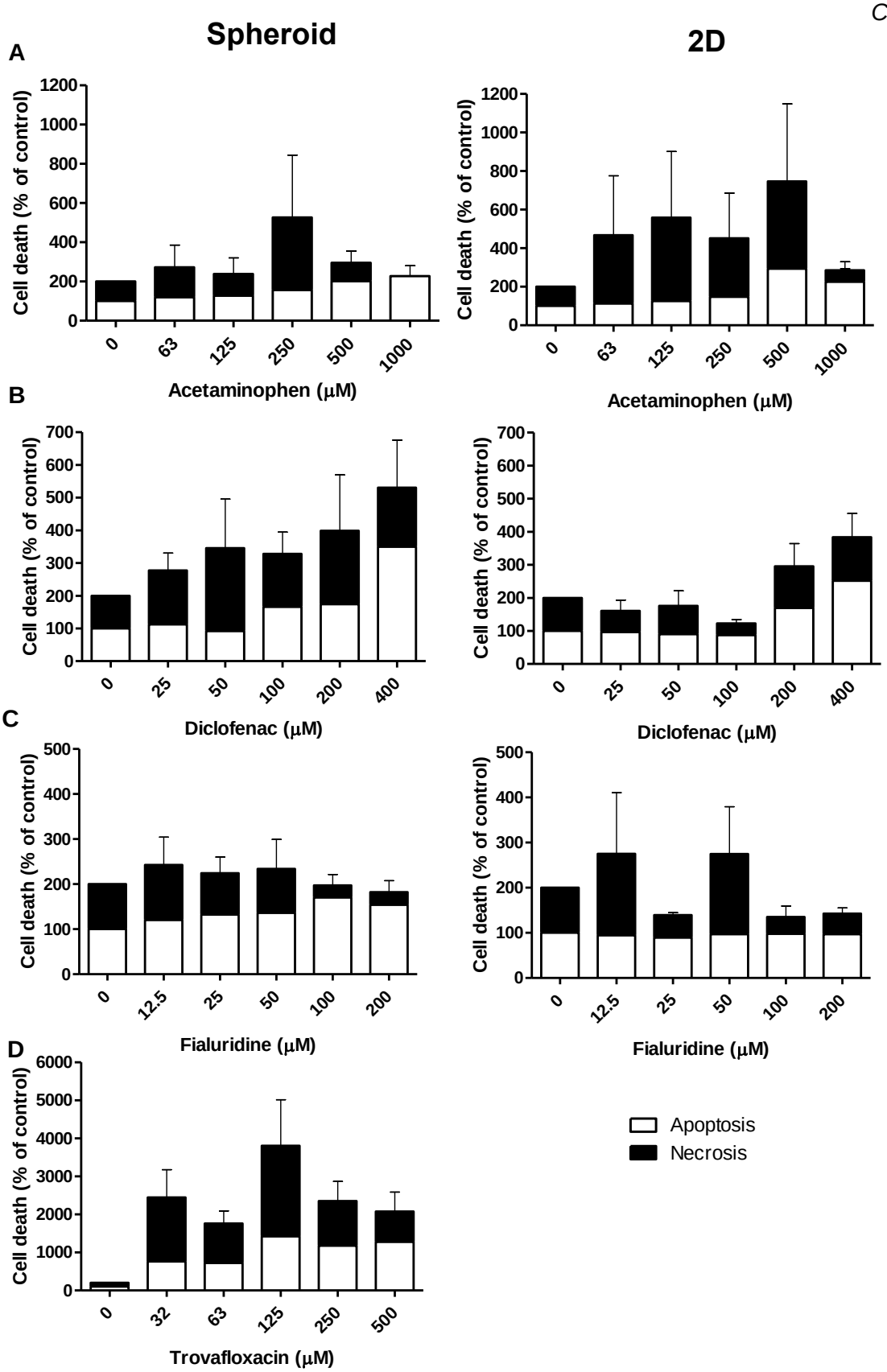

Figure 4.9. Keratin 18 biomarker release from spheroids. Spheroids and 2D C3A cells were treated with hepatotoxins (**A**) acetaminophen, (**B**) diclofenac, (**C**) fialuridine and (**D**) trovafloxacin, 20 spheroids pooled and supernatant analysed for keratin 18 by ELISA. Apoptosis was calculated from ck18 quantification and necrosis calculated from ck18 subtracted from total keratin 18. Data are represented as mean ± SEM (n=3 using 20 replicates) as a percentage of vehicle control.

Out of interest this analysis was repeated on supernatant from THP1 co-culture spheroids (Figure 4.10). A similar pattern of apoptotic ck18 release was observed, showing a dose-dependent increase. However, again necrosis did not correlate with the concentration of any of the drugs or overall cell viability from previous analysis (Figure 4.2). The apoptosis observed from THP1 co-culture spheroids was also significantly higher than that in C3A spheroids, correlating with the increased toxicity previously observed in the co-culture model (Figure 4.7).

miR-122 was analysed in the supernatant of spheroids treated with the same hepatotoxins, however negligible levels were detected in all of the samples (data not shown).

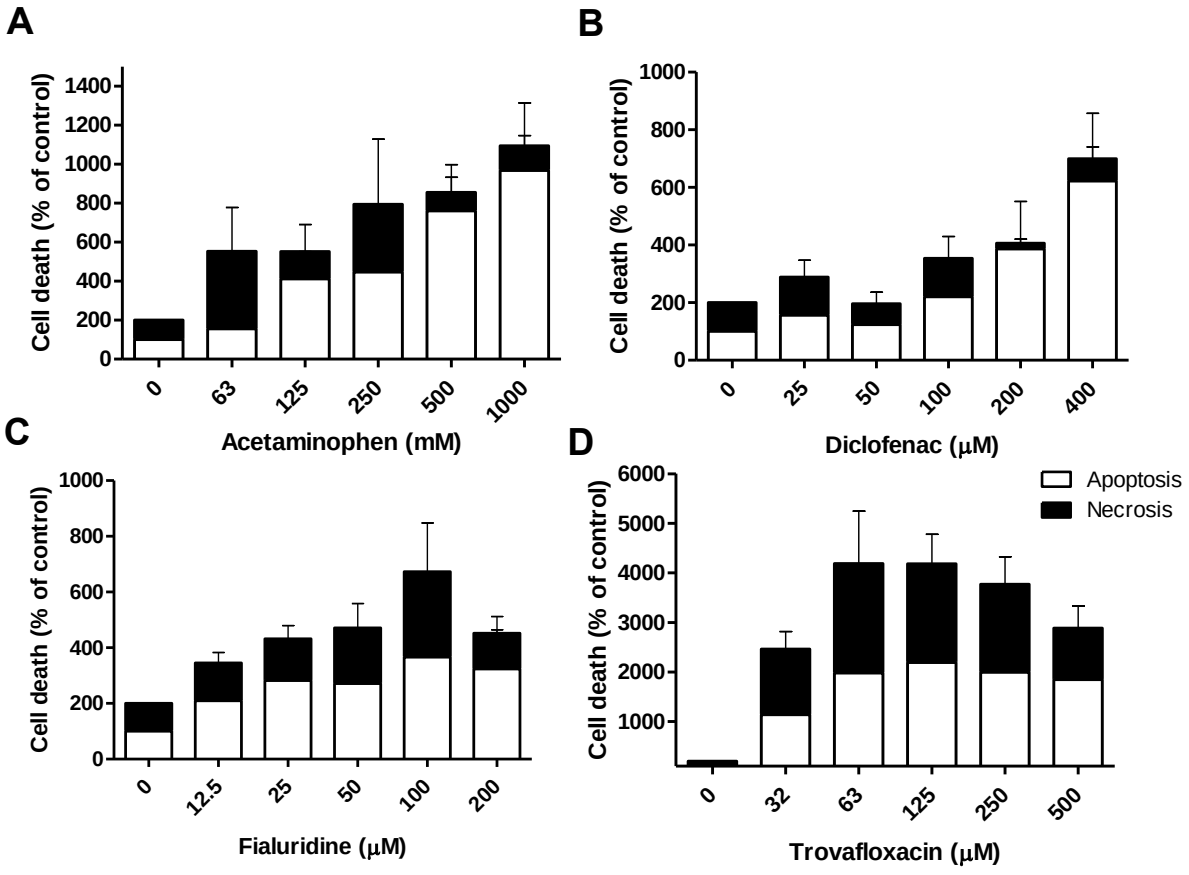

Figure 4.10. Keratin 18 biomarker release from THP1 co-culture spheroids. THP1 co-culture spheroids were treated with hepatotoxins (**A**) acetaminophen, (**B**) diclofenac, (**C**) fialuridine and (**D**) trovafloxacin, 20 spheroids pooled and supernatant analysed for keratin 18 by ELISA. Apoptosis was calculated from ck18 quantification and necrosis calculated from ck18 subtracted from total keratin 18. Data are represented as mean ± SEM (n=3 using 20 replicates) as a percentage of vehicle control.

4.4 Discussion

Compounds can cause DILI by a multitude of different mechanisms. For example, some hepatotoxins cause dysfunction of transporters or loss of structural integrity, such as diclofenac, nefazodone, bosentan, troglitazone and tolcapone (Fattinger et al. 2001; Kostrubsky et al. 2006; Smith 2003; Stricker 1992; Tujios and Fontana 2011). Consequentially bile is not effectively secreted into the bile ducts and toxic substances can build-up in and around the hepatocytes (Fattinger et al. 2001; Kaplowitz 2005; Kostrubsky et al. 2006; Kullak-Ublick 2000-2013; Tujios and Fontana 2011). As observed previously, C3A spheroids showed correct localisation of bile canalicular structures and transporter function, hence it could be predicted that any cholestatic compound interfering with this would be detected in the spheroids.

On the other hand it is often the metabolite of a compound which causes damage to the liver, being directly hepatotoxic or forming adducts with liver proteins. Examples of compounds with this as a suggested mechanism of toxicity include acetaminophen, diclofenac, nefazodone, amiodarone, perhexiline, tolcapone and troglitazone (Ashrafian et al. 2007; Jorga et al. 1999; Kalgutkar et al. 2005; Kaplowitz 2005; Smith 2003; Stricker 1992; Tujios and Fontana 2011; Zahno et al. 2011). It has been demonstrated that C3A spheroids display CYP enzyme activity with the ability to metabolise xenobiotic compounds (see Section 3.3.4), hence it is likely that drug metabolites would be formed in the spheroids and their toxic effects observed (Srivastava et al. 2010).

Many compounds have been suggested to cause injury through damage of mitochondria such as diclofenac, fialuridine, amiodarone and troglitazone (Begriche et al. 2011; Boelsterli and Lim 2007; Honkoop et al. 1997; Smith 2003). As the C3A

spheroids have functional mitochondria which can be analysed it detail, it is likely that disruption to mitochondrial respiration would be identified.

Furthermore, certain compounds target certain zones of the liver, such as acetaminophen (Tujios and Fontana 2011). Hence, the zonated function that was observed in the spheroid model may also be useful to the detection of toxins (Opie 1904). The C3A spheroids recapitulate functions from the periportal region and the perivenous region (as demonstrated in Section 3.3.2), herein it could be predicted that toxins affecting any area of the liver could be detected in this model.

Many studies suggest that an immune response is involved, and accentuates the toxicity of many hepatotoxins. Diclofenac and trovafloxacin are two compounds displaying evidence of immune or inflammatory-mediated toxicities (Shaw et al. 2010; Stricker 1992). In order for this damage to be detected, correct cell communications and signalling must be in place in an *in vitro* model, as well as the capability to alert or initiate an immune response.

A final and vitally important parameter to consider is the longevity of the *in vitro* model. Many hepatotoxins take a long time and often multiple exposures before toxicity ensues. This study was able to adopt a 4 day dosing strategy, with repeat dosing on day 2 for spheroid cultures. This was in order to better recapitulate the longer, repeated drug exposures experienced by patients but in a quick, simple, high-throughput drug screen. Monolayer cells however were only treated for 24 hours, as this is the typical dosing strategy for a 2D liver model and the cells become over-confluent and start to die after 48 hours in this culture condition.

Each of the twelve hepatotoxic compounds caused toxicity in the C3A spheroids and all but one of the compounds was more toxic to spheroids than in corresponding HepG2/ C3A 2D models (Ju et al. 2015; Lin and Will 2012). Furthermore 9 out of 12 compounds were more toxic to C3A spheroids than 2D human hepatocyte cultures,

and 5 out of 12 more toxic to spheroids than hepatocyte sandwich cultures (Richert et al. 2016), with the remaining compounds showing similar sensitivity. It is possible that these hepatotoxins would not have been identified to be toxic in the 2D *in vitro* liver models, yet the spheroid model clearly identified toxicity. It is possible that the direct cell-cell contacts and increased liver-specific structures and functions of spheroids led to these toxins being able to exert their effects. The lower enzyme activity, lack of transporter function, limited cell contacts and different mitochondrial function may be the reason these toxins were not detected in 2D. Since these results were obtained, other researchers have found that their 3D cultures are more predictive of hepatotoxicity than monolayers, supporting the conclusion that 3D cell culture increases sensitivity to hepatotoxins (Gunness et al. 2013; Ramaiahgari et al. 2014). Unfortunately not all of the compounds' effects were directly compared to 2D cultures and there was limited published information available about the toxicity of these compounds in C3A cells. A direct experimental comparison of the two culture techniques using the same cell types and dosing strategy would provide confirmative evidence as to whether 3D cell culture increases the sensitivity of the model.

Data obtained from commercially available InSphero primary human hepatocyte and Kupffer co-culture spheroids by AstraZeneca could be compared with data obtained from the C3A spheroids. The same twelve hepatotoxins and three non-DILI compounds were analysed using an identical repeat dosing strategy and cell viability analysis as was carried out with the C3A spheroids. In order to predict whether the spheroids detected the compounds to have a risk of DILI, a SM calculation was utilised, taking into account the highest non-toxic concentration (IC_{10}) and compound exposure values (C_{max}) (Mueller et al. 2015; Richert et al. 2016; Sison-Young et al. 2016). An SM value below 20 appeared to best distinguish hepatotoxic compounds from non-hepatotoxic compounds. Despite being created from a hepatoma cell line,

the C3A spheroids detected toxicity in a similar number of compounds as the InSphero hepatocyte spheroids. The C3A spheroids were able to correctly predict DILI in 10 out of 12 compounds tested compared to 8 out of 12 detected in InSphero, resulting in a sensitivity of 90.9 % and a specificity of 66 % for C3A spheroids, and a sensitivity of 88 % and a specificity of 66 % for the InSphero spheroids. This could be due to the liver-specific functions in the C3A spheroids being upregulated and allowing the compounds to exert their mechanism of toxicity in this model. Perhaps the C3A spheroids do not possess the appropriate mechanisms to prevent or repair damage cause by these toxins, accounting for the differences between toxicities observed in hepatocyte spheroids. Although exposure was accounted for, the concentrations of each compound in spheroid culture may be significantly different from the C_{max} *in vivo,* therefore the SM calculation may be considered irrelevant. Furthermore using an SM value of 20, may not have been appropriate for the InSphero model. Regardless, this sensitivity appears to be a huge improvement on the sensitivity reported for currently used *in vitro* systems (Olsen and Whalen 2009).

Nevertheless, one of the non-DILI compounds, pioglitazone, was also determined to have a risk of DILI in the C3A spheroid model as well as the InSphero spheroids. Pioglitazone is not known to cause liver damage, but can damage the heart (Chinnam et al. 2012). This false positive lowered the sensitivity and specificity of the spheroid models. This lack of specificity may be a key limitation of the C3A spheroids, suggesting that the model cannot distinguish between hepatotoxic compounds and those toxic to other tissues. Other cell lines show poor specificity to hepatotoxins when cultured in 2D (Atienzar et al. 2014). It is difficult to accurately predict sensitivity and specificity with only a small number of positive and negative compounds and many of the compounds tested may indeed be toxic to other organs as well as the liver. A further drug screen employing a larger panel of compounds

with more negative DILI compounds would help to more accurately determine the sensitivity and specificity of the C3A model to hepatotoxins. Furthermore a negative control experiment, using a non-liver cell line cultured in 2D and spheroids, would identify whether spheroid culture heightens the sensitivity of multiple cell types to toxicity, indicating that this phenomenon is not liver-specific and is unrelated to the origin of the model.

The next investigation was whether the presence of NPC increased the sensitivity of the spheroid model to hepatotoxins. LSEC, cryopreserved after isolation from human liver, were chosen. Endothelial cells are the second largest population of cells in the liver, with vital functions during liver homeostasis, as well as having a key role during liver damage and regeneration (Anderson 2015; Kmiec 2001). Secondly, it was decided that an immune cell should be included in the spheroids. THP1 cells were identified, a human monocytic cell line isolated from an acute monocytic leukaemia patient, as they display many of the properties and markers of human monocytes, with the ability to phagocytose, detect and respond to stress signals, release pro-inflammatory cytokines and differentiate into macrophages (Tsuchiya et al. 1980). It was hypothesised that these NPC could create a more *in vivo*-like microenvironment in the spheroids and in turn respond to human hepatotoxins with heightened sensitivity.

Firstly the presence of each cell type in the spheroids during the desired culture period was confirmed. Secondly a toxicological analysis was performed. A clear trend highlighted that the inclusion of LSEC in the model caused a small increase in the sensitivity of the model to hepatotoxins, the inclusion of THP1 cells increased this sensitivity further, and both cell types even further, which was reflected in the IC_{50} values obtained. This led to a higher sensitivity of 91.6 % in the NPC co-culture models. Amiodarone was correctly picked up using the co-culture spheroid models which went undetected in the C3A monoculture spheroids. Suggested mechanisms

of amiodarone toxicity include mitochondrial and lysosomal dysfunction as well as toxic metabolite formation (Bandyopadhyay et al. 1990; Begriche et al. 2011; Dake et al. 1985; Zahno et al. 2011). It is possible that the inclusion of NPC into the spheroid model created a more *in vivo*-like environment, with sensitive mitochondria and CYP enzyme activity, in which this toxin was able to exert its toxicological effects. Moreover, despite not being identified as hepatotoxic, ximelagatran caused significantly more toxicity in spheroids cultured with THP1 monocyte cells. The mechanism by which this compound causes DILI has yet to be specified, however from these results one could hypothesise that these immune cells aggravated ximelagatran toxicity in the spheroids, indicating a toxic mechanism involving the immune response or inflammation.

Other research groups have analysed the ability of liver spheroids to detect hepatotoxic compounds. Despite using the same cell type, Fey and Wrzesinski found higher IC_{50} values for acetaminophen, diclofenac and amiodarone in their C3A spheroids (Fey and Wrzesinski 2012). This could be explained by the fact they used acute dosing, rather than a repeat-dosing strategy as used in this chapter. There is now evidence that repeat dosing, as well as 3D cell culture, increases the sensitivity of a HepG2 model to hepatotoxins (Ramaiahgari et al. 2014). Since performing the toxicological analysis presented here, another study tested the same panel of compounds using a 14 day repeat-dosing strategy and found their human hepatocyte co-culture spheroids to detect 75 % of hepatotoxins, indicating similar predictivity as the co-culture spheroid model in this chapter (Richert et al. 2016). Furthermore Bell *et al.* 2016 adopted longer dosing protocols of 7 or 28 days in their human hepatocyte co-culture spheroids, identifying 5/5 of their hepatotoxins to have a risk of DILI using their criteria (Bell et al. 2016). These 5 compounds were also correctly identified as being hepatotoxic in the C3A spheroid model. A longer repeat dosing protocol could be implemented with the C3A spheroids, up 32 day drug

treatment - as it has been proven that C3A spheroids were viable and functional for this period. This may increase their ability to detect toxins which cause DILI after longer and more numerous exposures. It was additionally discovered that the age or culture time at which C3A spheroids were treated did not affect drug response, unlike hepatocyte spheroids (Ogihara et al. 2015), as both 3 day and 10 day old C3A spheroids produced similar dose-response curves and IC_{50} values. This was perhaps due to the long-term stability of the C3A spheroid model.

Further evidence has been published revealing that the inclusion of endothelial cells in *in vitro* liver models may have advantages. Kang *et al.* 2013 show expression of hepatocyte differentiation markers and urea synthesis from rat hepatocytes after co-culture with endothelial cells, with comparable results observed in liver cell lines once co-cultured (Kang et al. 2013; Ohno et al. 2009). Co-cultures of vascular endothelial cells and C3A cells have shown increased liver-specific function, including CYP expression and albumin synthesis, but conversely a decreased sensitivity to hepatotoxin acetaminophen (Nelson et al. 2015). This increased function could be mitigated by signalling between the two cell types and an alteration in the phenotypes of these cells due to the creation of a more liver-like microenvironment. Likewise, *in vitro* co-culture studies have found that Kupffer cells can modulate hepatocyte phenotype, including increases in liver-specific functions as well as responses to inflammatory stimuli which otherwise have no effect on the cells (West et al. 1986; Yagi et al. 1998). Kupffer cells can also detect and respond to hepatocyte stress caused by hepatotoxins *in vitro,* potentially making a co-culture model with higher sensitivity to hepatotoxins (Kegel et al. 2015). A model by Edling *et al.* 2009 showed that culturing immune cells with the liver cell line Huh-7 led to enhanced sensitivity to hepatotoxins (Edling et al. 2009). The results presented in this chapter support this evidence that including NPC in liver models increases their sensitivity to a range of hepatotoxic compounds. Further analysis could give insight

into the mechanism by which some of these hepatotoxins are working, potentially by damaging NPC, the structural integrity of the liver, or through immune-mediated mechanisms. It would also be interesting to see the direct effects of the compounds on the NPC alone.

One disadvantage of preclinical drug screening is that completely different analyses are used to detect liver damage *in vitro* than in a clinical situation. The question was asked whether three novel biomarkers, HMGB1, keratin 18 and miR-122, could be analysed in an *in vitro* liver spheroid model and whether or not the measurement of these biomarkers would enhance the ability of the spheroid model to detect hepatotoxins by providing additional sensitivity and information about the toxicity occurring. miR-122 could not be quantified from C3A spheroid supernatant. It was previously thought that HepG2 cells did not express miR-122 (Murakami et al. 2005; Wu et al. 2009), however more recently miR-122 has been identified in HepG2 cells (Kia et al. 2015), suggesting that passage number could cause this gene deletion. It is possible that the C3A cell line, a subclone of HepG2 cells, does not express this miR or perhaps the method used was not sensitive enough for *in vitro* detection of miR-122 and needs to be optimised for use with cell culture samples.

Additionally, the analysis of HMGB1 in cell and spheroid lysates proved to be challenging and non-quantitative. HMGB1 is released during cell death (Antoine et al. 2009b) therefore a reduction in expression intracellularly was expected at high drug concentrations; however the expression in the cell lysates was fairly consistent despite the compounds causing a reduction in cell viability. It is not known exactly how these biomarkers are released from cells. Clearly these markers must be studied further in order to understand how they are regulated, released from cells and at what time point they can be detected after initiation of cell damage. Utilising a technique such as mass spectrometry imaging may provide a more sensitive

analysis of these two novel biomarkers *in vitro,* as well as providing quantitative information.

The analysis of keratin 18 released from the spheroids into the supernatant was more informative. All four compounds appeared to cause a dose-dependent increase in apoptosis in the spheroids. Analysis of this novel biomarker therefore suggests that these compounds cause DILI primarily by increasing apoptosis. On the other hand, this contradicts clinical evidence that acetaminophen causes necrosis which leads to liver damage (Hinson et al. 2010; James et al. 2003) and previously both ck18 and fk18 were found to increase after acetaminophen overdose (Antoine et al. 2013). Additionally, the levels of this biomarker did not correlate with the levels of cell death observed, particularly as both 2D and 3D models released similar levels despite revealing increased cell death in spheroids. In light of this, despite providing mechanistic information as to the type of cell death occurring, this analysis did not improve the sensitivity of the model. Hence relying on these biomarkers as a measure of toxicity from a range of different compounds may give misleading conclusions. To summarise, more research is needed into these novel biomarkers before they can be relied upon for an accurate diagnosis of DILI *in vitro* or in the clinic.

4.4.1 Conclusion

C3A spheroids were found to be more sensitive to a small panel of hepatotoxins than a 2D model, with a similar sensitivity as a commercially available hepatocyte spheroid model. The inclusion of NPC in the C3A spheroids increased the sensitivity of the model further, leading to a higher number of compounds being identified as having a hepatotoxic risk and supporting evidence than NPC have a vital role in DILI. The analysis of novel biomarker keratin 18 provided information

about the mechanism of cell death caused by each hepatotoxin, however HMGB1 and miR-122 could not be quantified in the C3A spheroid model.

Chapter 5

Investigation of Drug-Induced Mitochondrial Dysfunction in a C3A Liver Spheroid Model

Contents

5.1 Introduction

Mitochondria are organelles which are vitally important to cell survival, whose primary role is to produce cellular energy through OXPHOS and the consequent production of ATP (Cooper 2000). If mitochondria were to be damaged, not only would this lead to a reduction in cellular energy and function, but mitochondrial dysfunction could cause the production of ROS, damage DNA and proteins and inevitably lead to oxidative stress, cell death and potential organ damage. 50 % of hepatotoxic compounds are thought to have mitochondrial liability (Begriche et al. 2011; Boelsterli and Lim 2007), with the direct consequence of some compounds causing disastrous failures in clinical trials due to undetected mitochondrial toxicity during preclinical screening (Honkoop et al. 1997). By analysing the effect of a compound on mitochondrial function during preclinical trials, potentially dangerous toxins could be detected earlier in the drug discovery process.

The basal mitochondrial functionality was previously determined from C3A cells (Section 3.3.6), and therefore this platform could be used to investigate the intricate differences in mitochondrial function caused by toxic compounds. The analysis of mitochondrial stress *in vitro* could potentially highlight compounds with mitochondrial liabilities in humans. Furthermore, this analysis may help to elucidate the mechanisms of action of numerous hepatotoxins with currently unconfirmed mechanisms of toxicity by revealing whether the toxin is interfering with cellular bioenergetics.

In vitro experiments are most often performed on immortalised cells, which have adapted to withstand hypoxic and acidic conditions and display continued rapid growth. Although under normal conditions these cell lines produce the majority of their energy through OXPHOS, they also have the increased ability to produce energy through glycolysis, as glucose (often in excessive concentrations in the

medium) is converted to pyruvate, yielding two ATP molecules (Diaz-Ruiz et al. 2011; Marroquin et al. 2007). Mitochondrial OXPHOS is therefore no longer essential for energy production (Dell' Antone 2012; Rodriguez-Enriquez et al. 2001), this phenomenon is known as the Crabtree effect. This characteristic can result in compounds which cause mitochondrial damage going undetected in these model systems as the cells are able to continue to produce energy by an alternate mechanism resulting in the drug having little impact on cell viability (Marroquin et al. 2007).

One way to overcome this problem and allow immortalised cells to produce energy through functional mitochondrial ATP production is by removing the key substrate for glycolysis. Once glucose is removed from culture medium and replaced with galactose, the cells are forced to undergo mitochondrial OXPHOS for energy production as the efficiency of glycolysis is vastly reduced (Marroquin et al. 2007; Reitzer et al. 1979). This change in metabolism, or inhibition of the Crabtree effect, has been shown to occur within as little as 4 hours under galactose conditions (Kamalian et al. 2015). Studies have also confirmed that this metabolic switch indeed raises the sensitivity of 2D cultured cells to known mitochondrial toxins, leading to an increased ability to detect mitochondrial liabilities in novel drug compounds (Kamalian et al. 2015; Marroquin et al. 2007). Evidence suggests that C3A cells under normal cell culture conditions may be under the Crabtree effect, as similar immortalised cell lines display this feature (Kamalian et al. 2015; Marroquin et al. 2007; Rodriguez-Enriquez et al. 2001). Furthermore, inhibition of the Crabtree effect has previously been possible in HepG2 cells (Kamalian et al. 2015; Marroquin et al. 2007). C3A cells are able to grow in glucose deficient media (Nibourg et al. 2012), hence evidence suggests that inhibition of the Crabtree effect using galactose conditions would be possible in these cells.

C3A spheroids have displayed the ability to detect a wide range of hepatotoxic compounds, working by a range of different mechanisms. In addition C3A cells possess different functional capabilities depending on whether cultured in 2D or 3D spheroids. The first aim of this chapter was to elucidate whether changes in mitochondrial respiration could be detected after treatment with hepatotoxins, in order to confirm the mechanism of action of these compounds. Secondly, the bioenergetic profile of C3A cells was investigated in 2D or spheroid culture and it was questioned whether it was possible to modify the bioenergetic profile of this spheroid model as an attempt to increase its mitochondrial susceptibility.

Hypothesis 1: It will be possible to monitor changes in mitochondrial function caused by toxic compounds in the C3A spheroid model, which may help to determine the mechanism by which a compound is causing toxicity.

Hypothesis 2: Control C3A cells will be under the Crabtree effect and by culturing in galactose conditions it will be possible to circumvent the Crabtree effect, subsequently rendering the model more sensitive to hepatotoxins with mitochondrial liabilities.

5.2 Materials and Methods

All drug compounds and galactose were purchased from Sigma Aldrich, Missouri, USA. DMEM no glucose and dialysed FBS were purchased from Thermo Scientific, Watham, USA.

5.2.1 Spheroid formation and culture

C3A cells were maintained and cultured in monolayers as previously described (Section 2.2.1). Spheroids were created using the LOT from 1000 C3A cells as described previously (Section 2.2.1). For monolayer experiments C3A cells were used at 100 % confluence.

5.2.2 Culturing spheroids in galactose conditions

DMEM no glucose was used to create the agarose for the plates, and spheroids were cultured in galactose media consisting of DMEM no glucose supplemented with 10 % dialysed FBS, 10 mM galactose, 1 % L-glutamine, 1 % sodium pyruvate, 1 % penicillin-streptomycin.

5.2.3 Compound treatment

For experiments analysing the effect of hepatotoxins on mitochondrial function and for the toxicological analysis in glucose and galactose conditions, spheroids were treated with hepatotoxic compounds using a 4 day repeat dosing strategy as previously described (Section 4.2.3). For the experiments comparing the effects of hepatotoxins in glucose and galactose conditions on mitochondrial function, spheroids were treated with hepatotoxic compounds' IC_{50} concentrations for a 24 hour incubation period. 2D monolayer cells were also treated with hepatotoxic compounds for 24 hours. For experiments using rotenone, spheroids were treated with rotenone in 0.5 % DMSO in galactose medium for either 2 hours or 24 hours.

5.2.5 Cell viability analysis

Cell viability was analysed as previously described (Section 4.2.4). Three replicates were used for each experiment. A dose-response curve was plotted and IC_{50} values determined.

5.2.6 Bradford assay for quantification of protein content

Bradford assays were performed as previously described (Section 3.2.4).

5.2.7 Analysis of mitochondrial stress by oxygen consumption analysis

Cell Mito Stress Tests were performed on spheroids as previously described (Section 3.2.11), however for Crabtree investigations only rotenone was added to port A of the cartridge. Data was analysed using a Seahorse XF Mito Stress Test Report Generator and data normalised to protein content. 6 replicates of spheroids or 2D monolayer wells were used for each experiment.

5.2.8 Statistical analysis

Data are representative of at least three independent experiments (n=3) and expressed as mean ± SEM. Graphs and statistical analyses were performed using GraphPad Prism 5. A Shapiro-Wilk normality test was performed on all data sets. Data which passed normality tests underwent analysis by a two-way ANOVA, those which did not underwent a non-parametric Kruskal-Wallis test. Significance was determined from a p value < 0.05. **** $p<0.0001$, *** $p< 0.001$ ** $p<0.01$, * $p< 0.05$.

5.3 Results

5.3.1 Monitoring changes in mitochondrial function induced by hepatotoxins

In order to investigate whether or not changes in mitochondrial function could be detected in C3A spheroids, a Cell Mito Stress Test was performed after drug treatment with several hepatotoxins under normal culture conditions. Figure 5.1 shows the OCR curve produced by spheroids treated with acetaminophen, diclofenac, fialuridine and trovafloxacin using the repeat-dosing protocol described in the previous chapter. From this data it was concluded that both concentrations of trovafloxacin were too toxic to cells, as basal OCR values were very low and the spheroids did not respond to the Mito Stress Test. Therefore data obtained for trovafloxacin was removed from further analysis in this experiment. The values obtained after drug treatment were compared to untreated vehicle control spheroids to see how the compounds might be interfering with normal mitochondrial function (Figure 5.2). None of the three hepatotoxins had a significant effect on any of the respiratory parameters in the spheroids, however small differences could be observed. Basal respiration was seen to decrease in a dose-dependent manner in response to acetaminophen and fialuridine. The amount of respiration linked to ATP production decreased in response to all toxins, to varying extents. Proton leak was increased by diclofenac but decreased by high concentrations of fialuridine. SRC increased dose-dependently in response to acetaminophen and diclofenac, as well as increasing in response to fialuridine. All compounds caused a decrease in NMR and coupling efficiency compared to control spheroids, with fialuridine having the largest effect on NMR. None of these differences were significantly different from control spheroids.

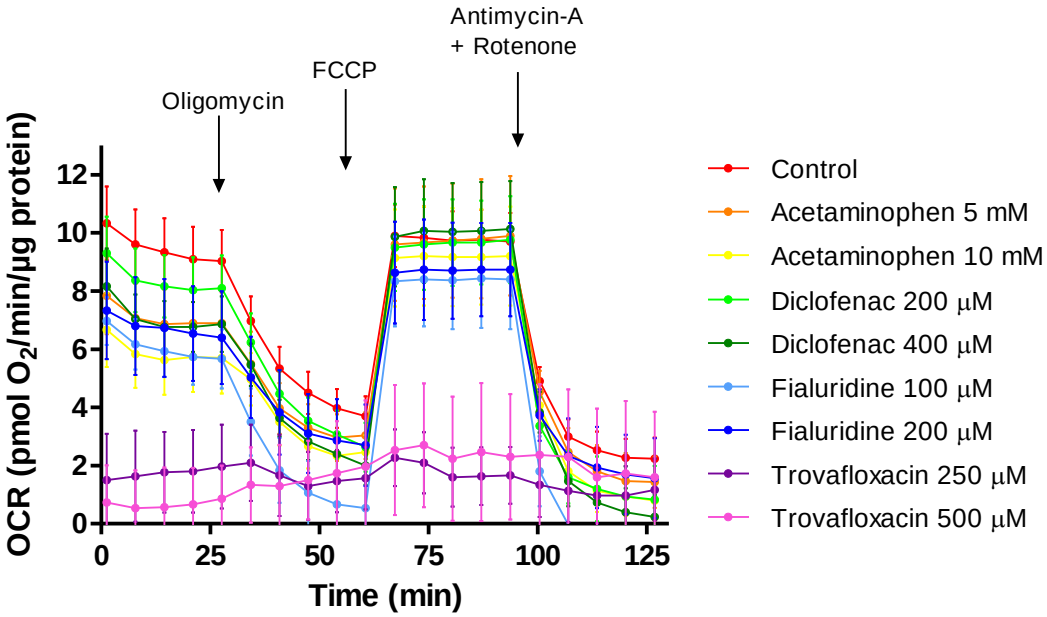

Figure 5.1. The effect of hepatotoxins on OCR in spheroids. Spheroids were treated with four hepatotoxins using a repeat-dosing strategy. A Mito Stress Test was performed using Seahorse technology. Raw OCR values (pmol O_2/min/µg protein) were plotted against time (min) for each drug treatment. Data represent mean ± SEM (n=3, 6 replicates).

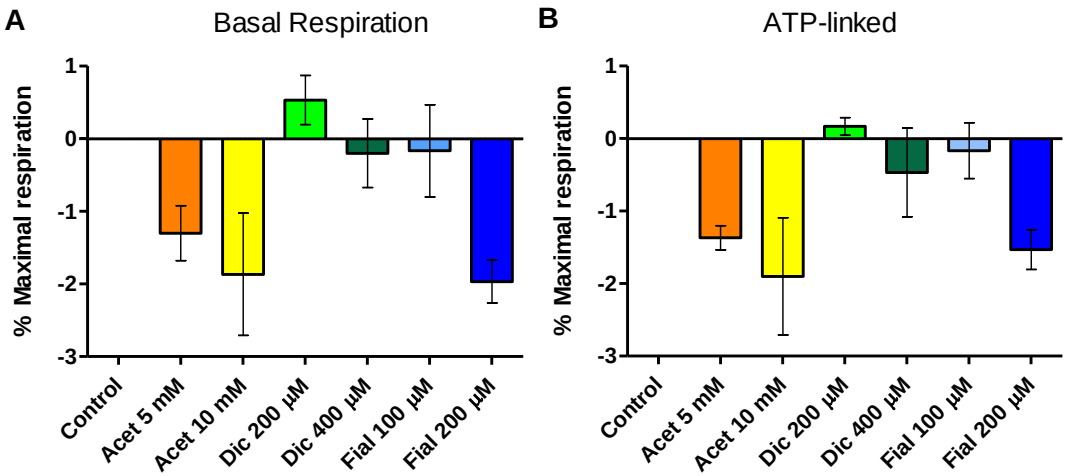

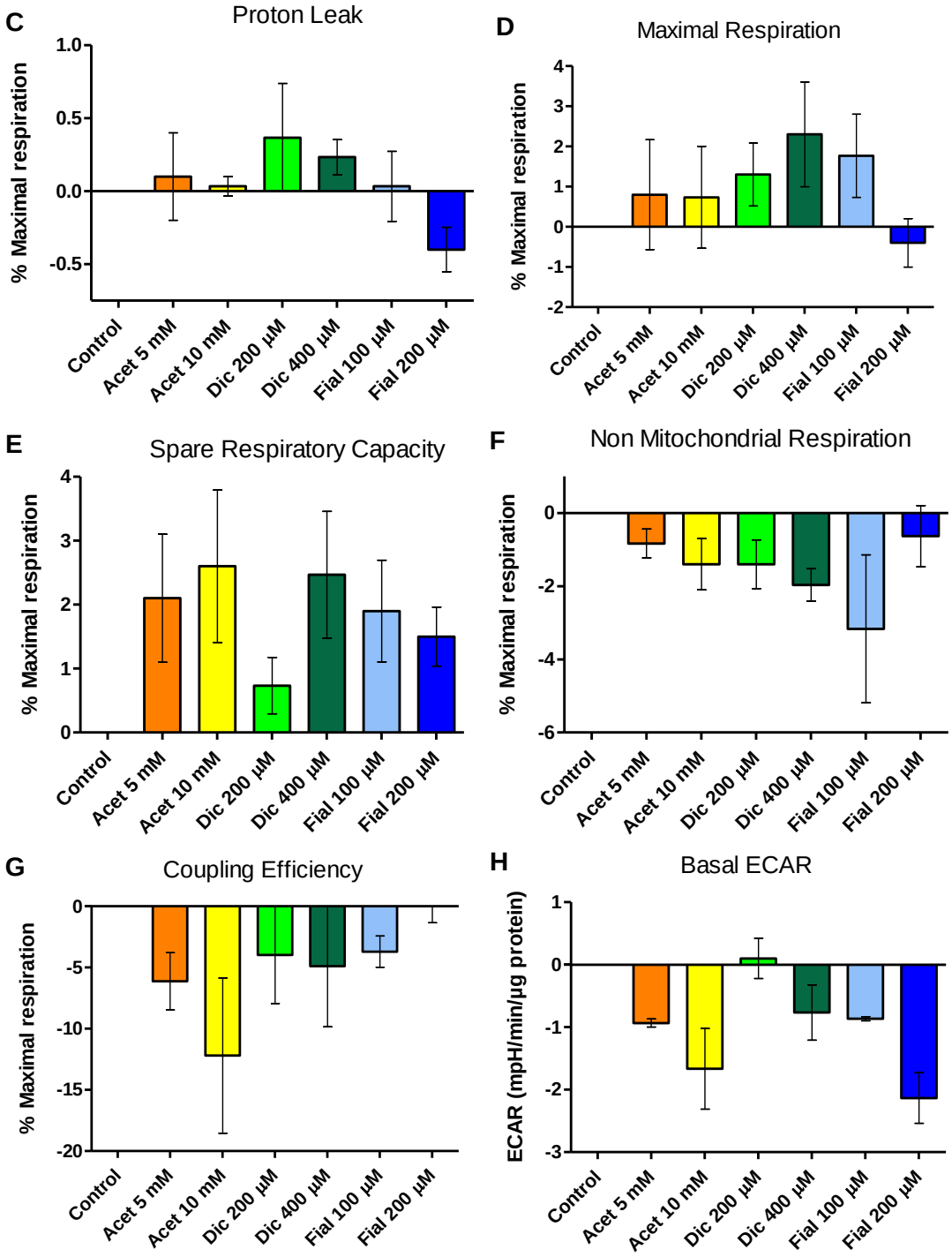

Figure 5.2. The effect of hepatotoxic compounds on mitochondrial function in spheroids. Spheroids were treated with two different concentrations of four hepatotoxins using a repeat-dosing protocol. A Mito Stress Test was performed using Seahorse technology and mitochondrial respiratory parameters calculated and plotted as a percentage of maximal respiration. Basal respiration, ATP-linked respiration, proton leak, maximal respiration, spare respiratory capacity, non-mitochondrial respiration, coupling efficiency and basal ECAR are plotted for each drug treatment (**A-H**). Data represent mean ± SEM normalised to untreated control values (n=3, 6 replicates).

It was next investigated how these results compared with the same compounds tested in 2D monolayer cultures (Figure 5.3). Only small differences were observed for all respiratory parameters between 2D and spheroids, indicating that these compounds affected the mitochondria in both 3D and 2D cell cultures similarly, despite previously confirming increased toxicity in spheroids.

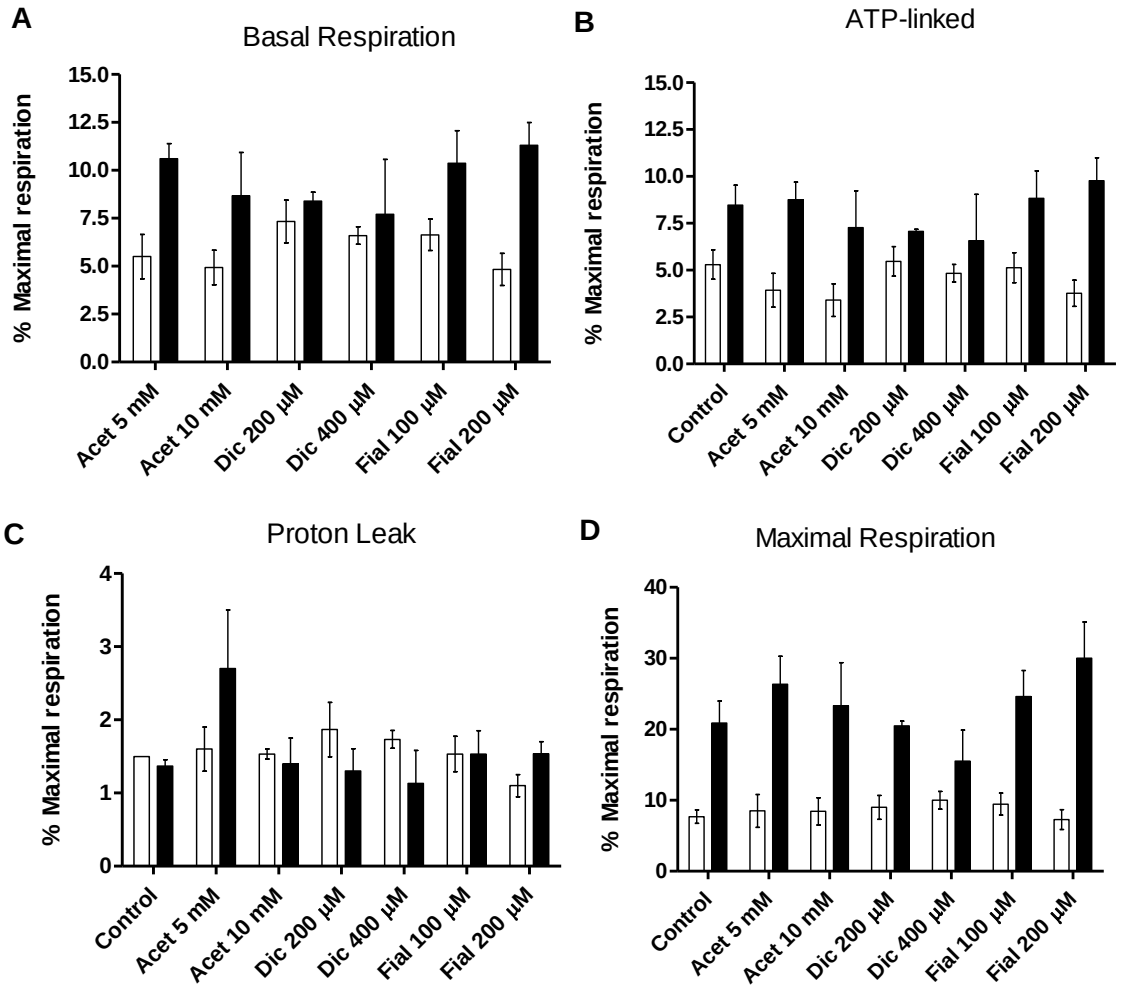

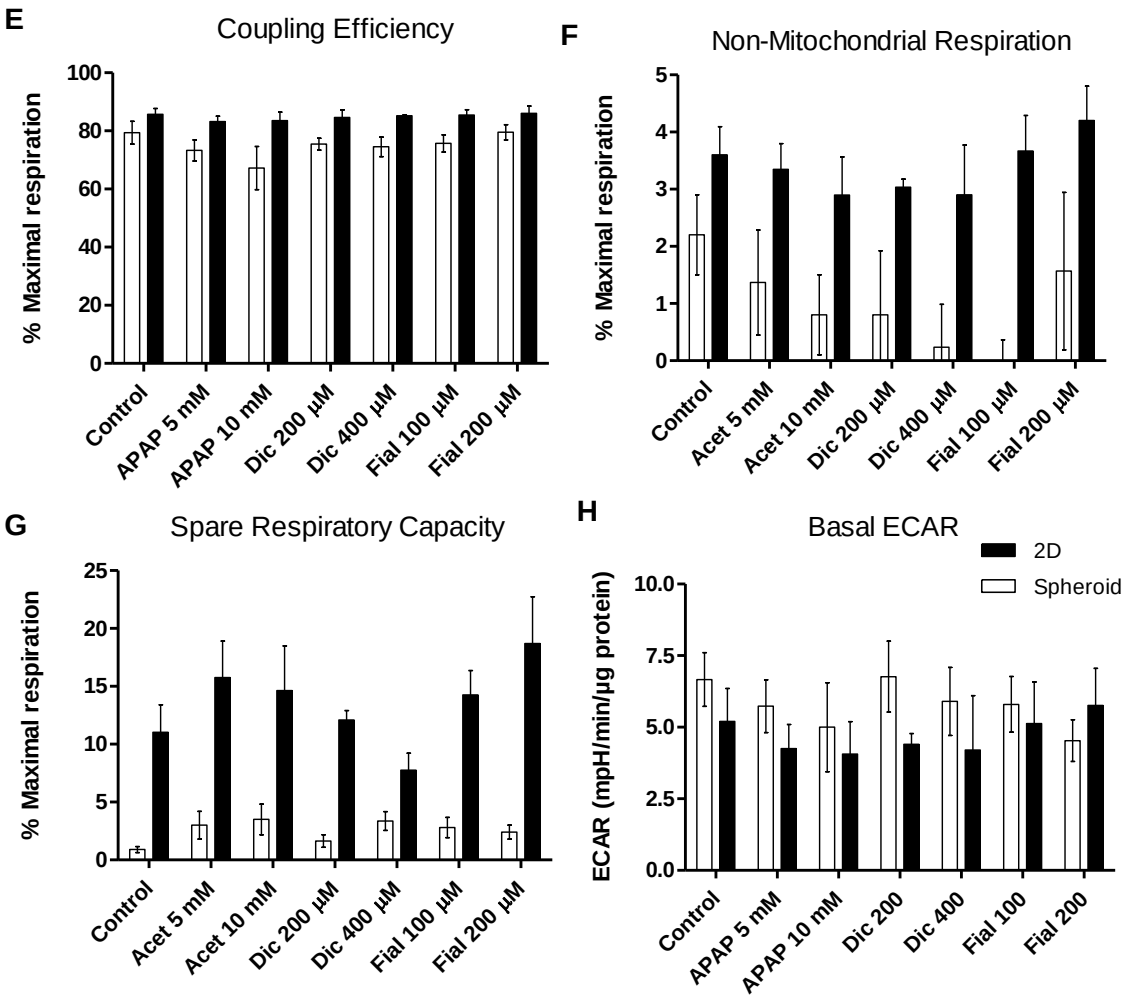

Figure 5.3. The effect of hepatotoxic compounds on mitochondrial function in spheroids and 2D C3A cells. Spheroids or 2D C3A cells were treated with two different concentrations of four hepatotoxins using a repeat-dosing protocol. A Mito Stress Test was performed using Seahorse technology and mitochondrial respiratory parameters calculated and plotted as a percentage of maximal respiration. Basal respiration, ATP-linked respiration, proton leak, maximal respiration, spare respiratory capacity, non-mitochondrial respiration, coupling efficiency and basal ECAR are plotted for each culture condition and drug treatment (**A-H**). Data represent mean ± SEM, (n=3, 6 replicates).

5.3.2 Circumventing the Crabtree effect in spheroids

Firstly it was determined whether C3A spheroids or 2D C3A cells were displaying the Crabtree effect. Subsequently, an investigation into whether or not the Crabtree effect could be circumvented was performed by culturing cells under galactose conditions. Basal respiration was analysed in control (glucose) spheroids (Figure 5.4A, black circle). Mitochondrial OCR (indicative of OXPHOS rate) was 8.9 ± 3.1 O_2/min/µg protein and basal ECAR (indicative of glycolysis rate) was 6.1 ± 0.5 mpH/min/µg protein in control spheroids (Dranka et al. 2011). The next part of the analysis involved treatment with rotenone, a mitochondrial complex I inhibitor. Spheroids cultured in glucose conditions saw a 4.5 O_2/min/µg protein decrease in OCR after treatment with rotenone, corresponding to a 50 % decrease. This suggests that rotenone successfully inhibited OXPHOS. A 1.8 mpH/min/µg protein (30 %) increase in ECAR was observed after rotenone exposure (Figure 5.4A black circle), although not significant, indicating a small up-regulation of glycolysis. These results indicate that the control glucose-cultured C3A spheroids were under the Crabtree effect to some extent, as once mitochondrial OXPHOS was reduced the cells compensated by increasing glycolytic capacity. It was then investigated whether a metabolic shift could be induced in C3A spheroids. Under galactose culture conditions basal mitochondrial OCR was similar to control spheroids at 8.7 ± 3.3 O_2/min/µg protein, however basal ECAR was lower in galactose conditions than control spheroids, at 4.6 ± 1.4 mpH/min/µg protein (Figure 5.4A, clear circle). This indicates lower levels of basal glycolysis, hence a metabolic shift, under these conditions (Dranka et al. 2011). Exposure to rotenone confirmed this alteration of energy metabolism in galactose conditions. Again a decrease in OCR was observed as OXPHOS was successfully inhibited, with a 5.4 pmol O_2/min/µg protein (62 %) drop. However the corresponding increase in ECAR previously observed in control spheroids did not occur under galactose conditions. A negligible 0.4

mpH/min/µg protein or 9 % increase in ECAR occurred after rotenone exposure in galactose-cultured C3A spheroids (Figure 5.4A, clear circle). This strongly suggests that any Crabtree effects observed in control, glucose-cultured, spheroids were abolished by using galactose culture conditions, as glycolytic capacity is unable to be increased in response to a decrease in mitochondrial respiratory capacity.

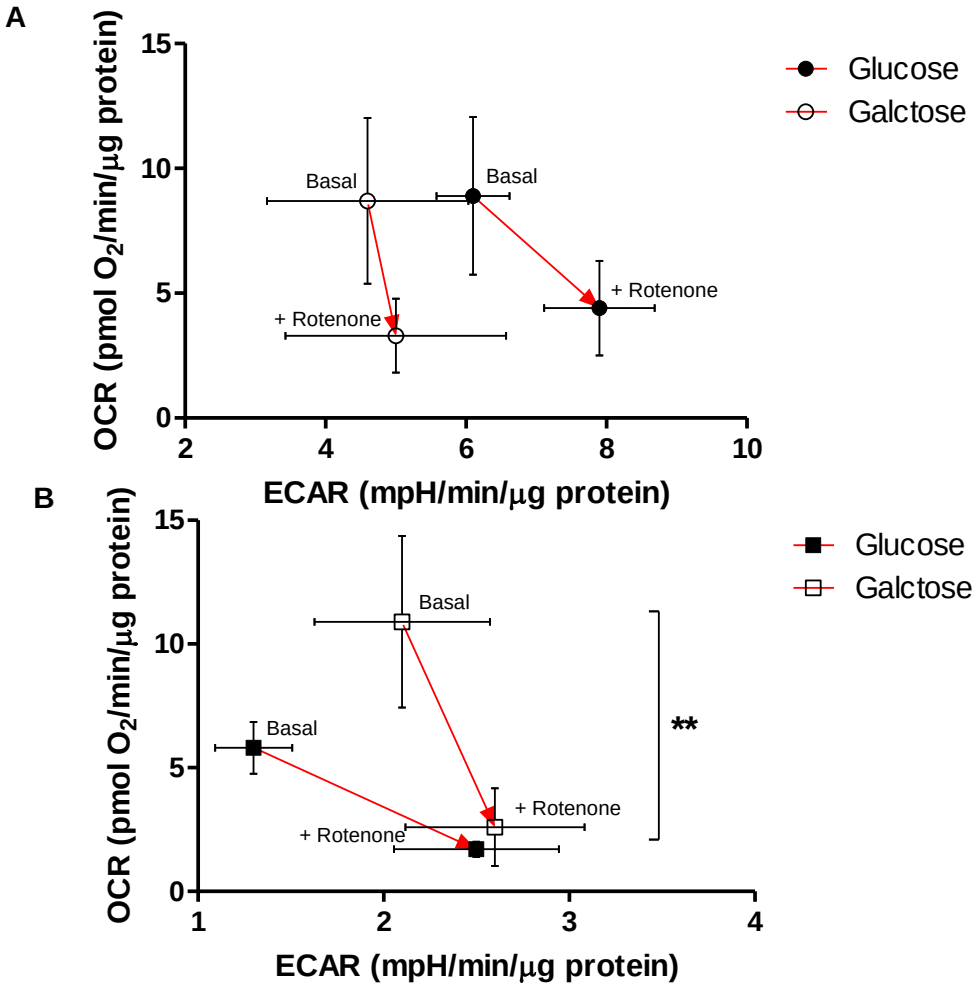

Figure 5.4. Effect of galactose conditions on mitochondrial OCR and ECAR. (**A**) Spheroids or (**B**) 2D C3A cells were acutely treated with rotenone after culture in glucose (black) or galactose (clear) conditions. Raw OCR values were plotted against raw ECAR values before and after exposure to rotenone. Data are represented as mean ± SEM, ** p<0.01, for galactose spheroids before and after exposure to rotenone (n=3 in triplicate).

This analysis was repeated in 2D C3A cells (Figure 5.4B). For 2D C3A cells basal ECAR was lower than in spheroids when using glucose medium, as seen previously (Figure 3.14). Control, glucose-cultured, 2D C3A cells had a basal OCR of 5.8 ± 1.0 O_2/min/µg protein and an ECAR of 1.3 ± 0.2 mpH/min/µg protein. Once exposed to rotenone OCR decreased by 4.1 pmol O_2/min/µg protein (70 %) and ECAR increased by 1.2 mpH/min/µg protein or 92 % (Figure 5.4B, black square). It appears that control 2D C3A cells were also under the Crabtree effect, as glycolysis was upregulated in response to decreased OCR. In fact a much larger increase in ECAR (92 %) compared to a 30 % increase was observed in 2D C3A cells, making the Crabtree effect more prominent in 2D cultured C3A cells. 2D C3A cells under galactose conditions responded similarly as when in spheroids, despite basal OCR and ECAR being higher than both 2D control and in spheroids, at 10.9 ± 3.5 pmol O_2/min/µg protein and 2.1 ± 0.5 mpH/min/µg protein respectively (Figure 5.4B, clear square). Once rotenone was added OCR decreased as expected, by 8.3 pmol O_2/min/µg protein, (76 %) in galactose-cultured cells. The increase in ECAR was again less in galactose conditions, only 23 %, 0.5 mpH/min/µg protein in 2D. This again indicates that control C3A cells are under the Crabtree effect and using galactose culture conditions abolishes this phenomenon.

Any differences in mitochondrial respiratory parameters were also elucidated in the two different conditions by performing a Mito Stress Test (Figure 5.5A). The analysis of mitochondrial function revealed that spheroids cultured in galactose had slightly higher basal respiration, ATP-linked respiration, proton leak and maximal respiration than control spheroids, but lower NMR, SRC and coupling efficiency (Figure 5.5B). These differences however were not significant.

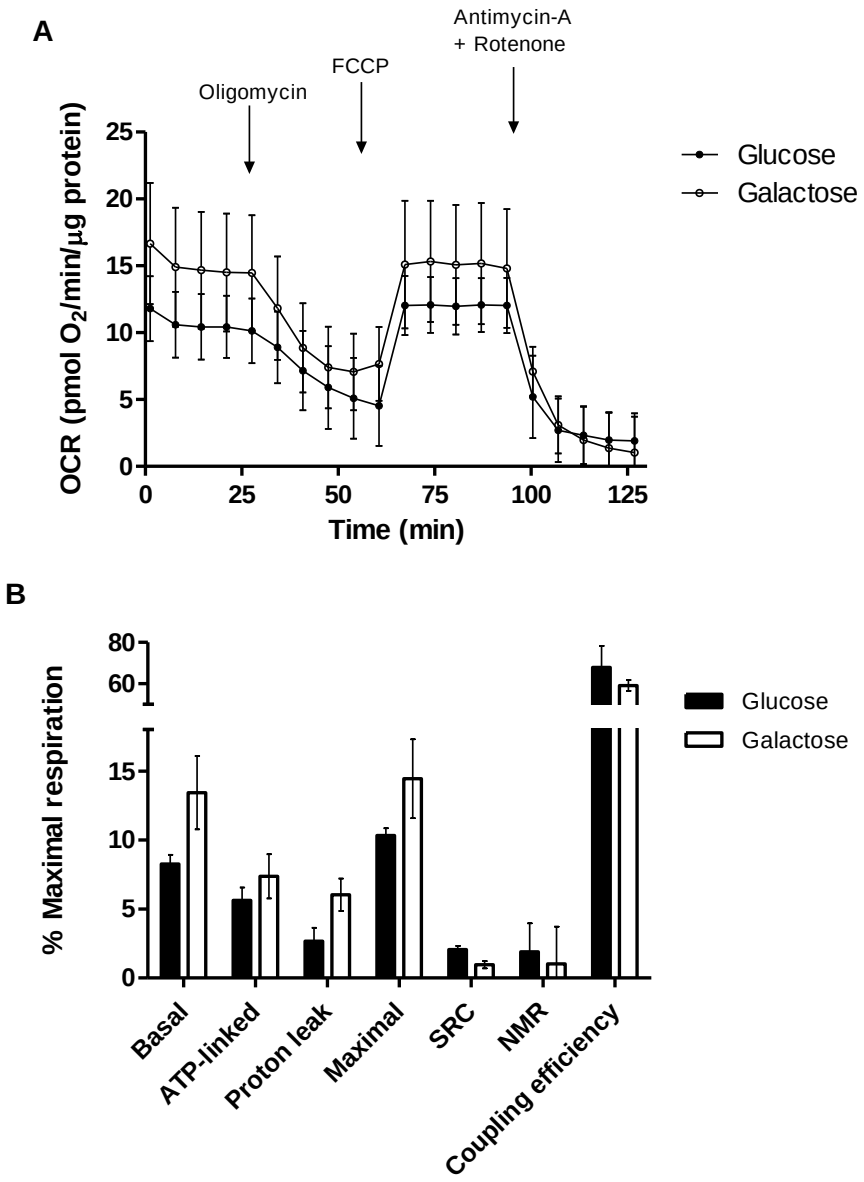

Figure 5.5. Effect of galactose conditions on mitochondrial function. A Mito Stress Test was performed on spheroids cultured in control glucose (black) or galactose (clear) conditions using Seahorse technology. (**A**) Raw OCR values (pmol O_2/min/µg protein) were plotted against time (min) for each culture condition; (**B**) Mitochondrial respiratory parameters were calculated and plotted as a percentage of maximal respiration. Basal respiration, ATP-linked respiration, proton leak, maximal respiration, spare capacity, non-mitochondrial respiration and coupling efficiency are plotted for each culture condition. Data represent mean ± SEM (n=3, 6 replicates).

Next, the toxicological effect of rotenone on spheroids cultured in both conditions was determined. Toxicity was observed in spheroids under both conditions in response to the complex I inhibitor. A decrease in cell viability was observed as drug concentrations increased, with no significant difference in toxicological

response under either condition (Figure 5.6A). As little as 6.2 µM rotenone caused toxicity in both conditions after a 24 hour incubation with spheroids. This toxicological analysis was repeated at lower concentrations of rotenone and a shorter incubation time, in order to separate any small differences between the two conditions (Figure 5.6B). Indeed, when using a lower concentration and shorter incubation period, rotenone was less toxic to glucose-cultured spheroids (Figure 5.6B, black circle), whereas galactose spheroids still suffered a larger reduction in cell viability (Figure 5.6B, clear circle), however these differences were not significant.

This analysis was repeated on C3A cells cultured in 2D to elucidate whether culture condition altered the susceptibility of the cells to this mitotoxin. Figure 5.7 shows the toxicity caused in both glucose and galactose conditions in 2D. At the lower concentrations of rotenone a significant difference in sensitivity can be observed, with barely any toxicity detected in glucose-cultured C3A cells and a large reduction in cell viability in galactose-cultured cells (Figure 5.7B). Table 5.3 compares IC_{50} values calculated from each culture condition. Correlating with the above data, galactose spheroids were more sensitive to rotenone, with a lower IC_{50} value of 0.65 µM in galactose conditions compared to 4.3 µM in control spheroids. Interestingly C3A cells had a different sensitivity to rotenone when cultured in 2D or 3D. Control spheroids were significantly more sensitive to rotenone than control monolayers. An IC_{50} value for glucose-cultured 2D C3A cells could not be calculated from the 2 hour incubation of rotenone as it did not cause enough toxicity. However from the 24 hour incubation the IC_{50} values were 3.2 µM and 4.7 µM for spheroids and monolayers respectively (Table 5.3).

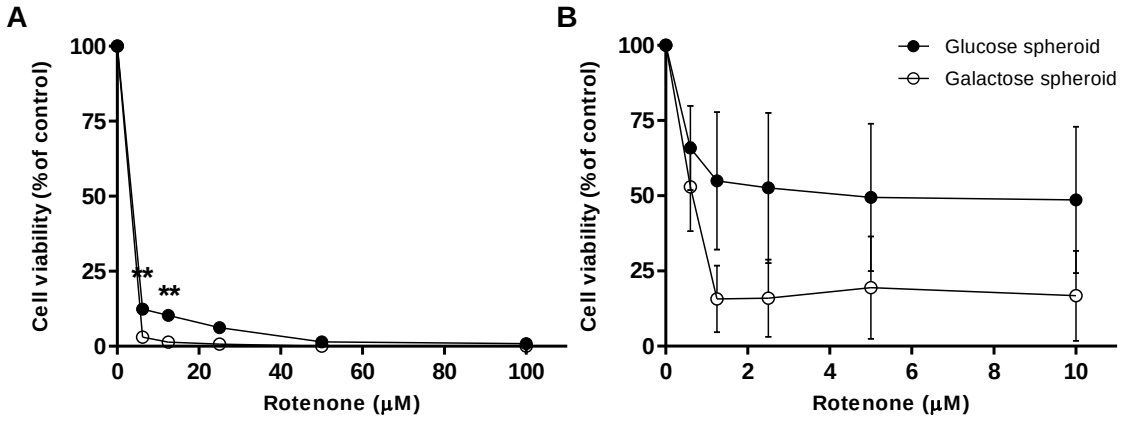

Figure 5.6. Galactose conditions increase the sensitivity of spheroids to mitotoxin rotenone. Spheroids were treated with (**A**) 100 μM rotenone for 24 hours or; (**B**) 10 μM rotenone for 2 hours, after culture in glucose or galactose conditions. Cell viability was analysed and plotted as a percentage of untreated control. Data are represented as mean ± SEM, ** p<0.01 (n=3 in triplicate).

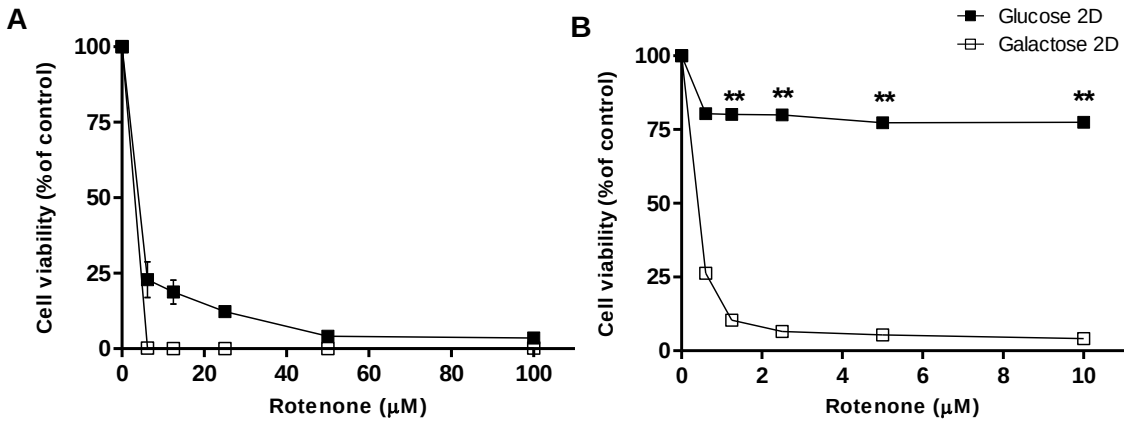

Figure 5.7. Galactose conditions increase the sensitivity of 2D C3A cells to mitotoxin rotenone. 2D C3A cells were treated with (**A**) 100 μM rotenone for 24 hours or; (**B**) 10 μM rotenone for 2 hours, after culture in glucose or galactose conditions. Cell viability was analysed and plotted as a percentage of untreated control. Data are represented as mean ± SEM, ** p<0.01 (n=3 in triplicate).

Rotenone incubation time (hours)	IC_{50} value in control spheroids (μM)	IC_{50} value in galactose spheroids (μM)	IC_{50} value in control 2D cells (μM)	IC_{50} value in galactose 2D cells (μM)
2	4.3	0.65	> 10	0.38
24	3.2 ***	2.7	4.7	2.7

Table 5.1. Sensitivity of spheroids and 2D C3A cells to mitotoxin rotenone. Spheroids and 2D C3A cells were treated with rotenone for 2 hours after culture in control glucose conditions or galactose conditions. Cell viability was analysed and IC_{50} values calculated. Data are represented as mean values, *** p<0.001 control spheroids compared to control 2D (n=3 in triplicate).

In order to visualise any differences in the number or location of mitochondria in glucose and galactose conditions, spheroids were stained with JC-1 and visualised by immunofluorescence. Figure 5.8 shows the expression and location of mitochondria (red) in relation to nuclei (blue) in both culture conditions. Numerous mitochondria can clearly be seen dispersed throughout the cell cytoplasm in both conditions with no clear difference in their localisation.

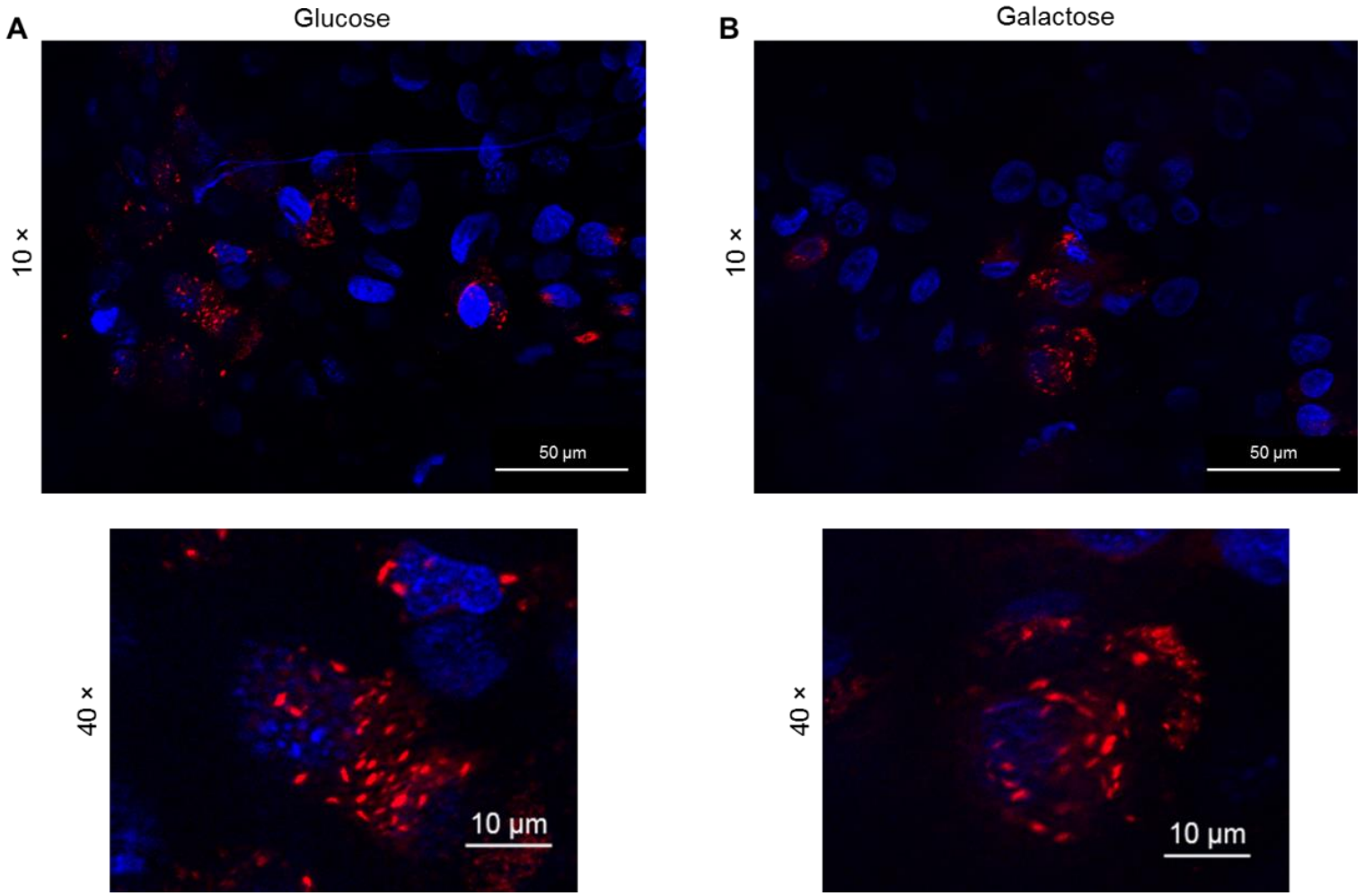

Figure 5.8. Mitochondrial location in spheroids cultured in glucose or galactose conditions. Spheroids were cultured in (**A**) control glucose conditions or; (**B**) galactose conditions, then incubated with 1 µM JC-1 mitochondrial stain (red) for 60 min then nuclei stained (blue) and imaged by confocal microscopy at 10 × or 40 × and represented as snap images. Scale bars = 50 µm.

5.3.3 Toxicological analysis of spheroids circumventing the Crabtree effect

Next the toxicity of the same four hepatotoxins were analysed under both glucose and galactose conditions. Dose-response curves for each compound are shown in Figure 5.9 and IC_{50} values in Table 5.4. Hepatotoxins caused toxicity in both the glucose and galactose-cultured spheroids. Trovafloxacin appeared to cause cell death at lower concentrations in galactose-cultured spheroids, indicated by a lower IC_{50} value of 25 µM compared to 65 µM, however the top concentrations affected the spheroids similarly. Diclofenac and acetaminophen appeared to be less toxic under galactose conditions, indicated by higher IC_{50} values for both. Diclofenac caused significantly less cell death in galactose-cultured spheroids than control. Fialuridine was equally toxic to both models (Figure 5.9).

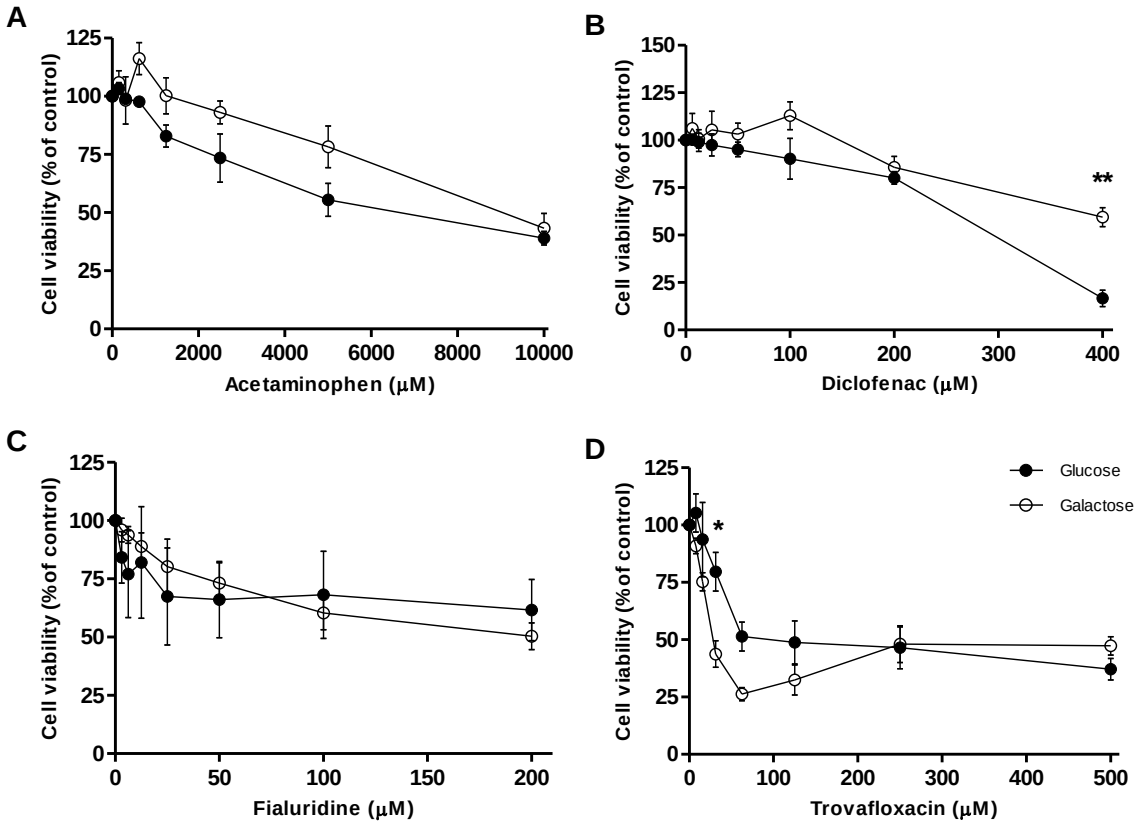

Figure 5.9. Toxicological analysis of spheroids cultured in galactose conditions. Spheroids were treated with four hepatotoxins (**A-D**) using a repeat-dosing protocol after culture in control glucose or galactose conditions. Cell viability was analysed and plotted as a percentage of vehicle control. Data are represented as mean ± SEM, ** p<0.01 (n=3 in triplicate).

Compound	IC_{50} value in control spheroids (μM)	IC_{50} value in galactose spheroids (μM)
Acetaminophen	7212	9240
Diclofenac	295	523 **
Trovafloxacin	65	25
Fialuridine	219	200

Table 5.2. Sensitivity of spheroids cultured in galactose conditions. Spheroids were treated with four hepatotoxins using a repeat-dosing protocol after culture in control glucose or galactose conditions. Cell viability was analysed and IC_{50} values calculated. Data is compared against IC_{50} values obtained for C3A spheroids cultured in control glucose conditions. Data are represented as mean values, ** p<0.01 (n=3 in triplicate).

This data was coupled with the effect of these compounds on mitochondrial respiration in both glucose and galactose conditions (Figure 5.10 and 5.11). The OCR curve produced after treatment with each hepatotoxin is plotted in Figure 5.9. In order to see any changes in mitochondrial function that occur before toxicity, spheroids were treated with the IC_{50} concentrations of each compound for 24 hours. No significant differences were observed in the response of galactose-cultured spheroids compared to control spheroids. Overall, basal respiration, respiration linked to ATP production, proton leak and maximal respiration were slightly higher in galactose conditions after treatment with all compounds and SRC and coupling efficiency were slightly lower. NMR increased after treatment with trovafloxacin only (Figure 5.11). The hepatotoxins therefore had no observable acute effect on glucose or galactose-cultured spheroids.

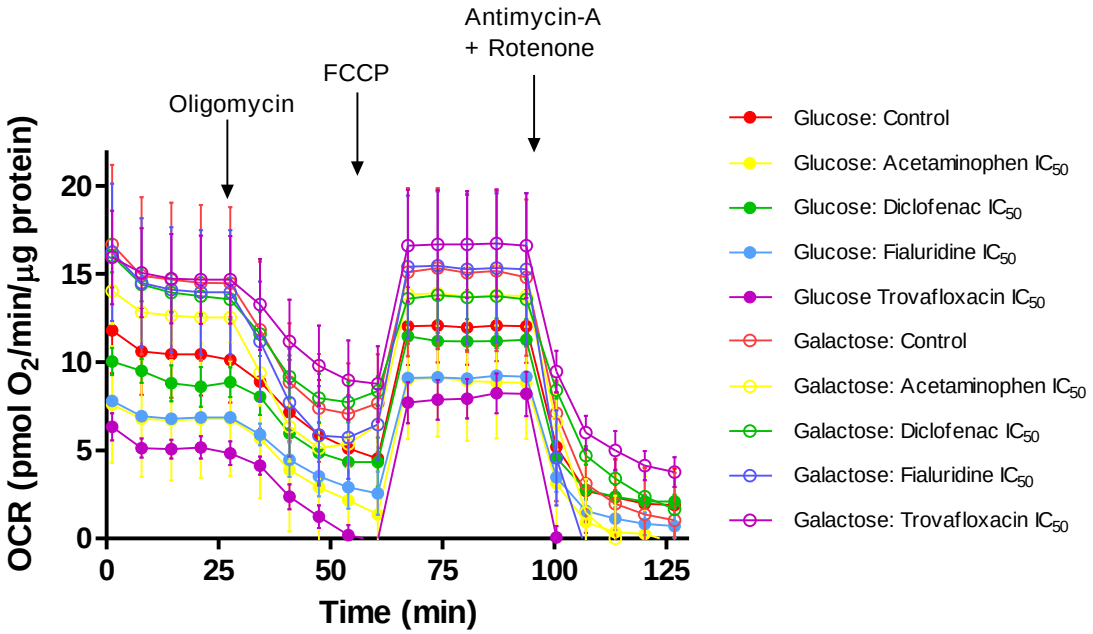

Figure 5.10. Effect of hepatotoxins on OCR in spheroids cultured in galactose conditions. Spheroids were treated with IC_{50} concentrations of four hepatotoxins for 24 hours after culture in control glucose (filled circle) or galactose (clear circle) conditions. A Mito Stress Test was performed using Seahorse technology. Raw OCR values (pmol O_2/min/µg protein) were plotted against time (min) for each drug treatment. Data represent mean ± SEM (n=3, 6 replicates).

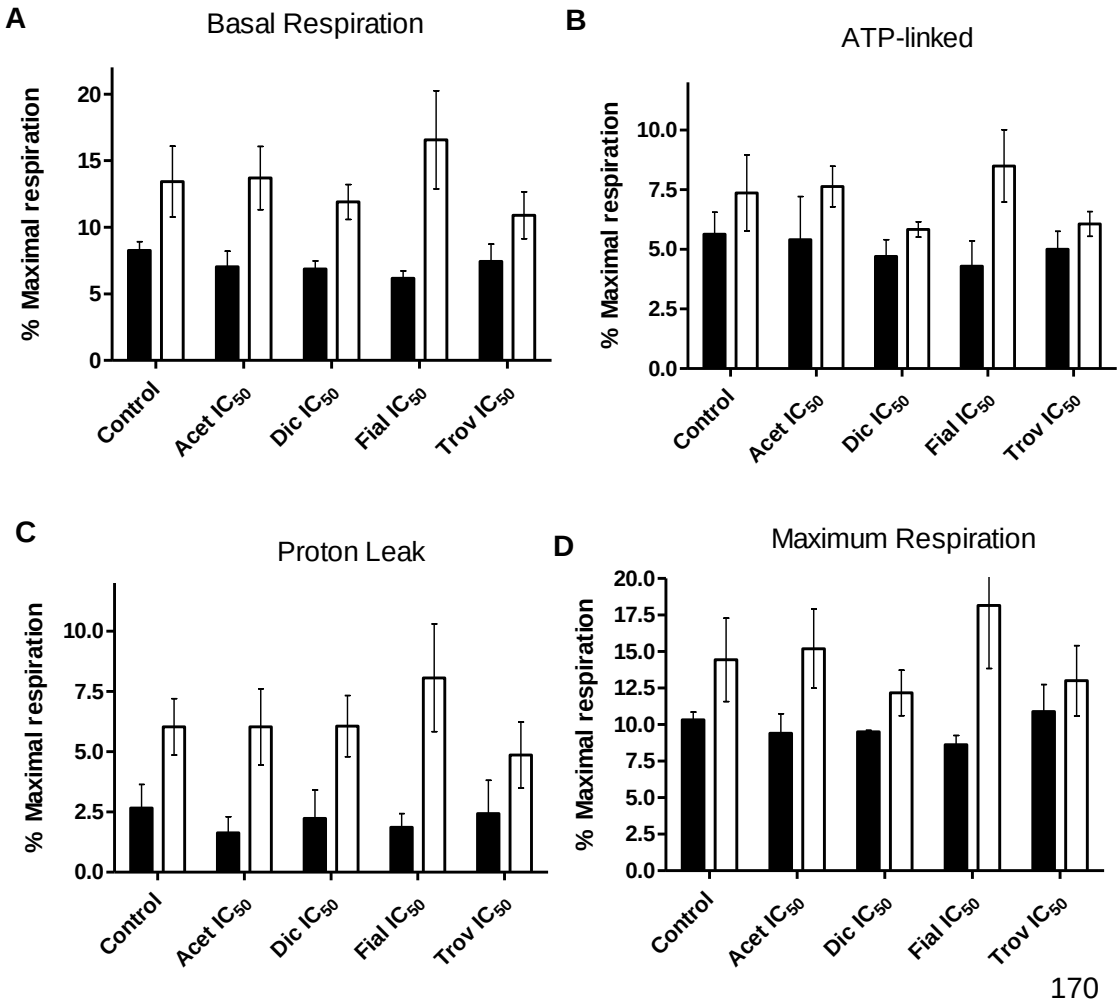

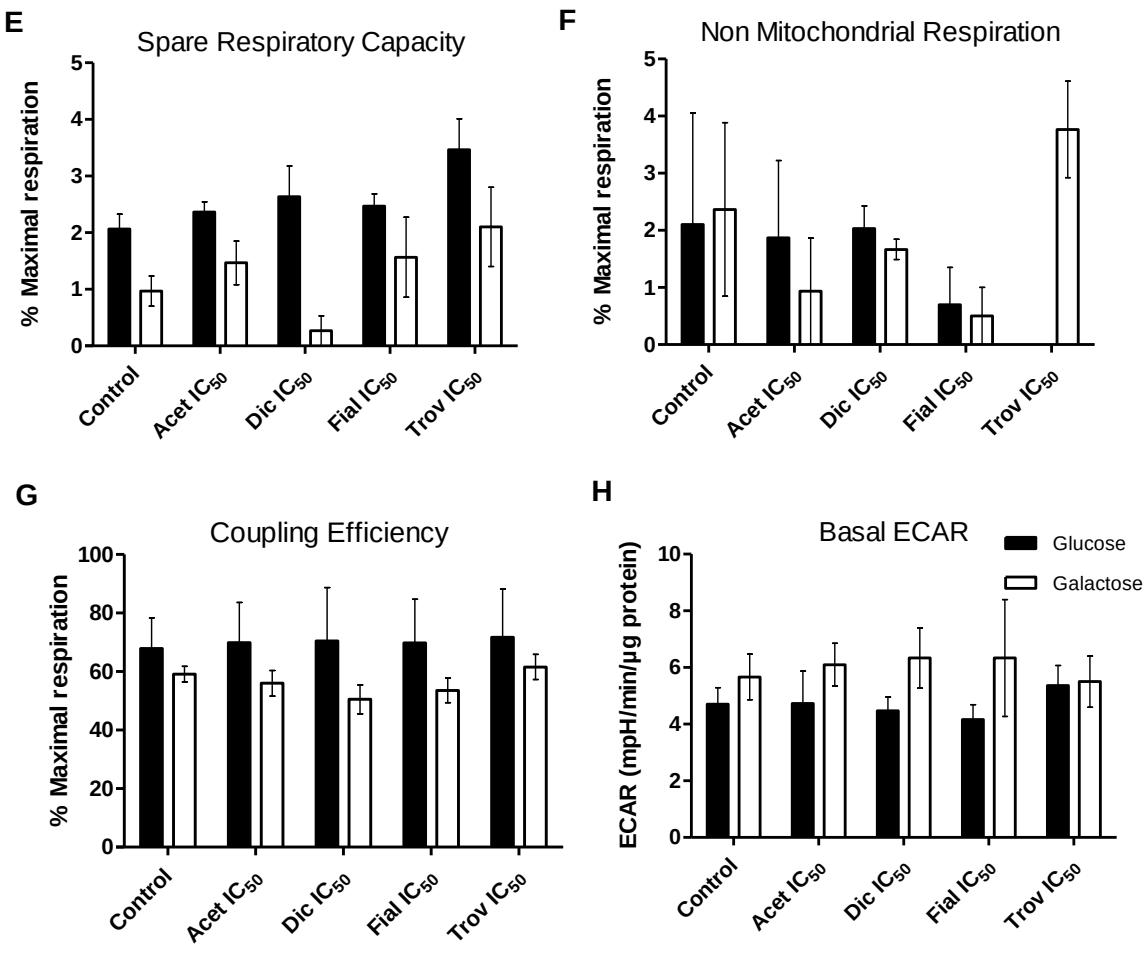

Figure 5.11. Effect of hepatotoxic compounds on mitochondrial function in spheroids cultured in galactose conditions. Spheroids were treated with IC_{50} concentrations of four hepatotoxins for 24 hours after culture in control glucose conditions or galactose conditions. A Mito Stress Test was performed using Seahorse technology and mitochondrial respiratory parameters calculated and plotted as a percentage of maximal respiration. Basal respiration, ATP-linked respiration, proton leak, maximal respiration, spare respiratory capacity, non-mitochondrial respiration, coupling efficiency and basal ECAR are plotted for each culture condition and drug treatment (**A-H**). Data represent mean ± SEM normalised to values obtained from control glucose conditioned spheroids (n=3, 6 replicates).

5.4 Discussion

It was previously revealed that the liver-specific functionality and phenotype of C3A cells was different depending upon whether cultured in 2D and 3D, as well as differences in the sensitivity to numerous hepatotoxins, with overall more human-relevant characteristics when cultured in spheroids. In this chapter the aim was to investigate the bioenergetic profile of C3A cells in 2D and 3D in more detail, as well as explore whether or not the C3A spheroid model could be tailored for the detection of hepatotoxins causing injury through mitochondrial damage.

Mitochondrial function was analysed in C3A spheroids after treatment with four hepatotoxins, in order to detect any subsequent signs of mitochondrial stress. The same repeat-dosing protocol was used as in the previous chapter, to identify any changes the drug might cause after longer, repeated dosing, as some hepatotoxins have been shown to only cause mitochondrial damage after a longer, repeated exposure. Changes in mitochondrial respiratory parameters could successfully be observed after exposure to hepatotoxins. A dose-dependent reduction in basal respiration was detected after treatment with acetaminophen and fialuridine, potentially due to increased ATP demand, inhibited ETC or decreased substrate supply (Hill et al. 2012). The same two compounds caused a decrease in respiration linked to ATP production, which may be due to damaged ETC, reduced ATP demand or low substrate availability (Hill et al. 2012). Another indicator of mitochondrial damage is a decrease in maximal respiration, or SRC, potentially caused by a decreased number of mitochondria or poor ETC integrity. A decrease in SRC results in the cells being less able to respond to oxidative stress or increased energy demand (Hill et al. 2012). Surprisingly, SRC and maximal respiration increased after treatment with all hepatotoxins, perhaps as the cells compensate for the increased stress caused by the hepatotoxins. NMR occurs from any other respiration occurring within the cell, mainly ROS production but also other

oxidases, interestingly levels decreased after hepatotoxin treatment (Hill et al. 2012). Every compound caused a decrease in coupling efficiency which could indicate mitochondrial damage due to electron transport being less efficiently linked to energy production (Brand and Nicholls 2011; Divakaruni et al. 2014; Hill et al. 2012). Hence, the ability to monitor changes in mitochondrial respiration using this method can provide more intricate information about the function of mitochondria and bioenergetics of an *in vitro* model.

Despite observing these changes in mitochondrial respiration after drug treatment, the values were not significantly different to control spheroids. Additionally, the effects on mitochondrial function within spheroid or 2D culture conditions were similar, despite previously showing that C3A spheroids were more sensitive to these hepatotoxins than 2D C3A cells. Hence the primary mechanism of toxicity of these compounds is unlikely to be via mitochondrial dysfunction. This is controversial, as acetaminophen, fialuridine and diclofenac have been previously stated to cause mitochondrial injuries (Boelsterli 2003; Honkoop et al. 1997; Kon et al. 2004; Moreno-Sanchez et al. 1999; Parmar et al. 1995). However, it is possible that the high concentrations of drug compound and repeat-dosing strategy were not appropriate for analysing mitochondrial function, as this would have created a high percentage of cell death in the spheroids, therefore the cells analysed were possibly either very unhealthy from the drug treatment or resistant to toxicity. For this reason, in later experiments spheroids were treated with IC_{50} concentrations for 24 hours, allowing for any acute effects of the compounds on mitochondria to be detected before significant cell death ensues.

The bioenergetic profile of C3A spheroids was next investigated. It was confirmed that under normal culture conditions the spheroids appeared to be under the Crabtree effect to some extent, with the ability to up-regulate glycolytic activity, as a compensatory mechanism for the decrease in mitochondrial energy production

when under stress (Dranka et al. 2011; Marroquin et al. 2007). It was further determined that one could circumvent the Crabtree effect by culturing the spheroids in galactose conditions. The modified spheroids had lower glycolytic activity, due to the unavailability of glucose in the culture medium, and were unable to up-regulate this process even after OXPHOS inhibition with rotenone. However, the differences between the two conditions were only small and non-significant, indicating that the control spheroids may in fact already rely heavily on mitochondria and OXPHOS for ATP production and only be capable of producing a small amount of energy via glycolysis, even when mitochondrial energy production is compromised. This contrast with the results found with 2D C3A cells, which were able to up-regulate glycolysis to a much larger extent. Perhaps this is because the cells in spheroids are not fully under the Crabtree effect, and 3D culture inhibits the ability of C3A cells to up-regulate glycolysis. This could help to explain why 2D C3A cells are less sensitive to hepatotoxins (as seen in Chapter 4), as 2D cells are able to produce more energy via glycolysis and continue to survive despite toxic insult.

Subsequently, the effect of rotenone on cell viability was analysed in spheroids under both conditions. Previous research revealed that HepG2 cells cultured in 2D showed increased sensitivity to rotenone when cultured in galactose conditions, whereas control HepG2 cells were resistant to rotenone toxicity (Kamalian et al. 2015; Marroquin et al. 2007). However, the C3A spheroids were sensitive to rotenone, with only a small difference in toxicity between glucose and galactose-cultured spheroids. Spheroids were also more sensitive to rotenone than 2D C3A cells in control conditions, indicating that the original spheroid model was susceptible and able to detect mitochondrial toxicity. This data provides evidence that the cells in the C3A spheroids are behaving more alike primary cells, using mitochondrial OXPHOS as their main energy production and as a result having

increased susceptibility to compounds which impair mitochondrial function (Marroquin et al. 2007).

The response of the spheroids to four hepatotoxins was analysed to see whether the galactose culture conditions increased the sensitivity of the spheroid model (Beggs et al. 2014; Boelsterli 2003; Honkoop et al. 1997; James et al. 2003; Kon et al. 2004; Moreno-Sanchez et al. 1999; Parmar et al. 1995; Shaw et al. 2010). The galactose-cultured spheroids were not significantly more sensitive to these hepatotoxins than control spheroids. Additionally, mitochondrial respiration parameters were not significantly altered in response to the four hepatotoxins. These data indicate that the control C3A spheroid model already had maximum susceptibility to the four toxins tested. This may be because these toxins are not targeting the mitochondria in the C3A spheroids and toxicity is caused through a different mechanism of action. Inhibition of ATPase activity and mitochondrial permeability transition have been suggested as mechanisms of acetaminophen-induced mitochondrial dysfunction (Kon et al. 2004; Parmar et al. 1995). Diclofenac has been indicated to inhibit mitochondrial ATP synthesis and uncouple OXPHOS, however the results in this chapter do not support this conclusion (Bort et al. 1999; Moreno-Sanchez et al. 1999; Syed et al. 2016). Fialuridine has been hypothesised to cause defects in mitochondrial DNA, resulting in an indirect inhibition of mitochondrial function (Tujios and Fontana, 2011). Despite the fact these compounds have been suggested to cause hepatotoxicity through mitochondrial damage, it has not yet been proven and perhaps mitochondrial dysfunction is not their main mechanism of toxicity.

Since conducting this research other groups have analysed respiratory parameters in C3A cells using a Seahorse technology. Bavli *et al.* were similarly able to detect mitochondrial toxicity induced by rotenone, as well as showing a clear effect of hepatotoxin troglitazone on mitochondrial respiratory parameters before toxicity is

observed (Bavli et al. 2016). This indicates that the analytical method used in this chapter is indeed capable of detecting mitochondrial toxicity in C3A cells, supporting the evidence that the hepatotoxins tested are not directly toxic to mitochondria. However it is possible that the mechanism of mitochondrial injury caused by the hepatotoxins tested is not detectable using the analysis carried out in this work.

There is a downside to using galactose to alter energy metabolism. Culturing cells for prolonged periods in galactose conditions has been shown to have a deleterious effect on the cells. Cells cultured in galactose have been shown to have increased mitophagy and mitochondrial degradation due to the up-regulated OXPHOS (Dombi et al. 2016; Melser et al. 2013; Van Laar et al. 2011).

5.4.1. Conclusion

In summary, the analysis of mitochondrial stress is possible in a C3A spheroid model and intricate changes in mitochondrial function can be identified. The C3A cell line's bioenergetic profile differs depending upon culture condition in that cells in 2D are under the Crabtree effect to a higher degree, whereas spheroids rely more heavily on OXPHOS. This results in the C3A spheroid model being susceptible to mitochondrial toxins without the need to culture in galactose conditions. It was identified that acetaminophen, diclofenac, fialuridine and trovafloxacin do not cause any detectable mitochondrial injury in the C3A liver spheroid model. The ability of the model to analyse intricate mitochondrial liabilities could reduce harm caused by mitochondrial toxins in clinical trials by detecting these dangerous chemicals earlier in the drug development process.

Chapter 6

Concluding Discussion

Contents

6.1 Introduction

As explained throughout this thesis, the overall aim was to develop a novel *in vitro* liver model in the hope of improving its likeness to the human liver in order to investigate DILI. The development of a more *in vivo*-like human-relevant liver model could potentially increase the sensitivity of the drug screening process. This research should contribute to reducing costs, producing safer medicines and consequently minimizing the numbers of adverse effects seen in patients by preventing compounds with hepatotoxic liabilities making it to clinical trials.

In this thesis, a 3D liver spheroid model was successfully developed utilising C3A cells and numerous important parameters were characterised, many of which had not been previously investigated. Once the structure and viability of the spheroids had been thoroughly interrogated and the models likeness to *in vivo* liver tissue discovered, it was further proven that the C3A spheroids were capable of performing numerous liver-specific functions. The enhanced structure and function of the liver spheroids resulted in high sensitivity to liver toxins. Moreover the effect of including NPC in the spheroid model was elucidated, which in fact further increased the sensitivity of the model to hepatotoxins. Finally the bioenergetic profile of C3A spheroids was confirmed, revealing an increased likeness of C3A cells to primary cells once cultured in 2D. Changes in mitochondrial respiration and biomarker release could be detected in response to drug compounds, allowing the mechanism of action of hepatotoxins to be probed in detail. This chapter will discuss the implications of this research and the ongoing efforts to enhance the understanding of the mechanisms of DILI and improve the detection of hepatotoxins preclinically.

6.2 Enhancements in the preclinical investigation of DILI

At the beginning of this project, exciting advancements were taking place in preclinical screening. Researchers were investigating the potential of novel, complex *in vitro* systems, fuelled by the ever increasing failures during drug trials. Simple 2D monoculture cell models were becoming outdated, unable to detect up to 40 % of hepatotoxic compounds and costing companies precious time and money (Xu et al. 2008) and with improvements in tissue culture and engineering, novel techniques were becoming more easily available. Figure 6.1 depicts some of the most common systems in which DILI is investigated.

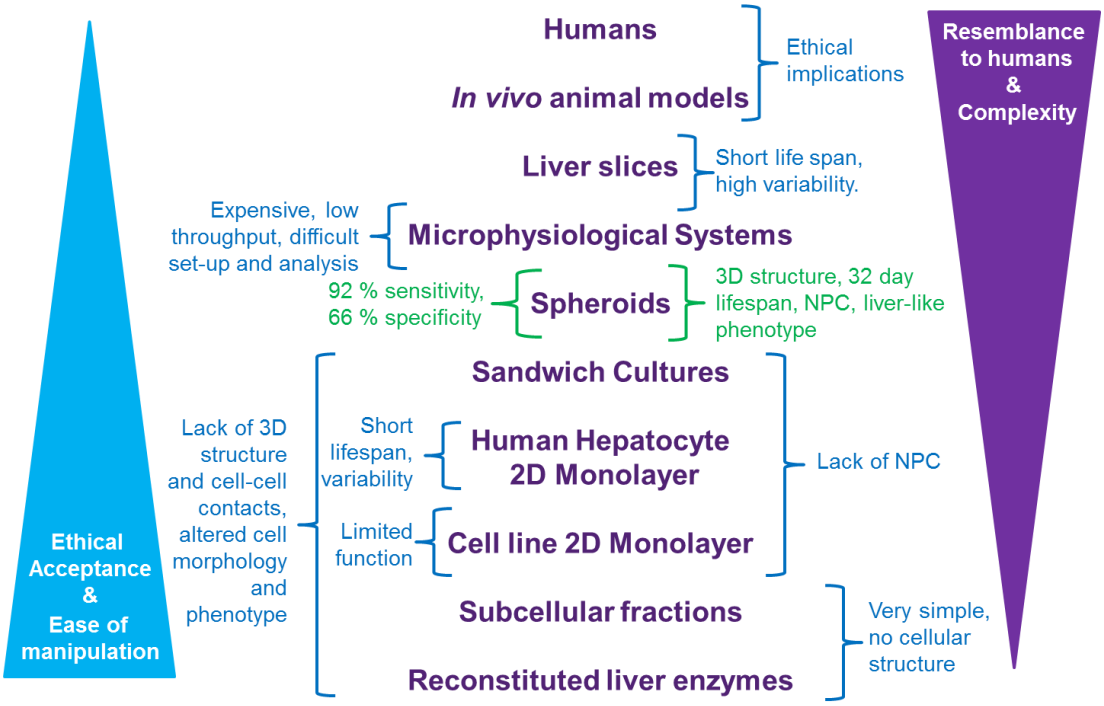

Figure 6. 1. Advancements in liver models. Numerous liver models are available for the investigation of DILI, these models range from the closest resemblance to humans with highest complexity to the most ethically accepted and easy to manipulate systems. With advancements in 3D cell culture, spheroid models have now been optimised and validated for use in drug safety screening, with numerous advantages over older *in vitro* models.

Clinical research into human DILI is essential, furthermore, animal studies are legally required to be performed on two separate species before a chemical can be tested in patients (Krewski et al. 2010). However, it is clear that *in vitro* models are absolutely crucial in order to detect human hepatotoxicity before entering clinical trials. These liver models tend to be human-relevant, inexpensive and with little limitation as to what experiments can be carried out. However, in the past, *in vitro* liver models have lacked complexity, resulting in systems which do not recapitulate human liver structure or function and consequently poorly predict hepatotoxicity (Xu et al. 2008).

Researchers have attempted numerous techniques in order to try and improve liver models, for instance investigating multiple different cell types such as primary hepatocytes, modified cell lines, stem cells, co-cultures as well as culturing with ECM or scaffolds (Godoy et al. 2013). For example, sandwich culture of hepatocytes can prolong their function and produce secondary structures. However, these models still have disadvantages, they do not represent a human liver, and have problems with variability and impracticalities performing the techniques (Godoy et al. 2013; van Zijl and Mikulits 2010). One of the most significant changes to *in vitro* drug testing was undoubtedly the emergence of 3D models. Spheroids, bioreactors and scaffolds have been used for many years in embryonic research and cancer therapeutics and more recently adapted in other areas of drug research (van Zijl and Mikulits 2010). Numerous research groups are now investigating the use of 3D liver models for drug testing, aiming to create organ-like structures in order to detect toxicity of novel drug compounds. 3D liver cell culture has proven on numerous occasions to display more *in vivo*-like structural and functional components when compared to monolayer cultures, correlating with an increased sensitivity to toxicants (Bell et al. 2016; Godoy et al. 2013; Ramaiahgari et al. 2014; Tostoes et al. 2012)

Spheroids appear to have become the one of most popular novel *in vitro* liver models, with multiple companies, such as InSphero and Organovo, now offering pre-formed spheroids to be shipped directly for drug screening purposes. With the advantages of being easier to create and manipulate than more complex novel cell culture techniques, spheroids are an attractive model to bridge the gap between the very simple and overly complex liver models. Furthermore, spheroids created from liver cell lines have the benefits of being more widely available and with less ethical implications than using liver slices or primary cells. These improvements are mirrored in the ability of liver spheroids to detect human hepatotoxins (Bell et al. 2016; Ramaiahgari et al. 2014; Richert et al. 2016; Tostoes et al. 2012). Hence, liver spheroids have immense potential for investigating DILI.

6.3 Potential of the C3A liver spheroid model for the investigation of DILI

How does the C3A spheroid model compare to other *in vitro* liver models? With increasingly complex cell culture models emerging, how do C3A spheroids fit into the drug screening process? Figure 6.2 depicts the important stages in the development of a novel drug compound. *In vitro* models are used in the drug development process to investigate the efficacy of a lead compound, as well as determine its kinetics and safety in humans. It is impossible to choose one perfect model for drug screening; one can however choose an appropriate model, or combination, in order to answer a specific research question.

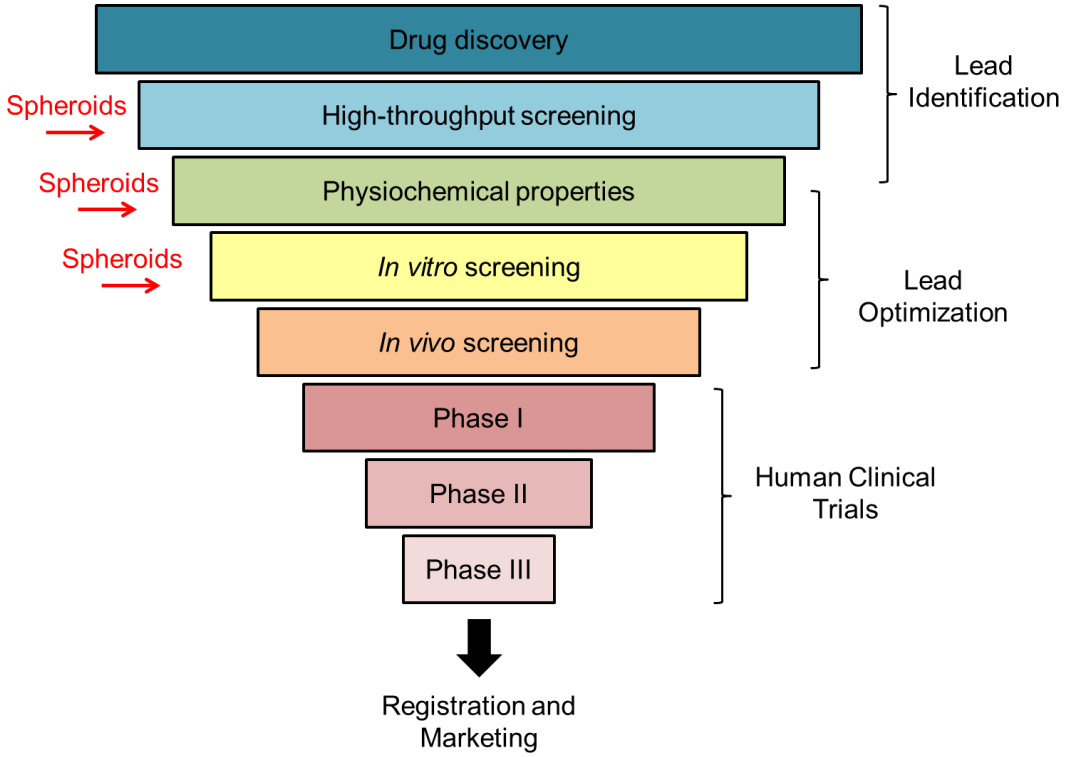

Figure 6.2. The drug development process. The development of a novel therapeutic compound firstly involves the discovery of a novel drug compound. This involved the identification of a lead compound with efficacy for the target of interest using high-throughput screening and analysing physicochemical properties. The next stage, lead optimisation, consists of *in vitro* and *in vivo* testing of these compounds to ensure safety and efficacy of the compound. Finally, clinical trials are performed before the drug can be marketed for clinical use. Spheroids could potentially be utilised at multiple stages of the drug development process.

For preclinical drug screening, an initial simple but effective screen is required to identify lead compounds. This drug screen must ideally be fast, high-throughput, inexpensive, reproducible, readily available and easy to analyse. The spheroid model developed in this thesis can be created in 72 hours, in 96-well plate format, from an inexpensive and reproducible cell line, with easy end-point analysis. Automated production and dosing of C3A spheroids is possible, and has been performed at AstraZeneca, further increasing the ease of use of this model. The biology of the C3A spheroids has been validated, with key parameters elucidated including 32 day lifespan, cell viability, proliferation rate, cell number, diameter, 3D cell morphology and secondary structures. Furthermore, the analysis of liver-specific functions of C3A spheroids revealed an increased likeness to *in vivo* functionality. In addition to this, C3A spheroids display a sensitivity of 90.9 % and specificity of 66 %, higher than that observed in established *in vitro* models (Olsen and Whalen 2009; Olson et al. 2000b). This evidence suggests the potential of a C3A spheroid model to detect hepatotoxins and improve upon the sensitivity of 2D culture models. Hence, C3A spheroids are a promising, novel, human-relevant *in vitro* model for high-throughput drug screening.

In addition, spheroids could be used further down the drug safety process. The C3A spheroid model can be cultured for at least 32 days, allowing for longer and repeated drug exposures, with the potential of analysing sub-acute or delayed drug effects. For a more in-depth analysis the spheroid model could be utilised to investigate the mechanism by which compounds are causing toxicity by analysing novel biomarkers of DILI, mitochondrial function, transporter inhibition or the effect of the compound on NPC. There is even the potential to use more complex spheroids to model liver diseases and examine the efficacy of therapeutic compounds.

6.4 Future potential for *in vitro* liver models

In the future, *in vitro* liver models are likely to become more advanced. Multi-compartmental microfluidics devices are now freely available, allowing the flow of media from one cell model to another, replicating the interaction of multiple different cell types, tissues or organs of the human body. This could involve compartments containing different NPC, allowing the circulation of soluble factors between the different cell types, or indeed the interaction of multiple organ systems with the liver compartment. Liver spheroids could be incorporated into a multi-compartmental model in order to recapitulate a human liver more precisely than 2D cultured cells. Studies have attempted to combine 3D spheroids with flow and the combination of these two techniques could further improve liver-specific functions and result in increased sensitivity to hepatotoxins, once practical difficulties are overcome (Esch et al. 2015; Lee et al. 2013; Tostoes et al. 2012). Novel 3D models have the ability to recreate complex structures incorporating multiple cell types and ECM due to the enhancements in chemical engineering and 3D printing. The production of an entire *in vitro* liver sinusoid structure is now possible, with a capillary compartment supplying a flow of oxygen and nutrients, a 3D mass of hepatocytes and NPC in the sinusoid themselves, secondary structures and a bile compartment to remove waste products produced by the hepatocytes (Choi et al. 2016; Toh et al. 2009; Williams D et al. 2012). Furthermore, in order to overcome some of the practical difficulties of using specialist *in vitro* models, these systems are likely to become more automated, with continuous monitoring of important parameters as well as automated sample collection or imaging in order to become more user friendly and produce higher volumes of data (Bhatia and Ingber 2014). The analysis of these systems is likely to also become more specialised, with technologies such as high-content screening becoming available and entirely automated analysis of end-points, the quantity of data obtained from these drug screens is ever increasing and

these analyses have the potential to have a higher predictivity than *in vivo* models (Ballard et al. 2016; Garside et al. 2014; Persson et al. 2014).

The possibility of replacing animal models with more human-relevant 3D models has been discussed, in order to improve on the 50 % of human hepatotoxins detected in animal studies (Olsen and Whalen 2009). *In vivo* experimentation will always receive criticism due to the unethical nature of causing harm to animals. Furthermore the vast genetic and environmental differences beckons the question as to whether these animal models are relevant to human toxicity (Krewski et al. 2010). Complex human-relevant *in vitro* liver models have immense potential to be used to analyse drug efficacy, ADME (adsorption, drug distribution, metabolism, excretion) and side effects, all of which could help determine a safe and efficacious dose for clinical trials (Ballard et al. 2016; Bhatia and Ingber 2014; Khetani et al. 2015a; Persson et al. 2014). The advantage of microfluidics offers more realistic thermodynamic properties of the model, allowing estimations of compounds exposures (Bhatia and Ingber 2014; Choucha Snouber et al. 2013; Dash et al. 2013; Esch et al. 2015; Khetani et al. 2015a; Rashidi et al. 2016). Furthermore, complex liver models could be used to investigate drug toxicity more intricately, with the possibility to model interactions between multiple organ systems and investigate the mechanisms of drug pharmacology and toxicity in detail (Bhatia and Ingber 2014; Khetani et al. 2015a). Therefore, although abolishing *in vivo* studies completely is unlikely, many animal-based assays could be replaced with an alternative *in vitro* test system. In the future these specialised liver models may have a vital role throughout the drug development process.

Bibliography

Meso-Scale Discovery (Accessed 12/04/2013). In.
Adams DH, Ju C, Ramaiah SK, Uetrecht J, Jaeschke H (2010) Mechanisms of immune-mediated liver injury. Toxicological sciences : an official journal of the Society of Toxicology 115(2):307-21 doi:10.1093/toxsci/kfq009
Amoah AGB, Gould BJ, Parke DV, Lockhart JDF (1986) Further-Studies on the Pharmacokinetics of Perhexiline-Maleate in Humans. Xenobiotica; the fate of foreign compounds in biological systems 16(1):63-68
Anderson CL (2015) The liver sinusoidal endothelium reappears after being eclipsed by the Kupffer cell: a 20th century biological delusion corrected. Journal of leukocyte biology 98(6):875-6 doi:10.1189/jlb.4VMLT0215-054R
Andersson U, Rauvala H (2011) Introduction: HMGB1 in inflammation and innate immunity. Journal of internal medicine 270(4):296-300 doi:10.1111/j.1365-2796.2011.02430.x
Antoine DJ, Dear JW, Starkey-Lewis P, et al. (2013) Mechanistic biomarkers provide early and sensitive detection of acetaminophen-induced acute liver injury at first presentation to hospital. Hepatology doi:10.1002/hep.26294
Antoine DJ, Jenkins RE, Dear JW, et al. (2012) Molecular forms of HMGB1 and keratin-18 as mechanistic biomarkers for mode of cell death and prognosis during clinical acetaminophen hepatotoxicity. Journal of Hepatology 56(5):1070-9
Antoine DJ, Mercer AE, Williams DP, Park BK (2009a) Mechanism-based bioanalysis and biomarkers for hepatic chemical stress. Xenobiotica; the fate of foreign compounds in biological systems 39(8):565-577 doi:10.1080/00498250903046993
Antoine DJ, Williams DP, Kipar A, et al. (2009b) High-mobility group box-1 protein and keratin-18, circulating serum proteins informative of acetaminophen-induced necrosis and apoptosis in vivo. Toxicoligical Sciences 112(2):521-31 doi:10.1093/toxsci/kfp235
Ashrafian H, Horowitz JD, Frenneaux MP (2007) Perhexiline. Cardiovascular drug reviews 25(1):76-97 doi:10.1111/j.1527-3466.2007.00006.x
Asthana A, Kisaalita WS (2012) Microtissue size and hypoxia in HTS with 3D cultures. Drug discovery today 17(15-16):810-7 doi:10.1016/j.drudis.2012.03.004
Atienzar FA, Novik EI, Gerets HH, et al. (2014) Predictivity of dog co-culture model, primary human hepatocytes and HepG2 cells for the detection of hepatotoxic drugs in humans. Toxicology and applied pharmacology 275(1):44-61 doi:10.1016/j.taap.2013.11.022
Bacon. B. R., O'Grady. J. G., Di Bisceglie. A. M., Lake. J. R. (2006) Comprehensive Clinical Hepatology. Elsevier Health Sciences
Bai S, Nasser MW, Wang B, et al. (2009) MicroRNA-122 inhibits tumorigenic properties of hepatocellular carcinoma cells and sensitizes these cells to sorafenib. The Journal of biological chemistry 284(46):32015-27 doi:10.1074/jbc.M109.016774
Ballard TE, Wang S, Cox LM, et al. (2016) Application of a Micropatterned Cocultured Hepatocyte System To Predict Preclinical and Human-Specific Drug Metabolism. Drug Metabolism and Disposition 44(2):172-179 doi:10.1124/dmd.115.066688
Bandyopadhyay S, Klaunig JE, Somani P (1990) Cytotoxic interactions of cardioactive cationic amphiphilic compounds in primary rat hepatocytes in culture. Hepatology 12(1):48-58
Baudoin R, Griscom L, Prot JM, Legallais C, Leclerc E (2011) Behavior of HepG2/C3A cell cultures in a microfluidic bioreactor. Biochem Eng J 53(2):172-181 doi:10.1016/j.bej.2010.10.007
Bavli D, Prill S, Ezra E, et al. (2016) Real-time monitoring of metabolic function in liver-on-chip microdevices tracks the dynamics of mitochondrial dysfunction. Proceedings of the National Academy of Sciences of the United States of America 113(16):E2231-40 doi:10.1073/pnas.1522556113

Beggs KM, Fullerton AM, Miyakawa K, Ganey PE, Roth RA (2014) Molecular mechanisms of hepatocellular apoptosis induced by trovafloxacin-tumor necrosis factor-alpha interaction. Toxicological sciences : an official journal of the Society of Toxicology 137(1):91-101 doi:10.1093/toxsci/kft226

Begriche K, Massart J, Robin MA, Borgne-Sanchez A, Fromenty B (2011) Drug-induced toxicity on mitochondria and lipid metabolism: mechanistic diversity and deleterious consequences for the liver. J Hepatol 54(4):773-94 doi:10.1016/j.jhep.2010.11.006

Bell CC, Hendriks DF, Moro SM, et al. (2016) Characterization of primary human hepatocyte spheroids as a model system for drug-induced liver injury, liver function and disease. Scientific reports 6:25187 doi:10.1038/srep25187

Bell CW, Jiang W, Reich CF, 3rd, Pisetsky DS (2006) The extracellular release of HMGB1 during apoptotic cell death. American Journal of Physiology: Cell Physiology 291(6):C1318-25

Bell LN, Chalasani N (2009) Epidemiology of idiosyncratic drug-induced liver injury. Seminars in liver disease 29(4):337-47 doi:10.1055/s-0029-1240002

Benichou C (1990) Criteria of drug-induced liver disorders. Report of an international consensus meeting. J Hepatol 11(2):272-6

Bhatia SN, Ingber DE (2014) Microfluidic organs-on-chips. Nature biotechnology 32:760-722

Bianchi ME, Beltrame M (1998) Flexing DNA: HMG-box proteins and their partners. American journal of human genetics 63(6):1573-7 doi:10.1086/302170

Biven K, Erdal H, Hagg M, et al. (2003) A novel assay for discovery and characterization of pro-apoptotic drugs and for monitoring apoptosis in patient sera. Apoptosis : an international journal on programmed cell death 8(3):263-8

Boelsterli UA (2003) Diclofenac-induced liver injury: a paradigm of idiosyncratic drug toxicity. Toxicology and applied pharmacology 192(3):307-22

Boelsterli UA, Lim PL (2007) Mitochondrial abnormalities--a link to idiosyncratic drug hepatotoxicity? Toxicology and applied pharmacology 220(1):92-107 doi:10.1016/j.taap.2006.12.013

Borges N (2003) Tolcapone-related liver dysfunction: implications for use in Parkinson's disease therapy. Drug safety 26(11):743-7

Bort R, Ponsoda X, Jover R, Gomez-Lechon MJ, Castell JV (1999) Diclofenac toxicity to hepatocytes: a role for drug metabolism in cell toxicity. The Journal of pharmacology and experimental therapeutics 288(1):65-72

Bouwens L, Baekeland M, De Zanger R, Wisse E (1986) Quantitation, tissue distribution and proliferation kinetics of Kupffer cells in normal rat liver. Hepatology 6(4):718-22

Brand MD, Nicholls DG (2011) Assessing mitochondrial dysfunction in cells. The Biochemical journal 435(2):297-312 doi:10.1042/BJ20110162

Calogero S, Grassi F, Aguzzi A, et al. (1999) The lack of chromosomal protein Hmg1 does not disrupt cell growth but causes lethal hypoglycaemia in newborn mice. Nature Genetics 22(3):276-80 doi:10.1038/10338

Castoldi M, Vujic Spasic M, Altamura S, et al. (2011) The liver-specific microRNA miR-122 controls systemic iron homeostasis in mice. The Journal of clinical investigation 121(4):1386-96 doi:10.1172/JCI44883

Cermelli S, Ruggieri A, Marrero JA, Ioannou GN, Beretta L (2011) Circulating microRNAs in patients with chronic hepatitis C and non-alcoholic fatty liver disease. PloS one 6(8):e23937 doi:10.1371/journal.pone.0023937

Chan HF, Zhang Y, Leong KW (2016) Efficient One-Step Production of Microencapsulated Hepatocyte Spheroids with Enhanced Functions. Small 12(20):2720-30 doi:10.1002/smll.201502932

Chang J, Nicolas E, Marks D, et al. (2004) miR-122, a mammalian liver-specific microRNA, is processed from hcr mRNA and may downregulate the high affinity cationic amino acid transporter CAT-1. RNA biology 1(2):106-13

Chang TT, Hughes-Fulford M (2009) Monolayer and spheroid culture of human liver hepatocellular carcinoma cell line cells demonstrate distinct global gene expression patterns and functional phenotypes. Tissue engineering Part A 15(3):559-67 doi:10.1089/ten.tea.2007.0434

Chinnam P, Mohsin M, Shafee LM (2012) Evaluation of acute toxicity of pioglitazone in mice. Toxicology international 19(3):250-4 doi:10.4103/0971-6580.103660

Cho CH, Park J, Nagrath D, et al. (2007) Oxygen uptake rates and liver-specific functions of hepatocyte and 3T3 fibroblast co-cultures. Biotechnology and bioengineering 97(1):188-99 doi:10.1002/bit.21225

Choi S (2003) Nefazodone (Serzone) withdrawn because of hepatotoxicity. CMAJ : Canadian Medical Association journal = journal de l'Association medicale canadienne 169(11):1187

Choi YY, Kim J, Lee SH, Kim DS (2016) Lab on a chip-based hepatic sinusoidal system simulator for optimal primary hepatocyte culture. Biomedical microdevices 18(4):58 doi:10.1007/s10544-016-0079-6

Choucha Snouber L, Bunescu A, Naudot M, et al. (2013) Metabolomics-on-a-chip of hepatotoxicity induced by anticancer drug flutamide and Its active metabolite hydroxyflutamide using HepG2/C3a microfluidic biochips. Toxicological sciences : an official journal of the Society of Toxicology 132(1):8-20 doi:10.1093/toxsci/kfs230

Cooper GM (2000) The Cell: A Molecular Approach, 2nd Edition edn. Sinauer Associates

Cotran RSK, Vinay; Fausto, Nelson; Nelso Fausto; Robbins, Stanley L.; Abbas, Abul K. (2005) Robbins and Cotran pathologic basic of disease (7th Ed). Elsevier Saunders

Cummings J, Ranson M, Lacasse E, et al. (2006) Method validation and preliminary qualification of pharmacodynamic biomarkers employed to evaluate the clinical efficacy of an antisense compound (AEG35156) targeted to the X-linked inhibitor of apoptosis protein XIAP. British journal of cancer 95(1):42-8 doi:10.1038/sj.bjc.6603220

Curcio E, Salerno S, Barbieri G, De Bartolo L, Drioli E, Bader A (2007) Mass transfer and metabolic reactions in hepatocyte spheroids cultured in rotating wall gas-permeable membrane system. Biomaterials 28(36):5487-97 doi:10.1016/j.biomaterials.2007.08.033

Dake MD, Madison JM, Montgomery CK, et al. (1985) Electron microscopic demonstration of lysosomal inclusion bodies in lung, liver, lymph nodes, and blood leukocytes of patients with amiodarone pulmonary toxicity. The American journal of medicine 78(3):506-12

Dash A, Simmers MB, Deering TG, et al. (2013) Hemodynamic flow improves rat hepatocyte morphology, function, and metabolic activity in vitro. Am J Physiol-Cell Ph 304(11):C1053-C1063 doi:10.1152/ajpcell.00331.2012

Dell' Antone P (2012) Energy metabolism in cancer cells: how to explain the Warburg and Crabtree effects? Medical hypotheses 79(3):388-92 doi:10.1016/j.mehy.2012.06.002

Diaz-Ruiz R, Rigoulet M, Devin A (2011) The Warburg and Crabtree effects: On the origin of cancer cell energy metabolism and of yeast glucose repression. Biochimica et biophysica acta 1807(6):568-76 doi:10.1016/j.bbabio.2010.08.010

Ding BS, Nolan DJ, Butler JM, et al. (2010) Inductive angiocrine signals from sinusoidal endothelium are required for liver regeneration. Nature 468(7321):310-5 doi:10.1038/nature09493

Divakaruni AS, Paradyse A, Ferrick DA, Murphy AN, Jastroch M (2014) Analysis and interpretation of microplate-based oxygen consumption and pH data. Methods in enzymology 547:309-54 doi:10.1016/B978-0-12-801415-8.00016-3

Domansky K, Inman W, Serdy J, Dash A, Lim MHM, Griffith LG (2010) Perfused multiwell plate for 3D liver tissue engineering. Lab on a chip 10(1):51-58 doi:10.1039/b913221j

Dombi E, Diot A, Morten K, et al. (2016) The m.13051G>A mitochondrial DNA mutation results in variable neurology and activated mitophagy. Neurology 86(20):1921-3 doi:10.1212/WNL.0000000000002688

Donato MT, Lahoz A, Castell JV, Gomez-Lechon MJ (2008) Cell lines: a tool for in vitro drug metabolism studies. Current drug metabolism 9(1):1-11

Dorst N, Oberringer M, Grasser U, Pohlemann T, Metzger W (2014) Analysis of cellular composition of co-culture spheroids. Annals of anatomy = Anatomischer Anzeiger : official organ of the Anatomische Gesellschaft 196(5):303-11 doi:10.1016/j.aanat.2014.05.038

Dranka BP, Benavides GA, Diers AR, et al. (2011) Assessing bioenergetic function in response to oxidative stress by metabolic profiling. Free Radical Bio Med 51(9):1621-1635 doi:10.1016/j.freeradbiomed.2011.08.005

Dufour DR, Lott JA, Nolte FS, Gretch DR, Koff RS, Seeff LB (2000) Diagnosis and monitoring of hepatic injury. I. Performance characteristics of laboratory tests. Clinical chemistry 46(12):2027-49

Dunn JC, Tompkins RG, Yarmush ML (1991) Long-term in vitro function of adult hepatocytes in a collagen sandwich configuration. Biotechnology progress 7(3):237-45 doi:10.1021/bp00009a007

Dutkowski R, Graf R, Clavien PA (2006) Rescue of the cold preserved rat liver by hypothermic oxygenated machine perfusion. Am J Transplant 6(5):903-912 doi:10.1111/j.1600-6143.2006.01264.x

Edling Y, Sivertsson LK, Butura A, Ingelman-Sundberg M, Ek M (2009) Increased sensitivity for troglitazone-induced cytotoxicity using a human in vitro co-culture model. Toxicol in Vitro 23(7):1387-95 doi:10.1016/j.tiv.2009.07.026

Edwards IR, Aronson JK (2000) Adverse drug reactions: definitions, diagnosis, and management. Lancet 356(9237):1255-9 doi:10.1016/S0140-6736(00)02799-9

Eriksson C, Gustavsson A, Kronvall T, Tysk C (2011) Hepatotoxicity by bosentan in a patient with portopulmonary hypertension: a case-report and review of the literature. Journal of gastrointestinal and liver diseases : JGLD 20(1):77-80

Esch MB, Prot JM, Wang YI, et al. (2015) Multi-cellular 3D human primary liver cell culture elevates metabolic activity under fluidic flow. Lab on a chip 15(10):2269-77 doi:10.1039/c5lc00237k

Esteller A (2008) Physiology of bile secretion. World J Gastroentero 14(37):5641-5649 doi:Doi 10.3748/Wjg.14.5641

Evankovich J, Cho SW, Zhang R, et al. (2010) High Mobility Group Box 1 Release from Hepatocytes during Ischemia and Reperfusion Injury Is Mediated by Decreased Histone Deacetylase Activity. Journal of Biological Chemistry 285(51):39888-39897 doi:10.1074/jbc.M110.128348

Farquhar MG, Palade GE (1963) Junctional complexes in various epithelia. The Journal of cell biology 17:375-412

Fattinger K, Funk C, Pantze M, et al. (2001) The endothelin antagonist bosentan inhibits the canalicular bile salt export pump: a potential mechanism for hepatic adverse reactions. Clinical pharmacology and therapeutics 69(4):223-31 doi:10.1067/mcp.2001.114667

Fey SJ, Wrzesinski K (2012) Determination of drug toxicity using 3D spheroids constructed from an immortal human hepatocyte cell line. Toxicological sciences : an official journal of the Society of Toxicology 127(2):403-11 doi:10.1093/toxsci/kfs122

Fey SJ, Wrzesinski K (2013) Microgravity spheroids as a reliable, long-term tool for predictive toxicology. Toxicology letters 221:S153-S153 doi:10.1016/j.toxlet.2013.05.318

Filippi C, Keatch SA, Rangar D, Nelson LJ, Hayes PC, Plevris JN (2004) Improvement of C3A cell metabolism for usage in bioartificial liver support systems. J Hepatol 41(4):599-605 doi:10.1016/j.jhep.2004.06.012

Fisher A, Croft-Baker J, Davis M, Purcell P, McLean AJ (2002) Entacapone-induced hepatotoxicity and hepatic dysfunction. Movement disorders : official journal of the Movement Disorder Society 17(6):1362-5; discussion 1397-1400 doi:10.1002/mds.10342

Friedrich J, Seidel C, Ebner R, Kunz-Schughart LA (2009) Spheroid-based drug screen: considerations and practical approach. Nature protocols 4(3):309-24 doi:10.1038/nprot.2008.226

Fromenty B, Pessayre D (1997) Impaired mitochondrial function in microvesicular steatosis. Effects of drugs, ethanol, hormones and cytokines. J Hepatol 26 Suppl 2:43-53

Funatsu K, Ijima H, Nakazawa K, Yamashita Y, Shimada M, Sugimachi K (2001) Hybrid artificial liver using hepatocyte organoid culture. Artificial organs 25(3):194-200

Garside H, Marcoe KF, Chesnut-Speelman J, et al. (2014) Evaluation of the use of imaging parameters for the detection of compound-induced hepatotoxicity in 384-well cultures of HepG2 cells and cryopreserved primary human hepatocytes. Toxicol in Vitro 28(2):171-181 doi:10.1016/j.tiv.2013.10.015

Gebhardt R (1992) Metabolic zonation of the liver: regulation and implications for liver function. Pharmacology & therapeutics 53(3):275-354

Gebhardt R, Hengstler JG, Muller D, et al. (2003) New hepatocyte in vitro systems for drug metabolism: metabolic capacity and recommendations for application in basic research and drug development, standard operation procedures. Drug metabolism reviews 35(2-3):145-213 doi:10.1081/DMR-120023684

Gerets HH, Tilmant K, Gerin B, et al. (2012) Characterization of primary human hepatocytes, HepG2 cells, and HepaRG cells at the mRNA level and CYP activity in response to inducers and their predictivity for the detection of human hepatotoxins. Cell biology and toxicology 28(2):69-87 doi:10.1007/s10565-011-9208-4

Gerlach JC, Mutig K, Sauer IM, et al. (2003) Use of primary human liver cells originating from discarded grafts in a bioreactor for liver support therapy and the prospects of culturing adult liver stem cells in bioreactors: A morphologic study. Transplantation 76(5):781-786 doi:10.1097/01.Tp.0000083319.36931.32

Gissen P, Arias IM (2015) Structural and functional hepatocyte polarity and liver disease. J Hepatol 63(4):1023-37 doi:10.1016/j.jhep.2015.06.015

Godoy P, Hewitt NJ, Albrecht U, et al. (2013) Recent advances in 2D and 3D in vitro systems using primary hepatocytes, alternative hepatocyte sources and non-parenchymal liver cells and their use in investigating mechanisms of hepatotoxicity, cell signaling and ADME. Archives of toxicology 87(8):1315-530 doi:10.1007/s00204-013-1078-5

Gomez-Lechon MJ, Donato MT, Castell JV, Jover R (2004) Human hepatocytes in primary culture: the choice to investigate drug metabolism in man. Current drug metabolism 5(5):443-62

Gomez-Lechon MJ, Jover R, Donato T, et al. (1998) Long-term expression of differentiated functions in hepatocytes cultured in three-dimensional collagen matrix. Journal of cellular physiology 177(4):553-62 doi:10.1002/(SICI)1097-4652(199812)177:4<553::AID-JCP6>3.0.CO;2-F

Grimes DR, Kelly C, Bloch K, Partridge M (2014) A method for estimating the oxygen consumption rate in multicellular tumour spheroids. Journal of the Royal Society, Interface / the Royal Society 11(92):20131124 doi:10.1098/rsif.2013.1124

Guguen-Guillouzo C, Corlu A, Guillouzo A (2010) Stem cell-derived hepatocytes and their use in toxicology. Toxicology 270(1):3-9 doi:10.1016/j.tox.2009.09.019

Guillouzo A, Corlu A, Aninat C, Glaise D, Morel F, Guguen-Guillouzo C (2007) The human hepatoma HepaRG cells: a highly differentiated model for studies of liver metabolism and toxicity of xenobiotics. Chemico-biological interactions 168(1):66-73 doi:10.1016/j.cbi.2006.12.003

Gunness P, Mueller D, Shevchenko V, Heinzle E, Ingelman-Sundberg M, Noor F (2013) 3D organotypic cultures of human HepaRG cells: a tool for in vitro toxicity studies. Toxicological sciences : an official journal of the Society of Toxicology 133(1):67-78 doi:10.1093/toxsci/kft021

Guo L, Dial S, Shi L, et al. (2011) Similarities and differences in the expression of drug-metabolizing enzymes between human hepatic cell lines and primary human hepatocytes. Drug metabolism and disposition: the biological fate of chemicals 39(3):528-38 doi:10.1124/dmd.110.035873

Guyot C, Lepreux S, Combe C, et al. (2006) Hepatic fibrosis and cirrhosis: the (myo)fibroblastic cell subpopulations involved. The international journal of biochemistry & cell biology 38(2):135-51 doi:10.1016/j.biocel.2005.08.021

Harrill AH, Roach J, Fier I, et al. (2012) The Effects of Heparins on the Liver: Application of Mechanistic Serum Biomarkers in a Randomized Study in Healthy Volunteers. Clinical Pharmacology & Therapeutics 92(2):214-220 doi:10.1038/clpt.2012.40

Herzog N, Hansen M, Miethbauer S, et al. (2015) Primary-like Human Hepatocytes Genetically Engineered to Obtain Proliferation Competence Display Hepatic Differentiation Characteristics in Monolayer and Organotypical Spheroid Cultures. Cell biology international doi:10.1002/cbin.10574

Hewitt NJ, Lechon MJ, Houston JB, et al. (2007) Primary hepatocytes: current understanding of the regulation of metabolic enzymes and transporter proteins, and pharmaceutical practice for the use of hepatocytes in metabolism, enzyme induction, transporter, clearance, and hepatotoxicity studies. Drug metabolism reviews 39(1):159-234 doi:10.1080/03602530601093489

Hill BG, Benavides GA, Lancaster JR, Jr., et al. (2012) Integration of cellular bioenergetics with mitochondrial quality control and autophagy. Biological chemistry 393(12):1485-1512 doi:10.1515/hsz-2012-0198

Hinson JA, Roberts DW, James LP (2010) Mechanisms of acetaminophen-induced liver necrosis. Handbook of experimental pharmacology(196):369-405 doi:10.1007/978-3-642-00663-0_12

Honkoop P, Scholte HR, de Man RA, Schalm SW (1997) Mitochondrial injury. Lessons from the fialuridine trial. Drug safety 17(1):1-7

InSphero (2016) InSphero. In.

James LP, Mayeux PR, Hinson JA (2003) Acetaminophen-induced hepatotoxicity. Drug metabolism and disposition: the biological fate of chemicals 31(12):1499-506 doi:10.1124/dmd.31.12.1499

Janko C, Filipovic MR, Munoz L, et al. (2013) Redox modulation of HMGB1-related signaling. Antioxidants & redox signaling doi:10.1089/ars.2013.5179

Jedlitschky G, Hoffmann U, Kroemer HK (2006) Structure and function of the MRP2 (ABCC2) protein and its role in drug disposition. Expert opinion on drug metabolism & toxicology 2(3):351-66 doi:10.1517/17425255.2.3.351

Jones W, Bianchi K (2015) Aerobic glycolysis: beyond proliferation. Frontiers in immunology 6:227 doi:10.3389/fimmu.2015.00227

Jorga K, Fotteler B, Heizmann P, Gasser R (1999) Metabolism and excretion of tolcapone, a novel inhibitor of catechol-O-methyltransferase. Brit J Clin Pharmaco 48(4):513-520 doi:DOI 10.1046/j.1365-2125.1999.00036.x

Ju SM, Jang HJ, Kim KB, Kim J (2015) High-Throughput Cytotoxicity Testing System of Acetaminophen Using a Microfluidic Device (MFD) in HepG2 Cells. Journal of toxicology and environmental health Part A 78(16):1063-72 doi:10.1080/15287394.2015.1068650

Kalgutkar AS, Vaz AD, Lame ME, et al. (2005) Bioactivation of the nontricyclic antidepressant nefazodone to a reactive quinone-imine species in human liver microsomes and recombinant cytochrome P450 3A4. Drug metabolism and disposition: the biological fate of chemicals 33(2):243-53 doi:10.1124/dmd.104.001735

Kamalian L, Chadwick AE, Bayliss M, et al. (2015) The utility of HepG2 cells to identify direct mitochondrial dysfunction in the absence of cell death. Toxicol in Vitro 29(4):732-40 doi:10.1016/j.tiv.2015.02.011

Kang YB, Rawat S, Cirillo J, Bouchard M, Noh HM (2013) Layered long-term co-culture of hepatocytes and endothelial cells on a transwell membrane: toward engineering the liver sinusoid. Biofabrication 5(4):045008 doi:10.1088/1758-5082/5/4/045008

Kaplowitz N (2005) Idiosyncratic drug hepatotoxicity. Nat Rev Drug Discov 4(6):489-499 doi:10.1038/nrd1750

Kasinskas RW, Venkatasubramanian R, Forbes NS (2014) Rapid uptake of glucose and lactate, and not hypoxia, induces apoptosis in three-dimensional tumor tissue culture. Integrative biology : quantitative biosciences from nano to macro doi:10.1039/c4ib00001c

Kasuya J, Sudo R, Mitaka T, Ikeda M, Tanishita K (2011) Hepatic stellate cell-mediated three-dimensional hepatocyte and endothelial cell triculture model. Tissue engineering Part A 17(3-4):361-70 doi:10.1089/ten.TEA.2010.0033

Kazama H, Ricci JE, Herndon JM, Hoppe G, Green DR, Ferguson TA (2008) Induction of immunological tolerance by apoptotic cells requires caspase-dependent oxidation of high-mobility group box-1 protein. Immunity 29(1):21-32 doi:10.1016/j.immuni.2008.05.013

Kegel V, Pfeiffer E, Burkhardt B, et al. (2015) Subtoxic Concentrations of Hepatotoxic Drugs Lead to Kupffer Cell Activation in a Human In Vitro Liver Model: An Approach to Study DILI. Mediators of inflammation 2015:640631 doi:10.1155/2015/640631

Keisu M, Andersson TB (2010) Drug-induced liver injury in humans: the case of ximelagatran. Handbook of experimental pharmacology(196):407-18 doi:10.1007/978-3-642-00663-0_13

Khetani SR, Berger DR, Ballinger KR, Davidson MD, Lin C, Ware BR (2015a) Microengineered liver tissues for drug testing. Journal of laboratory automation 20(3):216-50 doi:10.1177/2211068214566939

Khetani SR, Berger DR, Ballinger KR, Davidson MD, Lin C, Ware BR (2015b) Microengineered Liver Tissues for Drug Testing. Journal of laboratory automation doi:10.1177/2211068214566939

Kia R, Kelly L, Sison-Young RL, et al. (2015) MicroRNA-122: a novel hepatocyte-enriched in vitro marker of drug-induced cellular toxicity. Toxicological sciences : an official journal of the Society of Toxicology 144(1):173-85 doi:10.1093/toxsci/kfu269

Kmiec Z (2001) Cooperation of liver cells in health and disease. Advances in anatomy, embryology, and cell biology 161:III-XIII, 1-151

Knobeloch D, Ehnert S, Schyschka L, et al. (2012) Human hepatocytes: isolation, culture, and quality procedures. Methods in molecular biology 806:99-120 doi:10.1007/978-1-61779-367-7_8

Koenig S, Aurich H, Schneider C, et al. (2007) Zonal expression of hepatocytic marker enzymes during liver repopulation. Histochemistry and cell biology 128(2):105-14 doi:10.1007/s00418-007-0301-y

Kolios G, Valatas V, Kouroumalis E (2006) Role of Kupffer cells in the pathogenesis of liver disease. World journal of gastroenterology : WJG 12(46):7413-20

Kon K, Kim JS, Jaeschke H, Lemasters JJ (2004) Mitochondrial permeability transition in acetaminophen-induced necrosis and apoptosis of cultured mouse hepatocytes. Hepatology 40(5):1170-9 doi:10.1002/hep.20437

Kordes C, Sawitza I, Haussinger D (2008) Canonical Wnt signaling maintains the quiescent stage of hepatic stellate cells. Biochemical and biophysical research communications 367(1):116-23 doi:10.1016/j.bbrc.2007.12.085

Kordes C, Sawitza I, Haussinger D (2009) Hepatic and pancreatic stellate cells in focus. Biological chemistry 390(10):1003-12 doi:10.1515/BC.2009.121

Kordes C, Sawitza I, Muller-Marbach A, et al. (2007) CD133+ hepatic stellate cells are progenitor cells. Biochemical and biophysical research communications 352(2):410-7 doi:10.1016/j.bbrc.2006.11.029

Kostadinova R, Boess F, Applegate D, et al. (2013) A long-term three dimensional liver co-culture system for improved prediction of clinically relevant drug-induced hepatotoxicity. Toxicology and applied pharmacology 268(1):1-16 doi:10.1016/j.taap.2013.01.012

Kostrubsky SE, Strom SC, Kalgutkar AS, et al. (2006) Inhibition of hepatobiliary transport as a predictive method for clinical hepatotoxicity of nefazodone. Toxicological sciences : an official journal of the Society of Toxicology 90(2):451-9 doi:10.1093/toxsci/kfj095

Krewski D, Acosta D, Jr., Andersen M, et al. (2010) Toxicity testing in the 21st century: a vision and a strategy. Journal of toxicology and environmental health Part B, Critical reviews 13(2-4):51-138 doi:10.1080/10937404.2010.483176

Krishna M (2013) Microscopic anatomy of the liver. Clinical Liver Disease 2(S1):S4-S7

Krutzfeldt J, Stoffel M (2006) MicroRNAs: a new class of regulatory genes affecting metabolism. Cell metabolism 4(1):9-12 doi:10.1016/j.cmet.2006.05.009

Ku NO, Strnad P, Zhong BH, Tao GZ, Omary MB (2007) Keratins let liver live: Mutations predispose to liver disease and crosslinking generates Mallory-Denk bodies. Hepatology 46(5):1639-49 doi:10.1002/hep.21976

Kullak-Ublick GA (2000-2013) Drug-Induced Cholestatic Liver Disease

Kutay H, Bai S, Datta J, et al. (2006) Downregulation of miR-122 in the rodent and human hepatocellular carcinomas. Journal of cellular biochemistry 99(3):671-8 doi:10.1002/jcb.20982

Lasser KE, Allen PD, Woolhandler SJ, Himmelstein DU, Wolfe SM, Bor DH (2002) Timing of new black box warnings and withdrawals for prescription medications. Jama 287(17):2215-20

Laverty HG, Antoine DJ, Benson C, Chaponda M, Williams D, Park BK (2010) The potential of cytokines as safety biomarkers for drug-induced liver injury. European Journal of Clinical Pharmacology 66(10):961-976 doi:10.1007/s00228-010-0862-x

Lea JD, Clarke JI, McGuire N, Antoine DJ (2016) Redox-Dependent HMGB1 Isoforms as Pivotal Co-Ordinators of Drug-Induced Liver Injury: Mechanistic Biomarkers and Therapeutic Targets. Antioxidants & redox signaling 24(12):652-665 doi:10.1089/ars.2015.6406

LeCluyse EL, Alexandre E, Hamilton GA, et al. (2005) Isolation and culture of primary human hepatocytes. Methods in molecular biology 290:207-29

LeCluyse EL, Witek RP, Andersen ME, Powers MJ (2012) Organotypic liver culture models: meeting current challenges in toxicity testing. Critical reviews in toxicology 42(6):501-48 doi:10.3109/10408444.2012.682115

Lee SA, No da Y, Kang E, Ju J, Kim DS, Lee SH (2013) Spheroid-based three-dimensional liver-on-a-chip to investigate hepatocyte-hepatic stellate cell interactions and flow effects. Lab on a chip 13(18):3529-37 doi:10.1039/c3lc50197c

Lee WM (2003) Drug-induced hepatotoxicity. The New England journal of medicine 349(5):474-85 doi:10.1056/NEJMra021844

Limmer A, Knolle PA (2001) Liver sinusoidal endothelial cells: a new type of organ-resident antigen-presenting cell. Archivum immunologiae et therapiae experimentalis 49 Suppl 1:S7-11

Lin Z, Will Y (2012) Evaluation of drugs with specific organ toxicities in organ-specific cell lines. Toxicological sciences : an official journal of the Society of Toxicology 126(1):114-27 doi:10.1093/toxsci/kfr339

Liou IW, Larson AM (2008) Role of liver transplantation in acute liver failure. Seminars in liver disease 28(2):201-9 doi:10.1055/s-2008-1073119

Lippincott. J. B (1993) Diseases of the Liver, 7 edn. Wiley-Blackwell

Liu D, Fan J, Mei M, Ingvarsson S, Chen H (2009) Identification of miRNAs in a liver of a human fetus by a modified method. PloS one 4(10):e7594 doi:10.1371/journal.pone.0007594

Loi CM, Alvey CW, Vassos AB, Randinitis EJ, Sedman AJ, Koup JR (1999) Steady-state pharmacokinetics and dose proportionality of troglitazone and its metabolites. Journal of clinical pharmacology 39(9):920-926 doi:Doi 10.1177/00912709922008533

Loi CM, Randinitis EJ, Vassos AB, Kazierad DJ, Koup JR, Sedman AJ (1997) Lack of effect of type II diabetes on the pharmacokinetics of troglitazone in a multiple-dose study. Journal of clinical pharmacology 37(12):1114-1120

Longati P, Jia X, Eimer J, et al. (2013) 3D pancreatic carcinoma spheroids induce a matrix-rich, chemoresistant phenotype offering a better model for drug testing. BMC cancer 13:95 doi:10.1186/1471-2407-13-95

Mantovani A, Cassatella MA, Costantini C, Jaillon S (2011) Neutrophils in the activation and regulation of innate and adaptive immunity. Nature reviews Immunology 11(8):519-31 doi:10.1038/nri3024

Marroquin LD, Hynes J, Dykens JA, Jamieson JD, Will Y (2007) Circumventing the Crabtree effect: replacing media glucose with galactose increases susceptibility of HepG2 cells to mitochondrial toxicants. Toxicological sciences : an official journal of the Society of Toxicology 97(2):539-47 doi:10.1093/toxsci/kfm052

Materne EM, Ramme AP, Terrasso AP, et al. (2015) A multi-organ chip co-culture of neurospheres and liver equivalents for long-term substance testing. Journal of biotechnology 205:36-46 doi:10.1016/j.jbiotec.2015.02.002

Mavri-Damelin D, Damelin LH, Eaton S, Rees M, Selden C, Hodgson HJ (2008) Cells for bioartificial liver devices: the human hepatoma-derived cell line C3A produces urea but does not detoxify ammonia. Biotechnology and bioengineering 99(3):644-51 doi:10.1002/bit.21599

McKenzie R, Fried MW, Sallie R, et al. (1995) Hepatic failure and lactic acidosis due to fialuridine (FIAU), an investigational nucleoside analogue for chronic hepatitis B. The New England journal of medicine 333(17):1099-105 doi:10.1056/NEJM199510263331702

Melser S, Chatelain EH, Lavie J, et al. (2013) Rheb regulates mitophagy induced by mitochondrial energetic status. Cell metabolism 17(5):719-30 doi:10.1016/j.cmet.2013.03.014

Messner S, Agarkova I, Moritz W, Kelm JM (2013) Multi-cell type human liver microtissues for hepatotoxicity testing. Archives of toxicology 87(1):209-13 doi:10.1007/s00204-012-0968-2

Michalopoulos GK (2007) Liver regeneration. Journal of cellular physiology 213(2):286-300 doi:10.1002/jcp.21172

Moghe PV, Coger RN, Toner M, Yarmush ML (1997) Cell-cell interactions are essential for maintenance of hepatocyte function in collagen gel but not on matrigel. Biotechnology and bioengineering 56(6):706-11

Moreno-Sanchez R, Bravo C, Vasquez C, Ayala G, Silveira LH, Martinez-Lavin M (1999) Inhibition and uncoupling of oxidative phosphorylation by nonsteroidal anti-inflammatory drugs: study in mitochondria, submitochondrial particles, cells, and whole heart. Biochemical pharmacology 57(7):743-52

Mueller D, Koetemann A, Noor F (2011) Organotypic Cultures of HepG2 Cells for In Vitro Toxicity Studies. Journal of Bioengineering & Biomedical Science 1(S2):10

Mueller S, Guillouzo A, Hewitt P, Richert L (2015) Overview on liver cell models and their use in pharmaceutical drug toxicity testing. Toxicol in Vitro 14:172-186

Murakami Y, Yasuda T, Saigo K, et al. (2005) Comprehensive analysis of microRNA expression patterns in hepatocellular carcinoma and non-tumorous tissues. Oncogene 25(2537-2545)

Murphy SV, Atala A (2014) 3D bioprinting of tissues and organs. Nature biotechnology 32(8):773-85 doi:10.1038/nbt.2958

Navarro VJ, Senior JR (2006) Drug-related hepatotoxicity. The New England journal of medicine 354(7):731-9 doi:10.1056/NEJMra052270

Nelson LJ, Navarro M, Treskes P, et al. (2015) Acetaminophen cytotoxicity is ameliorated in a human liver organotypic co-culture model. Scientific reports 5:17455 doi:10.1038/srep17455

Nibourg GA, Chamuleau RA, van Gulik TM, Hoekstra R (2012) Proliferative human cell sources applied as biocomponent in bioartificial livers: a review. Expert opinion on biological therapy 12(7):905-21 doi:10.1517/14712598.2012.685714

Norris W, Paredes AH, Lewis JH (2008) Drug-induced liver injury in 2007. Current opinion in gastroenterology 24(3):287-97 doi:10.1097/MOG.0b013e3282f9764b

Nystrom S, Antoine DJ, Lundback P, et al. (2012) TLR activation regulates damage-associated molecular pattern isoforms released during pyroptosis. The EMBO journal doi:10.1038/emboj.2012.328

O'Brien PJ, Irwin W, Diaz D, et al. (2006) High concordance of drug-induced human hepatotoxicity with in vitro cytotoxicity measured in a novel cell-based model using high content screening. Archives of toxicology 80(9):580-604 doi:10.1007/s00204-006-0091-3

Ogihara T, Iwai H, Inoue T, et al. (2015) Utility of human hepatocyte spheroids for evaluation of hepatotoxicity. Fundamental Toxicological Sciences 2(1):41-48

Ohno M, Motojima K, Okano T, Taniguchi A (2009) Induction of drug-metabolizing enzymes by phenobarbital in layered co-culture of a human liver cell line and endothelial cells. Biological & pharmaceutical bulletin 32(5):813-7

Olanow CW (2000) Tolcapone and hepatotoxic effects. Tasmar Advisory Panel. Archives of neurology 57(2):263-7

Olive PL, Vikse C, Trotter MJ (1992) Measurement of oxygen diffusion distance in tumor cubes using a fluorescent hypoxia probe. International journal of radiation oncology, biology, physics 22(3):397-402

Olsen AK, Whalen MD (2009) Public perceptions of the pharmaceutical industry and drug safety: implications for the pharmacovigilance professional and the culture of safety. Drug safety 32(10):805-10 doi:10.2165/11316620-000000000-00000

Olson H, Betton G, Robinson D, et al. (2000a) Concordance of the toxicity of pharmaceuticals in humans and in animals. Regul Toxicol Pharm 32(1):56-67 doi:DOI 10.1006/rtph.2000.1399

Olson H, Betton G, Robinson D, et al. (2000b) Concordance of the toxicity of pharmaceuticals in humans and in animals. Regulatory toxicology and pharmacology : RTP 32(1):56-67 doi:10.1006/rtph.2000.1399

Omary MB, Ku NO, Toivola DM (2002) Keratins: guardians of the liver. Hepatology 35(2):251-7 doi:10.1053/jhep.2002.31165

Opie EL (1904) Zonal Necrosis of the Liver. The Journal of medical research 12(1):147-168 1

Ostapowicz G, Fontana RJ, Schiodt FV, et al. (2002) Results of a prospective study of acute liver failure at 17 tertiary care centers in the United States. Annals of internal medicine 137(12):947-54

Ozer J, Ratner M, Shaw M, Bailey W, Schomaker S (2008) The current state of serum biomarkers of hepatotoxicity. Toxicology 245(3):194-205 doi:10.1016/j.tox.2007.11.021

Parmar DV, Ahmed G, Khandkar MA, Katyare SS (1995) Mitochondrial ATPase: a target for paracetamol-induced hepatotoxicity. European journal of pharmacology 293(3):225-9

Persson M, Loye AF, Jacquet M, et al. (2014) High-content analysis/screening for predictive toxicology: application to hepatotoxicity and genotoxicity. Basic Clin Pharmacol Toxicol 115(1):18-23 doi:10.1111/bcpt.12200

Peshwa MV, Wu FJ, Sharp HL, Cerra FB, Hu WS (1996) Mechanistics of formation and ultrastructural evaluation of hepatocyte spheroids. In vitro cellular & developmental biology Animal 32(4):197-203

Poyck PP, Hoekstra R, Vermeulen JL, et al. (2008) Expression of glutamine synthetase and carbamoylphosphate synthetase i in a bioartificial liver: markers for the development of zonation in vitro. Cells, tissues, organs 188(3):259-69 doi:10.1159/000121609

Ramachandran SD, Schirmer K, Munst B, et al. (2015) In Vitro Generation of Functional Liver Organoid-Like Structures Using Adult Human Cells. PloS one 10(10):e0139345 doi:10.1371/journal.pone.0139345

Ramaiahgari SC, den Braver MW, Herpers B, et al. (2014) A 3D in vitro model of differentiated HepG2 cell spheroids with improved liver-like properties for repeated dose high-throughput toxicity studies. Archives of toxicology 88(5):1083-95 doi:10.1007/s00204-014-1215-9

Rashidi H, Alhaque S, Szkolnicka D, Flint O, Hay DC (2016) Fluid shear stress modulation of hepatocyte-like cell function. Archives of toxicology 90(7):1757-1761 doi:10.1007/s00204-016-1689-8

Reitzer LJ, Wice BM, Kennell D (1979) Evidence that glutamine, not sugar, is the major energy source for cultured HeLa cells. Journal of Biological Chemistry(254):2669-2676

Research. CotUoAi (2004) National Research Council (US) Committee to Update Science, Medicine, and Animals., Washington

Reuben A, Koch DG, Lee WM, Acute Liver Failure Study G (2010) Drug-induced acute liver failure: results of a U.S. multicenter, prospective study. Hepatology 52(6):2065-76 doi:10.1002/hep.23937

Riccalton-Banks L, Liew C, Bhandari R, Fry J, Shakesheff K (2003) Long-term culture of functional liver tissue: three-dimensional coculture of primary hepatocytes and stellate cells. Tissue engineering 9(3):401-10 doi:10.1089/107632703322066589

Richert L, Baze A, Parmentier C, et al. (2016) Cytotoxicity evaluation using cryopreserved primary human hepatocytes in various culture formats. Toxicology letters (in submission)

Rodriguez-Enriquez S, Juarez O, Rodriguez-Zavala JS, Moreno-Sanchez R (2001) Multisite control of the Crabtree effect in ascites hepatoma cells. European journal of biochemistry / FEBS 268(8):2512-9

Russo MW, Galanko JA, Shrestha R, Fried MW, Watkins P (2004) Liver transplantation for acute liver failure from drug induced liver injury in the United States. Liver transplantation : official publication of the American Association for the Study of Liver Diseases and the International Liver Transplantation Society 10(8):1018-23 doi:10.1002/lt.20204

Sainz B, Jr., TenCate V, Uprichard SL (2009) Three-dimensional Huh7 cell culture system for the study of Hepatitis C virus infection. Virology journal 6:103 doi:10.1186/1743-422X-6-103

Scaffidi P, Misteli T, Bianchi ME (2002) Release of chromatin protein HMGB1 by necrotic cells triggers inflammation. Nature 418(6894):191-5

Schutzer KM, Wall U, Lonnerstedt C, et al. (2004) Bioequivalence of ximelagatran, an oral direct thrombin inhibitor, as whole or crushed tablets or dissolved formulation. Curr Med Res Opin 20(3):325-331 doi:10.1185/030079903125003035

SeahorseBioscience (2016) Seahorse Bioscience. In.

Semler EJ, Ranucci CS, Moghe PV (2000) Mechanochemical manipulation of hepatocyte aggregation can selectively induce or repress liver-specific function. Biotechnology and bioengineering 69(4):359-69

Sempere LF, Freemantle S, Pitha-Rowe I, Moss E, Dmitrovsky E, Ambros V (2004) Expression profiling of mammalian microRNAs uncovers a subset of brain-expressed microRNAs with possible roles in murine and human neuronal differentiation. Genome biology 5(3):R13 doi:10.1186/gb-2004-5-3-r13

Sgro C, Clinard F, Ouazir K, et al. (2002) Incidence of drug-induced hepatic injuries: a French population-based study. Hepatology 36(2):451-5 doi:10.1053/jhep.2002.34857

Sharom FJ (2011) The P-glycoprotein multidrug transporter. Essays in biochemistry 50(1):161-78 doi:10.1042/bse0500161

Shaw PJ, Ganey PE, Roth RA (2010) Idiosyncratic drug-induced liver injury and the role of inflammatory stress with an emphasis on an animal model of trovafloxacin hepatotoxicity. Toxicological sciences : an official journal of the Society of Toxicology 118(1):7-18 doi:10.1093/toxsci/kfq168

Sison-Young RL, Lauschke VM, Johann E, et al. (2016) A multicenter assessment of single-cell models aligned to standard measures of cell health for prediction of acute hepatotoxicity. Archives of toxicology doi:10.1007/s00204-016-1745-4

Smith MT (2003) Mechanisms of troglitazone hepatotoxicity. Chemical research in toxicology 16(6):679-87 doi:10.1021/tx034033e

Srivastava A, Maggs JL, Antoine DJ, Williams DP, Smith DA, Park BK (2010) Role of reactive metabolites in drug-induced hepatotoxicity. Handbook of experimental pharmacology(196):165-94 doi:10.1007/978-3-642-00663-0_7

Starkey Lewis PJ, Dear J, Platt V, et al. (2011) Circulating microRNAs as potential markers of human drug-induced liver injury. Hepatology 54(5):1767-1776 doi:10.1002/hep.24538

Stricker BHCH (1992) Drug-Induced Hepatic Injury 2nd Ed. Elsvier, Amsterdam

Syed M, Skonberg C, Hansen SH (2016) Mitochondrial toxicity of diclofenac and its metabolites via inhibition of oxidative phosphorylation (ATP synthesis) in rat liver mitochondria: Possible role in drug induced liver injury (DILI). Toxicol in Vitro 31:93-102 doi:10.1016/j.tiv.2015.11.020

Szabo G, Bala S (2013) MicroRNAs in liver disease. Nature reviews Gastroenterology & hepatology 10(9):542-52 doi:10.1038/nrgastro.2013.87

Takahashi Y, Hori Y, Yamamoto T, Urashima T, Ohara Y, Tanaka H (2015) 3D spheroid cultures improve the metabolic gene expression profiles of HepaRG cells. Bioscience reports 35(3) doi:10.1042/BSR20150034

Thomas RJ, Bhandari R, Barrett DA, et al. (2005) The effect of three-dimensional co-culture of hepatocytes and hepatic stellate cells on key hepatocyte functions in vitro. Cells, tissues, organs 181(2):67-79 doi:10.1159/000091096

Toh YC, Lim TC, Tai D, Xiao G, van Noort D, Yu H (2009) A microfluidic 3D hepatocyte chip for drug toxicity testing. Lab on a chip 9(14):2026-35 doi:10.1039/b900912d

Tostoes RM, Leite SB, Serra M, et al. (2012) Human liver cell spheroids in extended perfusion bioreactor culture for repeated-dose drug testing. Hepatology 55(4):1227-36 doi:10.1002/hep.24760

Tsuchiya S, Yamabe M, Yamaguchi Y, Kobayashi Y, Konno T, Tada K (1980) Establishment and characterization of a human acute monocytic leukemia cell line (THP-1). International journal of cancer Journal international du cancer 26(2):171-6

Tujios S, Fontana RJ (2011) Mechanisms of drug-induced liver injury: from bedside to bench. Nature reviews Gastroenterology & hepatology 8(4):202-11 doi:10.1038/nrgastro.2011.22

Van Laar VS, Arnold B, Cassady SJ, Chu CT, Burton EA, Berman SB (2011) Bioenergetics of neurons inhibit the translocation response of Parkin following rapid mitochondrial depolarization. Human molecular genetics 20(5):927-40 doi:10.1093/hmg/ddq531

van Zijl F, Mikulits W (2010) Hepatospheres: Three dimensional cell cultures resemble physiological conditions of the liver. World journal of hepatology 2(1):1-7 doi:10.4254/wjh.v2.i1.1

Venereau E, Casalgrandi M, Schiraldi M, et al. (2012) Mutually exclusive redox forms of HMGB1 promote cell recruitment or proinflammatory cytokine release. Journal of Experimental Medicine 209(9):1519-1528 doi:10.1084/jem.20120189

Vermeir M, Annaert P, Mamidi RN, Roymans D, Meuldermans W, Mannens G (2005) Cell-based models to study hepatic drug metabolism and enzyme induction in humans. Expert opinion on drug metabolism & toxicology 1(1):75-90 doi:10.1517/17425255.1.1.75

Wang H, Bloom O, Zhang M, et al. (1999) HMG-1 as a late mediator of endotoxin lethality in mice. Science 285(5425):248-51 doi:7585 [pii]

Wang Z, Luo X, Anene-Nzelu C, et al. (2015) HepaRG culture in tethered spheroids as an in vitro three-dimensional model for drug safety screening. Journal of applied toxicology : JAT 35(8):909-17 doi:10.1002/jat.3090

Watkins PB (2005) Idiosyncratic liver injury: challenges and approaches. Toxicologic pathology 33(1):1-5 doi:10.1080/01926230590888306

Wells RG (2008) The role of matrix stiffness in regulating cell behavior. Hepatology 47(4):1394-400 doi:10.1002/hep.22193

West MA, Keller GA, Hyland BJ, Cerra FB, Simmons RL (1986) Further characterization of Kupffer cell/macrophage-mediated alterations in hepatocyte protein synthesis. Surgery 100(2):416-23

Wheeler MD (2003) Endotoxin and Kupffer cell activation in alcoholic liver disease. Alcohol research & health : the journal of the National Institute on Alcohol Abuse and Alcoholism 27(4):300-6

Williams D, Shipley S, Ellis MJ, et al. (2012) Novel in vitro and mathematical models for the prediction of chemical toxicity. Toxicology Research

Winkler S, Hempel M, Bruckner S, et al. (2015) Mouse white adipose tissue-derived mesenchymal stem cells gain pericentral and periportal hepatocyte features after differentiation in vitro, which are preserved in vivo after hepatic transplantation. Acta physiologica 215(2):89-104 doi:10.1111/apha.12560

Wong SF, No da Y, Choi YY, Kim DS, Chung BG, Lee SH (2011) Concave microwell based size-controllable hepatosphere as a three-dimensional liver tissue model. Biomaterials 32(32):8087-96 doi:10.1016/j.biomaterials.2011.07.028

Wrzesinski K, Fey SJ (2013) After trypsinisation, 3D spheroids of C3A hepatocytes need 18 days to re-establish similar levels of key physiological functions to those seen in the liver. Toxicology Research 2(2):123-135 doi:10.1039/c2tx20060k

Wrzesinski K, Magnone MC, Hansen LV, et al. (2013) HepG2/C3A 3D spheroids exhibit stable physiological functionality for at least 24 days after recovering from trypsinisation. Toxicology Research 2(3):163-172 doi:10.1039/c3tx20086h

Wrzesinski K, Rogowska-Wrzesinska A, Kanlaya R, et al. (2014) The cultural divide: exponential growth in classical 2D and metabolic equilibrium in 3D environments. PloS one 9(9):e106973 doi:10.1371/journal.pone.0106973

Wu X, Wu SQ, Tong L, et al. (2009) miR-122 affects the viability and apoptosis of hepatocellular carcinoma cells. Scand J Gastroentero 44(11):1332-1339 doi:10.3109/00365520903215305

Xia L, Hong X, Sakban RB, et al. (2016) Cytochrome P450 induction response in tethered spheroids as a three-dimensional human hepatocyte in vitro model. Journal of applied toxicology : JAT 36(2):320-9 doi:10.1002/jat.3189

Xu J, Wu C, Che X, et al. (2011) Circulating microRNAs, miR-21, miR-122, and miR-223, in patients with hepatocellular carcinoma or chronic hepatitis. Molecular carcinogenesis 50(2):136-42 doi:10.1002/mc.20712

Xu JJ, Henstock PV, Dunn MC, Smith AR, Chabot JR, de Graaf D (2008) Cellular imaging predictions of clinical drug-induced liver injury. Toxicological sciences : an official journal of the Society of Toxicology 105(1):97-105 doi:10.1093/toxsci/kfn109

Yagi K, Sumiyoshi N, Nakashima Y, et al. (1998) Stimulation of liver functions in hierarchical co-culture of bone marrow cells and hepatocytes. Cytotechnology 26(1):5-12 doi:10.1023/A:1007938118602

Yamada S, Maruyama I (2007) HMGB1, a novel inflammatory cytokine. Clinica Chimica Acta 375(1-2):36-42 doi:10.1016/j.cca.2006.07.019

Yang H, Lundback P, Ottosson L, et al. (2012) Redox modification of cysteine residues regulates the cytokine activity of high mobility group box-1 (HMGB1). Molecular medicine 18(1):250-9 doi:10.2119/molmed.2011.00389

Zahno A, Brecht K, Morand R, et al. (2011) The role of CYP3A4 in amiodarone-associated toxicity on HepG2 cells. Biochemical pharmacology 81(3):432-441 doi:10.1016/j.bcp.2010.11.002

Zhang Y, Jia Y, Zheng R, et al. (2010) Plasma microRNA-122 as a biomarker for viral-, alcohol-, and chemical-related hepatic diseases. Clinical chemistry 56(12):1830-8 doi:10.1373/clinchem.2010.147850

Zhou Y, Qin S, Wang K (2013) Biomarkers of drug-induced liver injury. Current Biomarker Findings 3:1-9

Zinchenko YS, Schrum LW, Clemens M, Coger RN (2006) Hepatocyte and kupffer cells co-cultured on micropatterned surfaces to optimize hepatocyte function. Tissue engineering 12(4):751-61 doi:10.1089/ten.2006.12.751